The University Of Sheffield.

HYBRID CONTROL OF HUMAN-INDUCED VIBRATION

By

Nima Noormohammadi

A thesis submitted for the Degree of Doctor of Philosophy (PhD) at the

The University of Sheffield

Department of Civil and structural Engineering

January 2014

To Maral

To Raheleh (Akhtar), Davar and Rama

Abstract

A key objective in the design of any sports stadium is to include the maximum number of spectators with minimum obstruction in the visual cone. This functional requirement often results in employing one or more cantilevered tiers, which in turn culminates in more slender grandstands often with relatively low natural frequencies and modal damping ratios. These natural frequencies may sometimes fall in the range of frequencies of human movement, which can possibly excite the structure in resonance resulting in vibration serviceability issues. One of the available techniques to reduce excessive responses is to use passive vibration control techniques such as Tuned Mass Dampers (TMD). However, the off-tuning problem is a potential drawback of this technique, whereby changes in natural frequencies caused by crowd-structure interaction may detune the TMDs.

This thesis presents a study into the possibility of using Hybrid Tuned Mass Dampers (HTMDs) to augment the vibration serviceability of structures. An appropriate control algorithm is developed. It shows a comparative analysis of vibration mitigation performances that are likely to be attained by utilising the proposed HTMD. Also, an appropriate control scheme is utilised with the proposed HTMD to deal with the off-tuning issues in TMDs caused by crowd loading, and is shown to be effective.

In addition, it shows a comparative experimental investigation of a passive TMD and a prototype HTMD applied on a slab strip structure. The most effective control algorithm to enhance the performance of the HTMD and also deal with the off-tuning problem is investigated. The experimental results verify the developed simulation studies and also demonstrate the effectiveness of employing a HTMD considering both structural response and cost (actuator effort).

Acknowledgement

I would like to express profound gratitude to my supervisor, Professor Paul Reynolds, for his invaluable support, encouragement, supervision and useful suggestions throughout this research work. His moral support and continuous guidance enabled me to complete my work successfully. I am also highly thankful to Dr Donald Nyawako for his valuable suggestions throughout this study.

Life would not have been the same without the support of my wife, Maral Saifzadeh. The encouragement, kindness and support of you is highly appreciated, I know the word ‘thank you’ is not enough. I am as ever, especially indebted to my parents, and Mrs Akhtar Vojdan Shemshadi Mr Davar Noormohammadi and my brother, Mr Rama Noormohammadi for their love and support throughout my life. I also wish to thank my other family members, Behrang, Shamsi, Bahman, Shoghra and Shahram.

Also thanks to members of the Vibration Engineering Section: Alex, James, Sharon, Arun, Emma, Erfan, Chris and Vito for your company and support over the past years.

Finally, I wish to express my appreciation to all my friends who shared their love and experiences with me.

Nima Noormohammadi

Memorandum

The accompanying thesis entitled “Hybrid Control of Human-Induced Vibration” is submitted for the degree of Doctor of Philosophy in the Faculty of Engineering at the University of Sheffield. The thesis is based entirely on the independent work carried out by the author in The University of Sheffield between December 2009 and January 2014 under the supervision of Professor Paul Reynolds. All the work and ideas recorded are original except where acknowledged in the text or by reference. The work contained in the thesis has not previously been submitted for a degree or diploma at this, or any other, University or Examining Body.

Nima Noormohammadi

January 2014

Table of Contents

List of Figures

List of Tables

Notations

c_{act} Damping coefficient of the actuator

c_{as} Damping coefficient of active spectators

c_p Damping coefficient of the passive TMD

c_{ps} Damping coefficient of passive spectators

c_s Damping coefficient of the empty structure

f_{act} Natural frequency of the actuator

f_{beat} Frequency of the crowd activity (frequency of the music beat)

f_p Natural frequency of the TMD

f_s Fundamental natural frequency of the empty structure

$\bar{f}$ Frequency ratio between TMD and structure

k_{act} Stiffness of the actuator

k_{as} Stiffness of active spectators

k_p Stiffness of the passive TMD

k_{ps} Stiffness of passive spectators

k_s Stiffness of the empty structure

m_{act} Mass of the actuator

m_{as} Mass of active spectators

m_{ep} Mass of each person

m_p Mass of the passive TMD

m_{ps} Mass of passive spectators

m_s Mass of the empty structure

$\bar{m}$ Mass ratio between TMD and structure

r_p Penalty Factor in GA and Penalty Method

s Laplace Transform operator

v_{act} Force-voltage characteristic of the actuator

x_{act} Absolute displacement of the actuator mass

x_{as} Absolute displacement of the active spectators

$x_{p,rel}$ Relative displacement of the TMD mass

x_p Absolute displacement of the TMD mass

x_{ps} Absolute displacement of the passive spectators

x_s Absolute displacement of the structure

$\dot{x}_{act}$ Absolute velocity of the actuator mass

$\dot{x}_{as}$ Absolute velocity of the active spectators

$\dot{x}_{p,rel}$ Relative velocity of the TMD mass

$\dot{x}_{p}$ Absolute velocity of the TMD mass

$\dot{x}_{ps}$ Absolute velocity of the passive spectators

$\dot{x}_{s}$ Absolute velocity of the structure

$\ddot{x}_{act}$ Absolute acceleration of the actuator mass

$\ddot{x}_{as}$ Absolute acceleration of the active spectators

$\ddot{x}_{p,rel}$ Relative acceleration of the TMD mass

$\ddot{x}_{p}$ Absolute acceleration of the TMD mass

$\ddot{x}_{ps}$ Absolute acceleration of the passive spectators

$\ddot{x}_{s}$ Absolute acceleration of the structure

A_{DVF} State matrix in SS model, structure with attached AMD

$A_{HTMD,S}$ State matrix in SS model, structure with attached HTMD in stadium model

A_{HTMD} State matrix in SS model, structure with attached HTMD

A_{lqr} State matrix in SS model, structure with attached HTMD using LQR

$A_{TMD,S}$ State matrix in SS model, structure with attached TMD in stadium model

A_{TMD} State matrix in SS model, structure with attached TMD

$A_{unc,S}$ State matrix in SS model, structure with attached TMD in stadium model

A_{unc} State matrix in SS model, uncontrolled structure

B_{DVF} Input matrix in SS model, structure with attached AMD

$B_{HTMD,S}$ Input matrix in SS model, structure with attached HTMD in stadium model

B_{HTMD} Input matrix in SS model, structure with attached HTMD

B_{lqr} Input matrix in SS model, structure with attached HTMD using LQR

$B_{TMD,S}$ Input matrix in SS model, structure with attached TMD in stadium model

B_{TMD} Input matrix in SS model, structure with attached TMD

$B_{unc,S}$ Input matrix in SS model, structure with attached TMD in stadium model

B_{unc} Input matrix in SS model, uncontrolled structure

C_{DVF} Output matrix in SS model, structure with attached AMD

$C_{HTMD,S}$ Output matrix in SS model, structure with attached HTMD in stadium model

C_{HTMD} Output matrix in SS model, structure with attached HTMD

$C_{TMD,S}$ Output matrix in SS model, structure with attached TMD in stadium model

C_{TMD} Output matrix in SS model, structure with attached TMD

$C_{unc,S}$ Output matrix in SS model, structure with attached TMD in stadium model

C_{unc} Output matrix in SS model, uncontrolled structure

D_{DVF} Feed through matrix in SS model, structure with attached AMD

$D_{HTMD,S}$ Feed through matrix in SS model, structure with attached HTMD in stadium model

D_{HTMD} Feed through matrix in SS model, structure with attached HTMD

$D_{TMD,S}$ Feed through matrix in SS model, structure with attached TMD in stadium model

D_{TMD} Feed through matrix in SS model, structure with attached TMD

$D_{unc,S}$ Feed through matrix in SS model, structure with attached TMD in stadium model

D_{unc} Feed through matrix in SS model, uncontrolled structure

$F_{c,act}$ Damping force of the actuator

F_{ext} External force on the main structure (e.g. human jumping force)

$F_{I,act}$ Inertia force of the actuator

F_i Objective Function of the ith frequency in GA

$F_{k,act}$ Stiffness force of the actuator

$\mathrm{G_{act}}$ TF of the actuator

$\mathrm{G_{as,1,S}}$ TF of the active spectators relates to the acceleration of the structure in stadium model

$\mathrm{G_{as,2,S}}$ TF of the active spectators relates to the internal force in stadium model

G_{filter} Filter transfer function

$G_{GLF,i}$ Generated Load Factor of ith harmonic

G_i Constraint Function of the ith frequency in GA

$\mathrm{G_{int}}$ Integrator block transfer function

$\mathrm{G_{p,1,S}}$ TF of the TMD/HTMD relates to the acceleration of the structure in stadium model

$G_{p,1}$ TF of the TMD relates to the acceleration of the structure

$G_{p,2,S}$ TF of the TMD/HTMD relates to the inertia force of the actuator in stadium model

$G_{p,2}$ TF of the TMD relates to the inertia force of the actuator

G_{Plant} TF between structure/TMD response and actuator's inertia force

$G_{ps,1,S}$ TF of the passive spectators relates to the acceleration of the structure in stadium model

$G_{s,1,TMD,S}$ TF of the structure (with attached TMD/HTMD) relates to external force in stadium model

$G_{s,1,TMD}$ TF of the structure (with attached TMD/HTMD) relates to the TMD's dynamics

$G_{s,1,unc,S}$ TF of the uncontrolled structure relates to external force in stadium model

$G_{s,2,TMD,S}$ TF of the structure (with attached TMD/HTMD) relates to the TMD dynamics in stadium model

$G_{s,2,TMD}$ TF of the structure (with attached TMD/HTMD) relates to the external force

$G_{s,2,unc,S}$ TF of the uncontrolled structure relates to the active spectator in stadium model

$G_{s,2,unc}$ TF of the uncontrolled structure relates to the external force

$G_{s,3,TMD,S}$ TF of the structure (with attached TMD/HTMD) relates to the active spectator in stadium model

$G_{s,3,unc,S}$ TF of the uncontrolled structure relates to the passive spectator in stadium model

$G_{s,4,TMD,S}$ TF of the structure (with attached TMD/HTMD) relates to the passive spectator in stadium model

G_{xx} Auto Power Spectral Density of input signal

G_{xy} Cross Power Spectral Density between input and output

G_{yx} Cross Power Spectral Density between output and input

G_{yy} Auto Power Spectral Density of output signal

$H_{HTMD,S}$ TF between external force and structural response for stadium model with HTMD

H_{HTMD} TF between external force and structural response for controlled structure with HTMD

$H_{TMD,S}$ TF between external force and structural response for controlled stadium model with TMD

H_{TMD} TF between external force and structural response for controlled structure with TMD

$H_{unc,S}$ TF between external force and structural response for uncontrolled stadium model

H_{unc} TF between external force and structural response for uncontrolled structure

K_1 Feedback gain, displacement of the TMD

K_2 Feedback gain, acceleration of the main structure

K_3 Feedback gain, velocity of the main structure

K_4 Feedback gain, velocity of the TMD

K_5 Feedback gain, acceleration of the TMD

K_{DVF} Direct Velocity Feedback gain

K_i Feedback gain

K_{lqr} LQR feedback gain matrix

P_{as} Internal periodic jumping force in active spectators

P_{lqr} Solution of the Riccati Differential Equation in LQR method

Q_{lqr} State weighting matrix in LQR method

R_{lqr} Control weighting matrix in LQR method

U_{act} Developed force in the electromagnetic coils of actuator

U_{DVF} Input vector in SS model, structure with attached AMD

$U_{HTMD,S}$ Input vector in SS model, structure with attached HTMD in stadium model

U_{HTMD} Input vector in SS model, structure with attached HTMD

U_{lqr} Input vector in SS model, structure with attached HTMD using LQR

$U_{TMD,S}$ Input vector in SS model, structure with attached TMD in stadium model

U_{TMD} Input vector in SS model, structure with attached TMD

$U_{unc,S}$ Input vector in SS model, structure with attached TMD in stadium model

U_{unc} Input vector in SS model, uncontrolled structure

$V_{in,act}$ Input voltage of the actuator

$X_{1,DVF}$ State of the SS model, displacement of the structure with attached AMD

$X_{1,\mathrm{H}TMD,S}$ State of the SS model, displacement of the structure with attached HTMD in stadium model

$X_{1,\mathrm{H}TMD}$ State of the SS model, displacement of the structure with attached HTMD

$X_{1,TMD,S}$ State of the SS model, displacement of the structure with attached TMD in stadium model

$X_{1,TMD}$ State of the SS model, displacement of the structure with attached TMD

$X_{1,unc,S}$ State of the SS model, displacement of the structure with attached TMD in stadium model

$X_{1,unc}$ State of the SS model, displacement of the uncontrolled structure

$X_{10,\mathrm{H}TMD,S}$ State of the SS model, velocity of the active mass in HTMD in stadium model

$X_{11,\mathrm{H}TMD,S}$ State of the SS model, acceleration of the active mass in HTMD in stadium model

$X_{2,DVF}$ State of the SS model, velocity of the structure with attached AMD

$X_{2,\mathrm{H}TMD,S}$ State of the SS model, velocity of the structure with attached HTMD in stadium model

$X_{2,\mathrm{H}TMD}$ State of the SS model, velocity of the structure with attached HTMD

$X_{2,TMD,S}$ State of the SS model, velocity of the structure with attached TMD in stadium model

$X_{2,TMD}$ State of the SS model, velocity of the structure with attached TMD

$X_{2,unc,S}$ State of the SS model, velocity of the structure with attached TMD in stadium model

$X_{2,unc}$ State of the SS model, velocity of the uncontrolled structure

$X_{3,\mathrm{H}TMD,S}$ State of the SS model, displacement of the passive mass in HTMD in stadium model

$X_{3,\mathrm{H}TMD}$ State of the SS model, displacement of the passive mass in HTMD

$X_{3,TMD,S}$ State of the SS model, displacement of the passive mass in TMD in stadium model

$X_{3,TMD}$ State of the SS model, displacement of the TMD mass in passive TMD

$X_{3,unc,S}$ State of the SS model, displacement of the active spectators DOF in TMD in stadium model

$X_{4,\mathrm{H}TMD,S}$ State of the SS model, velocity of the passive mass in HTMD in stadium model

$X_{4,\mathrm{H}TMD}$ State of the SS model, velocity of the passive mass in HTMD

$X_{4,TMD,S}$ State of the SS model, velocity of the passive mass in TMD in stadium model

$X_{4,TMD}$ State of the SS model, velocity of the TMD mass in passive TMD

$X_{4,unc,S}$ State of the SS model, velocity of the active spectators DOF in TMD in stadium model

$X_{5,DVF}$ State of the SS model, displacement of the active mass in AMD

$X_{5,\mathrm{H}TMD,S}$ State of the SS model, displacement of the active spectators DOF in HTMD in stadium model

$X_{5,\mathrm{H}TMD}$ State of the SS model, displacement of the active mass in HTMD

$X_{5,TMD,S}$ State of the SS model, displacement of the active spectators DOF in TMD in stadium model

$X_{5,unc,S}$ State of the SS model, displacement of the passive spectators DOF in TMD in stadium model

$X_{6,DVF}$ State of the SS model, velocity of the active mass in AMD

$X_{6,\mathrm{H}TMD,S}$ State of the SS model, velocity of the active spectators DOF in HTMD in stadium model

$X_{6,\mathrm{H}TMD}$ State of the SS model, velocity of the active mass in HTMD

$X_{6,TMD,S}$ State of the SS model, velocity of the active spectators DOF in TMD in stadium model

$X_{6,unc,S}$ State of the SS model, velocity of the passive spectators DOF in in stadium model TMD

$X_{7,DVF}$ State of the SS model, acceleration of the active mass in AMD

$X_{7,\mathrm{H}TMD,S}$ State of the SS model, displacement of the passive spectators DOF in HTMD in stadium model

$X_{7,\mathrm{H}TMD}$ State of the SS model, acceleration of the active mass in HTMD

$X_{7,TMD,S}$ State of the SS model, displacement of the passive spectators DOF in TMD in stadium model

$X_{8,\mathrm{H}TMD,S}$ State of the SS model, velocity of the passive spectators DOF in in stadium model HTMD

$X_{8,TMD,S}$ State of the SS model, velocity of the passive spectators DOF in in stadium model TMD

$X_{9,\mathrm{H}TMD,S}$ State of the SS model, displacement of the active mass in HTMD in stadium model

X_{act} Laplace transform of the actuator response

X_{DVF} State vector in SS model, structure with attached AMD

$X_{HTMD,S}$ State vector in SS model, structure with attached HTMD in stadium model

X_{HTMD} State vector in SS model, structure with attached HTMD

X_{lqr} State vector in SS model, structure with attached HTMD using LQR

X_p Laplace transform of the TMDresponse

X_{Resp} Reponses of the structure or TMD (i.e. acceleration, velocity or displacement)

X_S Laplace transform of the empty structure response

$X_{TMD,S}$ State vector in SS model, structure with attached TMD in stadium model

X_{TMD} State vector in SS model, structure with attached TMD

$X_{unc,S}$ State vector in SS model, structure with attached TMD in stadium model

X_{unc} State vector in SS model, uncontrolled structure

$\dot{X}_{1,DVF}$ Derivative of the state of the SS model, velocity of the structure with attached AMD

$\dot{X}_{1,HTMD,S}$ Derivative of the state of the SS model, velocity of the structure with attached HTMD in stadium model

$\dot{X}_{1,HTMD}$ Derivative of the state of the SS model, velocity of the structure with attached HTMD

$\dot{X}_{1,TMD,S}$ Derivative of the state of the SS model, velocity of the structure with attached TMD in stadium model

$\dot{X}_{1,TMD}$ Derivative of the state of the SS model, velocity of the structure with attached TMD

$\dot{X}_{1,unc,S}$ Derivative of the state of the SS model, velocity of the structure with attached TMD in stadium model

$\dot{X}_{1,unc}$ Derivative of the state of the SS model, velocity of the uncontrolled structure

$\dot{X}_{10,HTMD,S}$ Derivative of the state of the SS model, acceleration of the active mass in HTMD in stadium model

$\dot{X}_{11,HTMD,S}$ Derivative of the state of the SS model, derivative of the acceleration of the active mass in HTMD in stadium model

$\dot{X}_{2,DVF}$ Derivative of the state of the SS model, acceleration of the structure with attached AMD

$\dot{X}_{2,HTMD,S}$ Derivative of the state of the SS model, acceleration of the structure with attached HTMD in stadium model

$\dot{X}_{2,HTMD}$ Derivative of the state of the SS model, acceleration of the structure with attached HTMD

$\dot{X}_{2,TMD,S}$ Derivative of the state of the SS model, acceleration of the structure with attached TMD in stadium model

$\dot{X}_{2,TMD}$ Derivative of the state of the SS model, acceleration of the structure with attached TMD

$\dot{X}_{2,unc,S}$ Derivative of the state of the SS model, acceleration of the structure with attached TMD in stadium model

$\dot{X}_{2,unc}$ Derivative of the state of the SS model, acceleration of the uncontrolled structure

$\dot{X}_{3,HTMD,S}$ Derivative of the state of the SS model, velocity of the passive mass in HTMD in stadium model

$\dot{X}_{3,HTMD}$ Derivative of the state of the SS model, velocity of the passive mass in HTMD

$\dot{X}_{3,TMD,S}$ Derivative of the state of the SS model, velocity of the passive mass in TMD in stadium model

$\dot{X}_{3,TMD}$ Derivative of the state of the SS model, velocity of the TMD mass in passive TMD

$\dot{X}_{3,unc,S}$ Derivative of the state of the SS model, velocity of the active spectators DOF in TMD in stadium model

$\dot{X}_{4,HTMD,S}$ Derivative of the state of the SS model, acceleration of the passive mass in HTMD in stadium model

$\dot{X}_{4,HTMD}$ Derivative of the state of the SS model, acceleration of the passive mass in HTMD

$\dot{X}_{4,TMD,S}$ Derivative of the state of the SS model, acceleration of the passive mass in TMD in stadium model

$\dot{X}_{4,TMD}$ Derivative of the state of the SS model, acceleration of TMD mass in passive TMD

$\dot{X}_{4,unc,S}$ Derivative of the state of the SS model, acceleration of the active spectators DOF in TMD in stadium model

$\dot{X}_{5,DVF}$ Derivative of the state of the SS model, velocity of the active mass in AMD

$\dot{X}_{5,HTMD,S}$ Derivative of the state of the SS model, velocity of the active spectators DOF in HTMD in stadium model

$\dot{X}_{5,HTMD}$ Derivative of the state of the SS model, velocity of the active mass in HTMD

$\dot{X}_{5,TMD,S}$ Derivative of the state of the SS model, velocity of the active spectators DOF in TMD in stadium model

$\dot{X}_{5,unc,S}$ Derivative of the state of the SS model, velocity of the passive spectators DOF in TMD in stadium model

$\dot{X}_{6,DVF}$ Derivative of the state of the SS model, acceleration of the active mass in AMD

$\dot{X}_{6,HTMD,S}$ Derivative of the state of the SS model, acceleration of the active spectators DOF in HTMD in stadium model

$\dot{X}_{6,HTMD}$ Derivative of the state of the SS model, acceleration of the active mass in HTMD

$\dot{X}_{6,TMD,S}$ Derivative of the state of the SS model, acceleration of the active spectators DOF in TMD in stadium model

$\dot{X}_{6,unc,S}$ Derivative of the state of the SS model, acceleration of the passive spectators DOF in TMD in stadium model

$\dot{X}_{7,DVF}$ Derivative of the state of the SS model, derivative of the acceleration of the active mass in AMD

$\dot{X}_{7,HTMD,S}$ Derivative of the state of the SS model, velocity of the passive spectators DOF in HTMD in stadium model

$\dot{X}_{7,HTMD}$ Derivative of the state of the SS model, derivative of the acceleration of the active mass in HTMD

$\dot{X}_{7,TMD,S}$ Derivative of the state of the SS model, velocity of the passive spectators DOF in TMD in stadium model

$\dot{X}_{8,HTMD,S}$ Derivative of the state of the SS model, acceleration of the passive spectators DOF in HTMD in stadium model

$\dot{X}_{8,TMD,S}$ Derivative of the state of the SS model, acceleration of the passive spectators DOF in TMD in stadium model

$\dot{X}_{9,HTMD,S}$ Derivative of the state of the SS model, velocity of the active mass in HTMD in stadium model

$\dot{X}_{DVF}$ Derivative of state vector in SS model, structure with attached AMD

$\dot{X}_{HTMD,S}$ Derivative of state vector in SS model, structure with attached HTMD in stadium model

$\dot{X}_{HTMD}$ Derivative of state vector in SS model, structure with attached HTMD

$\dot{X}_{lqr}$ Derivative of state vector in SS model, structure with attached HTMD using LQR

$\dot{X}_{TMD,S}$ Derivative of state vector in SS model, structure with attached TMD in stadium model

$\dot{X}_{TMD}$ Derivative of state vector in SS model, structure with attached TMD

$\dot{X}_{unc,S}$ Derivative of state vector in SS model, structure with attached TMD in stadium model

$\dot{X}_{unc}$ Derivative of state vector in SS model, uncontrolled structure

$Y_{1,DVF}$Output of the SS model, displacement of the structure with attached AMD

$Y_{1,HTMD,S}$Output of the SS model, displacement of the structure with attached TMD in stadium model

$Y_{1,HTMD}$Output of the SS model, displacement of the structure with attached TMD

$Y_{1,TMD,S}$Output of the SS model, displacement of the structure with attached TMD in stadium model

$Y_{1,TMD}$ Output of the SS model, displacement of the structure with attached TMD

$Y_{1,unc,S}$Output of the SS model, displacement of the structure with attached TMD in stadium model

$Y_{1,unc}$ Output of the SS model, displacement of the uncontrolled structure

$Y_{2,DVF}$Output of the SS model, velocity of the structure with attached AMD

$Y_{2,HTMD,S}$Output of the SS model, velocity of the structure with attached TMD in stadium model

$Y_{2,HTMD}$Output of the SS model, velocity of the structure with attached TMD

$Y_{2,TMD,S}$Output of the SS model, velocity of the structure with attached TMD in stadium model

$Y_{2,TMD}$ Output of the SS model, velocity of the structure with attached TMD

$Y_{2,unc,S}$Output of the SS model, velocity of the structure with attached TMD in stadium model

$Y_{2,unc}$ Output of the SS model, velocity of the uncontrolled structure

$Y_{3,DVF}$Output of the SS model, acceleration of the structure with attached AMD

$Y_{3,HTMD,S}$Output of the SS model, acceleration of the structure with attached TMD in stadium model

$Y_{3,HTMD}$Output of the SS model, acceleration of the structure with attached TMD

$Y_{3,TMD,S}$Output of the SS model, acceleration of the structure with attached TMD in stadium model

$Y_{3,TMD}$ Output of the SS model, acceleration of the structure with attached TMD

$Y_{3,unc,S}$Output of the SS model, acceleration of the structure with attached TMD in stadium model

$Y_{3,unc}$ Output of the SS model, acceleration of the uncontrolled structure

$Y_{4,HTMD,S}$Output of the SS model, displacement of the passive mass in HTMD TMD in stadium model

$Y_{4,HTMD}$Output of the SS model, displacement of the passive mass in HTMD TMD

$Y_{4,TMD,S}$Output of the SS model, displacement of the passive mass in TMD in stadium model

$Y_{4,TMD}$ Output of the SS model, displacement of the TMD mass in passive TMD

$Y_{5,HTMD,S}$ Output of the SS model, velocity of the passive mass in HTMD in stadium model

$Y_{5,HTMD}$Output of the SS model, velocity of the passive mass in HTMD

$Y_{5,TMD,S}$ Output of the SS model, velocity of the passive mass in TMD in stadium model

$Y_{5,TMD}$ Output of the SS model, velocity of the TMD mass in passive TMD

$Y_{6,HTMD,S}$Output of the SS model, acceleration of the passive mass in HTMD in stadium model

$Y_{6,HTMD}$Output of the SS model, acceleration of the passive mass in HTMD

$Y_{6,TMD,S}$Output of the SS model, acceleration of the passive mass in TMD in stadium model

$Y_{6,TMD}$ Output of the SS model, acceleration of the TMD mass in passive TMD

$Y_{7,DVF}$Output of the SS model, displacement of the active mass in AMD

$Y_{7,HTMD,S}$Output of the SS model, displacement of the active mass in HTMD in stadium model

$Y_{7,HTMD}$Output of the SS model, displacement of the active mass in HTMD

$Y_{8,DVF}$Output of the SS model, velocity of the active mass in AMD

$Y_{8,HTMD,S}$Output of the SS model, velocity of the active mass in HTMD in stadium model

$Y_{8,HTMD}$Output of the SS model, velocity of the active mass in HTMD

$Y_{9,DVF}$Output of the SS model, inertia force of the actuator in AMD

$Y_{9,HTMD,S}$Output of the SS model, inertia force of the actuator in HTMD in stadium model

$Y_{9,HTMD}$Output of the SS model, inertia force of the actuator in HTMD

ε_{act} Low pass filter element coefficient of the actuator

ξ_{act} Damping ratio of the actuator

ξ_p Damping ratio of the TMD

ξ_s Damping ratio of the empty structure

ρ_{jump} Crowd effectiveness factor

Abbreviations

SDOF: Single Degree Of Freedom

DOF: Degree Of Freedom

EMA: Experimental Modal Analysis

TF: Transfer Function

FRF: Frequency Response Function

LQR: Linear Quadratic Regulator

SS: State Space

TMD: Tuned Mass Damper

HTMD: Hybrid Tuned Mass Damper

GA: Genetic Algorithm

OF: Objective Function

S.T.: Subject To

RL: Root Locus

SISO: Single Input-Single Output

MISO: Multi Input-Single Output

MIMO: Multi Input- Multi Output

SIMO: Single Input- Multi Output

AVC: Active Vibration Control

AMD: Active Mass Damper

DVF: Direct Velocity Feedback

GLF: Generated Load Factor

DLF: Dynamic Load Factor

PSD: Power Spectral Density

MTVV: Maximum Transient Vibration Value

RMS: Root Mean Square

1. Introduction

In recent years there has been a trend to design sports stadia in such a way as to have higher capacities for spectators in addition to providing a clearer visual field. Therefore, many designs have incorporated one or more cantilevered tiers. However, using cantilevers may result in grandstands with increased slenderness and which often have lower fundamental natural frequencies and modal damping ratios. These natural frequencies might fall in the range of excitation frequencies produced by human activities, potentially resulting in resonant responses. This can result in a vibration serviceability problem and can potentially be a safety concern if spectators become alarmed by the responses and a crowd panic situation develops.

Past solutions to deal with observed or anticipated vibration serviceability problems have been mainly passive methods, such as tuned mass dampers (TMDs). These techniques have exhibited problems such as lack of performance and off-tuning caused by human-structure interaction. To address this issue, research is currently underway to investigate the possible application of hybrid TMDs (HTMDs), which are a combination of active and passive control, to improve the vibration serviceability of such structures under human excitation.

Hybrid control contains an integration of passive and active control systems. It is created by the combination of active and passive segments (also known as composite active-passive controllers) to reduce structural response mostly by energy dissipation through the passive part, whereas the active part is included to improve its performance. In hybrid control systems the active part is smaller and less power is required than for a fully active system.

This thesis presents a combined analytical and experimental programme of research carried out to investigate the potential of HTMDs for mitigation of vibrations in crowd-occupied stadium structures. The active part of the HTMD is expected to be advantageous in both the enhancement of vibration control performance and also to provide adaptability when structural characteristics change due to the variable crowd occupation.

1.1. Thesis outline

This research work is presented in eight chapters. Chapter 1 briefly introduces the subject of vibration serviceability in stadia and different relevant methods for mitigation of these vibrations. It also presents an introduction to the HTMD as a possible solution and the focus of this research. Chapter 2 is the literature review section, which describes the background to vibration mitigation methods that have been employed in civil engineering structures in the past to suppress human-induced vibrations. It also has a review on various control algorithms related to HTMDs. Chapter 3 presents the development of structural model (both controlled and un-controlled) with AMD (Active Mass Damper), TMD (Tuned Mass Damper) and HTMD (Hybrid Tuned Mass Damper) attached. Also, different control algorithms are investigated and compared.

Chapter 4 introduces a new HTMD gain optimisation method using a Genetic Algorithm. The performance of the proposed optimised HTMD is compared against that of the AMD and TMD. Chapter 5 studies the off-tuning issue as one of the known disadvantages of passive TMD. It introduces two control algorithms in HTMD to deal with off-tuning problem.

Chapter 6 presents an experimental investigation utilising a prototype HTMD on a laboratory structure and compares its performance against the uncontrolled structure and the structure controlled with a passive TMD and AMD. Chapter 7 describes a simulation study of the application of HTMD on a cantilevered seating deck in a stadium. It describes the development of the stadium model using real measurement data and compares the structural response using TMD and HTMD. Chapter 8 presents conclusions and some recommendation for further studies.

2. Literature Review

2.1. Introduction

Advanced material technologies and building design codes often lead to slender structures with low fundamental natural frequencies. These structures, grandstands and concert arenas for instance, are sometimes susceptible to human movements such as walking, running, bobbing and jumping [1]–[8]. This happens particularly when humans' jumping and walking frequencies or their harmonics are close to a structural natural frequency [9]. The feeling of fear and discomfort in building occupants due to high levels of vibration is an important consideration for vibration serviceability and safety [10]–[12].

For instance, there have been some footbridges mostly in town areas and under pedestrian forces that are designed more slender for artistic reasons. One important problem in designing medium to long span footbridges is to reduce vibrations caused by wind load or pedestrians. [13].

2.1.1. Structural Vibration Control

During the past few decades, structural control has attracted the attention of many researchers in this field. The aim is to reduce excessive vibration using appropriate methods [14], [15]. A range of vibration control techniques have been introduced and applied to improve different structural vibration performance such as seismic and wind induced vibration. These can be classified as follows [16]:

- Passive Vibration Control
- Active Vibration Control
- Semi-Active Vibration Control (Controlled Passive)
- Hybrid Vibration Control (Active+Passive)

In Passive Control methods, the vibration energy is dissipated by introduction of additional material or devices to the primary structures, which raises their damping and sometimes stiffness. Passive control methods do not require an external power source. Generally, it is also relatively easy to design them [11]. However, they have relatively poor performance, particularly for low-level vibrations where they might not be fully engaged.

In active control, a control force is applied to a structure by applying external power via an actuator. This method adds energy to the structure that is intended to oppose the vibration caused by a disturbance. However, this method has some disadvantages, such as possible loss of external power, requirement of actuators, high running cost and high power demand in case of large disturbance forces [9], [11].

A semi-active control system can be considered as a passive system where its damping and/or stiffness can be changed in real time, without introducing additional energy to the controlled structure [17], [18]. They are sometimes known as controlled passive devices which is probably a more accurate term [11]. Semi-active controllers have many advantages. They are relatively cheap, require low power and are relatively simple devices without too many mechanical parts. Also because external energy is not applied directly to the structure, these devices are inherently stable. An important advantage for both hybrid and semi-active systems is their ability to work as purely passive systems in case of external power failure [9], [18]–[21].

However, there are some problems with semi-active controllers. One of the most important issues is highly complex and nonlinear nature of the control algorithms used. This means it is difficult to define the required relationship between damper force and the structural response that will give the best mitigation performance [10], [22].

Hybrid control is usually a combination of passive and active control systems. It can be either a switching between or integration of active and passive parts. Most proposed hybrid controllers are the switching system type [15]. Where hybrid controllers are based on integration of active and passive parts (also known as composite active-passive controller), they reduce structural response mainly by dissipating energy through the passive part, whereas the active part reduces the sensitivity of the system to changes in structural dynamic properties and also enhances its performance. Because the force capacity of the active part is small in comparison with the passive part, lower power is required than purely active systems. In addition, the size of the active element is comparatively smaller than

those in purely active controllers and leads to fewer installation problems [2], [18], [21].

These methods have been applied successfully in other disciplines such as seismic and wind induced vibration control. The focus of this work is to examine the potential application of hybrid control on civil structures subjected to human induced vibration.

It should be noted that the main difference between vibration due to human activities (e.g. in stadia) in contrast with wind and seismic induced vibration is the presence of human-structure interaction phenomenon that results in alteration of the dynamic of the primary structure. This can be a challenge for the controlling method since some types such as passive control is set to work in a specific bandwidth frequency.

2.1.2. Vibration Serviceability of Grandstands

Large audiences can be attracted by a pop concert and it has been largely usual to occupy sport stadia or concert arenas for these events. In addition, the spectator's behaviour has been changed to have more jumping and dancing activities during concerts. Hence, grandstands compared to their original designs encounter more severe loading. It is known that the population of people can produce remarkable dynamic loads especially when rhythmic jumping exists in their movements. This situation may happen with some kinds of aerobics and dance activities. If the frequency of this load coincides with a resonant frequency of a structure, a high level of vibration might be expected. This is an important consideration for sport stadia, concert arenas and other similar types of structure, especially in those with long-span cantilever [1], [8], [23]–[30].

Vibration serviceability issues in stadia have been reported during some live events and sport matches. To remedy these problems, various different methods have been applied including adding extra columns, temporary struts, trussing below cantilevers, viscous dampers and using Tuned Mass Dampers [8], [17], [31], [32].

One of the key issues in stadia is the phenomenon of human-structure interaction. This is the result of the combination of human occupants and the main structure which changes the structural dynamic properties. Since the activities of the occupants generally change during a live event, the properties of the structure can vary as well.

This can occur by presence of both active and passive spectators in the stadium. Active spectator refers to that group of people who have movement activities such as jumping or bouncing. Passive people on the other hand do not have any considerable motion such as those mentioned before [8], [33]–[37]. This has been investigated practically during a number of live events [36], [38]–[40].

The problem therefore may arise that passive control technologies, such as tuned mass dampers, may become detuned as a result of the changing structural properties during a sports or concert event. Consequently, there should be a new proposed device that can deal with this problem by changing its frequency of operation in addition to have the capacity to deal with the magnitude of the excitation force (e.g. people's jumping or bounding).

2.2. Vibration Control

In general, there are four types of structural vibration control including passive, active, semi-active and hybrid control methods. [41]. These methods are in addition to the structural modification and/or changing of their applications. These will be described and considered in more detail in this section.

2.2.1. Passive Vibration Control

In passive vibration control the reduction of vibration can be achieved by adding extra materials and/or devices to dissipate vibration energy. Hence it does not require external energy. Passive vibration methods can be employed in different type of vibration such as seismic, wind, machinery and human induced vibration [42]–[44].

The are various mechanisms by which passive systems may operate, such as metal yielding, frictional sliding, transformation of the phases in metals and viscoelastic deformation in solid or liquid materials and fluid orifices. Some examples of passive controllers are tuned mass dampers, base isolation, viscoelastic dampers, metallic yield dampers, friction dampers, viscous fluid dampers and tuned liquid dampers [18]

Passive vibration control techniques have many advantages including simplicity in design, inherently stable systems and relatively lower cost [9], [12], [14], [16]–[18], [45]–[48].

However, passive control methods typically have a number of drawbacks, such as lack of damping capacity and poor performance of tuned dampers when structural dynamic properties change (off-tuning) [16], [21].

2.2.1.1. Tuned Mass Damper

A Tuned Mass Damper (TMD) is a conventional passive control method to decrease the response of flexible structures such as skyscrapers or long bridges. It consists of a mass, spring and damper, which interact with the structure to which they are attached to dissipate vibration energy. A TMD acts as a secondary moving mass attached to the main structure with frequency tuned close to the natural frequency of the primary system. The TMD vibrates out of phase of the main system and hence vibration energy of the structure is transferred to the auxiliary mass, to be dissipated through the TMD damping element. TMDs are tuned to operate in a specific frequency which is mostly one of the structural dominant mode's frequency. This is why TMDs are effective mostly in resonant cases where the frequency of the external force is around the frequency of the structure. Dynamic properties of TMDs (i.e. mass, damping and stiffness) are not time varying [3], [13], [20], [46], [49]–[54].

TMDs have been widely used to mitigate vibration in civil, mechanical and aerospace structures and many theoretical and practical researchers have been performed in this area [17], [18], [20], [45]. TMDs have been found to be an effective device to reduce human induced vibration caused by pedestrian activities on footbridges [4].

However, there are some limitations in employing TMDs. Their performance depends highly on the amount of added mass and if the mass is too small the effect of a TMD is limited. Also, since the dynamic properties of structures typical vary during the occupation of the building, the TMDs may not remain well tuned and their performance may reduce. TMDs are sensitive to off-tuning and also they have a narrow effective frequency band. Also, TMDs are generally efficient when the primary structure has light damping and hence are not particularly effective for heavily damped structures. Moreover, the TMD inertial mass may continue to vibrate after the vibration of the primary structure supressed and this may lead to undesirable motion [2]–[4], [13], [20], [46], [47], [50], [52], [54]–[57].

2.2.2. Active Control

The performance of active vibration control is based on force generation using an external source of energy. In this method, a control force is imparted to the structure through an actuator which aims to counteract the vibration caused by disturbance forces [16], [41], [58]. In this method, the disturbance (input) force and/or the response of the structure is monitored continuously and the output information is employed to calculate and generate the appropriate control force [59].

The force generator can be in the form of a shaker or actuator [9]. Generally an active scheme consists of sensors and actuators in combination with a digital control unit (Figure 2-1) [3], [14], [16]. The magnitude and/or frequency of the actuator's force changes in real-time. The control force depends on different factors such as target structure's acceleration or velocity [41].

Active bracing and active mass damper (AMD) are typical examples of active control devices. Active control approach is the combination of several engineering disciplines such as electronic engineering, computer engineering, control engineering and materials engineering [18].

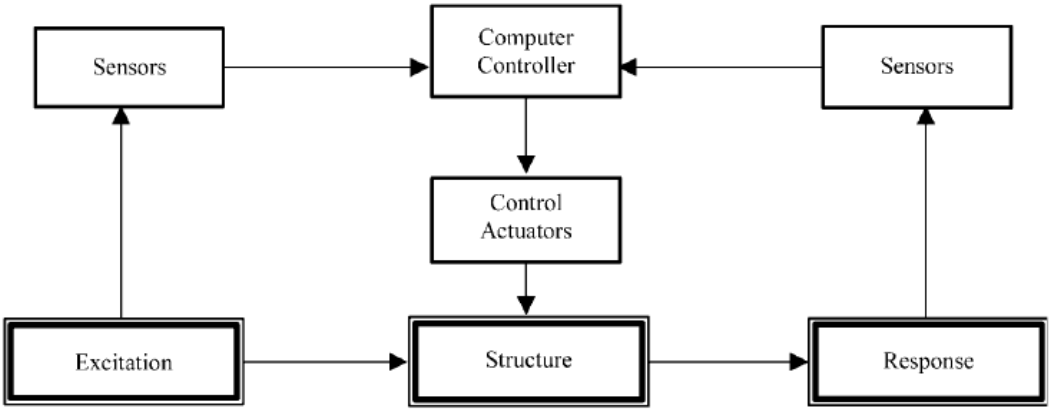

Figure 2-1- Schematic of a structure with active vibration controller [18]

If the control force is calculated and generated by measuring external excitation, the term feed-forward control is used. However, if the control force calculation depends on both structural response and external excitation, the term feedback control is used [59]. Feedback control can be employed when the external force is not measureable.

Active control technologies have a number of advantages. They have multi-usage abilities such as working in wind and earthquake engineering and also control of

human induced vibration in civil structures. Also, there are wide selections of control strategies depending on the main purpose of the control. For instance, the control algorithm for people serenity in non-dangerous vibration (vibration serviceability) is different from the control algorithm for building safety in earthquake. This is due to different reasons such as differences in the nature of the disturbance load [18].

However, active control also has some disadvantages. Issues such as reliability, price and energy saving of active controllers should be carefully considered [16]. Also in civil engineering, uncertainties and non-linearity nature of structures introduce complexity to the system. In addition, types of actuators and sensors could be highly complicated and massive in size (for actuators) when required control forces are large [11], [59]–[63].

Also, active control method highly depends on external power source and this can be a limitation of its performance [21], [64], [65]. In addition, the frequency band width of the controller is limited due to the dynamics of the actuator and it might be a restriction for its performance [46].

2.2.2.1.Active Tuned Mass Damper

Active TMD (ATMD) is a TMD that has active external force acting on the structure to reduce the vibration level. This active force element is applied to the structure through the inertia mass [65]–[69]. In fact, the actuator is placed between the primary and auxiliary structure (Figure 2-2) [52]. First studies on active TMD were performed by [70].

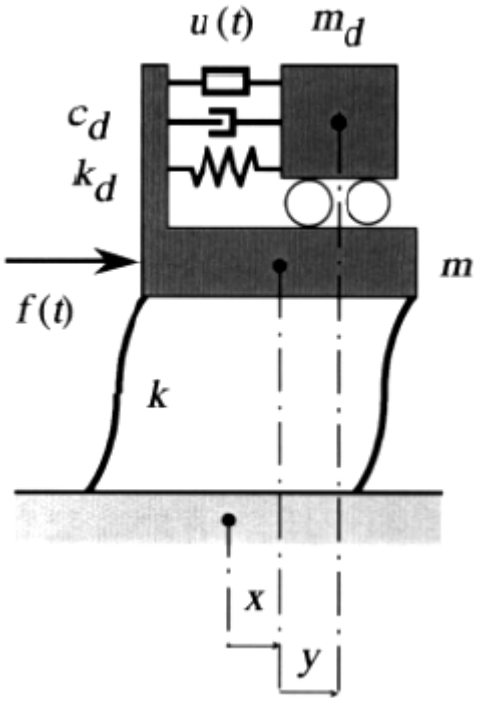

Figure 2-2- Active TMD [51]

The operational frequency band width of the ATMDs are wider than passive TMDs [71].

2.2.3. Semi-Active Control

Semi-active control has been introduced as a method in which the parameters of the system (e.g. stiffness and damping) can be optimised and changed in real time. The basic energy dissipation principles of semi-active control belong to passive control [16]. In fact, there is no active force generation in both passive and semi-active control [47]. Initial employment of semi-active control was on car suspension systems including vehicle body acceleration and vertical movement of the axles [72].

There are different kinds of semi-active control devices such as electro-rheological (ER), magneto-rheological (MR) dampers [14], active variable stiffness (AVS), active variable damping (AVD) [73]–[75] and magnetically tuned mass damper (MTMD) [57].

Semi-active control has many benefits including less external power requirement in comparison with active control and relative reliability on loss of power, since it can operate on batteries. Also, semi-active devices have better performance in comparison with passive control techniques in systems with uncertainties. They can

deal with off-tuning problems. Semi-active devices (such as semi-active dampers) have relatively simple mechanical design. In contrast with active control, semi-active control is inherently stable. Also the frequency bandwidth of semi-active control is wide (when it is employed in TMDs) [4], [9], [13], [18]–[20], [47], [49].

However, semi-active control has some disadvantages as well. Its performance depends highly on the type of control algorithm, which can be very complex [10], [13], [19], [49], [76]–[78]. Also, semi-active control requires nonlinear control algorithms due to its inherent nonlinear force-velocity relationship [10], [13], [72], [79], [80]. Generally, there is no particular 'closed form' analysis of such systems since their characteristics are time-varying, although some approximate methods have been proposed [81].

A magnetorheological (MR) fluid damper is a particular type of semi-active device in which the viscosity of the fluid within the damper is controlled through application of a magnetic field. This magnetic field can be varied in real-time and is controlled by a control voltage determined by complex control algorithms. A closed loop feedback control is often employed to update the control voltage by considering the actual and desired damping force in addition to the reaction capability of device. MR dampers have been widely used for semi-active controller devices such as SATMDs [4], [10], [11], [19], [49], [79], [82]–[97].

MR Fluids are a type of material in which the material's behaviour changes from free-flowing viscous liquid to semi-solid material in the presence of magnetic field (Figure 2-3). In fact when there is magnetic field, the particles in MR Damper obtain the chain formation and causes restriction in moving fluid [13], [19], [22], [49], [84], [88], [98]–[105].

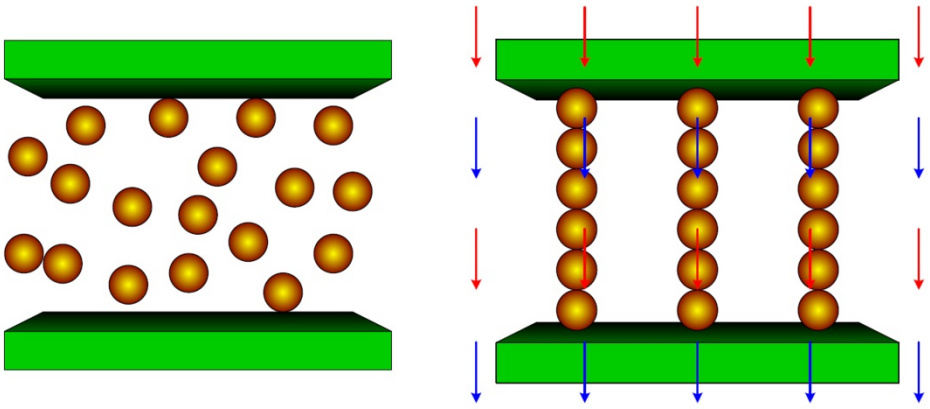

Figure 2-3- Schematic of MR Fluids operation

Electrorheological (ER) dampers are similar to MR damper. However, the viscosity of the damper changes in the presence of electrical field rather that magnetic field. ER fluids transfer from liquid to solid material when subjected to electrical field [15], [106]. ER dampers have some disadvantages such as safety problems, relatively high-price, requirement of high level of electricity and power sources and limitation in obtainable yield stress. In addition, ER dampers are much larger in size in comparison with MR dampers [18].

2.2.3.1.Semi-Active Tuned Mass Damper

As it was mentioned before, a semi-active tuned mass damper (SATMD) is a TMD with changeable damping and/or stiffness elements (Figure 2-4) [9], [65], [107]. An important aspect of SATMD is the ability of it to be tuned to wider range of frequencies and damping in comparison with passive TMDs [9], [20]

Many studies show that semi-active TMDs have more effect rather than conventional TMDs in the presence of off-tuning and also dynamic response reduction [9], [20], [22], [49], [79], [108]–[111].

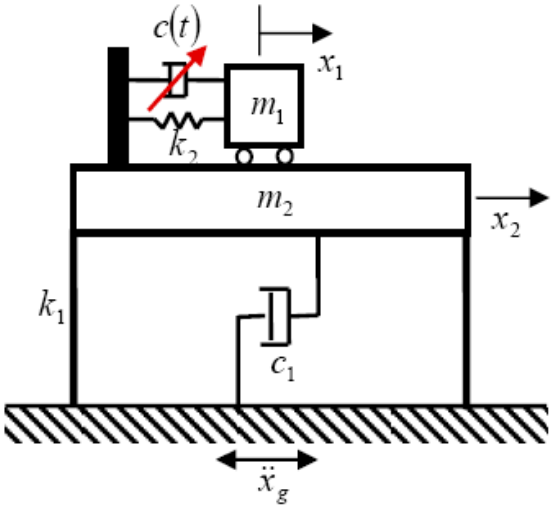

Figure 2-4- Schematic of a structure with attached SATMD [49]

2.2.4. Hybrid Control

As noted previously, both active and passive control methods have some advantages and drawbacks. In an attempt to use the benefits of both and at the same time to deal with many of the disadvantages, hybrid control methods have been introduced [16]. A hybrid controller is a combination of passive and active control systems [12], [45], [47], [65], [112], which is an attractive option for structural vibration control [12], [21], [50], [113], [114].

Different types of hybrid control have been introduced. An active-passive switching system is a type of hybrid device in which the system can be changed between active and passive control automatically. For instance, for a tall building when the level of vibration is low (e.g. wind or moderate earthquake induced vibration), the system can operate as a purely active system. However, when the vibration magnitude increases, perhaps in response to more severe earthquake excitation, the system shifts to a purely passive operation to avoid over-heating or overloading of the active components. This system has been practically implemented in some real structures [12], [50], [115]–[119].

Another classification of hybrid control devices are integrated active-passive devices. In these systems, both the active and passive parts of the system work simultaneously. A hybrid tuned mass damper (HTMD) is an example of this type of

hybrid control. This consists of a TMD controlled actively by an additional active mass [2], [18], [45], [54], [120].

2.2.4.1.Hybrid Tuned Mass Damper

HTMD is the combination of a passive TMD with an active element (actuator), as shown in Figure 2-5. The active part of the system increases the movement of the passive mass, which increases its inertia force. This leads to a system in which its inertia force can be changed in real-time [41], [56], [121]–[124], [51], [52], [54].

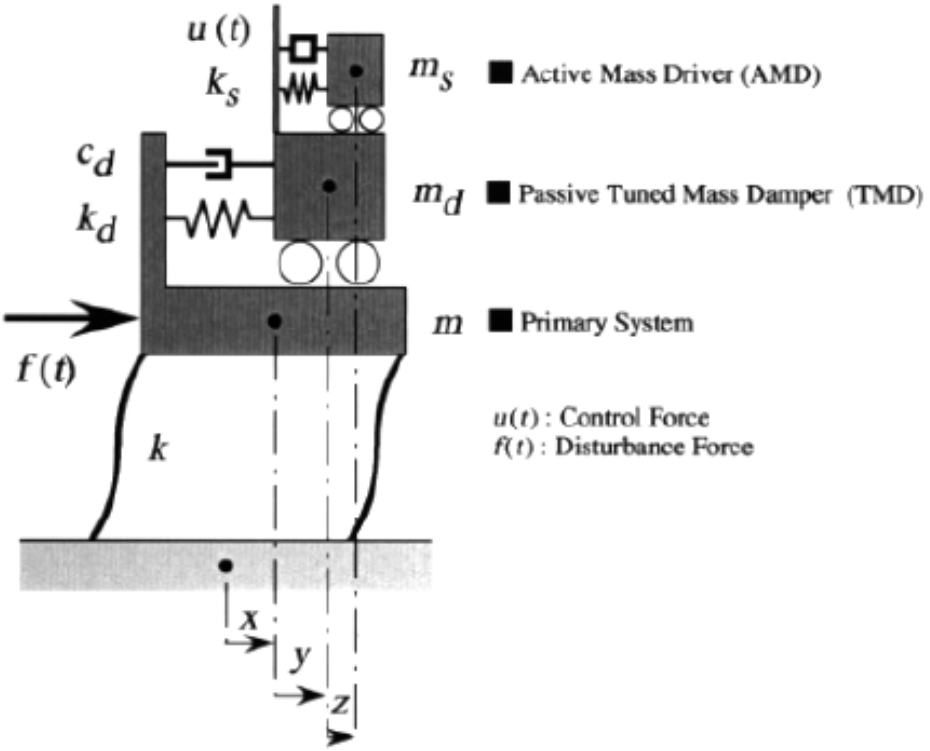

Figure 2-5- Schematic of HTMD [51]

Since the active element is relatively smaller in hybrid systems, power requirements are typically lower than for purely active systems. The passive part provides the majority of the energy dissipation capacity, whereas the active part both enhances the performance of the passive element and increases the robustness of the system to changes in structural dynamic properties (i.e. off-tuning). Another important advantage of hybrid systems is their ability to work as purely passive systems in case of power failure. HTMDs are appropriate devices to control both low and high frequency vibrations. In the presence of large magnitude vibration forces (e.g. during an earthquake), an HTMD still requires only a low power source. Moreover, the

TMD acts as a mechanical filter to reduce higher frequency vibration to the active part of the system [2], [3], [18], [21], [50], [52], [56], [64], [65], [121], [125]–[127].

2.3. Off-Tuning

Off-tuning occurs when the frequency of a controlled mode of the structure changes. There are various causes of off-tuning, including changes in structural frequency, inappropriate choice of TMD's parameters, effect of live loads and environmental factors (such as temperature) [9], [20], [46], [47].

For instance, in slender structures such as footbridges, human loads might cause the structures to behave in an unexpected way. The pedestrian mass may be high in comparison with the mass of the bridge structure and sometimes under-estimated. This leads to a significantly lower natural frequency than the original structure.

Off-tuning is an important issue for TMDs since the operational frequency of a TMD is very narrow and it is set to a particular structural frequency [47], [48], [56], [71]. Experimental and numerical investigations have shown that the performance of a TMD can be reduced when the main structural properties such as frequency changes [57].

Considering on the off-tuning problem as one of the possible results of human-structure interaction in human induced vibration control, passive control methods such as TMD could be a non-practical solution to remediate the excessive vibration since the operation range of TMD is set to certain band of frequency. However HTMD on the other hand can be a possible solution to deal with this issue since the active part of HTMD can act as a tuning system.

2.4. Control Algorithms

An important consideration for HTMD design is control force generated by the actuator which can be calculated through combination of displacement, velocity and acceleration of the structure and TMD by applying different gain coefficients. Choosing the type and optimisation of the gains is an important factor to achieve the proper ability of the controller [3], [4], [13], [128].

The choice of control algorithm is an important factor to produce appropriate command voltages and the performance of the controller is highly dependent on this.

The type of algorithm depends on the non-linearity of the system, accessibility of feedback measurement and the number of devices to be used in the structure. The capacity of generated force in actuators should also be considered [19], [49], [65], [129]. The goal of control algorithm is to reduce the error between desired and actual structural response and/or to change some particular parameters linked to the structural response [2], [13].

2.4.1. PID Control

The basics of PID control consists of the proportional, integral and derivative components of the response of the structure multiplied by their corresponding feedback gains [46]. Direct response feedback gains have an important role in control algorithm since they have a large effect on the final structural response [130]. However in reality, PID control is more complex in the presence of filtering and different compensators (such as actuator, sensor, etc.)

Acceleration feedback is an early and appropriate approach which consists of a gain multiply by acceleration of the structure and gives the control force [3], [128]. Also, other kinds of direct response gains such as velocity and displacement of the structure and TMD's mass were employed as a suitable control scheme for HTMDs. These type of control enhances the damping and inertia of the passive part of the system [2].

2.4.2. Optimal Control

Optimal control methods are conventional methods that have been employed widely and generally in the control area. [13], [19], [49], [75], [88], [91], [94], [131]–[134]. The role of this form of control is to make the states of the systems almost equal to zero [46].

There are different types of optimal control methods such as Linear Quadratic Regulator (LQR) and Linear Quadratic Gaussian (LQG).

2.4.2.1.Linear Quadratic Regulator (LQR)

LQR is the most common type of optimal control. In LQR method, it is assumed that all states of the system are measurable. The goal of using this method is to place the poles of the structure in a way that results in more damping. [13], [46], [53], [119], [134], [135].

However, since the LQR control only works with the states of the system (i.e. displacement and velocity or velocity and acceleration), it is not possible to use this method to employ all responses of the system (i.e. displacement, velocity and acceleration at the same time). Author explains and shows its application in active control and HTMD on further chapters.

2.4.2.2.State Derivative Feedback by LQR

Since it is not possible to measure all the state of the systems and sometimes it is possible to measure the derivative of the system (e.g. acceleration instead of the velocity), a modified version of LQR is introduced [134] to apply LQR on derivative of the states of the system instead of the states directly. This is useful when velocity and acceleration of the system is considered instead of velocity and displacement [130], [134], [136].

Although using this method make it possible to work with the derivative of the states (e.g. velocity and acceleration), still the ability of using all outputs (i.e. displacement, velocity and acceleration) is missed from this method. The application and performance of modified LQR in active control and HTMD is described in further chapters.

2.4.2.3.Output Derivative Feedback by LQR

Sometimes it is not possible to measure all the states of the system and the output matrix does not have all the state's measurements. Hence, it is possible to use this modified version of LQR method in which the output matrix of a system's sate space is considered for LQR method [134]. This is useful especially when the acceleration of the system is measurable [136]. This is addressed later on other chapters.

2.4.3. Optimisation

In different control methods, defining the proper control parameters (such as feedback control gain, TMD's parameters, etc.) is an important and sometimes complex issue. The "Optimisation" term here explains different methods to calculate these parameters appropriately.

Most structures are complex and inherently nonlinear and calculating the proper dynamic modelling is an important issue. Therefore, using conventional control algorithms are not suitable for these types of problems. Having a MDOF (Multi

Degree of Freedom System) is an example of a complex system. Modern control optimisation and techniques is an appropriate method to be employed instead of conventional methods for these types of problems [21], [137]–[139].

Also, since obtaining the closed-form solution of the TMD/HTMD with damping element is not possible, it is necessary to use numerical optimisation methods. This means that it is not possible to mathematically solve the conventional equation of motions for MDOF system in the presence of damping element and generate a parametric relation between structural response and TMD's parameters [47], [48], [56], [57], [71], [121], [140].

There are also different conventional optimisation methods (Figure 2-6) such as gradient-based or Hessian local optimisation in which the objective function is smooth and the aim is to achieve a local optimisation. Random search technique is another optimisation method which is considered as a very basic method. It is an unintelligent method since it only studies the search space randomly. Compared to some more developed techniques such as Genetic Algorithm, this method performs the random search without linking to earlier results. Also random search is considered as time consuming method in more complex problems [138].

Mathematical programming or optimization techniques	Stochastic process techniques	Statistical methods
Calculus methods	Statistical decision theory	Regression analysis
Calculus of variations	Markov processes	Cluster analysis, pattern recognition
Nonlinear programming	Queueing theory	
Geometric programming	Renewal theory	Design of experiments
Quadratic programming	Simulation methods	Discriminate analysis (factor analysis)
Linear programming	Reliability theory	
Dynamic programming		
Integer programming		
Stochastic programming		
Separable programming		
Multiobjective programming		
Network methods: CPM and PERT		
Game theory		
Modern or nontraditional optimization techniques		
Genetic algorithms		
Simulated annealing		
Ant colony optimization		
Particle swarm optimization		
Neural networks		
Fuzzy optimization		

Figure 2-6- Different optimisation techniques [139]

Stochastic Hill Climbing as another method also has the disadvantage of reaching the first (i.e. local minimum) instead of the global one. To avoid this, the procedure must be repeated several times. This method is not suitable when there is more than one local minimum point. However this is a simple and quick method [138].

Simulated Annealing is a similar method as Stochastic Hill Climbing with the difference of avoiding local optimum points. It is a competitive method with GA. However, these two have some differences on the type of searching in the population of the possible solutions. GA has wider range of the solution [138].

2.4.3.1. Genetic Algorithm

GA is the most popular approach in evolutionary computation techniques. It is a search and optimisation method first introduced by John Holland in 1975 [14], [138]. GA has been successfully applied in many optimisation fields. It follows Darwin's rule of natural selection. The higher probability to pass to the next generation is with the individual which is more fit with the defined aim's objective [14], [138]. This algorithm is based on information trading of each member in community and comprehensive search [22], [141], [142].

GA has many advantages in comparison with other optimisation methods. It has a simple concept (Figure 2-7) and there is no requirement of gradient information. It has a wide application and any optimisation problem can employ GA. Also it is possible to use GA in combination with other methods such as Fuzzy Logic or Neural Network and even traditional techniques. It is a more reliable and quicker approach for more complex problems. Also since there is no complex mathematical requirement of the objective function and because GA is based on evolution of objective function, it can be applied to non-linear discrete or continuous constraint or unconstraint search spaces. Also, GA is a parallel method in which the calculation speed is significantly higher. Also as it noted earlier, GA looks for the population of points instead of one single point. "GAs are something worth trying when everything else has failed or when we know absolutely nothing of the search space" [138].

However, defining an appropriate fitness function, population size, rates for mutation and cross over and also type of selection are some of the challenges when using GAs [138].

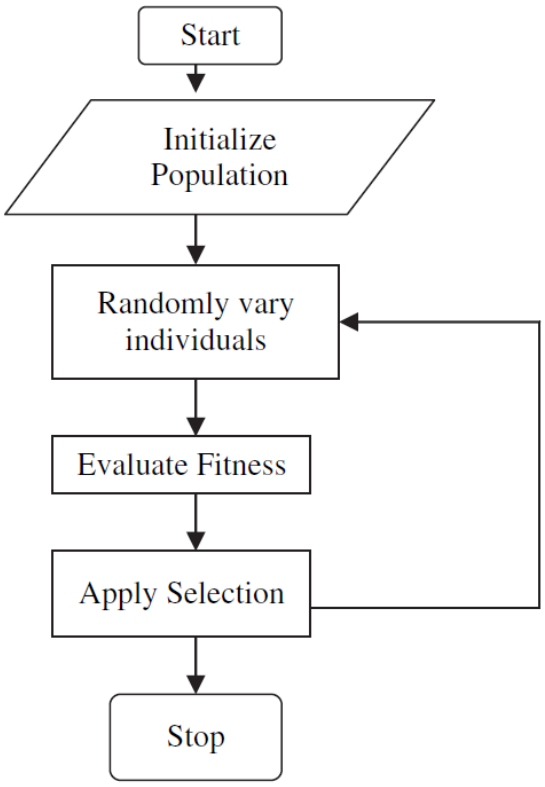

Figure 2-7- Schematic of an Evolutionary Algorithm [138]

GAs have been applied in civil engineering problems since a few decades ago. It is very effective in solving complex problems and its application in civil engineering has been improving with the aid of computer science development [137], [138].

2.4.3.2. Fuzzy Control

Fuzzy Logic Control (FLC) has drawn the consideration of control engineers recently. It is appropriate for nonlinear and uncertain cases where the design data are unclear. It consists of "fuzzication interface, rule base, decision making and a de-fuzzication interface to simulate logical reasoning of human beings". FLC initial parameters are hard to determine and it is found by error and trail methods. However, it is possible to use some other conventional method in parallel with FLC. Also, FLC performance depends on the mathematical formulation of the system [21], [46], [112], [137], [139], [143].

2.4.3.3. Neural networks

Neural Network is a strong and appropriate approach to be employed in complex non-linear structures. Hence, it is sometimes mixed with conventional control

methods [22]. It consists of mathematical functions which based on training and learning from measured data. In the area of structural control, Neural Network mostly is employed for state estimations [46]. Author shows and explains the application of some of these methods in further chapters. Several of these methods are modelled and compared to each other and the most appropriate method for the application of HTMD is introduced.

2.5. Summary

To summarise, there are different methods of vibration control with advantages and disadvantages depends on the type of vibration and application of the controller. For instance, active control was employed to reduce the vibration level caused by human activities (e.g. walking) in office floors [31], [144]–[148] or passive tuned mass damper (TMD) is used for controlling the human induced vibration in footbridges [17].

One of the known issues in human induced vibration control is the human-structure interaction phenomenon. This results in changing in the primary structure's dynamic properties (such as frequency and damping of a cantilever in grandstand). Hence, passive control could be an inappropriate method of control when the effect of human-structure interaction is significant since they mean to work in a specific range of dynamic properties. Active control on the other hand has the ability to operate in a wider range of frequency. However, they could have the cost problem for large structures such as stadium since large actuators might be needed in order to control the higher magnitude of excitation force (e.g. spectator's jumping force in a stadium). Hence, neither passive TMD nor Active Mass Damper (AMD) has been employed to control human-induced vibration in larger structures such as grandstand when the level of excitation force is larger and also the human-structure interaction effect is significant.

Considering on both performance (e.g. vibration reduction in a wider range of frequency) and cost (e.g. using large actuator in the presence of large vibration force), the available human induced vibration control techniques could be an inappropriate method. On the other hand, HTMD systems proved to be highly effective solution for control of vibrations due to wind and earthquake [41], [56],

[121]–[124], [51], [52], [54]. However, HTMD has not been used for reducing human-induced vibration.

This thesis is grounded on the hypothesis that HTMD is an effective method to reduce human-induced vibrations of grandstands. Author, in the present study, will introduce Hybrid Tuned Mass Damper as a type of hybrid control technique to reduce the vibration control for larger scales of the vibration forces (such as in stadium) with a wider frequency range of operation. In addition, author will employ Genetic Algorithm as one of the available optimisation methods to generate the appropriate parameter for the proposed device. The performance of proposed device will be considered both analytically and experimentally.

3. Development and application of HTMD for controlling human-induced vibration

A shorter version of this chapter was presented and published in [149].

3.1. Introduction

As previously discussed in Chapter 2, a hybrid damper is a combination of different primary control technologies. In this research work, the Hybrid Tuned Mass Damper (HTMD) is the combination of a passive TMD with an active element (actuator) on top. The performance of the passive TMD is improved by the additional active part.

In this chapter, analytical models of an empty structure in addition to the structure with passive TMD, AMD and HTMD attached will be developed. These models are to be developed in both transfer function and state space formulations. Following a review of these models, the properties of the passive TMD (and passive part of the HTMD) will be calculated using two different approaches. An active vibration control (AVC) scheme using an inertial actuator (AMD) is also developed.

Three different control algorithms for the HTMD, based on past research and enhanced by further developments proposed by the author, are then investigated to develop the most suitable technique for HTMD design. In addition, two approaches are employed to check the closed-loop stability. All created analytical models will be verified experimentally later in chapter 6.

3.2. Model of the uncontrolled structure

The laboratory structure used in this study is a simply supported post-tensioned concrete slab strip with span 10.8 m, width 2.0 m and depth 0.275 m. The total weight of the slab is approximately 15 tonnes and its dynamic properties established from measurements are presented elsewhere [145], [146], [150].

Based on the first bending mode of vibration modelled as a SDOF system (Figure 3-1), the structure has natural frequency $f_s = 4.44\,\text{Hz}$ with modal mass $m_s = 7150\,\text{kg}$ and damping ratio of $\xi_s = 0.5\%$. The derived damping coefficient and stiffness are $c_s = 1976\,\text{N.sec/m}$ and $k_s = 5{,}588{,}071\,\text{N/m}$, respectively. This mode is susceptible to human activities such as walking [151]. Rayleigh damping is

assumed for the structure since in civil engineering structures damping mostly corresponds with stiffness and mass element [146].

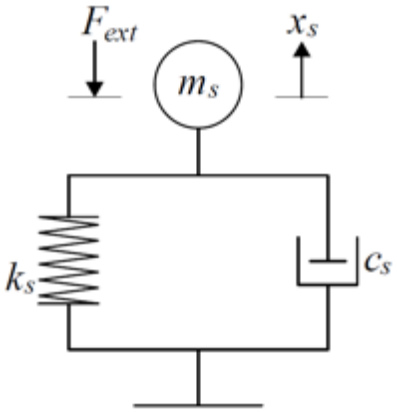

Figure 3-1- SDOF model of the uncontrolled structure

The equation of motion of the uncontrolled structure subjected to external force (F_{ext}) is generated as

$$m_s\ddot{x}_s(t) + c_s\dot{x}_s(t) + k_s x_s(t) = F_{ext}(t) \quad \textbf{(3.1)}$$

3.2.1. Open loop structural model using transfer function formulation

The open loop system (Figure 3-2) has the output (i.e. acceleration, velocity or displacement of the structure) in response to the input (i.e. external force such as human jumping force) in the absence of structural control.

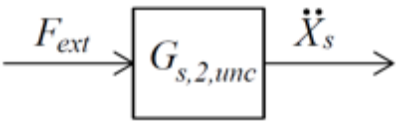

Figure 3-2- Block diagram arrangement of the uncontrolled structure as a SDOF system

Converting (3.1) from time domain to Laplace domain,

$$m_s s^2 X_s(s) + c_s s X_s(s) + k_s X_s(s) = F_{ext}(s) \quad \textbf{(3.2)}$$

hence the transfer function (TF) is given by

$$\frac{X_s(s)}{F_{ext}(s)} = \frac{1}{m_s s^2 + c_s s + k_s} \quad \textbf{(3.3)}$$

where $F_{ext}(s)$ and $X_s(s)$ are the Laplace transforms of the external force and structural displacement response, respectively. To achieve the output as acceleration instead of displacement in the structure TF, equation **(3.3)** is multiplied by a s^2 term. Hence $G_{s,2,unc}$, the accelerance TF between external force and the response is calculated as:

$$H_{unc} = G_{s,2,unc} = \frac{X_s(s)s^2}{F_{ext}(s)} = \frac{s^2}{m_s s^2 + c_s s + k_s} \quad \textbf{(3.4)}$$

Figure 3-1 shows a comparison between the proposed SDOF model of the structure and the corresponding measured transfer function below 10 Hz. Higher structural modes are omitted since their contribution in this frequency range is small [146]. Also, it should be noted that the frequency of the structure in Figure 3-1 has been reduced to 4.33 Hz from 4.44 Hz due to the existence of an additional mass on the slab during the measurements (which was the locked TMD acting as a passive mass on the structure).

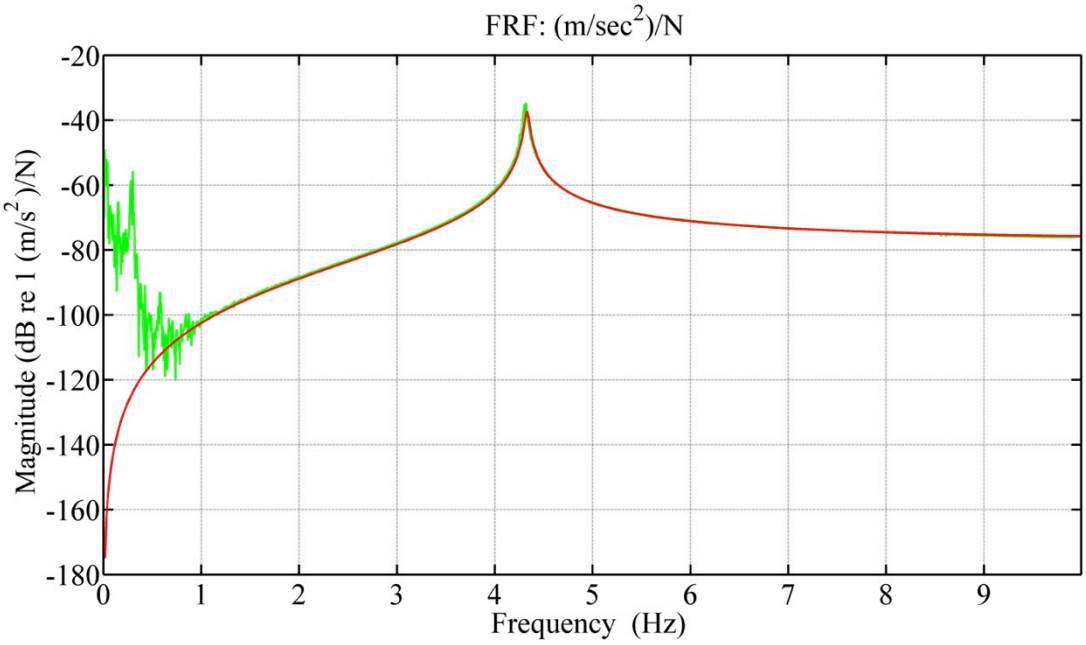

Figure 3-3- FRF of the uncontrolled structure, structure model (red); experimental measurement (green)

3.2.2. Open loop structural model using state space formulation

To use some optimal control design techniques such as linear quadratic regulator (LQR), it is more convenient to derive a state space (SS) model of the system. Based on equation (3.1), the states of uncontrolled structure are introduced as

$$\begin{Bmatrix} X_{1,unc} = x_s \\ X_{2,unc} = \dot{x}_s \end{Bmatrix} \therefore \begin{Bmatrix} \dot{X}_{1,unc} = X_{2,unc} \\ \dot{X}_{2,unc} = \ddot{x}_s \end{Bmatrix} \quad \textbf{(3.5)}$$

Hence, the SS representation of the system in the form of $\dot{X}_{unc} = A_{unc}X_{unc} + B_{unc}U_{unc}$ is developed as

$$\begin{Bmatrix} \dot{X}_{1,unc} \\ \dot{X}_{2,unc} \end{Bmatrix} = \begin{bmatrix} 0 & 1 \\ -\frac{(k_s)}{m_s} & -\frac{(c_s)}{m_s} \end{bmatrix} * \begin{Bmatrix} X_{1,unc} \\ X_{2,unc} \end{Bmatrix} + \begin{bmatrix} 0 \\ \frac{1}{m_s} \end{bmatrix} * \{F_{ext}\} \quad \textbf{(3.6)}$$

To obtain displacement, velocity and acceleration of the system as outputs in the form of $Y_{unc} = C_{unc}X_{unc} + D_{unc}U_{unc}$, the output matrix is established as

$$\begin{Bmatrix} Y_{1,unc} \\ Y_{2,unc} \\ Y_{3,unc} \end{Bmatrix} = \begin{bmatrix} 1 & 0 \\ 0 & 1 \\ -\frac{(k_s)}{m_s} & -\frac{(c_s)}{m_s} \end{bmatrix} * \begin{Bmatrix} X_{1,unc} \\ X_{2,unc} \end{Bmatrix} + \begin{bmatrix} 0 \\ 0 \\ \frac{1}{m_s} \end{bmatrix} * \{F_{ext}\} \quad \textbf{(3.7)}$$

3.3. Model of the structure with attached TMD

The tuned mass damper (TMD) used in this research work comprises of a mass attached to the main structure with a spring and a damper element as shown by the model in Figure 3-1. The model of the system is a 2 DOF arrangement including the primary structure as the first DOF and the passive TMD as the second DOF of the model.

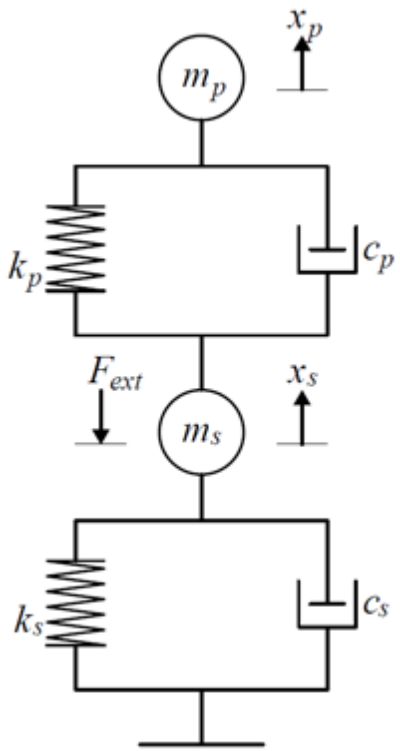

Figure 3-4- 2DOF model of the structure with attached TMD

The set of equations of motions of the system with attached TMD subjected to external force (F_{ext}) are given by

$$\begin{cases} m_s\ddot{x}_s(t) + (c_s + c_p)\dot{x}_s(t) + (k_s + k_p)x_s(t) - c_p\dot{x}_p(t) - k_p x_p(t) = F_{ext}(t) \\ m_p\ddot{x}_p(t) + c_p\dot{x}_p(t) + k_p x_p(t) - c_p\dot{x}_s(t) - k_p x_s(t) = 0 \end{cases} \quad \textbf{(3.8)}$$

3.3.1. Open loop structural model using transfer function formulation

Figure 3-5 shows the transfer function (TF) arrangement of the system, which is an open loop scheme. However, as is illustrated in Figure 3-5, the motion of the TMD is dependent on the acceleration of the structure and conversely the response of the structure is dependent on the dynamic interaction between it and the TMD. Hence, there are feedbacks between these two components of the model.

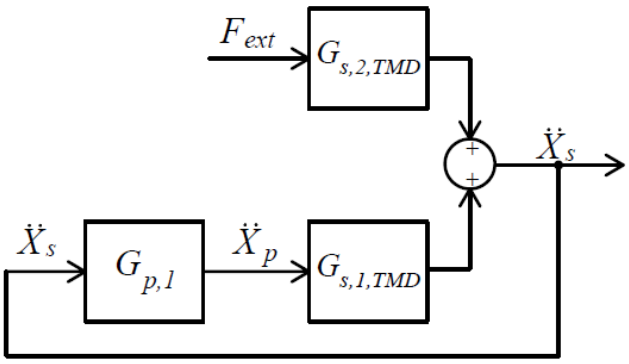

Figure 3-5- Block diagram arrangement of the structure with attached TMD as a 2DOF system

Converting (3.8) from time domain to Laplace domain results in

$$\begin{cases} m_s s^2 X_s(s) + (c_s + c_p) s X_s(s) + (k_s + k_p) X_s(s) - c_p s X_p(s) - k_p X_p(s) \\ \qquad = F_{ext}(s) \\ m_p s^2 X_p(s) + c_p s X_p(s) + k_p X_p(s) - c_p s X_s(s) - k_p X_s(s) = 0 \end{cases} \quad \textbf{(3.9)}$$

Rearranging (3.9) in terms of $X_s(s)$, $X_p(s)$ and $F_{ext}(s)$ leads to

$$\begin{cases} [m_s s^2 + (c_s + c_p) s + (k_s + k_p)] X_s(s) - [c_p s + k_p] X_p(s) = F_{ext}(s) \\ [m_p s^2 + c_p s + k_p] X_p(s) - [c_p s + k_p] X_s(s) = 0 \end{cases} \quad \textbf{(3.10)}$$

Defining $G_{s,1,TMD}$, $G_{s,2,TMD}$ and $G_{p,1}$ by considering the acceleration as the output of each block (i.e. by multiplying s^2 term) then

$$G_{s,1,TMD} = \frac{X_s(s)s^2}{X_p(s)s^2} = \frac{c_p s + k_p}{m_s s^2 + (c_s + c_p) s + (k_s + k_p)} \quad \textbf{(3.11)}$$

and

$$G_{s,2,TMD} = \frac{X_s(s)s^2}{F_{ext}(s)} = \frac{s^2}{m_s s^2 + (c_s + c_p) s + (k_s + k_p)} \quad \textbf{(3.12)}$$

and

$$G_{p,1} = \frac{X_p(s)s^2}{X_s(s)s^2} = \frac{c_p s + k_p}{m_p s^2 + c_p s + k_p} \quad \textbf{(3.13)}$$

Substituting (3.11), (3.12) and (3.13) into (3.10), the final TF of the system becomes as

$$\begin{cases} \ddot{x}_s = \ddot{x}_p \mathrm{G}_{\mathrm{s,1,TMD}} + F_{ext} \mathrm{G}_{\mathrm{s,2,TMD}} \\ \ddot{x}_p = \ddot{x}_s \mathrm{G}_{\mathrm{p,1}} \end{cases} \quad \textbf{(3.14)}$$

Combining two parts of the equations generates the final transfer function ($\mathrm{H_{TMD}}$) between the structural response and external force as

$$\begin{aligned} &\ddot{x}_s = \left(\ddot{x}_s \mathrm{G}_{\mathrm{p,1}}\right) \mathrm{G}_{\mathrm{s,1,TMD}} + F_{ext} \mathrm{G}_{\mathrm{s,2,TMD}} \\ &\therefore \left(1 - \mathrm{G}_{\mathrm{p,1}} \mathrm{G}_{\mathrm{s,1,TMD}}\right) \ddot{x}_s = F_{ext} \mathrm{G}_{\mathrm{s,2,TMD}} \end{aligned} \quad \textbf{(3.15)}$$

Then

$$\mathrm{H_{TMD}} = \frac{\ddot{x}_s}{F_{ext}} = \frac{\mathrm{G}_{\mathrm{s,2,TMD}}}{1 - \mathrm{G}_{\mathrm{p,1}} \mathrm{G}_{\mathrm{s,1,TMD}}} \quad \textbf{(3.16)}$$

which is represented in Figure 3-5.

3.3.2. Open loop structural model using state space formulation

Considering equation (3.8), the states of the system are introduced as

$$\begin{aligned} &X_{TMD} = \begin{Bmatrix} X_{1,TMD} = x_s \\ X_{2,TMD} = \dot{x}_s \\ X_{3,TMD} = x_p \\ X_{4,TMD} = \dot{x}_p \end{Bmatrix} \\ &\therefore \dot{X}_{TMD} \begin{Bmatrix} \dot{X}_{1,TMD} = X_{2,TMD} \\ \dot{X}_{2,TMD} = \ddot{x}_s \\ \dot{X}_{3,TMD} = X_{4,TMD} \\ \dot{X}_{4,TMD} = \ddot{x}_p \end{Bmatrix} \end{aligned} \quad \textbf{(3.17)}$$

Hence, the SS representation of the model in the form of $\dot{X}_{TMD} = A_{TMD} X_{TMD} + B_{TMD} U_{TMD}$ is given by

$$\begin{Bmatrix} \dot{X}_{1,TMD} \\ \dot{X}_{2,TMD} \\ \dot{X}_{3,TMD} \\ \dot{X}_{4,TMD} \end{Bmatrix} = \begin{bmatrix} 0 & 1 & 0 & 0 \\ -\frac{(k_s + k_p)}{m_s} & -\frac{(c_s + c_p)}{m_s} & \frac{k_p}{m_s} & \frac{c_p}{m_s} \\ 0 & 0 & 0 & 1 \\ \frac{k_p}{m_p} & \frac{c_p}{m_p} & -\frac{k_p}{m_p} & -\frac{c_p}{m_p} \end{bmatrix} * \begin{Bmatrix} X_{1,TMD} \\ X_{2,TMD} \\ X_{3,TMD} \\ X_{4,TMD} \end{Bmatrix} + \begin{bmatrix} 0 \\ \frac{1}{m_s} \\ 0 \\ 0 \end{bmatrix} * \{F_{ext}\} \quad \textbf{(3.18)}$$

To have displacement, velocity and acceleration of the structure and TMD as outputs in the form of $Y_{TMD} = C_{TMD}X_{TMD} + D_{TMD}U_{TMD}$, the output matrix is introduced as

$$\begin{Bmatrix} Y_{1,TMD} \\ Y_{2,TMD} \\ Y_{3,TMD} \\ Y_{4,TMD} \\ Y_{5,TMD} \\ Y_{6,TMD} \end{Bmatrix} = \begin{bmatrix} 1 & 0 & 0 & 0 \\ 0 & 1 & 0 & 0 \\ \frac{(k_s + k_p)}{m_s} & -\frac{(c_s + c_p)}{m_s} & \frac{k_p}{m_s} & \frac{c_p}{m_s} \\ 0 & 0 & 1 & 0 \\ 0 & 0 & 0 & 1 \\ \frac{k_p}{m_p} & \frac{c_p}{m_p} & -\frac{k_p}{m_p} & -\frac{k_p}{m_p} \end{bmatrix} * \begin{Bmatrix} X_{1,TMD} \\ X_{2,TMD} \\ X_{3,TMD} \\ X_{4,TMD} \end{Bmatrix} + \begin{bmatrix} 0 \\ 0 \\ \frac{1}{m_s} \\ 0 \\ 0 \\ 0 \end{bmatrix} * \{F_{ext}\} \quad \textbf{(3.19)}$$

3.3.3. TMD parameter optimisation

The design of a TMD involves the calculation of its mass, stiffness and damping. To design these parameters, it is assumed that the structure is a SDOF system based on the first mode of vibration, since for the structure under consideration it is dominant and the target mode for control. Table 3-1 summarises the key parameters of the SDOF primary structure, which were discussed in section 3.2.

Table 3-1-Structural parameters employed in TMD design

m_s (kg)	c_s (N.sec/m)	k_s (MN/m)	f_s (Hz)	ξ_s
7,150	1,976	5.59	4.44	0.5%

To calculate the TMD parameters, two methods are employed. The first method is the classical tuning method initially introduced by den Hartog [152] and improved by Tsai and Lin [153]. Next, the author introduces an optimisation method using a genetic algorithm (GA) and the results of these two approaches are compared and assessed.

3.3.3.1.Optimisation of TMD parameters using the classical method

According to [153], the frequency ratio and damping ratio of the TMD can be determined following these formulas:

$$\bar{f} = \left(\frac{\sqrt{1-0.5\bar{m}}}{1+\bar{m}} + \sqrt{1-2{\xi_s}^2} - 1\right) - \left[2.375 - 1.034\sqrt{\bar{m}} - 0.426\bar{m}\right]\xi_s\sqrt{\bar{m}} - \left(3.730 - 16.903\sqrt{\bar{m}} + 20.496\bar{m}\right){\xi_s}^2\sqrt{\bar{m}} \quad \textbf{(3.20)}$$

$$\xi_p = \sqrt{\frac{3\bar{m}}{8(1+\bar{m})(1-0.5\bar{m})}} + \left(0.151\xi_s - 0.170{\xi_s}^2\right) + \left(0.163\xi_s - 4.980{\xi_s}^2\right)\bar{m} \quad \textbf{(3.21)}$$

Where

$$\bar{m} = \frac{m_p}{m_s} \quad \textbf{(3.22)}$$

which is usually chosen by the designer,

$$\bar{f} = \frac{f_p}{f_s} \quad \textbf{(3.23)}$$

and

$$\xi_p = \frac{c_p}{2\sqrt{k_p m_p}} \quad \textbf{(3.24)}$$

Choosing $\overline{m}$ as 4.8% and substituting parameters of Table 3-1 into the equations (3.20), (3.21) and (3.22), the TMD parameters are calculated as shown in Table 3-2.

Table 3-2-TMD parameters using classical method

$\overline{m}$	$\bar{f}$	f_p (Hz)	ξ_p (%)	m_p (kg)	c_p (Ns/m)	k_p (N/m)
4.76%	0.94	4.18	13.33%	340	2,379	235,436

3.3.3.2.Optimisation of TMD parameters using a GA approach

Use of a GA as a searching method has been employed to explore in the area of feasible response and generate an optimised solution in that region, which gives the TMD parameters. Figure 3-6 shows the FRF of a SDOF system with and without a TMD attached to it. The TMD is used here to minimise the response of the structure (($H_{TMD}(\omega_i)$), the blue line) within a desirable band of frequencies (i.e. $\omega_0 < \omega_i < \omega_n$) by choosing the best possible parameters of the TMD (i.e. mass, damping and stiffness). However, it should be noticed that the FRF of the controlled structure should be inside the boundary of the FRF of the uncontrolled structure ($H_{unc}(\omega_i)$) to avoid higher responses at non-resonant frequencies. Consequently, for each ω_i, the response of the controlled structure due to the external force ($H_{TMD}(\omega_i)$) should be as minimum as possible. Also for each ω_i, the response of the controlled structure due to the external force ($H_{TMD}(\omega_i)$) should be less than the response of the uncontrolled structure ($H_{unc}(\omega_i)$) at the same frequency (ω_i). Hence, the objective function of the optimisation problem is to minimise the FRF function of the 2DOF system (i.e. including the structure and the TMD, the blue line) within the constraint of the FRF of the uncontrolled structure (red line).

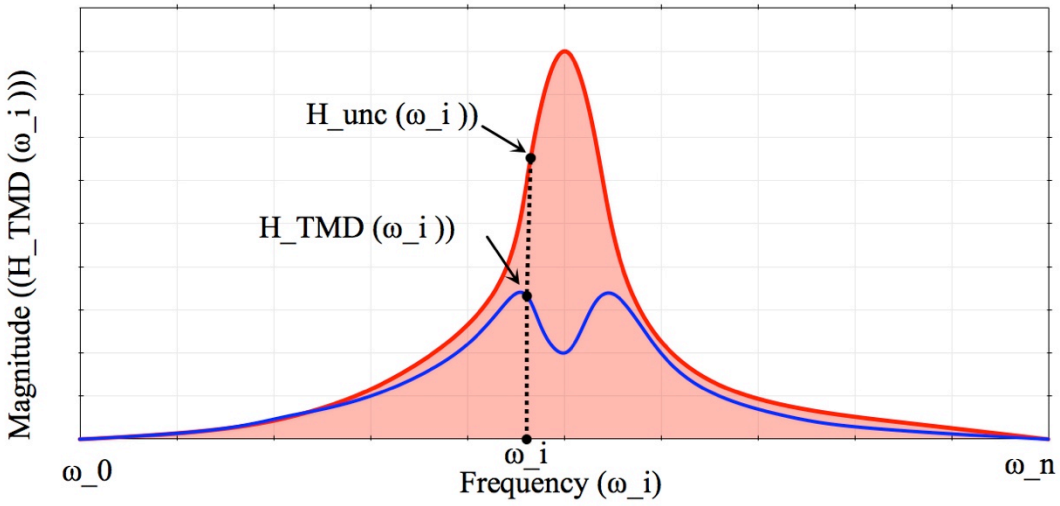

Figure 3-6- FRF of the controlled structure with TMD (blue) and uncontrolled structure (red) to be used in the GA

The optimisation problem is generated as

$$\text{O.F.: } \min(H_{TMD}(\omega_i)), \quad \omega_0 < \omega_i < \omega_n \tag{3.25}$$

$$\text{Constraint: } S.T. \quad H_{TMD}(\omega_i) < H_{unc}(\omega_i) \therefore H_{TMD}(\omega_i) - H_{unc}(\omega_i) < 0 \quad \omega_0 < \omega_i < \omega_n \tag{3.26}$$

where H_{unc} and H_{TMD} are the FRF functions (TF) between the external force and structural acceleration for uncontrolled and controlled (with TMD) structures, respectively. These functions were derived in sections 3.2.1 and 3.3.1.

In (3.4) and (3.16), substituting $s = j\omega_i$ where $j = \sqrt{-1}$, H_{unc} and H_{TMD} become

$$H_{unc}(\omega_i) = \frac{(j\omega_i)^2}{\mathrm{m_s}(j\omega_i)^2 + \mathrm{c_s}(j\omega_i) + \mathrm{k_s}} \tag{3.27}$$

$$H_{TMD}(\omega_i) = -(j\omega_i)^2 / [\left(\frac{(c_p(j\omega_i)+k_p)^2}{(m_p(j\omega_i)^2+c_p(j\omega_i)+k_p)^2(m_s(j\omega_i)^2+(c_s+c_p)(j\omega_i)+(k_s+k_p))} - 1\right) * \left(m_s(j\omega_i)^2 + (c_s + c_p)(j\omega_i) + (k_s + k_p)\right)] \tag{3.28}$$

It should be noted that the magnitude of FRF is the absolute value (complex magnitude) of these transfer functions.

In addition, the constraint function becomes as

$$(-(j\omega_i)^2/[\left(\frac{(c_p(j\omega_i)+k_p)^2}{(m_p(j\omega_i)^2+c_p(j\omega_i)+k_p)^2\left(m_s(j\omega_i)^2+(c_s+c_p)(j\omega_i)+(k_s+k_p)\right)}-1\right)*$$
$$\left(m_s(j\omega_i)^2+\left(c_s+c_p\right)(j\omega_i)+\left(k_s+k_p\right)\right)])-\frac{(j\omega_i)^2}{\mathrm{m_s}(j\omega_i)^2+\mathrm{c_s}(j\omega_i)+\mathrm{k_s}} \quad \textbf{(3.29)}$$

Based on (3.28) and (3.29), this is a multi-objective nonlinear function with nonlinear semi-infinite constrains. To apply a GA to this problem, the penalty function method is introduced to create a fitness function of the GA as [138], [139]

$$Fitness\ Function = F_i + r_p \sum_{i=1}^{n} G_i \quad \textbf{(3.30)}$$

The role of the penalty function is to convert the constrained problem to unconstrained. In the penalty method, usually some information about the infeasible solutions (the solutions out of the constraint) is required. This is achieved by a slight violation of the constraints [138], [139]. In (3.30) r_p is the Penalty Factor, G_i is the Constraint Function, F_i is the Objective Function for the ith frequency and n is the number of discreet frequencies. Implementing (3.30), both the OF and the constraint function convert to a single fitness function which can be applied using the MATLAB Optimisation Toolbox [138], [154], Multi-Objective Genetic Algorithm.

Table 3-3- GA parameters for optimisation of TMD parameters

Number of variables	3
Population Size	200
Selection Function	Tournament
Tournament Size	2
Reproduction/ Crossover fraction	0.8
Mutation function	Adaptive feasible
Crossover / Crossover fraction	Intermediate, ratio:1.0
Migration Direction	Forward
Migration fraction	0.2
Migration Interval	20
Pareto population fraction	0.35
Fitness Limit	Infinity
Stall generations	100
Function tolerance	10^{-5}
Fitness function evaluation	In serial

Using the properties in Table 3-3 for GA, the optimised critical values (TMD parameters) are shown in Table 3-4. It should be noted that the upper and lower bounds of the GA are very important since these define the area of choosing the critical values. In this case, these bounds are the practical feasibility of the TMD's parameters (i.e. mass, spring and damper). Hence, the lower bound is set to [m_p=100 c_p=100 k_p=50,000] and the upper band to [m_p=340 c_p=4,000 k_p=500,000]. It took 282 iterations to calculate the optimised parameters. In addition, r_p, the penalty factor was changed from 10^1 to 10^{100}. However, there is not a large difference between the outputs of the optimisation (TMD parameters) by changing r_p and it was concluded that this number has not a significant effect on the result. This is the maximum of 3% changing in the result.

Table 3-4- TMD parameters obtained using GA

f_p (Hz)	ξ_p (%)	m_p (kg)	c_p (Ns/m)	k_p (N/m)
4.42	11.38	335	2117	258,095

Figure 3-1 shows the FRF magnitude plot of the results from both Table 3-2 and Table 3-4 in comparison to that from the uncontrolled structure.

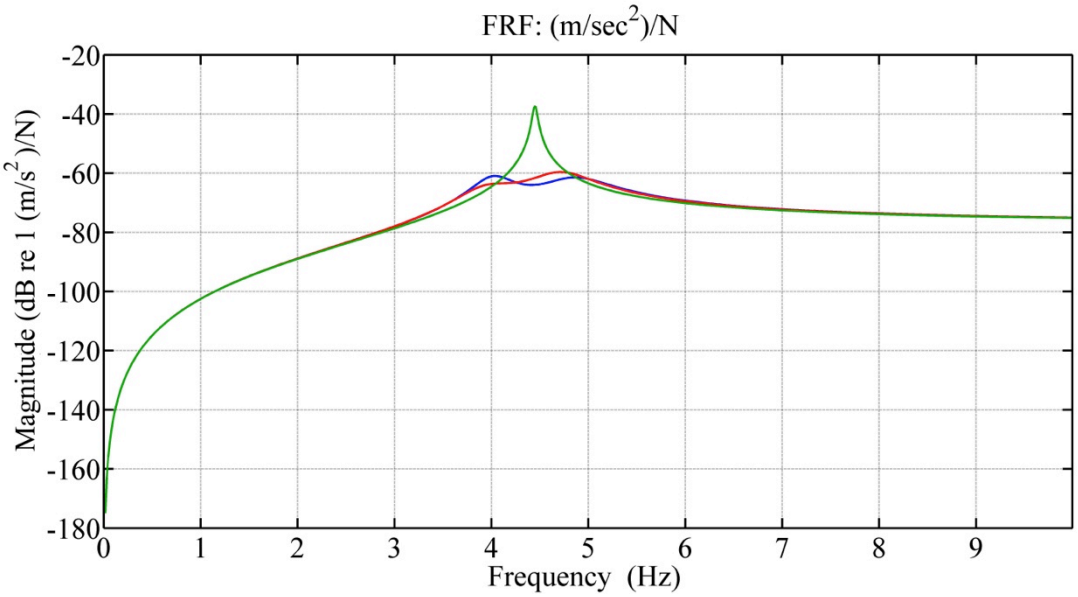

Figure 3-7- FRF of the uncontrolled structure (green) in comparison with structure with TMD using classical design (red) and TMD designed with GA (blue)

Both the classical and GA methods generate suitable TMD parameters. However, the GA approach gives more equal peaks of lower magnitude in comparison to the classical method. Using GA for optimising TMD parameters verifies the proposed methodology by the author and will be employed in optimising HTMD parameters (i.e. control gains).

It should be noted that both classical and GA optimisation method have violation of boundary (i.e. responses out of the boundary of the uncontrolled structure). This could be firstly due to the narrower band of resonant frequency of the considered structure. Also for GA optimisation, since Penalty Function method is employed, violation of the boundary is expected.

3.4. HTMD model

The hybrid tuned mass damper (HTMD) in this research work comprises of a TMD with an actuator attached on top as shown by the schematic in Figure 3-8. The structural vibration energy is dissipated primarily through the passive part and the

active element improves the performance of the system by addressing the off-tuning problem and mobilisation of passive TMD under low level vibrations. The active element can also be used to augment the damping force provided by the passive part of the TMD.

As illustrated in Figure 3-8, the model of the system is a 3DOF arrangement including the main structure as the first DOF, the passive TMD as the second DOF and an active actuator with inertial mass as the third DOF of the model. m_{act}, c_{act} and k_{act} are the mass, damping and stiffness of the actuator DOF, respectively. x_{act} is the absolute displacement of the active mass of the actuator.

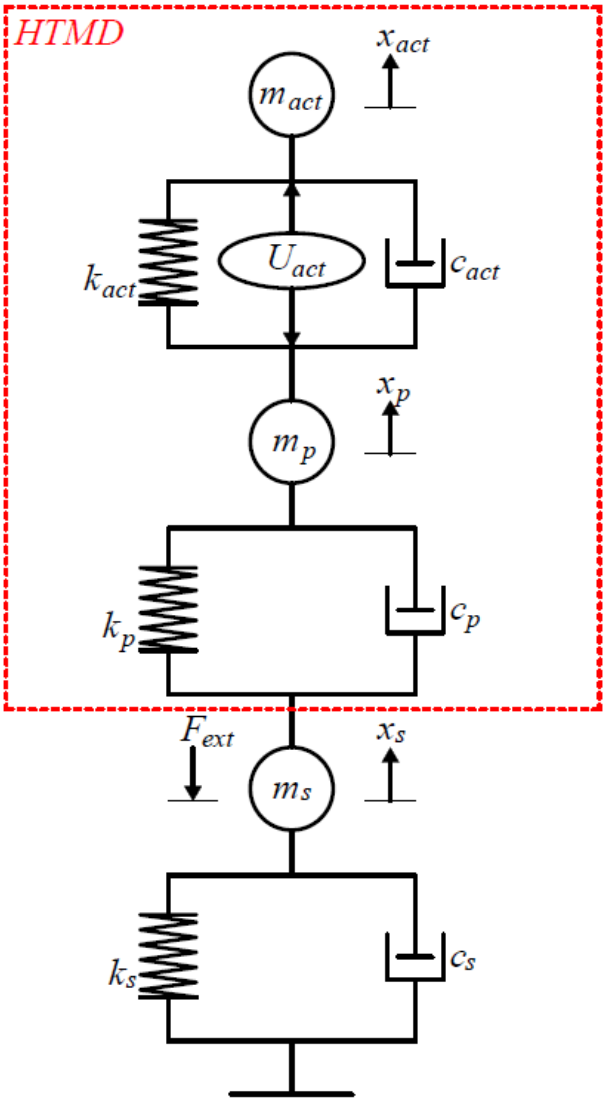

Figure 3-8- 3DOF model of the structure with attached HTMD

The equations of motion of the system with attached HTMD subjected to external force (F_{ext}) and force developed in the electromagnetic coils of actuator (U_{act}) are given by

a) $m_s\ddot{x}_s(t) + (c_s + c_p)\dot{x}_s(t) + (k_s + k_p)x_s(t) - c_p\dot{x}_p(t) - k_p x_p(t) = F_{ext}(t)$

b) $m_p\ddot{x}_p(t) + (c_p + c_{act})\dot{x}_p(t) + (k_p + k_{act})x_p(t) - c_p\dot{x}_s(t) - k_p x_s(t) - c_{act}\dot{x}_{act}(t) - k_{act}x_{act}(t) = U_{act}(t)$ **(3.31)**

c) $m_{act}\ddot{x}_{act}(t) + c_{act}\dot{x}_{act}(t) + k_{act}x_{act}(t) - c_{act}\dot{x}_p(t) - k_{act}x_p(t) = -U_{act}(t)$

3.4.1. Model of the actuator

The actuator used in this research work is an APS Dynamics Model 400 electrodynamic shaker which connects to an amplifier and generates an inertia force from the acceleration of the active mass [146]. This force also acts on the TMD as a reaction force. The actuator inertia force is controlled by applying a control voltage (maximum of 2.0 volt) to its amplifier. There are two operation modes; voltage and current mode. In this research, the voltage mode has been used and in this mode it can produce the harmonic force with the magnitude of around maximum 450 N) [155], [156].

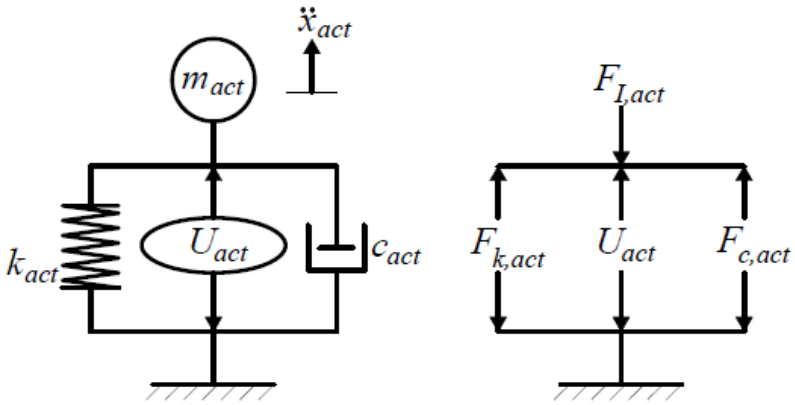

Figure 3-9- Free body diagram of the actuator

Writing the equation of motion for the actuator mass

$$m_{act}\ddot{x}_{act}(t) + c_{act}\dot{x}_{act}(t) + k_{act}x_{act}(t) = U_{act}(t) \quad \textbf{(3.32)}$$

Converting this in terms of force where $F_{I,act}$, $F_{c,act}$ and $F_{k,act}$ are inertia, damping and stiffness forces of the actuator, then:

$$F_{I,act}(t) + F_{c,act}(t) + F_{k,act}(t) = \mathrm{U_{act}}(t)$$
$$\therefore F_{I,act}(t) = -F_{c,act}(t) - F_{k,act}(t) + \mathrm{U_{act}}(t) \quad \textbf{(3.33)}$$

where

$$\mathrm{U_{act}}(t) = v_{act} V_{in,act} \quad \textbf{(3.34)}$$

$V_{in,act}$ is the input voltage of the actuator and v_{act} is the force-voltage characteristic of the actuator. Considering Figure 3-9 and equation (3.33), it is possible to replace the actuator DOF with just one inertia force (i.e. $F_{I,act}$) as in Figure 3-10.

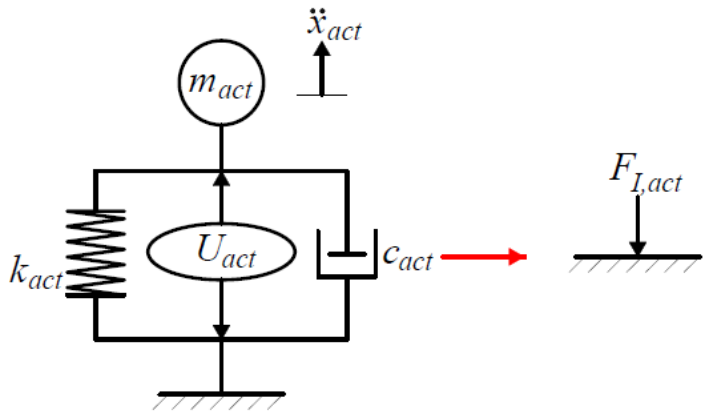

Figure 3-10- Replacing actuator DOF with the inertia force of actuator

Combining (3.32) and (3.34) and transforming it to Laplace domain generates

$$\frac{X_{act}(s)}{V_{in,act}(s)} = \frac{v_{act}}{m_{act}s^2 + c_{act}s + k_{act}} \quad \textbf{(3.35)}$$

having

$$\mathrm{F_{I,act}}(t) = \mathrm{m_{act}}\ddot{\mathrm{x}}_{\mathrm{act}}(t) \therefore \mathrm{F_{I,act}}(s) = \mathrm{m_{act}} X_{act} s^2 \quad \textbf{(3.36)}$$

Substituting (3.36) into (3.35) leads to

$$\frac{\mathrm{F_{I,act}}(s)}{V_{in,act}(s)} = \frac{m_{act} v_{act} s^2}{m_{act} s^2 + c_{act} s + k_{act}} \quad \textbf{(3.37)}$$

[147] showed that (3.37) needs a low pass element to be a third order model as a more realistic model of the actuator. Hence, $\mathrm{G_{act}}$, the TF between input voltage and inertia force of the actuator becomes

$$G_{act} = \frac{\mathrm{F_{I,act}}(s)}{V_{in,act}(s)} = \frac{m_{act} v_{act} s^2}{m_{act} s^2 + c_{act} s + k_{act}} * \frac{1}{s + \varepsilon_{act}} \quad \textbf{(3.38)}$$

where ε_{act} is the coefficient of the low pass filter element of the actuator. Figure 3-11 illustrates this TF. Also, the FRF of the actuator is demonstrated in Figure 3-12. This figure shows that for instance, at the frequency of around 2.5 Hz, for 1 volt of input voltage, there will be around 250 N inertia force from actuator. Considering on 2 volt maximum, the maximum actuator inertia force will be around 500 N.

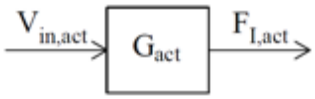

Figure 3-11- TF of the actuator

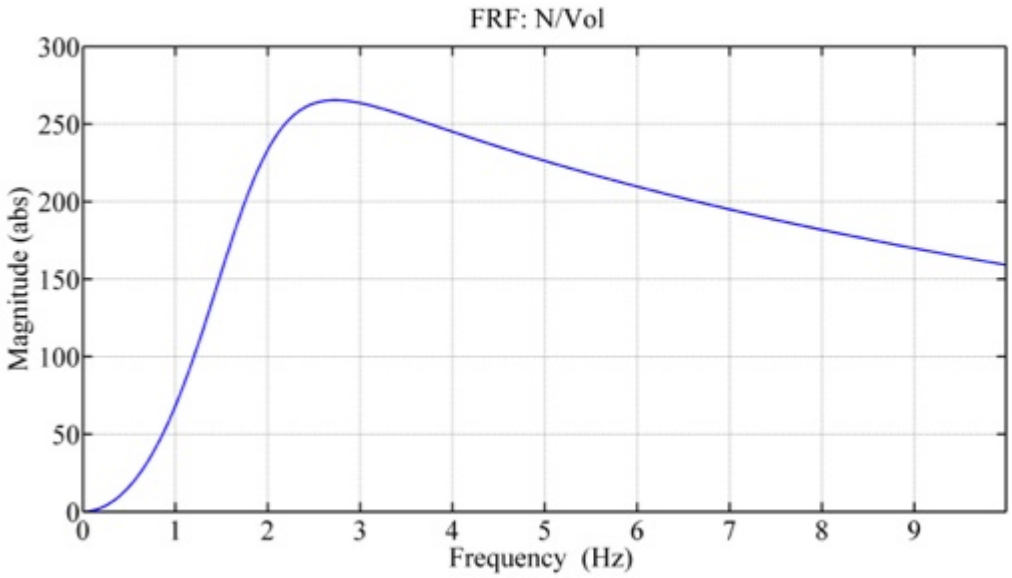

Figure 3-12- FRF of the actuator

Table 3-5 shows the properties of the actuator [146].

Table 3-5-Dynamic properties of the actuator

f_{act} (Hz)	ζ_{act}	m_a (kg)	c_{act} (N.sec/m)	k_{act} (N/m)	v_{act} (N/v)	ε_{act}
2.00	52%	30.0	392	4737	418.9	8*2π

3.4.2. Closed loop model of the structure incorporating the HTMD

Considering equation (3.31) and also reflecting the discussion in section 3.4.1, the 3DOF model of the structure with attached HTMD in Figure 3-8 is modified to Figure 3-13.

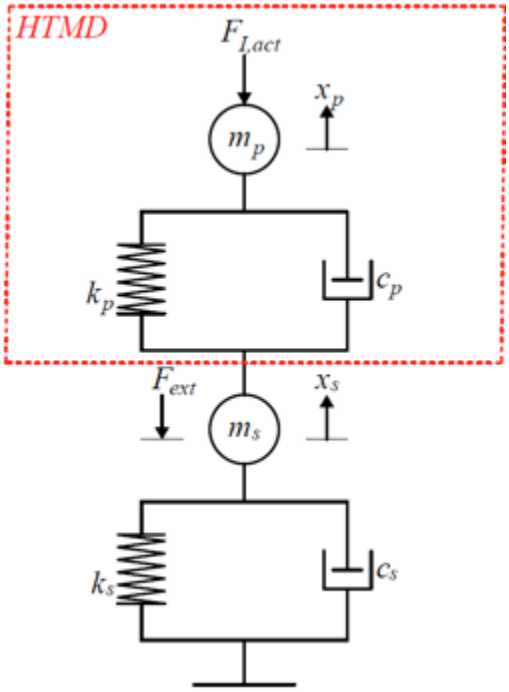

Figure 3-13- 2DOF model of the HTMD

Hence, the equations of motion of the system are generated as

$$\begin{cases} m_s\ddot{x}_s(t) + (c_s + c_p)\dot{x}_s(t) + (k_s + k_p)x_s(t) - c_p\dot{x}_p(t) - k_p x_p(t) = F_{ext}(t) \\ m_p\ddot{x}_p(t) + c_p\dot{x}_p(t) + k_p x_p(t) - c_p\dot{x}_s(t) - k_p x_s(t) = F_{I,act}(t) \end{cases} \quad \textbf{(3.39)}$$

Where the $F_{I,act}(t)$ can be calculated according to the TF between the actuator control voltage and inertia force in section 3.4.1. This control voltage is calculated and generated using suitable control algorithms that will be discussed later.

3.4.2.1. Transfer function of the HTMD

Figure 3-14 shows the TF arrangement of the model. It is a closed loop system. As the sketch illustrates, both responses of the TMD mass and structure are measured and fed back to the controller. These two responses are in terms of acceleration since this is the most convenient motion parameter for practical measurement. Then, it is the act of controller to calculate and generate the control voltage for the actuator, which then produces the inertia force acting on the TMD mass.

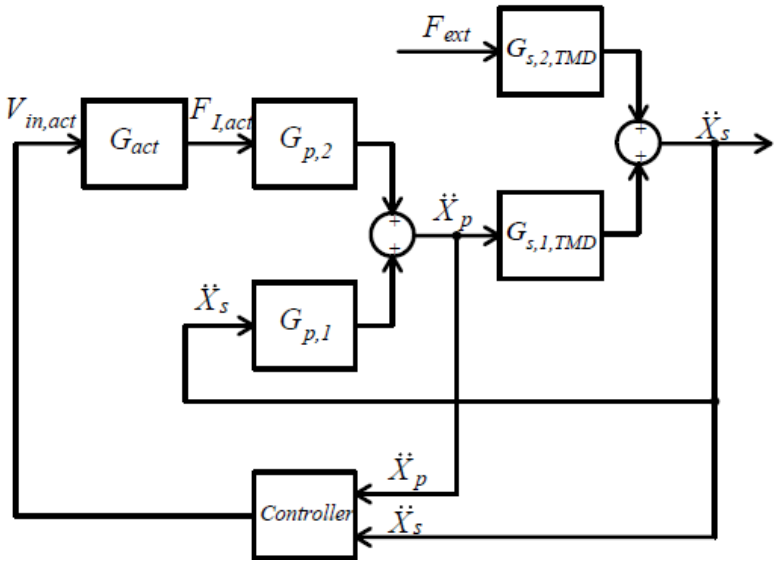

Figure 3-14- Block diagram arrangement of the structure with attached HTMD

Converting equation (3.39) from time domain to Laplace domain leads to

$$\begin{cases} m_s s^2 X_s(s) + (c_s + c_p) s X_s(s) + (k_s + k_p) X_s(s) - c_p s X_p(s) - k_p X_p(s) \\ \qquad = F_{ext}(s) \\ m_p s^2 X_p(s) + c_p s X_p(s) + k_p X_p(s) - c_p s X_s(s) - k_p X_s(s) = F_{I,act}(t) \end{cases} \quad \textbf{(3.40)}$$

Rearranging (3.40) in terms of $X_s(s)$, $X_p(s)$, $F_{ext}(s)$ and $F_{I,act}(s)$ results in

$$\begin{cases} [m_s s^2 + (c_s + c_p) s + (k_s + k_p)] X_s(s) - [c_p s + k_p] X_p(s) = F_{ext}(s) \\ [m_p s^2 + c_p s + k_p] X_p(s) - [c_p s + k_p] X_s(s) = F_{I,act}(s) \end{cases} \quad \textbf{(3.41)}$$

In comparison with the passive TMD, the response of the TMD mass depends on the actuator force as well as the acceleration of the main structure. Hence, $G_{p,2}$, the TF

between the acceleration of the TMD mass and the inertia force of the actuator is introduced as

$$\mathrm{G_{p,2}} = \frac{\mathrm{X_p(s)s^2}}{F_{I,act}(\mathrm{s})} = \frac{\mathrm{s^2}}{m_p s^2 + c_p s + k_p} \quad \textbf{(3.42)}$$

Substituting (3.11), (3.12), (3.13) and (3.42) into (3.41), the final TF of the system becomes

$$\begin{cases} \ddot{x}_s = \ddot{x}_p \mathrm{G_{s,1,TMD}} + F_{ext} \mathrm{G_{s,2,TMD}} \\ \ddot{x}_p = \ddot{x}_s \mathrm{G_{p,1}} + F_{I,act} \mathrm{G_{p,2}} \end{cases} \quad \textbf{(3.43)}$$

Combining these equations generates the final transfer function between the structural response and external force ($\mathrm{H_{HTMD}}$) as

$$\ddot{x}_s = \left(\ddot{x}_s \mathrm{G_{p,1}} + F_{I,act} \mathrm{G_{p,2}}\right) \mathrm{G_{s,1,TMD}} + F_{ext} \mathrm{G_{s,2,TMD}} \quad \textbf{(3.44)}$$

It will be shown in further sections that since $F_{I,act}$ depends on the response of the structure and TMD, it is possible to simplify equation (3.45) by substituting $\ddot{x}_s$ and $\ddot{x}_p$ in $F_{I,act}$. Hence, the HTMD transfer function takes the form of

$$\mathrm{H_{HTMD}} = \frac{\ddot{x}_s}{F_{ext}} \quad \textbf{(3.45)}$$

This is represented in Figure 3-14.

3.4.2.2.State space model of the HTMD

To include the dynamic properties (TF) of the actuator in the SS model, the inverse Laplace transform is applied on equation (3.38) and it is written in terms of acceleration instead of inertia force, hence

$$\frac{X_{act}(s)}{V_{in,act}(s)} = \frac{v_{act} m_{act}}{(m_{act})s^3 + (m_{act}\varepsilon_{act} + c_{act})s^2 + (c_{act}\varepsilon_{act} + k_{act})s + (k_{act}\varepsilon_{act})}$$

$$\therefore (m_{act})\ddot{x}_{act}(\mathrm{t}) + (m_{act}\varepsilon_{act} + c_{act})\ddot{x}_{act}(\mathrm{t}) + (c_{act}\varepsilon_{act} + k_{act})\dot{x}_{act}(\mathrm{t}) + (k_{act}\varepsilon_{act})x_{act}(t) = v_{act} m_{act} V_{in,act}(t) \quad \textbf{(3.46)}$$

Setting $\dot{X}_{7,\mathrm{H}TMD} = \ddot{x}_{act}$ leads to

$$\dot{X}_{7,HTMD} = \frac{1}{m_{act}}(v_{act}m_{act}V_{in,act} - (m_{act}\varepsilon_{act} + c_{act})X_{7,HTMD} - (c_{act}\varepsilon_{act} + k_{act})X_{6,HTMD} - (k_a\varepsilon_{act})X_{5,HTMD}) \quad \textbf{(3.47)}$$

This is included in SS model as follows. Considering equation (3.39), the states of the system are introduced as

$$\begin{Bmatrix} X_{1,\mathrm{H}TMD} = x_s \\ X_{2,\mathrm{H}TMD} = \dot{x}_s \\ X_{3,\mathrm{H}TMD} = x_p \\ X_{4,\mathrm{H}TMD} = \dot{x}_p \\ X_{5,\mathrm{H}TMD} = x_{act} \\ X_{6,\mathrm{H}TMD} = \dot{x}_{act} \\ X_{7,\mathrm{H}TMD} = \ddot{x}_{act} \end{Bmatrix} \therefore \begin{Bmatrix} \dot{X}_{1,\mathrm{H}TMD} = X_{2,\mathrm{H}TMD} \\ \dot{X}_{2,\mathrm{H}TMD} = \ddot{x}_s \\ \dot{X}_{3,\mathrm{H}TMD} = X_{4,\mathrm{H}TMD} \\ \dot{X}_{4,\mathrm{H}TMD} = \ddot{x}_p \\ \dot{X}_{5,\mathrm{H}TMD} = X_{6,\mathrm{H}TMD} \\ \dot{X}_{6,\mathrm{H}TMD} = X_{7,\mathrm{H}TMD} \\ \dot{X}_{7,\mathrm{H}TMD} = \ddot{x}_{act} \end{Bmatrix} \quad \textbf{(3.48)}$$

Hence, the SS representation of the system in the form of $\dot{X}_{HTMD} = A_{HTMD}X_{HTMD} + B_{HTMD}U_{HTMD}$ becomes as

$$\begin{Bmatrix} \dot{X}_{1,HTMD} \\ \dot{X}_{2,HTMD} \\ \dot{X}_{3,HTMD} \\ \dot{X}_{4,HTMD} \\ \dot{X}_{5,HTMD} \\ \dot{X}_{6,HTMD} \\ \dot{X}_{7,HTMD} \end{Bmatrix} = \begin{bmatrix} 0 & 1 & 0 & 0 & \cdots \\ -\frac{(k_s + k_p)}{m_s} & -\frac{(c_s + c_p)}{m_s} & \frac{k_p}{m_s} & \frac{c_p}{m_s} & \cdots \\ 0 & 0 & 0 & 1 & \cdots \\ \frac{k_p}{m_p} & \frac{c_p}{m_p} & -\frac{k_p}{m_p} & -\frac{c_p}{m_p} & \cdots \\ 0 & 0 & 0 & 0 & \cdots \\ 0 & 0 & 0 & 0 & \cdots \\ 0 & 0 & 0 & 0 & \cdots \end{bmatrix} \quad \textbf{(3.49)}$$

$$\begin{bmatrix} \cdots & 0 & 0 & 0 \\ \cdots & 0 & 0 & 0 \\ \cdots & 0 & 0 & 0 \\ \cdots & 0 & 0 & 0 \\ \cdots & 0 & 1 & 0 \\ \cdots & 0 & 0 & 1 \\ \cdots & -\frac{(k_{act} * \varepsilon_{act})}{m_{act}} & -\frac{(c_{act} * \varepsilon_{act} + k_{act})}{m_{act}} & -\frac{(m_{act} * \varepsilon_{act} + c_{act})}{m_{act}} \end{bmatrix}$$

$$\begin{Bmatrix} X_{1,\mathrm{H}TMD} \\ X_{2,\mathrm{H}TMD} \\ X_{3,\mathrm{H}TMD} \\ X_{4,\mathrm{H}TMD} \\ X_{5,\mathrm{H}TMD} \\ X_{6,\mathrm{H}TMD} \\ X_{7,\mathrm{H}TMD} \end{Bmatrix} + \begin{bmatrix} 0 & 0 & 0 \\ \frac{1}{m_s} & 0 & 0 \\ 0 & 0 & 0 \\ 0 & \frac{1}{m_p} & 0 \\ 0 & 0 & 0 \\ 0 & 0 & 0 \\ 0 & 0 & v_{act} \end{bmatrix} \begin{Bmatrix} F_{ext} \\ F_{I,act} \\ V_{in,act} \end{Bmatrix}$$

It should be noted that the TF of the actuator (representing the actuator dynamics) is included in the SS representation. To achieve the output as displacement, velocity and acceleration of the structure and TMD; and also displacement, velocity and inertia force of actuator in the form of $Y_{HTMD} = C_{HTMD}X_{HTMD} + D_{HTMD}U_{HTMD}$, the output matrix is introduced as

$$\begin{Bmatrix} Y_{1,HTMD} \\ Y_{2,HTMD} \\ Y_{3,HTMD} \\ Y_{4,HTMD} \\ Y_{5,HTMD} \\ Y_{6,HTMD} \\ Y_{7,HTMD} \\ Y_{8,HTMD} \\ Y_{9,HTMD} \end{Bmatrix} = \begin{bmatrix} 1 & 0 & 0 & 0 & \cdots \\ 0 & 1 & 0 & 0 & \cdots \\ -\frac{(k_s+k_p)}{m_s} & -\frac{(c_s+c_p)}{m_s} & \frac{k_p}{m_s} 0 & \frac{c_p}{m_s} & \cdots \\ 0 & 0 & 1 & 0 & \cdots \\ 0 & 0 & 0 & 1 & \cdots \\ \frac{k_p}{m_p} & \frac{c_p}{m_p} & -\frac{k_p}{m_p} & -\frac{c_p}{m_p} & \cdots \\ 0 & 0 & 0 & 0 & \cdots \\ 0 & 0 & 0 & 0 & \cdots \\ 0 & 0 & 0 & 0 & \cdots \end{bmatrix}$$

$$\begin{bmatrix} \cdots & 0 & 0 & 0 \\ \cdots & 0 & 0 & 0 \\ \cdots & 0 & 0 & 0 \\ \cdots & 0 & 0 & 0 \\ \cdots & 0 & 0 & 0 \\ \cdots & 0 & 0 & 0 \\ \cdots & 1 & 0 & 0 \\ \cdots & 0 & 1 & 0 \\ \cdots & 0 & 0 & m_{act} \end{bmatrix} \begin{Bmatrix} X_{1,\mathrm{H}TMD} \\ X_{2,\mathrm{H}TMD} \\ X_{3,\mathrm{H}TMD} \\ X_{4,\mathrm{H}TMD} \\ X_{5,\mathrm{H}TMD} \\ X_{6,\mathrm{H}TMD} \\ X_{7,\mathrm{H}TMD} \end{Bmatrix} + \begin{bmatrix} 0 & 0 & 0 \\ 0 & 0 & 0 \\ \frac{1}{m_s} & 0 & 0 \\ 0 & 0 & 0 \\ 0 & 0 & 0 \\ 0 & \frac{1}{m_p} & 0 \\ 0 & 0 & 0 \\ 0 & 0 & 0 \\ 0 & 0 & 0 \end{bmatrix} \begin{Bmatrix} F_{ext} \\ F_{I,act} \\ V_{in,act} \end{Bmatrix} \quad \textbf{(3.50)}$$

3.5. Model of the structure with attached AMD (Active Control)

In this research work for comparative purposes, an active vibration control (AVC) approach is designed. This is a simple direct velocity feedback (DVF) scheme [31], [146], [157] where the same actuator as was used in the HTMD is placed on the structure to control the first mode of the vibration. The velocity of the structure with appropriate gain factor applied is the control feedback signal. Figure 3-15 shows the model of the structure with AVC technique. It should be noted that as was derived previously, the actuator DOF is replaced with the generated inertia force. Hence, the inertia force of the actuator mass acts directly on the structure as the control force.

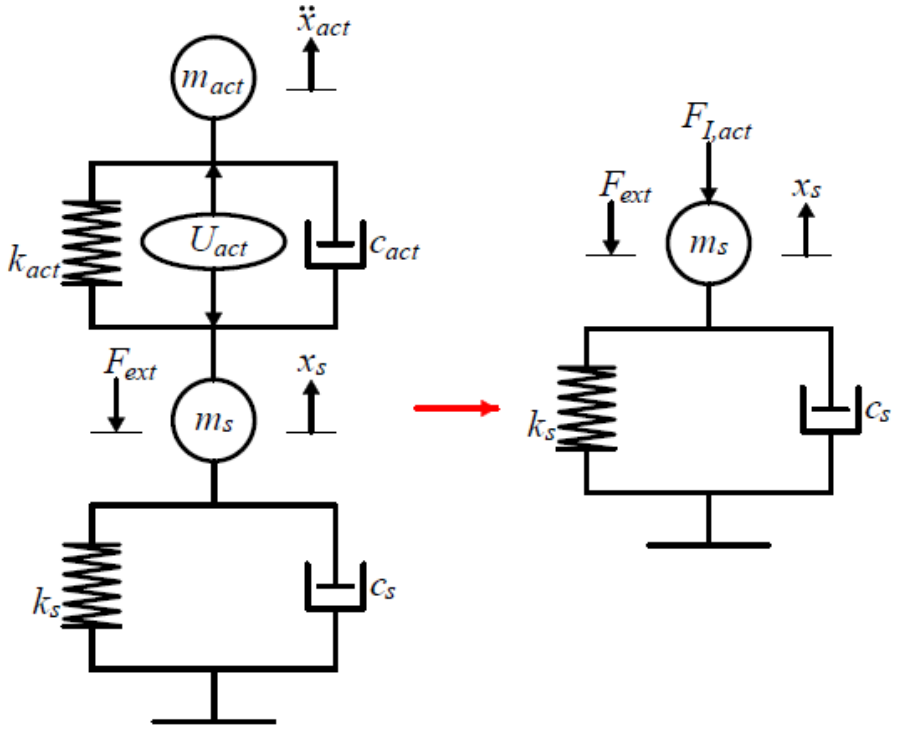

Figure 3-15- model of the structure with attached AMD

The equation of motion of the system with attached AMD (Active Mass Damper) subjected to external force (F_{ext}) and inertia force of the actuator ($F_{I,act}$) is given by

$$m_s\ddot{x}_s(t) + c_s\dot{x}_s(t) + k_s x_s(t) = F_{ext}(t) + F_{I,act}(t) \quad \textbf{(3.51)}$$

where $F_{I,act}(t)$ can be calculated according to the transfer function between $V_{in,act}$ (control input voltage) and $F_{I,act}$ in equation (3.38). Also, in DVF the control

voltage can be calculated using equation (3.52) where K_{DVF} is the feedback control gain,

$$V_{in,act} = K_{DVF}\dot{x}_s \quad \textbf{(3.52)}$$

The SS representation of the system in the form of $\dot{X}_{DVF} = A_{DVF}X_{DVF} + B_{DVF}U_{DVF}$ becomes

$$\begin{Bmatrix} \dot{X}_{1,DVF} \\ \dot{X}_{2,DVF} \\ \dot{X}_{5,DVF} \\ \dot{X}_{6,DVF} \\ \dot{X}_{7,DVF} \end{Bmatrix} = \begin{bmatrix} 0 & 1 & \cdots \\ -\frac{(k_s)}{m_s} & -\frac{(c_s)}{m_s} & \cdots \\ 0 & 0 & \cdots \\ 0 & 0 & \cdots \\ 0 & 0 & \cdots \end{bmatrix}$$
$$\begin{bmatrix} \cdots & 0 & 0 & 0 \\ \cdots & 0 & 0 & 0 \\ \cdots & 0 & 1 & 0 \\ \cdots & 0 & 0 & 1 \\ \cdots & -\frac{(k_{act}\varepsilon_{act})}{m_{act}} & -\frac{(c_{act}\varepsilon_{act}+k_{act})}{m_{act}} & -\frac{(m_{act}\varepsilon_{act}+c_{act})}{m_{act}} \end{bmatrix} \quad \textbf{(3.53)}$$
$$* \begin{Bmatrix} X_{1,DVF} \\ X_{2,DVF} \\ X_{5,DVF} \\ X_{6,DVF} \\ X_{7,DVF} \end{Bmatrix} + \begin{bmatrix} 0 & 0 & 0 \\ \frac{1}{m_s} & \frac{1}{m_s} & 0 \\ 0 & 0 & 0 \\ 0 & 0 & 0 \\ 0 & 0 & v_{act} \end{bmatrix} * \begin{Bmatrix} F_{ext} \\ F_{I,act} \\ V_{in,act} \end{Bmatrix}$$

The actuator dynamics are again included in the SS representation. To achieve the output as displacement, velocity and acceleration of the structure and also displacement, velocity and inertia force of actuator in the form of $Y_{DVF} = C_{DVF}X_{DVF} + D_{DVF}U_{DVF}$, the output matrix is introduced as

$$\begin{Bmatrix} Y_{1,DVF} \\ Y_{2,DVF} \\ Y_{3,DVF} \\ Y_{7,DVF} \\ Y_{8,DVF} \\ Y_{9,DVF} \end{Bmatrix} = \begin{bmatrix} 1 & 0 & \cdots \\ 0 & 1 & \cdots \\ -\frac{(k_s)}{m_s} & -\frac{(c_s)}{m_s} & \cdots \\ 0 & 0 & \cdots \\ 0 & 0 & \cdots \\ 0 & 0 & \cdots \end{bmatrix} \quad \textbf{(3.54)}$$

$$\begin{matrix}\cdots & 0 & 0 & 0\\ \cdots & 0 & 0 & 0\\ \cdots & 0 & 0 & 0\\ \cdots & 1 & 0 & 0\\ \cdots & 0 & 1 & 0\\ \cdots & 0 & 0 & m_{act}\end{matrix} * \begin{Bmatrix} X_{1,DVF}\\ X_{2,DVF}\\ X_{5,DVF}\\ X_{6,DVF}\\ X_{7,DVF}\end{Bmatrix} + \begin{bmatrix} 0 & 0 & 0\\ 0 & 0 & 0\\ \frac{1}{m_s} & \frac{1}{m_s} & 0\\ 0 & 0 & 0\\ 0 & 0 & 0\\ 0 & 0 & 0\end{bmatrix} * \begin{Bmatrix} F_{ext}\\ F_{I,act}\\ V_{in,act}\end{Bmatrix}$$

3.5.1. Simulation

Since the proposed AVC method is a single-input-single-output (SISO) system, it is possible to use root locus (RL) analysis to determine the appropriate control gain. The aim is to have the highest possible damping on the structure using the AVC technique within the limitations of the actuator capacity and stability. Figure 3-16 shows the RL plot of the proposed system.

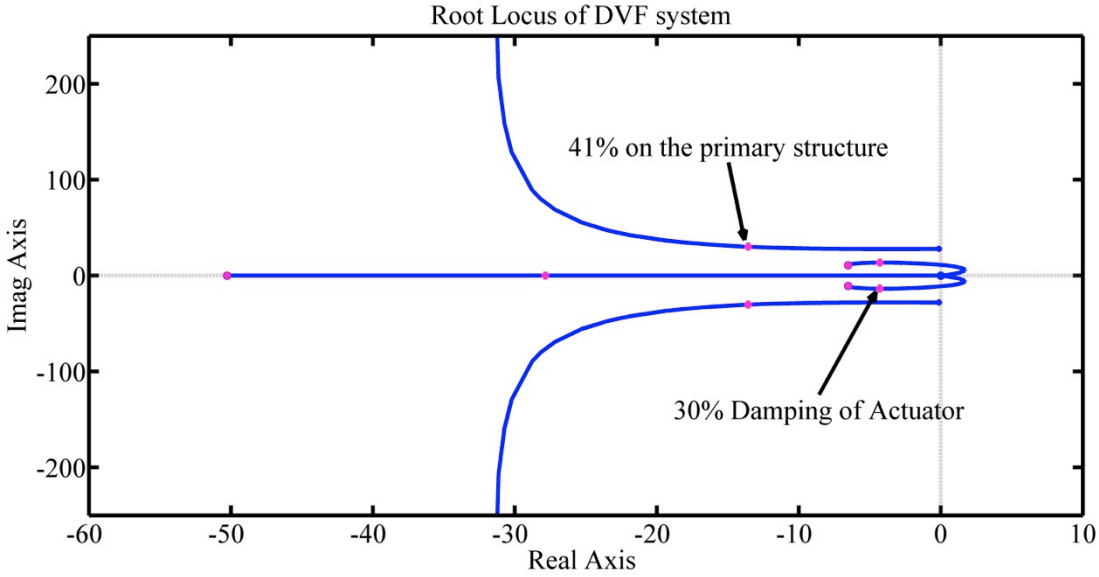

Figure 3-16- Root locus of the DVF technique

According to Figure 3-16 the DVF gain is calculated as $K_{DVF} = 521$. Also, since the poles of the closed loop system are on the left hand side of the *s*-plane plot, then the system is stable. By applying this gain within the proposed state space model, Figure 3-17 is generated. This is the accelerance FRF between external excitation and structural acceleration response.

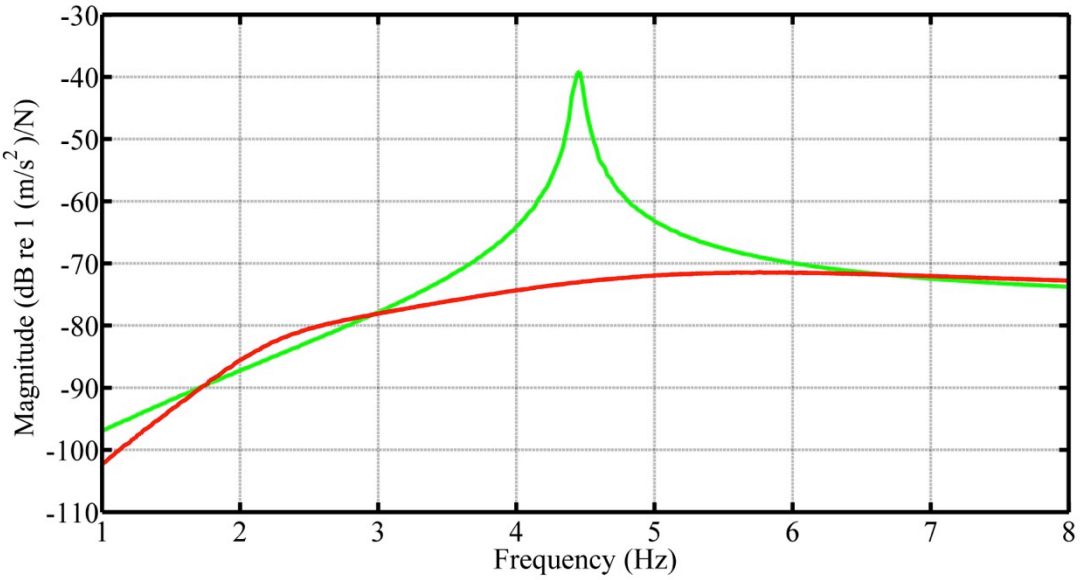

Figure 3-17- FRF of the uncontrolled structure (green) in comparison with structure with AMD (red)

As the figure demonstrates, the peak of the FRF is reduced from 0.0135 $(m/s^2)/N$ to 0.0002 $(m/s^2)/N$ when the AMD is acting on the structure, which corresponds to a 98% reduction in response compared with the uncontrolled structure. The performance of this AMD will be compared later against the performance of both the TMD and HTMD.

3.6. Control Algorithm

Based on Figure 3-14, developing a control algorithm is the key challenge to develop the controller block in a way to produce an appropriate actuator drive signal (voltage) from the measured response of the system. This signal is fed to the actuator (through the amplifier) and generates the control force that is acting on the TMD mass.

As mentioned in Chapter 2, there are a number of recommendations from other authors [2], [3], [51], [52], [158]–[161] for designing the control algorithm for an HTMD. These suggestions are mostly based on measurement of one or two responses of the structure and/or TMD (e.g. acceleration of the structure, velocity of the TMD mass, etc.) and multiplying these by appropriate gains before feeding them back to the actuator as the input voltages. Also, there are various recommendations to optimise these gains.

Herein, the author investigates first the effect of different type of gains (including those types suggested from other authors and those proposed new gains in this research) on the structure. Then, some methods are suggested to optimise the appropriate gains.

3.6.1. Direct Response Feedback

The response of the TMD in the equations of motion is given in terms of absolute values. It means, for instance, $\ddot{x}_p$ is the absolute acceleration of the TMD. However, by replacing the absolute terms with relative (i.e. $\ddot{x}_p$, $\dot{x}_p$ and x_p with $\ddot{x}_{p,rel}$, $\dot{x}_{p,rel}$ and $x_{p,rel}$ respectively) where

$$\begin{cases} \ddot{x}_{p,rel}(t) = \ddot{x}_p(t) - \ddot{x}_s(t) \\ \dot{x}_{p,rel}(t) = \dot{x}_p(t) - \dot{x}_s(t) \\ x_{p,rel}(t) = x_p(t) - x_s(t) \end{cases} \quad \textbf{(3.55)}$$

Then equation (3.8) is converted to

$$\begin{cases} m_s\ddot{x}_s(t) + c_s\dot{x}_s(t) + k_s x_s(t) - c_p\dot{x}_{p,rel}(t) - k_p x_{p,rel}(t) = F_{ext}(t) \\ m_p\left(\ddot{x}_s(t) + \ddot{x}_{p,rel}(t)\right) + c_p\dot{x}_{p,rel}(t) + k_p x_{p,rel}(t) = 0 \end{cases} \quad \textbf{(3.56)}$$

In (3.56), substituting the second part of the equation into the first part leads to

$$(m_s + m_p)\ddot{x}_s(t) + c_s\dot{x}_s(t) + k_s x_s(t) = F_{ext}(t) - m_p\ddot{x}_{p,rel}(t) \quad \textbf{(3.57)}$$

This means that the absolute inertia force of the TMD (i.e. $m_p\ddot{x}_{p,rel}(t)$) acts to attenuate the external force acting on the main structure. It means having more inertia force from the TMD causes more attenuation of the structural vibration. The goal of HTMD is to achieve a TMD with higher inertia force. On the other side and by modifying the second part of the equation (3.56) as

$$m_p\ddot{x}_{p,rel}(t) + c_p\dot{x}_{p,rel}(t) + k_p x_{p,rel}(t) = -m_p\ddot{x}_s(t) \quad \textbf{(3.58)}$$

This shows the acceleration of the main structure ($\ddot{x}_s(t)$) acts as an external force (excitation) on the TMD. The higher acceleration of the structure leads to higher acceleration of the TMD, which leads to more inertia force of the TMD. This inertia force attenuates the structural acceleration.

Now considering the equation of motion of the HTMD in (3.39) and replacing $F_{I,act}(t)$ with $K_i X_{Resp}$ where X_{Resp} is the response of the structure or TMD (i.e. displacement, velocity or acceleration) and K_i is the feedback gain then

$$\begin{cases} m_s\ddot{x}_s(t) + (c_s + c_p)\dot{x}_s(t) + (k_s + k_p)x_s(t) - c_p\dot{x}_p(t) - k_p x_p(t) = F_{ext}(t) \\ m_p\ddot{x}_p(t) + c_p\dot{x}_p(t) + k_p x_p(t) - c_p\dot{x}_s(t) - k_p x_s(t) = K_i X_{Resp}(t) \end{cases} \quad \textbf{(3.59)}$$

Based on (3.59) and also following the discussion of (3.57) and (3.58) leads to the conclusion that the first feedback gain should based on the acceleration of the structure which causes the TMD to have more acceleration and produces more inertia force. Hence combining (3.58) and second part of (3.59) and set $X_{Resp} = \ddot{x}_s(t)$ leads to

$$\begin{aligned} &m_p\ddot{x}_{p,rel}(t) + c_p\dot{x}_{p,rel}(t) + k_p x_{p,rel}(t) = -m_p\ddot{x}_s(t) + K_i\,\ddot{x}_s(t) \therefore \\ &m_p\ddot{x}_{p,rel}(t) + c_p\dot{x}_{p,rel}(t) + k_p x_{p,rel}(t) = (-m_p + K_i\,)\ddot{x}_s(t) \end{aligned} \quad \textbf{(3.60)}$$

This shows that using acceleration of the structure as a feedback results in the TMD having more inertia force. This can be described as the ‘driving force’ [159] of HTMD.

To regulate the damping force of the TMD, it is possible to adjust the second feedback of the system, which is the velocity of the TMD (i.e. $X_{Resp} = \dot{x}_p(t)$). Then (3.59) is converted to

$$\begin{aligned} &m_p\ddot{x}_p(t) + c_p\dot{x}_p(t) + k_p x_p(t) - c_p\dot{x}_s(t) - k_p x_s(t) = K_i\dot{x}_p(t) \therefore \\ &m_p\ddot{x}_p(t) + (c_p - K_i)\dot{x}_p(t) + k_p x_p(t) - c_p\dot{x}_s(t) - k_p x_s(t) = 0 \end{aligned} \quad \textbf{(3.61)}$$

(3.61) shows that feedback of the velocity of the TMD imparts an active damping force on the TMD. This can be called the ‘damping force’ of the HTMD [159].

Also, utilising acceleration and displacement of the TMD as feedbacks (i.e. replacing X_{Resp} with $\ddot{x}_p(t)$ and $x_p(t)$) causes the TMD mass and stiffness to be changed actively. Hence, the frequency of the TMD can be adjusted and hence tuned to the demanded frequency. This can be called the 'tuning force' of the TMD [162].

3.6.1.1.Simulations

To see the effect of each feedback on the structure, a numerical study is performed on the structure discussed in section 3.2 using the HTMD model proposed in section 3.4. The feedback terms considered are velocity and acceleration of the structure in addition to the displacement, velocity and acceleration of the TMD. The effects of these feedback terms are investigated individually in addition to combinations of them. Variation in both modal frequencies and magnitude of the FRF are considered.

Feedback gain ranges for individual response parameters

The initial step is to generate the range of gain factors that are going to be applied to the feedback terms. To achieve this, a RL analysis is employed based on the stability of the closed loop system proposed in Section 3.4.2. It should be noted that since the RL method is applicable for SISO systems and having more than one feedback leads to a MISO/MIMO system, it is necessary to apply RL for each feedback individually. This results in a range for each feedback gain that causes the system to be stable. The author shows later (in Section 4.1.2) that by using a combination of these ranges of feedback gains secures the stability of the system.

Based on TF of the system in 3.4.2 and replacing $V_{in,act}$ with $K_i X_{Resp}$ in the controller block in Figure 3-14, it is possible to employ RL to check the range of the stability of the system for each gain. Figure 3-18, Figure 3-19, Figure 3-20, Figure 3-21 and Figure 3-22 show the RL plots for different feedbacks. In addition, Table 3-6 illustrates the range of the gains that ensures the stability of the system.

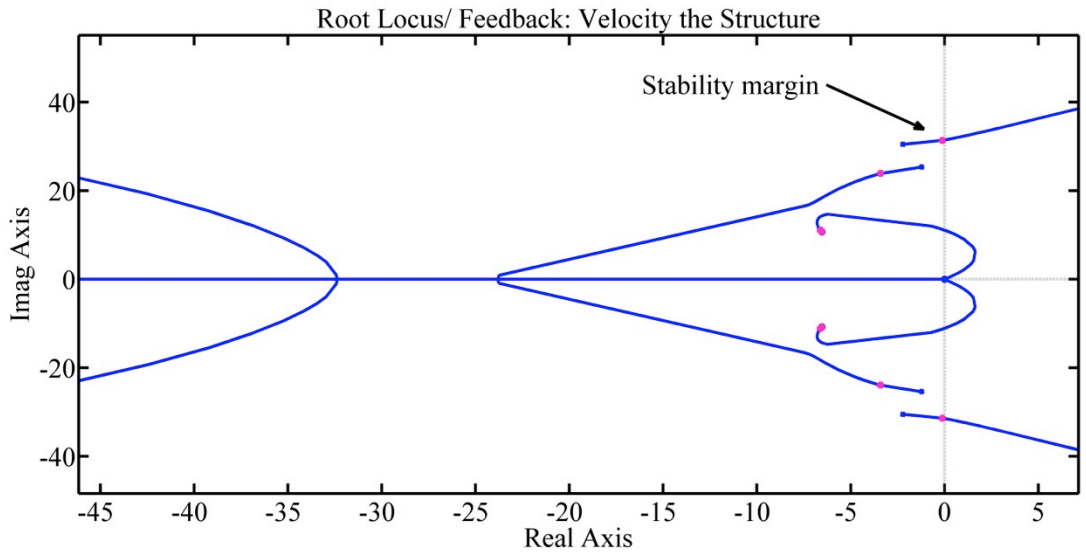

Figure 3-18- RL analysis, velocity of the structure as the response feedback.

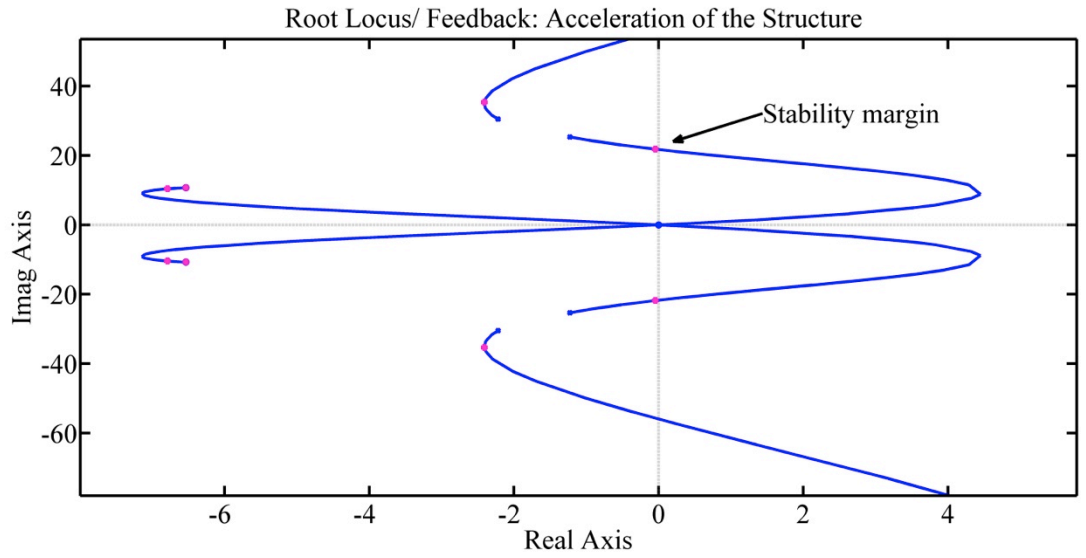

Figure 3-19- RL analysis, acceleration of the structure as the response feedback.

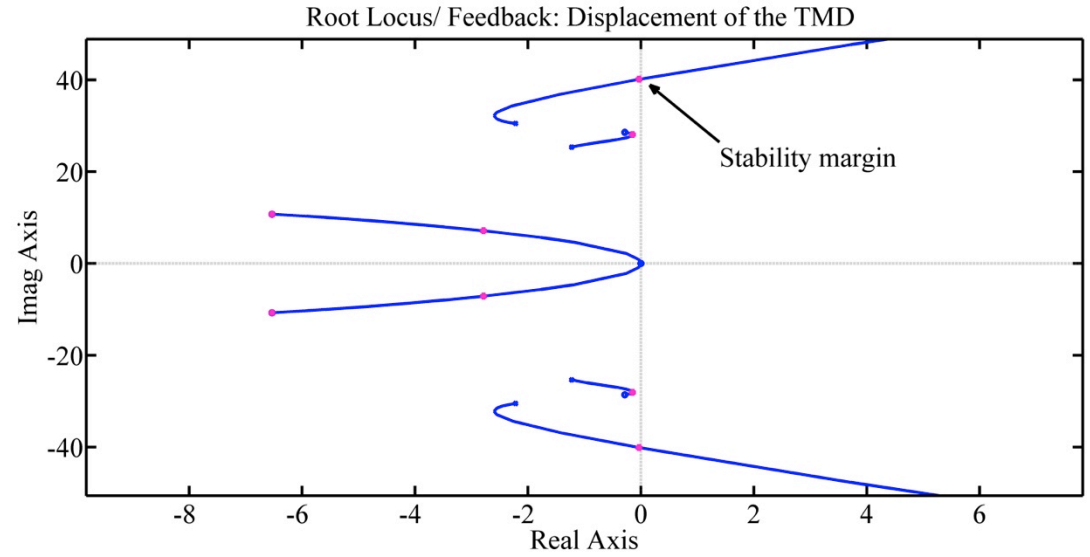

Figure 3-20- RL analysis, displacement of the TMD as the response feedback.

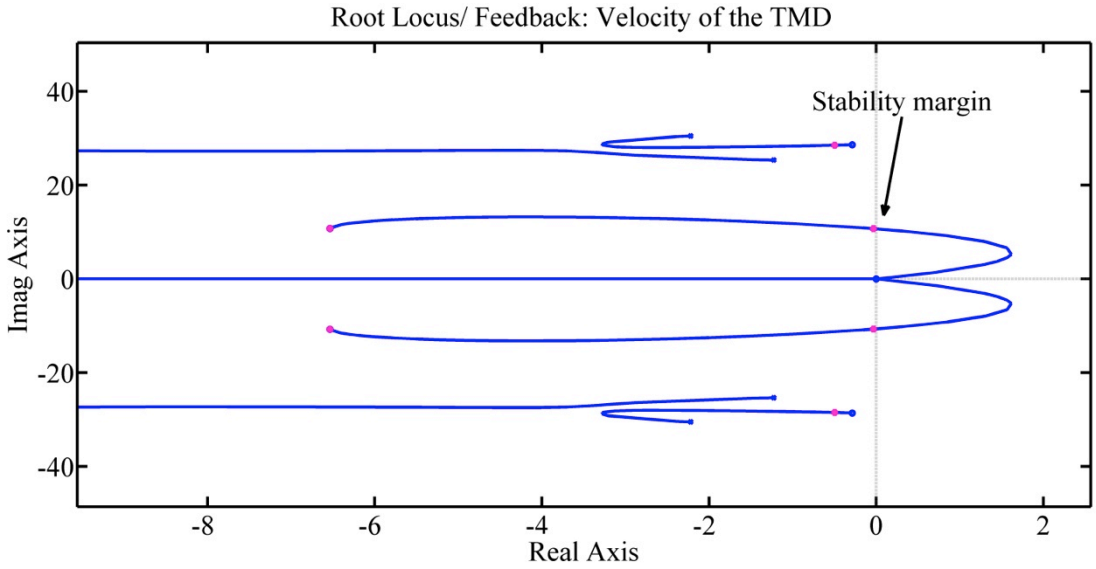

Figure 3-21- RL analysis, velocity of the TMD as the response feedback.

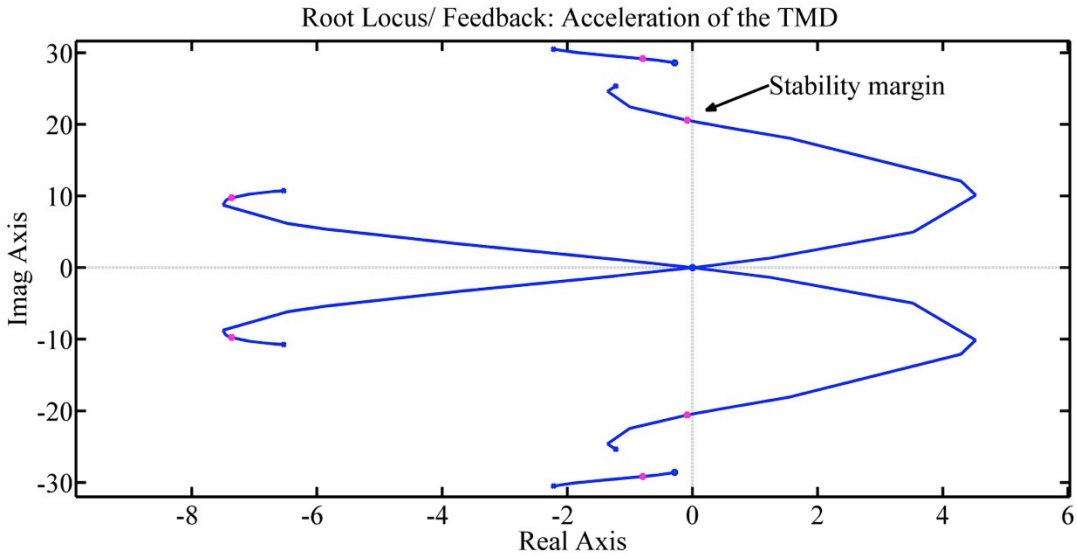

Figure 3-22- RL analysis, acceleration of the TMD as the response feedback.

It should be noted that these RL plots are zoomed to the region of interest. Hence, all loci are not presented in the plots.

Table 3-6- Stability range of the gains

Type of response feedback	Gain Range
K_3, Velocity of the main structure, $X_{Resp} = \dot{x}_s$	[-58,0]
K_2, Acceleration of the main structure, $X_{Resp} = \ddot{x}_s$	[-6.30,0]
K_1, Displacement of the TMD, $X_{Resp} = x_p$	[-1330,0]
K_4, Velocity of the TMD, $X_{Resp} = \dot{x}_p$	[-100,0]
K_5, Acceleration of the TMD, $X_{Resp} = \ddot{x}_p$	[-0.835,0]

All these ranges were confirmed experimentally by manually changing the individual gains of the system in the lab which will be discussed further in Chapter 6.

Manual optimisation of gain pairs

For the simulations, the properties of the structure and TMD summarised in Table 3-1 and Table 3-4 are used. In addition, the model proposed in Section 3.4 is employed. A MATLAB script is created to generate the FRF of the system between external force (F_{ext}) and structural acceleration ($\ddot{x}_s$). Then the peaks of these FRF magnitudes and their corresponding frequencies are calculated. The smallest FRF

number in the graph corresponds to the appropriate sets of gain (less acceleration) as the most appropriate gain for each type of feedback is chosen.

Figure 3-23 shows a contour plot of the combination of the structural acceleration and TMD velocity versus maximum magnitude of the FRF. Figure 3-24 and Figure 3-25 show the same results with structural acceleration and velocity and also structural acceleration and TMD displacement for feedback respectively. Table 3-7 summarises the results from plots generated from different combinations of gain pairs.

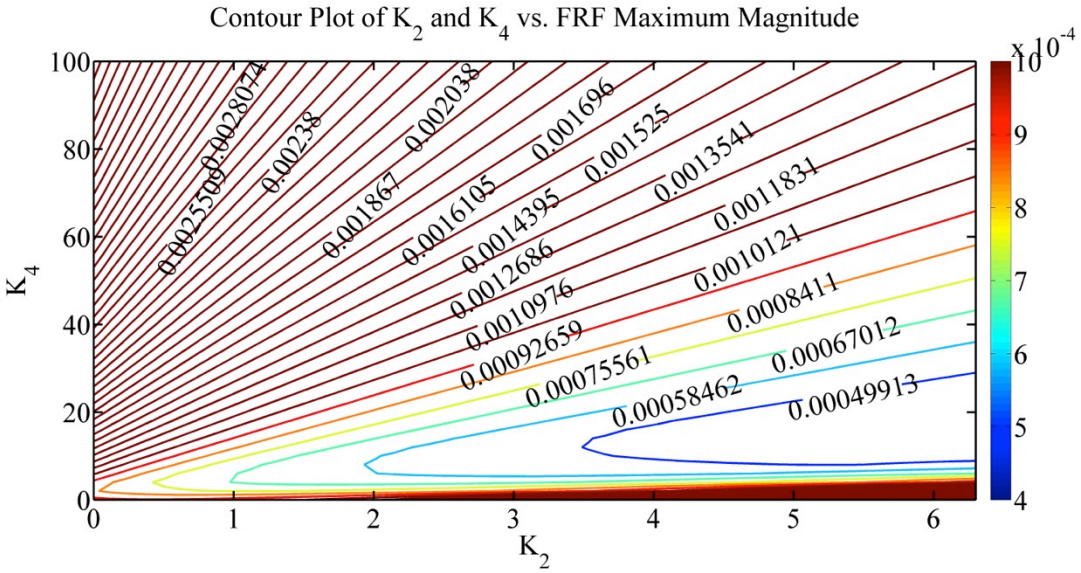

Figure 3-23- Contour plot of variation of structural acceleration and TMD velocity gains against maximum of FRF magnitude.

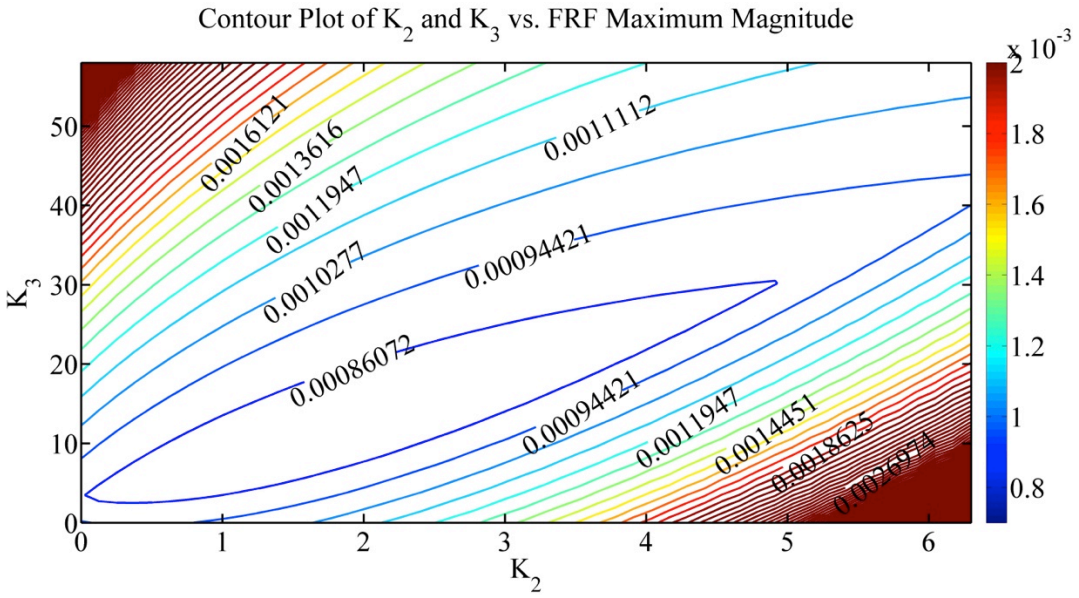

Figure 3-24- Contour plot of variation of structural acceleration and velocity gains against maximum of FRF magnitude

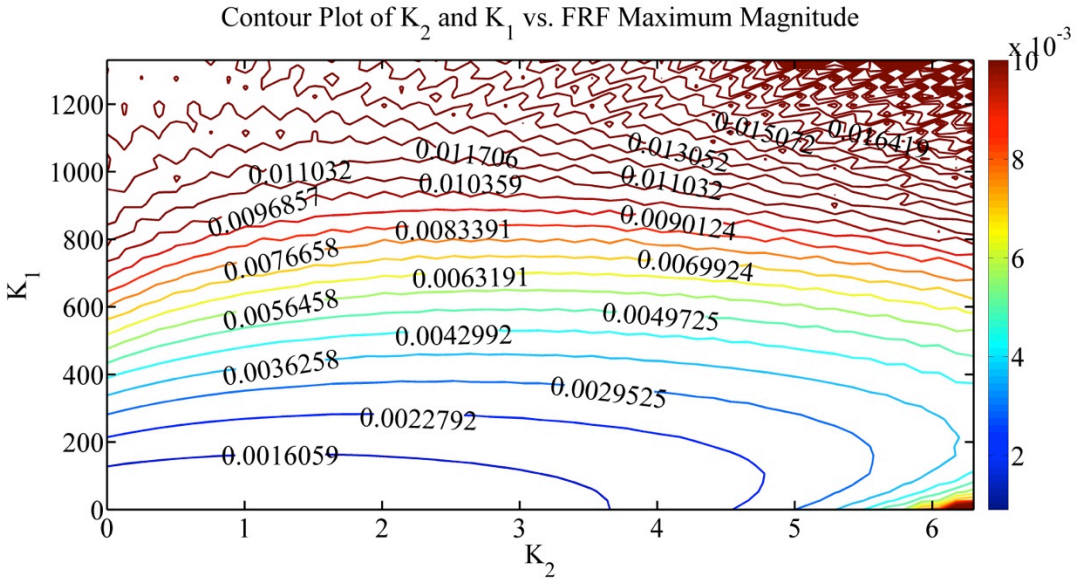

Figure 3-25-Contour plot of variation of structural acceleration and TMD displacement gains against maximum of FRF magnitude

Table 3-7 shows the minimum of the maximum magnitude of the FRFs for different gains. It should be noted that K_3 is feedback gain of the velocity of the main structure, K_2 is feedback gain of acceleration of the main structure, K_1 is feedback gain of displacement of the TMD, K_4 is feedback gain of velocity of the TMD and K_5 is feedback gain of the acceleration of the TMD.

Table 3-7- Peak of FRF response and corresponding frequencies for different gains

Gain Type	Gains	Min. of the FRF max ($m/sec^2/N$)	Frequency of the 1st FRF peak (Hz)	Frequency of the 2nd FRF peak (Hz)	Range of frequency of the 1st FRF peak (Hz)	Range of frequency of the 2nd FRF peak (Hz)
TMD	0	0.00095	4.06	4.87	-	-
K_3	-3.19	0.00086	4.06	4.87	3.91-4.06	4.87-4.98
K_2	-0.441	0.00093	3.96	4.98	3.47-4.06	4.87-5.71
K_1	0.00	0.00095	4.06	4.87	4.06-4.47	4.87-6.33
K_4	-2.5	0.00085	4.17	4.74	4.06-4.23	4.50-4.87
K_5	-0.036	0.00087	4.03	4.85	3.33-4.06	4.66-4.87
K_2 and K_4	-6.30& -20.00	0.00041	-	5.32	3.43-4.25	4.50-5.74
K_2 and K_3	-1.764 & -10.44	0.00078	3.79	5.20	3.39-4.05	4.87-5.71
K_2 and K_1	-0.378 & 0.00	0.00093	3.97	4.96	3.47-4.47	4.87-6.73
K_2 and K_5	-1.008 & -0.096	0.00082	3.80	5.01	3.05-4.06	4.66-5.71
K_4 and K_3	-2.00& -1.16	0.00084	4.13	4.77	3.91-4.22	4.50-4.98
K_4 and K_1	-2.00& 0.00	0.00085	4.13	4.77	4.06-4.47	4.18-6.65
K_4 and K_5	-2.00& 0.00	0.00085	4.13	4.77	3.20-4.14	4.50-4.87
K_1 and K_3	0.00& -3.48	0.00086	4.05	4.87	3.91-4.47	4.87-6.41
K_1 and K_5	0.00& -0.032	0.00087	4.02	4.85	3.33-4.47	4.66-6.33
K_5 and K_3	-0.016& -1.74	0.00086	4.04	4.87	3.17-4.06	4.66-4.98

Comparing the result of each single and gain pair in Table 3-7 with the equivalent passive TMD leads to Table 3-8, which can be used to draw some conclusions about employing single and couple feedback gains in HTMD.

Table 3-8- Comparison of the response reduction and frequency variation for different gains against passive TMD

Gain Type	Further reduction of FRF maximum magnitude	Changing of the frequency of the 1st FRF peak	Changing of the frequency of the 2nd FRF peak
TMD	0%	0%	0%
K_3	9%	4%	-2%
K_2	2%	15%	-17%
K_1	0%	-10%	-29%
K_4	11%	-4%	8%
K_5	8%	18%	4%
K_2 and K_4	57%	-5% to 16%	-18% to 8%
K_2 and K_3	18%	17%	-17%
K_2 and K_1	2%	-10% to 15%	-38%
K_2 and K_5	14%	25%	-17% to 4%
K_4 and K_3	12%	-4% to 4%	-2% to 8%
K_4 and K_1	11%	-10%	-37% to 14%
K_4 and K_5	11%	-2 % to 21%	8%
K_1 and K_3	9%	-10% to 4%	-32%
K_1 and K_5	8%	-10% to 18%	-30% to 4%
K_5 and K_3	9%	22%	-2% to 4%

As Table 3-8 reveals, employing one feedback gain does not have a large influence on response reduction. However, employing two gains improves the reduction in the maximum response. The combination of K_2 and K_4 has the most structural acceleration response reduction in comparison with passive TMD. Hence, using one response feedback gain is not an appropriate choice.

If we consider the effect of each gain on the variation of the frequency, it can be concluded from Table 3-8 that the combination of the displacement and acceleration of TMD feedback (i.e. K_1 and K_5) with different gains has a significant effect on the changing of frequencies of both peaks of the FRF. This means that to tune the TMD to a new frequency, it is an appropriate choice to employ K_1 and K_5 as tuning gains. Moreover, using velocity of the structure as a feedback does not have a large influence neither on response magnitude nor on modifying the frequencies because the damping forces imparted by the actuator are small and have little influence on the structural damping.

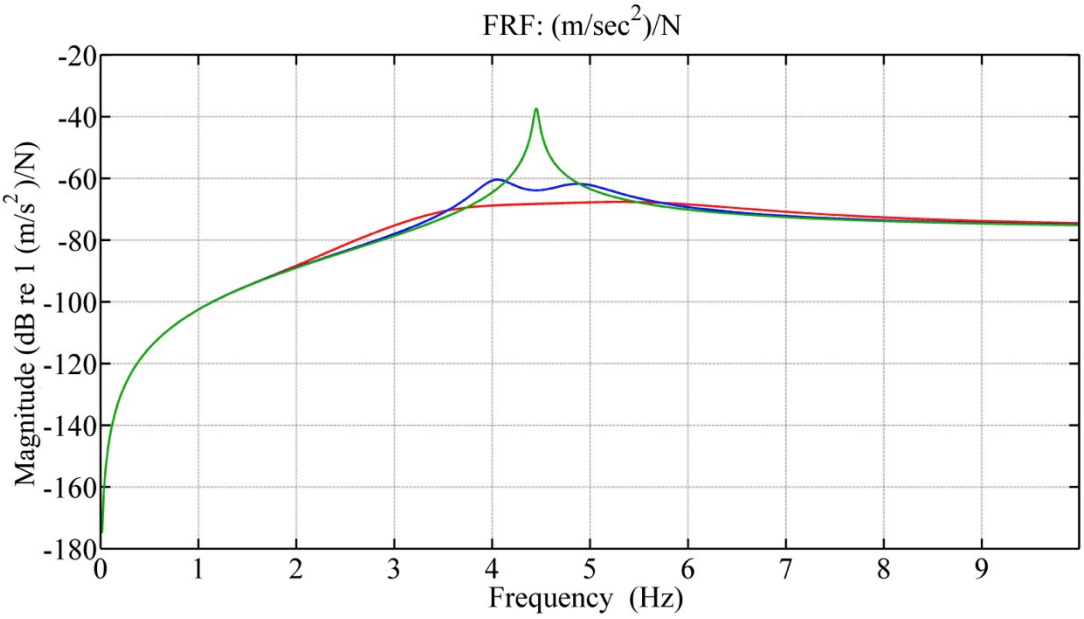

Figure 3-26- FRF of the uncontrolled structure (green) in comparison with structure with TMD (blue) and HTMD with manually optimised gains (red)

Figure 3-26 shows the result of the simulation with K_2 and K_4 employed on HTMD as feedback gains. This result is compared with the TMD designed in Section 3.3.3. Table 3-9 shows the comparison of the peak response reduction between TMD and HTMD. As illustrated, there is a significant reduction in the response of the structure using HTMD in comparison with passive TMD. HTMD has 56% reduction in the maximum FRF response and 40% response reduction at the resonance frequency compared with passive TMD.

Table 3-9- Simulation result comparison of the manual optimised gains

	Uncontrolled Structure	Structure with TMD	Structure with HTMD
Max. response magnitude ($m/s^2/N$)	0.0135	0.00095	0.00041
Reduction of the max. response	-	93%	97%
Response magnitude at resonance ($m/s^2/N$)	0.0135	0.00064	0.00038
Reduction of response at resonance	-	95%	97%

The manual optimisation method presented here can be employed for initial design of the system. However, there are some limitations of using this method. Firstly, since it is time consuming to utilise a small increment for the gains, it is possible to miss global maximum points of responses and only achieve local maxima. In addition, for the same reason it is not possible to combine more than two gains and check the effect of that on structure (i.e. driving force gain, active damping force gain and tuning force gains). Also, there exists the chance for the peaks of FRF to be outside of the boundary as discussed in Section 3.3.3.2. Hence, although the minimum responses between FRF peaks have been chosen in the above tables, these peaks could be outside the boundary of the uncontrolled structure FRF that leads to increase of the response at the non-resonant frequencies.

To deal with this, the author introduces other optimisation methods which will be discussed here.

3.6.2. LQR control

As previously noted, linear quadratic regulator (LQR) is an optimal control method which involves minimising a selected cost function for a dynamic system. In this section, two LQR approaches are introduced. For the first LQR method, the common method described in [163] is chosen. In this method, the states of the system (i.e. displacement and velocity of the structure and TMD) are concerned. In the second

method, the derivative of the states (i.e. velocity and acceleration of the structure and TMD) are used instead as the feedback parameters of the system, as derived in [134]. The results of the two methods are then compared.

3.6.2.1.LQR on the states of the system

In a SS system such as $\dot{X}_{lqr} = A_{lqr}X_{lqr} + B_{lqr}U_{lqr}$ the goal of LQR is to determine the control action $U_{lqr} = -K_{lqr}X_{lqr}$ to minimise the cost function J_{lqr} where K_{lqr} is the LQR feedback gain matrix, U_{lqr} is the control force and X_{lqr} is the state matrix of the system. The quadratic cost function is described as

$$J_{lqr} = \int_0^\infty \left({X_{lqr}}^T Q_{lqr} X_{lqr} + {U_{lqr}}^T R_{lqr} U_{lqr}\right) dt \quad \textbf{(3.62)}$$

Q_{lqr} and R_{lqr} are state and control weighting matrices, respectively, and K_{lqr} can be determined from following equation

$$K_{lqr} = {R_{lqr}}^{-1} {B_{lqr}}^T P_{lqr} \quad \textbf{(3.63)}$$

where P_{lqr} can be generated by solving the following Riccati differential equation.

$${A_{lqr}}^T P_{lqr} + P_{lqr} A_{lqr} - P_{lqr} B_{lqr} {R_{lqr}}^{-1} {B_{lqr}}^T P_{lqr} + Q_{lqr} = 0 \quad \textbf{(3.64)}$$

In addition, Q_{lqr} and R_{lqr} can be calculated from the following equations.

a) $Q_{ii,lqr} = \frac{1}{{X_{i,lqr}}^2}$

b) $R_{jj,lqr} = \rho_{lqr} \frac{1}{{U_{j,lqr}}^2}$ **(3.65)**

Where ρ_{lqr} is a trade-off factor between controller (actuator) and response, $X_{i,lqr}$ is the range of the states and $U_{j,lqr}$ is the range of the controller effort. According to BS6472 [164], the maximum RMS acceleration for the frequency of 4.5 Hz (fisrt vertical modal frequency of the structure) is 0.005 m/s^2. Converting the acceleration

to the velocity and displacement by multiplying with $\frac{1}{(4.5*2\pi)}$ and $\frac{1}{(4.5*2\pi)^2}$ respectively, Table 3-10 is generated which is the range of the states (i.e. $X_{i,lqr}$).

Table 3-10- Range of the structure states and derivative of states at 4.5 Hz to be used in LQR

State	Maximum accepted RMS value
Structure acceleration (m/s^2)	0.005
Structure velocity (m/s)	0.0001768
Structure displacement (m)	0.00000625

Also, considering the response of the TMD as other states of the system and using same methodology, it is possible to calculate the maximum range of the system states relating to the TMD based on the maximum displacement of the TMD mass of 0.1 m. Then by multiplying it by $(4.5 * 2\pi)$ and $(4.5 * 2\pi)^2$ to get maximum range of the velocity and acceleration of the TMD respectively, it is possible to generate Table 3-11. It should be mentioned the limit of the TMD displacement arises from the practical restriction of the prototype HTMD which will be discussed further in Chapter 6.

Table 3-11- Range of the TMD states and derivative of states at 4.50Hz to be used in LQR

State	Maximum accepted value
TMD acceleration (m/s^2)	80
TMD velocity (m/s)	2.8
TMD displacement (m)	0.1

Based on the maximum capability of the actuator (U_{lqr}) as discussed in chapter 3.4.1, the maximum possible voltage input to the actuator is 2.0 V. Consequently, it is possible to create the Q_{lqr} and R_{lqr} matrices. Now, if we consider the Figure 3-27 as the standard form of the feedback control, it is possible to modify the state space model introduced in Section 3.4.2.2. This should have the control voltage as the only input vector of the state space model by rejecting the external excitation force (i.e.

F_{ext}) as an input and considering it as the disturbance. Hence, the new state space system is introduced as equations (3.66).

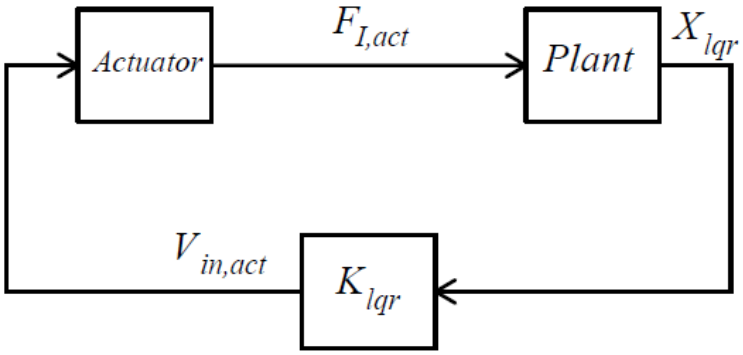

Figure 3-27- Configuration of the feedback system using LQR on system states

a) $A_{lqr} = A_{HTMD}$

b) $X_{lqr} = X_{HTMD}$

c) $B_{lqr} = \begin{bmatrix} 0 \\ 0 \\ 0 \\ 0 \\ 0 \\ 0 \\ v_{act} \end{bmatrix}$ **(3.66)**

d) $U_{lqr} = \{V_{in,act}\}$

It should be noted that the modified state space system is employed only to calculate the LQR feedback matrix (i.e. K_{lqr}). Then K_{lqr} is applied to the original state space model that was introduced in Section 3.4.2.2 and all the simulations are executed based on that model.

Now, based on equations (3.66) and also Table 3-10 and Table 3-11, it is possible to construct Q_{lqr} and R_{lqr} as follows:

$$Q_{lqr} = \begin{bmatrix} \frac{1}{0.00000625^2} & 0 & 0 & 0 & 0 & 0 & 0 \\ 0 & \frac{1}{0.0001768^2} & 0 & 0 & 0 & 0 & 0 \\ 0 & 0 & \frac{1}{0.1^2} & 0 & 0 & 0 & 0 \\ 0 & 0 & 0 & \frac{1}{2.8^2} & 0 & 0 & 0 \\ 0 & 0 & 0 & 0 & 0 & 0 & 0 \\ 0 & 0 & 0 & 0 & 0 & 0 & 0 \\ 0 & 0 & 0 & 0 & 0 & 0 & 0 \end{bmatrix} \quad \textbf{(3.67)}$$

and

$$R_{lqr} = \rho_{lqr} \left[\frac{1}{2.0^2}\right] \quad \textbf{(3.68)}$$

ρ_{lqr} in this study is calculated by employing the sensitivity approach and is based on the change in the response by varying ρ_{lqr} to achieve the desirable result. It should be mentioned that decreasing ρ_{lqr} leads to putting more effort on the actuator. Therefore, there should be a balance between the control performance and the actuator capability. Solving the LQR equations and setting $\rho_{lqr} = 10^{-24}$ results in the following feedback matrix which will be employed for later simulation (Section 3.6.2.3).

$$K_{lqr} = [\,423.94 \quad -24.82 \quad -121.85 \quad -4.59 \quad 0 \quad 0 \quad 0] \quad \textbf{(3.69)}$$

The last four columns are calculated as zero since there is no effect on these states as they relate to the actuator dynamics.

3.6.2.2.LQR on the derivatives of the states

As previously discussed, employing acceleration of the structure as one of the feedback parameters is important in terms of reduction in response using the HTMD. However, since acceleration of the structure (and TMD as well) is not a state of the system (i.e. it is a derivative of a state) it is not possible to use the normal LQR method as an optimal technique. However, [134] introduced a new technique in

which the derivative of the system is employed instead of the state itself (Figure 3-28).

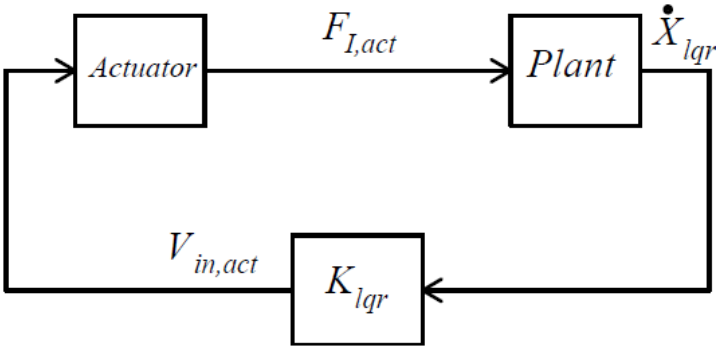

Figure 3-28- Configuration of the feedback system using modified LQR on derivative of the system state

It means that instead of using $U_{lqr} = -K_{lqr}X_{lqr}$, the new method proposed to use $U_{lqr} = -K_{lqr}\dot{X}_{lqr}$. Then, the modified quadratic cost function is described as

$$J_{lqr} = \int_0^\infty \left(\dot{X}_{lqr}{}^T Q_{lqr} \dot{X}_{lqr} + U_{lqr}{}^T R_{lqr} U_{lqr}\right) dt \qquad \textbf{(3.70)}$$

The modified K_{lqr} can be determined from following equation.

$$K_{lqr} = R_{lqr}{}^{-1} B_{lqr}{}^T A_{lqr}{}^{-T} P_{lqr} \qquad \textbf{(3.71)}$$

And the modified P_{lqr} can be generated by solving the following Riccati differential equation.

$$A_{lqr}{}^{-T} P_{lqr} + P_{lqr} A_{lqr}{}^{-1} - P_{lqr} A_{lqr}{}^{-1} B_{lqr} R_{lqr}{}^{-1} B_{lqr}{}^T A_{lqr}{}^{-T} P_{lqr} + Q_{lqr} = 0 \qquad \textbf{(3.72)}$$

In addition, due to using the derivative of the state, the modified Q_{lqr} is introduced as

$$Q_{lqr} = \begin{bmatrix} \frac{1}{0.0001768^2} & 0 & 0 & 0 & 0 & 0 & 0 \\ 0 & \frac{1}{0.005^2} & 0 & 0 & 0 & 0 & 0 \\ 0 & 0 & \frac{1}{2.8^2} & 0 & 0 & 0 & 0 \\ 0 & 0 & 0 & \frac{1}{80^2} & 0 & 0 & 0 \\ 0 & 0 & 0 & 0 & 0 & 0 & 0 \\ 0 & 0 & 0 & 0 & 0 & 0 & 0 \\ 0 & 0 & 0 & 0 & 0 & 0 & 0 \end{bmatrix} \quad \textbf{(3.73)}$$

Applying a similar sensitivity approach makes it possible to generate ρ_{lqr}. Solving the modified LQR equations and setting $\rho_{lqr} = 10^{-24}$ results in the following feedback matrix which will be employed later in the simulation (Section 3.6.2.3).

$$K_{lqr} = [-2.89 \quad -1.12 \quad -6.65 \quad 0.02 \quad 0 \quad 0 \quad 0] \quad \textbf{(3.74)}$$

Similar to the previous approach, the last four columns are calculated as zero since there is no effect on these states as they relate to the actuator dynamics. Furthermore, the velocities of the structure and TMD have are very small numbers in comparison with their applicable ranges.

3.6.2.3.Simulation

To simulate the system, the proposed state space model in Section 3.4.2.2 was programmed in MATLAB Simulink [165] using the dynamic properties of the structure and TMD calculated before in addition to the LQR feedback gain matrices determined for both proposed methods.

Figure 3-29 shows the FRF results of these simulations. The two LQR techniques are compared against the passive TMD.

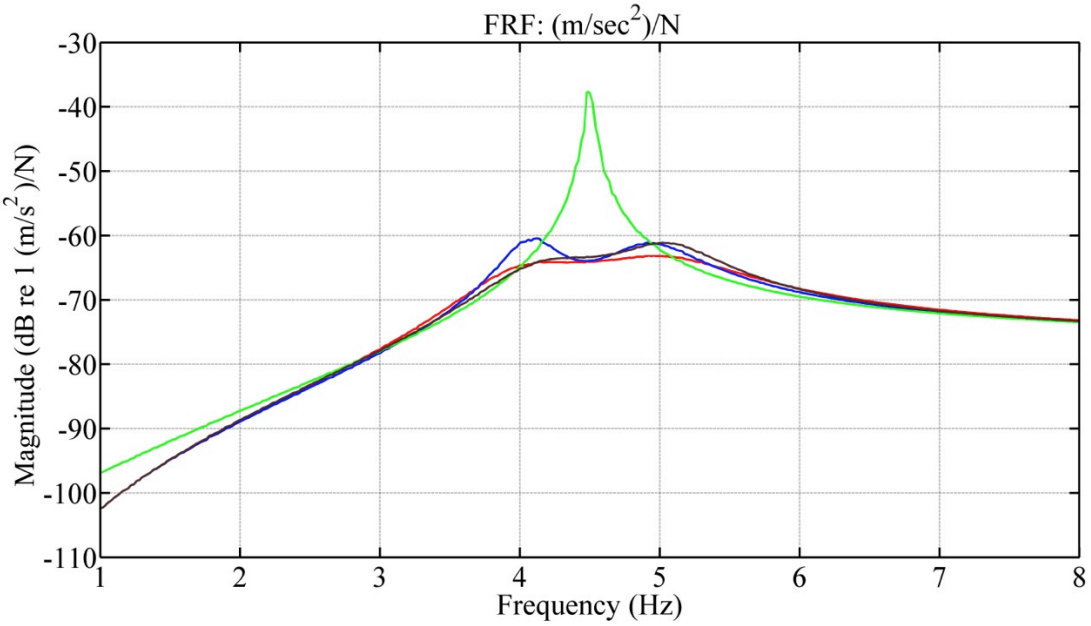

Figure 3-29- FRF of the uncontrolled structure (green) in comparison with structure with TMD (blue) and HTMD with modified LQR (red) and HTMD with conventional LQR (brown)

Table 3-12 gives a numerical comparison of the different techniques. The modified LQR method has the reduction of 27% and 35% for the peak of the FRF and FRF's response at the resonant frequency respectively in comparison with passive TMD. Meanwhile, the conventional LQR technique has the reduction of 8% and 29% for the peak of the FRF and FRF's response on resonant frequency respectively in comparison with passive TMD.

Table 3-12- Simulation result comparison of LQR methods and passive TMD

	Uncontrolled Structure	Structure with TMD	HTMD with conventional LQR	HTMD with modified LQR
Max. response magnitude ($m/s^2/N$)	0.0135	0.00095	0.00087	0.00069
Reduction of the max. response	-	93%	94%	95%
Response magnitude at resonance ($m/s^2/N$)	0.0135	0.00064	0.00067	0.00062
Reduction of response at resonance	-	95%	95%	95%

3.7. Closed loop stability of the system

A stability check of a closed-loop system is an important aspect in active control methods [7], [145]. One of the methods to determine the stability of a closed loop system is to investigate whether or not the poles of the system lie on the left hand plane of the *s*-plane plot. If so, the system is asymptotically stable [166].

The stability of a SIMO system can be investigated by using two techniques. First by evaluating the zeros of the closed loop system (i.e. roots of $1 + K_c(s)G(s)$ where $K_c(s)G(s)$ is the transfer function of the loop in Figure 3-30). Second, by using the Nyquist plot of $K_c(s)G(s)$ and considering whether it does not encircle point (-1,0) [150], [163].

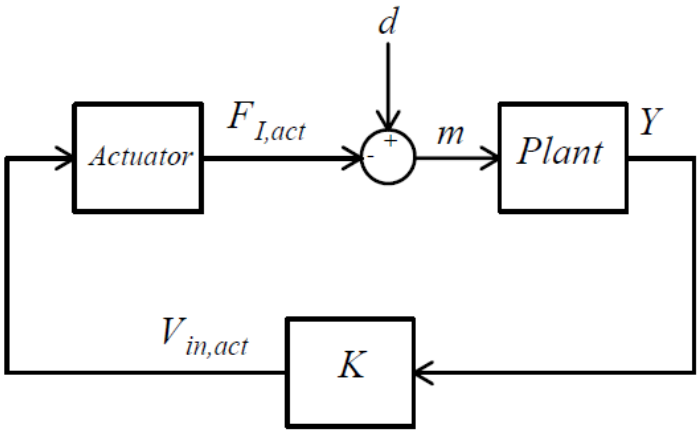

Figure 3-30- Block diagram of typical feedback control scheme

Developing the closed loop transfer function from Figure 3-30 leads to

a) $m = d - F_{I,act} \;\; \therefore m = d - \{k\}\{Y\}G_{act}$

b) $\{Y\} = m\{G_{Plant}\}$ **(3.75)**

Substituting two parts of the equation results in

$$\frac{d}{m} = \{k\}\{G_{Plant}\}G_{act} \quad \textbf{(3.76)}$$

Where $\{k\}$ is the feedback vector of the different types of outputs (i.e. structure or TMD responses) and $\{G_{Plant}\}$ is the vector of the transfer functions between the structure or TMD responses and the control force.

For the first technique, the zeros of the following equation should be on the left hand side of the *s*-plane .

$$1 + \{k\}\{G_{Plant}\}G_{act} \quad \textbf{(3.77)}$$

For the second technique, the Nyquist plot of the following equation should not encircle point (-1,0).

$$\{k\}\{G_{Plant}\}G_{act} \quad \textbf{(3.78)}$$

From the state space model presented in Section 3.4.2.2 it is possible to generate transfer functions (i.e. G_{Plant}) between different structural/TMD responses (i.e. Y_{HTMD}) and the control force (i.e. $F_{I,act}$) using the MATLAB [165] 'SS2TF' function (equations (3.79)). In addition, G_{act} is derived from equation (3.38). Depending on the type of control (e.g. LQR, modified LQR, Direct Response Feedback, etc.) the $\{k\}$ matrix can be generated.

a) $G\_(Plant,1) = (1.421e-014\,s\text{^}6 + 1.364e-012\,s\text{^}5 + 0.0008698\,s\text{^}4 + 0.1668\,s\text{^}3 + 7.787\,s\text{^}2 + 97.97\,s + 887.1)/(s\text{^}7 + 69.98\,s\text{^}6 + 2854\,s\text{^}5 + 1.21e005\,s\text{^}4 + 2.318e006\,s\text{^}3 + 5.654e007\,s\text{^}2 + 5.492e008\,s + 4.957e9)$

b) $G\_(Plant,2) = (2.842e-014\,s\text{^}6 + 0.0008698\,s\text{^}5 + 0.1668\,s\text{^}4 + 7.787\,s\text{^}3 + 97.97\,s\text{^}2 + 887.1\,s - 7.629e-006)/(s\text{^}7 + 69.98\,s\text{^}6 + 2854\,s\text{^}5 + 1.21e005\,s\text{^}4 + 2.318e006\,s\text{^}3 + 5.654e007\,s\text{^}2 + 5.492e008\,s + 4.957e9)$

c) $G\_(Plant,3) = (0.0008698\,s\text{^}6 + 0.1668\,s\text{^}5 + 7.787\,s\text{^}4 + 97.97\,s\text{^}3 + 887.1\,s\text{^}2 - 2.384e-007\,s - 4.768e-006)/(s\text{^}7 + 69.98\,s\text{^}6 + 2854\,s\text{^}5 + 1.21e005\,s\text{^}4 + 2.318e006\,s\text{^}3 + 5.654e007\,s\text{^}2 + 5.492e008\,s + 4.957e9)$

d) $G\_(Plant,4) = (1.421e-014\,s\text{^}6 + 0.003077\,s\text{^}5 + 0.1966\,s\text{^}4 + 5.189\,s\text{^}3 + 188.7\,s\text{^}2 + 2109\,s + 2.041e004)/(s\text{^}7 + 69.98\,s\text{^}6 + 2854\,s\text{^}5 + 1.21e005\,s\text{^}4 + 2.318e006\,s\text{^}3 + 5.654e007\,s\text{^}2 + 5.492e008\,s + 4.957e9)$ **(3.79)**

e) $G\_(Plant,5) = (0.003077\,s\text{^}6 + 0.1966\,s\text{^}5 + 5.189\,s\text{^}4 + 188.7\,s\text{^}3 + 2109\,s\text{^}2 + 2.041e004\,s - 6.676e-006)/(s\text{^}7 + 69.98\,s\text{^}6 + 2854\,s\text{^}5 + 1.21e005\,s\text{^}4 + 2.318e006\,s\text{^}3 + 5.654e007\,s\text{^}2 + 5.492e008\,s + 4.957e9)$

f) $G\_(Plant,6) = (0.003077\,s\text{^}7 + 0.1966\,s\text{^}6 + 5.189\,s\text{^}5 + 188.7\,s\text{^}4 + 2109\,s\text{^}3 + 2.041e004\,s\text{^}2 - 1.192e-007\,s - 2.861e-006)/(s\text{^}7 + 69.98\,s\text{^}6 + 2854\,s\text{^}5 + 1.21e005\,s\text{^}4 + 2.318e006\,s\text{^}3 + 5.654e007\,s\text{^}2 + 5.492e008\,s + 4.957e9)$

where $G_{Plant,1}$ to $G_{Plant,6}$ are the transfer functions between $F_{I,act}$ and displacement, velocity and acceleration of the structure and TMD respectively.

3.7.1. Stability of the closed loop system using the Direct Response Feedback method

Figure 3-31 shows the pole-zero map of the structure with HTMD attached using the manually optimized gains discussed in Section 3.6.1.1. This is the scenario with acceleration of the structure and velocity of the TMD as two feedbacks. As demonstrated, all poles and zeros of the closed loop system are on the left hand side of the *s*-plane, which shows a stable system.

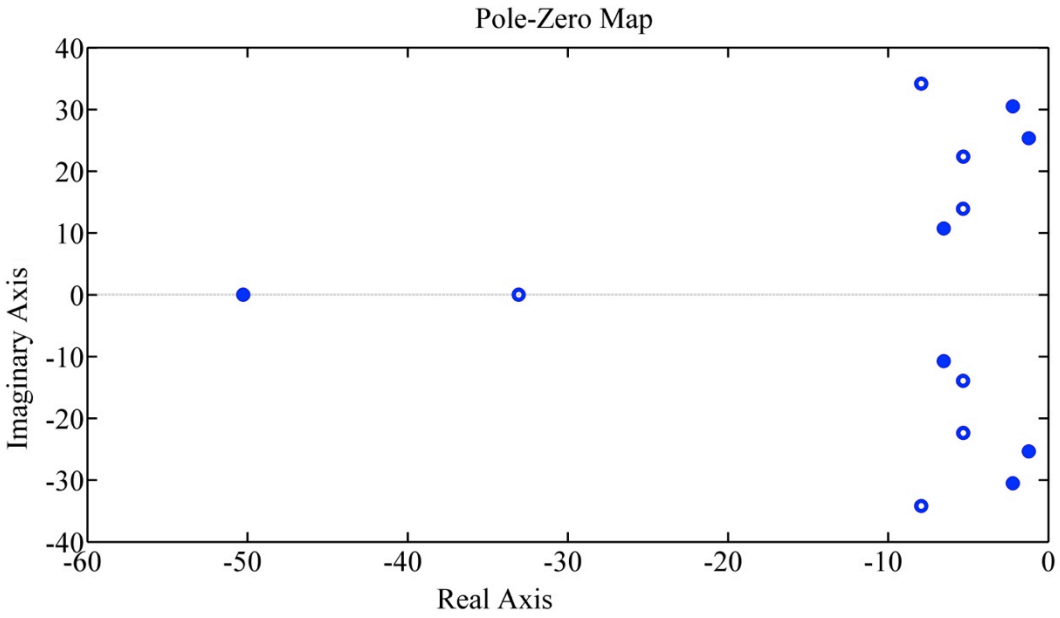

Figure 3-31- Pole-Zero map of the closed loop HTMD system using manually optimised gains

Figure 3-32 illustrates the Nyquist plot of the same system. Clearly, there is no encirclement around point (-1,0) and hence this guarantees the stability of the closed loop system.

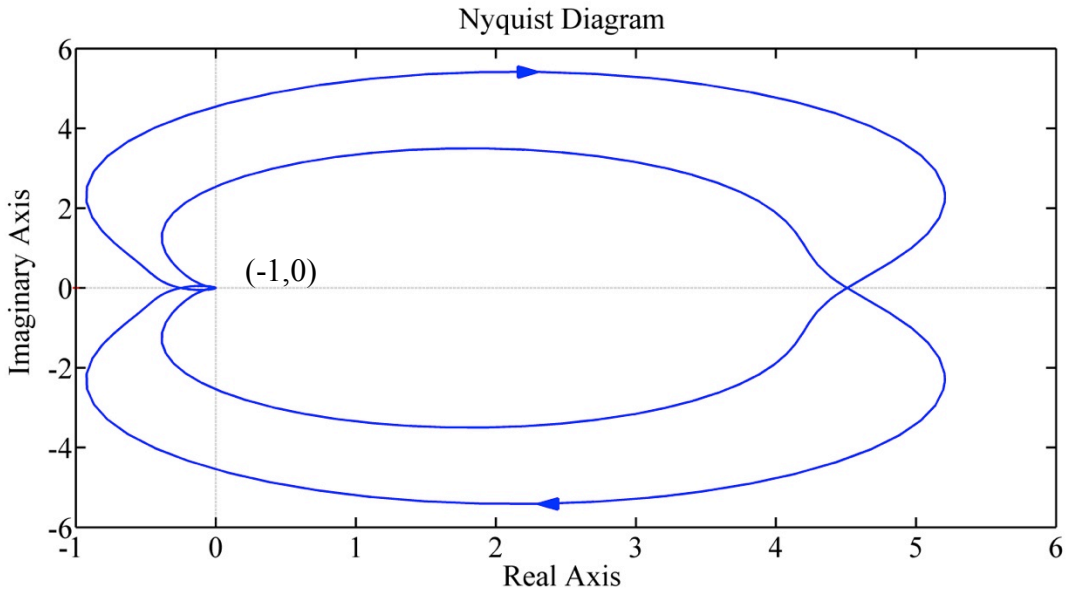

Figure 3-32- Nyquist plot of the closed loop HTMD system using manually optimised gains

3.7.2. Stability of the closed loop system using LQR method on the states of the system

Figure 3-33 shows the pole-zero map of the structure with HTMD attached using the conventional LQR method discussed in Section 3.6.1.1. This is the scenario with displacement and velocity of both structure and TMD used as four feedback gains. As demonstrated, all poles and zeros of the closed loop system are on the left hand side of the *s*-plane, which shows a stable system.

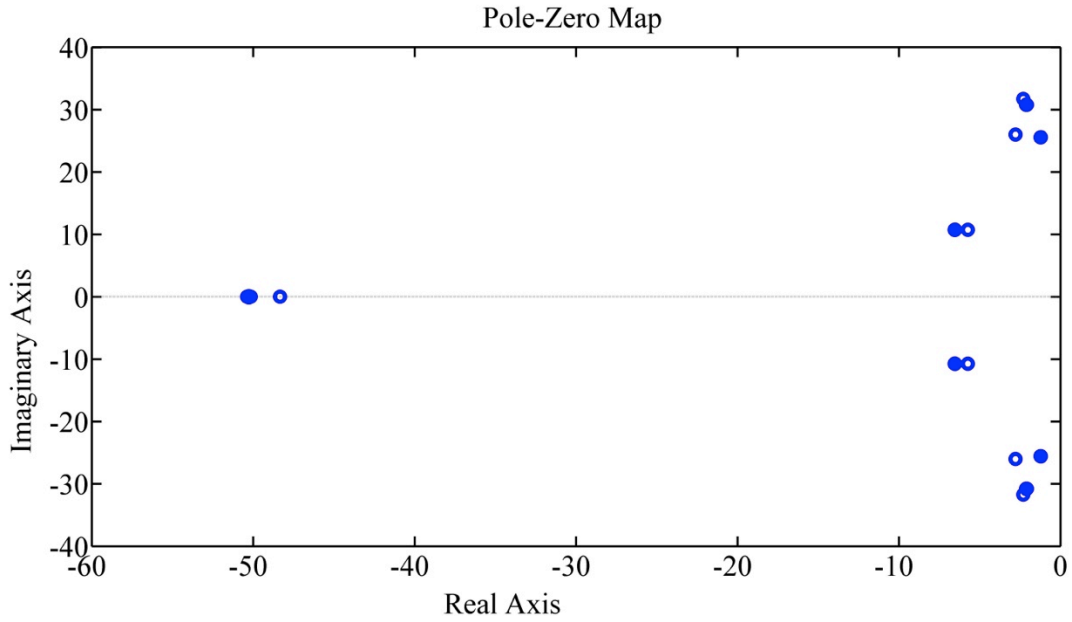

Figure 3-33- Pole-Zero map of the closed loop HTMD system using conventional LQR method

Figure 3-34 illustrates the Nyquist plot of the same system. Clearly, there is no encirclement around point (-1,0) and this secures the stability of the closed loop system.

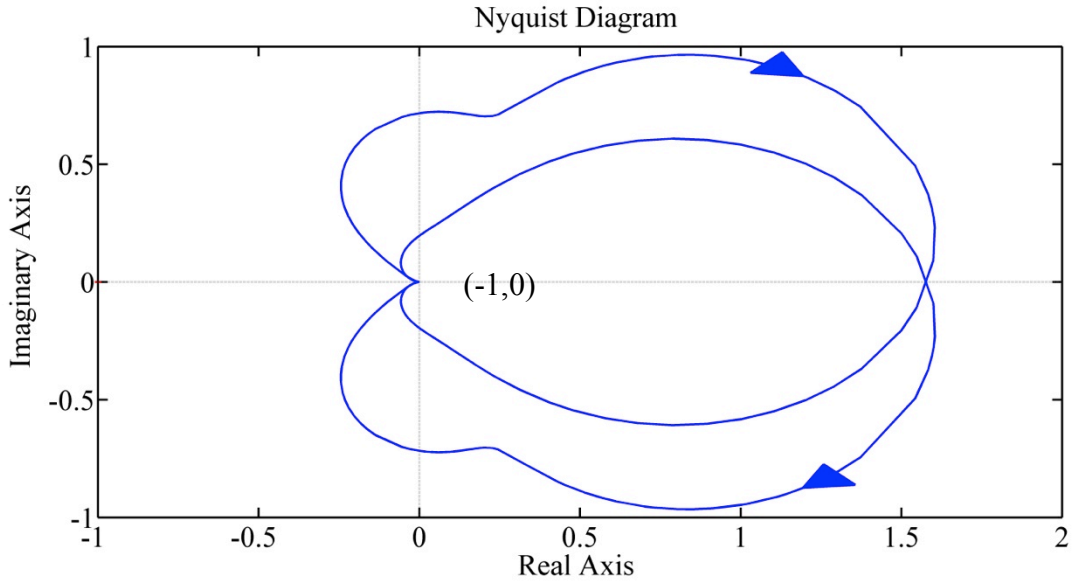

Figure 3-34- Nyquist plot of the closed loop HTMD system using conventional LQR method

3.7.3. Stability of the closed loop system using LQR method on the derivative of the states

Figure 3-35 shows the pole-zero map of the structure with HTMD attached using modified LQR method discussed in chapter 3.6.1.1. This is the scenario with velocity and acceleration of both structure and TMD used as four feedback gains. As demonstrated, all poles and zeros of the closed loop system are on the left hand side of the *s*-plane, which shows a stable system.

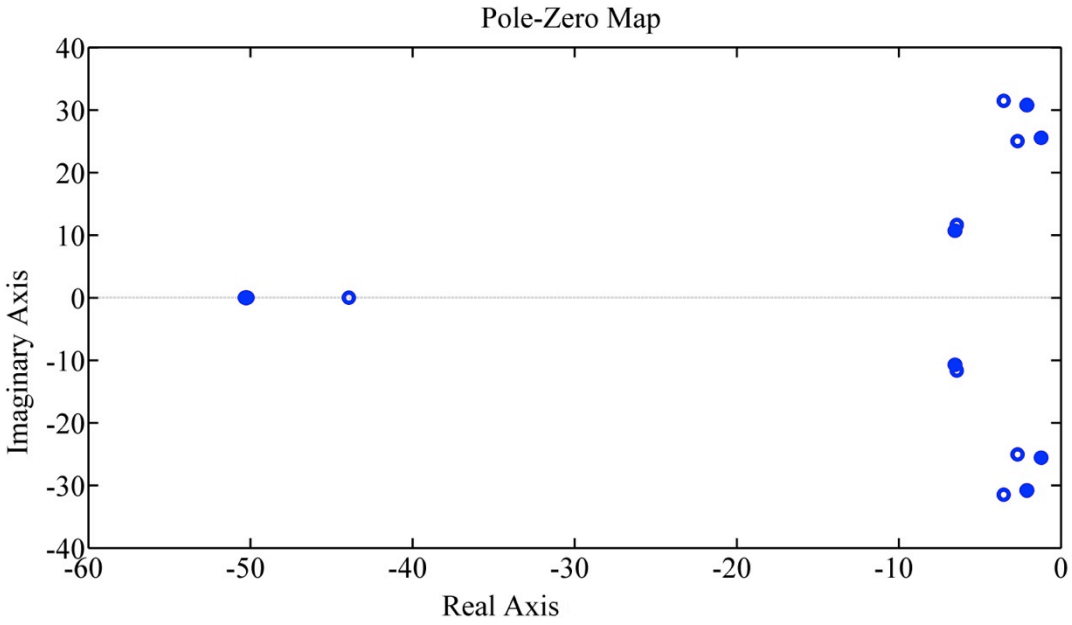

Figure 3-35- Pole-Zero map of the closed loop HTMD system using modified LQR method

Figure 3-36 illustrates the Nyquist plot of the same system. Clearly, there is no encirclement around point (-1,0) and this secures the stability of the closed loop system.

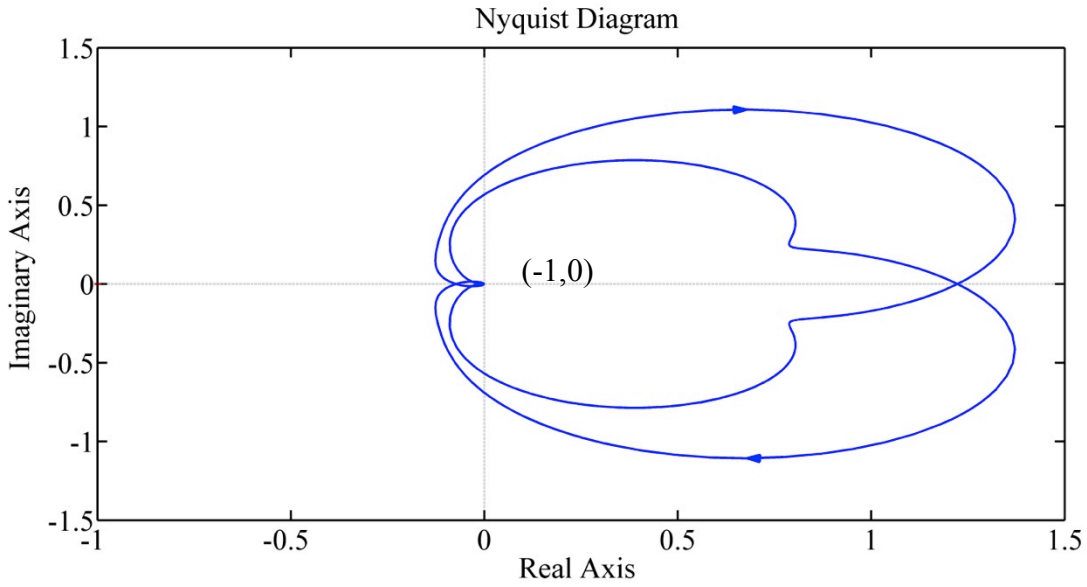

Figure 3-36- Nyquist plot of the closed loop HTMD system using modified LQR method

3.8. Conclusion and result discussion

In this chapter, a set of models for the structure with TMD, AMD and HTMD attached were derived (These models will be further investigated and compared with experimental results in chapters 6). Then, three different control schemes will be proposed.

In the first method, responses (i.e. displacement, velocity or acceleration) of both the TMD and primary structure were employed as the feedback-signal. To determine appropriate gains, a manual optimisation method was employed to check different gains and calculate the minimum structural response. Using this method makes it possible firstly to determine an appropriate combination of the gains and secondly to calculate the appropriate gains in the achieved combination. This method shows the largest reduction in response compared with conventional and modified LQR methods which are proposed as two additional techniques. However, due to the large amount of calculation, firstly it is not possible to check more than two combinations of gains. Also, using smaller incremental steps is highly costly since it increases the required computational effort. Hence the chance of missing the global minimum and achieving a local minimum response exists. However, the greatest advantage of

applying this technique is to investigate the behaviour and effect of each gain on the system.

Conversely, using conventional and modified LQR methods are two formal methods in the case of time and cost of simulation. However, since each method is restricted to either states or derivative of states of the system, it is not possible to use all demanded combination of the gains which were investigated in the first method (e.g. using displacement of TMD as a state in the combination with acceleration of the TMD as the derivative of the state). Hence, the performance of HTMD is lower than for the first technique.

Combining the results of the three proposed methods leads to the idea of applying a more suitable optimization method which can search through the areas of the responses and then generate the most appropriate control gains which ensure the minimum response inside the boundary of the uncontrolled structure. The new proposed method should be applicable for use with any combination of gains.

Hence author will introduce an optimisation technique using a genetic algorithm is introduced in the next chapter which can evaluate any combinations of gains (not only two) and derive the most appropriate gains through that.

4. Optimisation of HTMD system

As previously demonstrated, choosing and optimising the feedback control gains is a key aspect of HTMD performance. An approach is required that can produce the minimum possible structural response with optimum feedback gains combination and good computational efficiency.

Hence, the author introduces a new optimisation approach using a genetic algorithm (GA). The study presented here will illustrate that the GA approach can find a set of gains of any combination which causes the structure to have the minimum possible response. Then, the stability of the closed-loop system is investigated.

Finally, a numerical simulation using MATLAB Simulink is carried out to investigate three main aspects. Firstly, a comparison of the response reductions in the frequency domain between different control methods is presented. Then, a time domain analysis of structural response to a modelled jumping force is carried out and the response of the structure is checked against appropriate limits. Finally, the amount of power required for the HTMD and AMD is determined and hence the actuator effort is investigated for each method.

4.1. Gain optimisation

Herein, the author employs a similar technique as proposed in Section 3.3.3.2, except that the same parameters of the passive TMD are used as previously and it is the feedback gains which need to be optimised. Hence, the critical variables are changed from TMD parameters (i.e. mass, damping and stiffness) to the HTMD control gains (i.e. K_i).

Also, to investigate the effect of all relevant gain factors simultaneously and to explore which combination of gains is most suitable, all five feedback gains from Table 3-6 are chosen as critical variables.

4.1.1. Gain optimisation using GA

As Figure 4-1 illustrates, the aim of using the HTMD is to minimize the response of the structure in a desirable band of frequencies (ω_i) by using appropriate control gains. Hence, the critical values of the GA are the gains of the feedback system which should be optimized in a way that reduces the FRF of the structure

($H_{HTMD}(\omega_i)$) as the objective function. However, it should be noted that the FRF of the controlled structure should be inside the boundary of the FRF of the uncontrolled structure ($H_{unc}(\omega_i)$) to avoid higher responses at non-resonant frequencies. This means for each ω_i, the response of the controlled structure due to the external force ($H_{HTMD}(\omega_i)$) should be as minimum as possible. Also for each ω_i, the response of the controlled structure due to the external force ($H_{HTMD}(\omega_i)$) should be less than the response of the uncontrolled structure ($H_{unc}(\omega_i)$) at the same frequency (ω_i). Using this explanation makes it possible to define the problem in optimisation standard language.

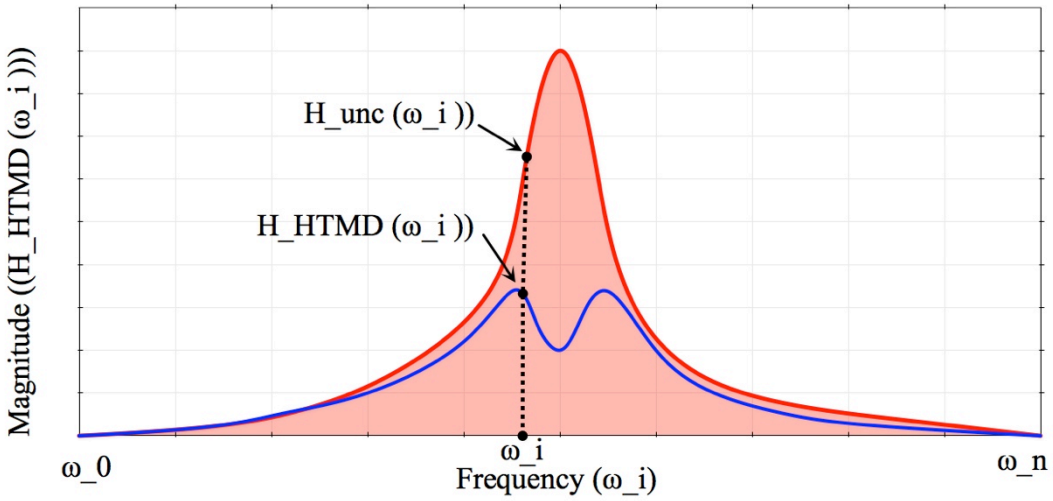

Figure 4-1- FRF magnitude plot of an uncontrolled structure (red) and controlled with HTMD (blue)

Considering Equation (3.44) and substituting the actuator input voltage ($V_{in,act}$) with the feedback signal as equation (4.1), H_{HTMD} is generated using all feedback signals (both states and derivative of states of the primary structure and TMD).

$$V_{in,act} = K_3\dot{x}_s + K_2\,\ddot{x}_s + K_1\,x_p + K_4\,\dot{x}_p + K_5\,\ddot{x}_p \qquad \textbf{(4.1)}$$

Then H_{HTMD} becomes

$$H_{HTMD} = \frac{G_{s,2,TMD}}{\frac{G_{s,1,TMD} * \left(G_{p,1} + G_{act} * G_{p,2} * (K_2 + K_3 * G_{int})\right)}{G_{act} * G_{p,2} * \left(K_1 * {G_{int}}^2 + K_4 * G_{int} + K_5\right) - 1} + 1} \qquad \textbf{(4.2)}$$

where G_{int} is an integrator block. As Equation (4.2) demonstrates, all feedback gains (K_1 to K_5) are included in this transfer function. By generating H_{HTMD} and H_{unc} it is possible to create the objective function (OF) and constraint function (CF).

Defining the optimisation problem

The definition of the optimisation problem involves generating the OF and CF, which are formulated in terms of the FRF as a proxy for system performance. Hence, to generate the FRF of both the controlled and uncontrolled structure, it is possible to replace the s term in H_{HTMD} and H_{unc} with $j\omega_i$ where $j = \sqrt{-1}$. Consequently, by recalling the transfer functions from Section 3.4.2.1, H_{HTMD} becomes

$$
\begin{aligned}
&H_{HTMD} = \omega_i^2 \,/ \cdots \\
&\cdots \left(\left(k_p + c_p * \omega_i * j\right) * \left(\frac{k_p + c_p * \omega_i * j}{-m_p * \omega_i^2 + c_p * \omega_i * j + k_p} + \cdots\right.\right. \\
&\cdots \left.\left(m_a^2 * v_a * \omega_i^4 * \left(K_2 - \frac{K_3 * j}{\omega_i}\right)\right) \,/\right. \\
&\cdots \left[(\varepsilon_{act} + \omega_i * j) * (-m_a * \omega_i^2 + c_a * \omega_i * j + k_a) * \left(-m_p * \omega_i^2 + \right.\right. \\
&\left.\left. c_p * \omega_i * j + k_p\right)\right])) / \\
&\cdots / (((m_a^2 * v_{act} * \omega_i^4 * \left(\frac{K_1}{\omega_i^2} - K_5 + \frac{K_4 * j}{\omega_i}\right)) / \cdots \\
&\cdots ((\varepsilon_{act} + \omega_i * j) * (-m_a * \omega_i^2 + c_a * \omega_i * j + k_a) * \left(-m_p * \omega_i^2 + \right. \\
&\left. c_p * \omega_i * j + k_p\right) + 1) * \left(k_p + k_s - m_s * \omega_i^2 + \omega_i * \left(c_p + c_s\right) * j\right)
\end{aligned}
\qquad \textbf{(4.3)}
$$

All variables in equation (4.3) are predetermined except K_1 to K_5. These are the critical values which should be optimised in such a way that Equation (4.3) is minimised at each frequency ω_i. Hence the OF is:

$$\text{OF}: \min(H_{HTMD}(\omega_i)), \quad \omega_0 < \omega_i < \omega_n \qquad \textbf{(4.4)}$$

and this is subject to the constraint:

$$\text{CF}: \quad H_{HTMD}(\omega_i) < H_{unc}(\omega_i) \therefore H_{HTMD}(\omega_i) - H_{unc}(\omega_i) < 0$$
$$\omega_0 < \omega_i < \omega_n \qquad \textbf{(4.5)}$$

Equations (4.4) and (4.5) show that this optimisation problem is a multi-objective non-linear function with non-linear semi-infinite constraints. Similar to the TMD parameters optimisation, a penalty function method is used to create a fitness function of the GA as:

$$Fitness\ Function = H_{HTMD}(\omega_i) + r_p \sum_{i=1}^{n} H_{HTMD}(\omega_i) - H_{unc}(\omega_i) \qquad \textbf{(4.6)}$$

where r_p is the penalty factor and n is the number of the discreet frequencies. Implementing (4.6), both the OF and CF are converted to a single fitness function which can be utilised in the Multi-Objective Genetic Algorithm from the MATLAB Optimisation Toolbox [154]. The GA properties in Table 3-3 are used, except for the number of variables which has changed from 3 to 5.

Table 4-1 illustrates the results of GA, which are the optimum critical values (i.e. feedback gains). In addition the properties in Table 3-1 and Table 3-4 as the properties of the primary structure and passive TMD are employed. Also ω_i is set from 0 to 10 Hz with an increment of 0.05 Hz.

Table 4-1- HTMD feedback gains using GA

K_3 (Vol.sec/m)	K_2 (Vol.sec^2/m)	K_1 (Vol /m)	K_4 (Vol.sec/m)	K_5 (Vol.sec^2/m)
0	-5.95	-191.17	-15.28	-0.151

It should be noted that the upper and lower bands of the GA are very important since this is the region in which the critical values are chosen. To generate these two bands, the stability ranges of the gains which are calculated from RL approach (Table 3-6) are employed. Hence, the lower band is set to [K_3=-58 K_2=-6.30 K_1=-1330 K_4=-100 K_5=-0.835] and the upper band to [K_3=0 K_2=0 K_1=0 K_4=0 K_5=0]. Using these bands ensures the initial stability of the closed loop system before further stability check.

137 iterations were required to converge on the optimised parameters. In addition, the penalty factor r_p was changed from 10^1 to 10^{100}. However, there was not a large alteration between the outputs of the optimisation (HTMD gains). This is the maximum of 5% variation. Also, the effect of changing the lower band of K_3 from -58 to 0 was investigated and it was concluded that this gain does not have significant influence on the response reduction and hence is redundant.

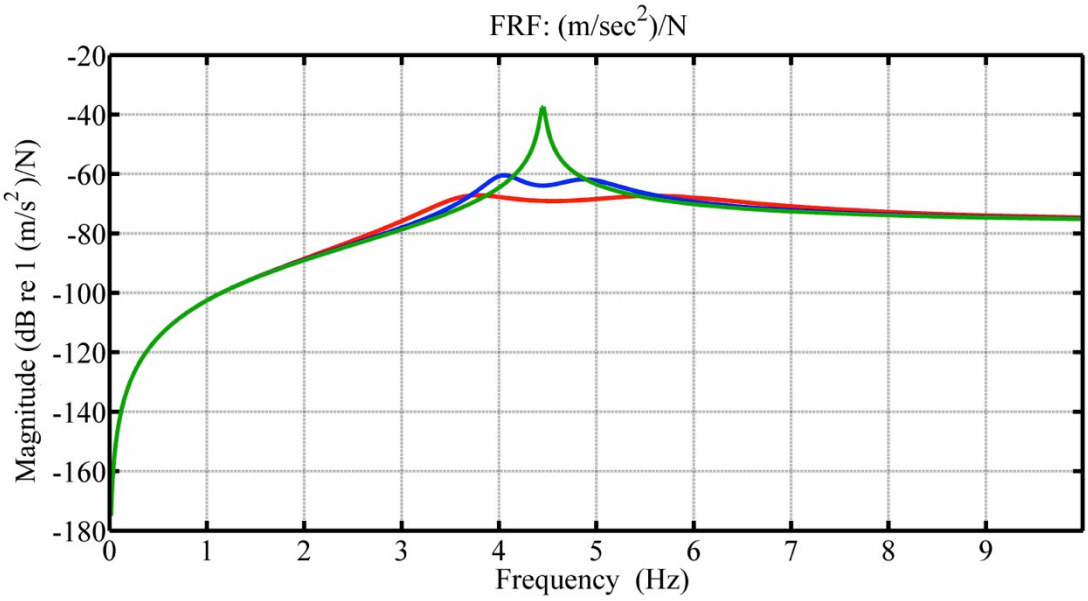

Figure 4-2- FRF of the uncontrolled structure (green) in comparison with structure with TMD (blue) and HTMD with GA employed (red)

Figure 4-2 shows a comparison of the FRFs of the uncontrolled structure, structure controlled with TMD and structure controlled with HTMD. Also, Table 4-2 shows a numerical comparison of the response reduction. It can be noted that the HTMD has 54% and 45% reduction in FRF peak and magnitude of the resonant response, respectively, in comparison with the passive TMD.

Table 4-2- Comparison of results using gains determined from GA

	Uncontrolled structure	Structure with TMD	Structure with HTMD
Max. response magnitude ($m/s^2/N$)	0.0135	0.00095	0.000438
Reduction of the max. response	-	93%	97%
Response magnitude at resonance ($m/s^2/N$)	0.0135	0.000639	0.000352
Reduction of response at resonance	-	95%	97%

4.1.2. Closed loop stability of the control system

The same methods with similar type of transfer function as discussed in chapter 3.7 were used to check the stability of the closed loop system. Figure 4-3 shows the pole-zero map of the structure with HTMD attached using gains determined from the GA (Table 4-1). As can be seen, all poles and zeros of the $1 + \{k\}\{G_{Plant}\}G_{act}$ are on the left hand side of the s-plane which indicates a stable system.

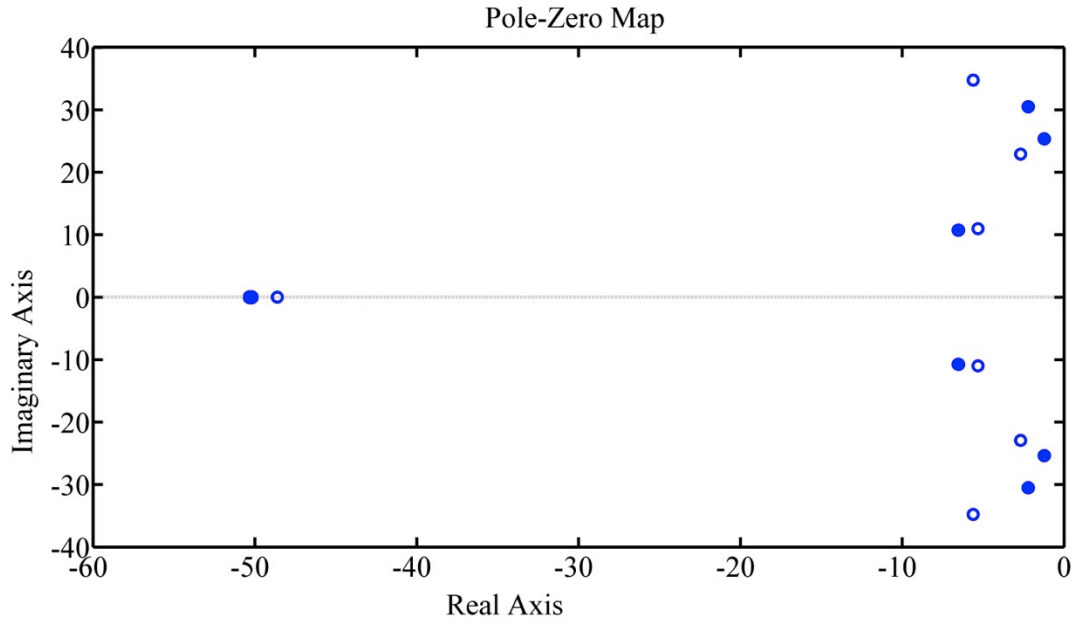

Figure 4-3- Pole-Zero map of the closed loop HTMD system using GA optimised gains

Also, Figure 4-4 shows the Nyquist plot of $\{k\}\{G_{Plant}\}G_{act}$. Clearly, there is no encirclement around point (-1,0) hence indicating the stability of the closed loop system.

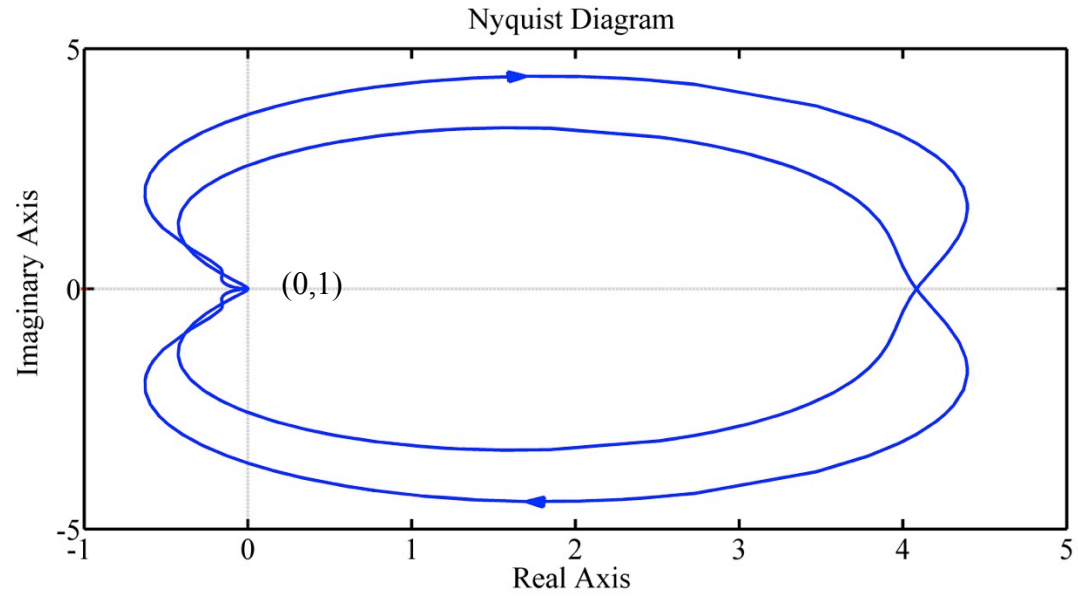

Figure 4-4- Nyquist plot of the closed loop HTMD system using GA optimised gains

4.2. Analytical simulations

In this section, the models, properties, control algorithm and gains that were proposed and designed previously are employed to run a number of analytical simulations. Both time and frequency domain analysis are carried out. The MATLAB Simulink package [165] was employed to analyse the previously proposed state space models.

4.2.1. Excitation forces

Two specific excitations were used for these simulations. First, a random white noise excitation is applied to the uncontrolled structure and controlled structure using passive TMD, AMD (direct velocity feedback) and HTMD with different control algorithms (including conventional LQR, modified LQR and GA). Using the calculated responses, the frequency response functions were determined through appropriate Fourier analysis and used for comparison of the performance of the various controllers.

Second, a simulation was carried out using a modelled measured human jumping force to evaluate both the control performance of the various controllers and also to assess the actuator effort, based on both device capability and required electrical power. To do this, the actuator inertia force (control force) and input voltage were assessed.

It should be noted that the main reason of choosing jumping as human activity in contrast with bouncing or jogging is that the magnitude of the jumping force is higher than the other types of activity and it is considered as more human energetic activity relevant to design of the stadium.

Random excitation

To perform a frequency response function analysis and to characterise the response of the structure, a random noise signal was applied as an input to the simulation. The signal was generated using the Data Physics digital spectrum analyser [167] and was used as input force for both the analytical simulations and later experimental work.

The random noise signal generated had frequency span of 0-50 Hz and peak magnitude of 2.0 V, which was appropriate for use as an input voltage signal to the

actuator amplifier. This type of signal is appropriate for classification of the system transfer functions. The Data Physics spectrum analyser [167] produces a random signal that has a uniform spectral density across the chosen frequency range and has zero mean value as Gaussian amplitude distribution [167]. A time domain plot of the signal is shown in Figure 4-5.

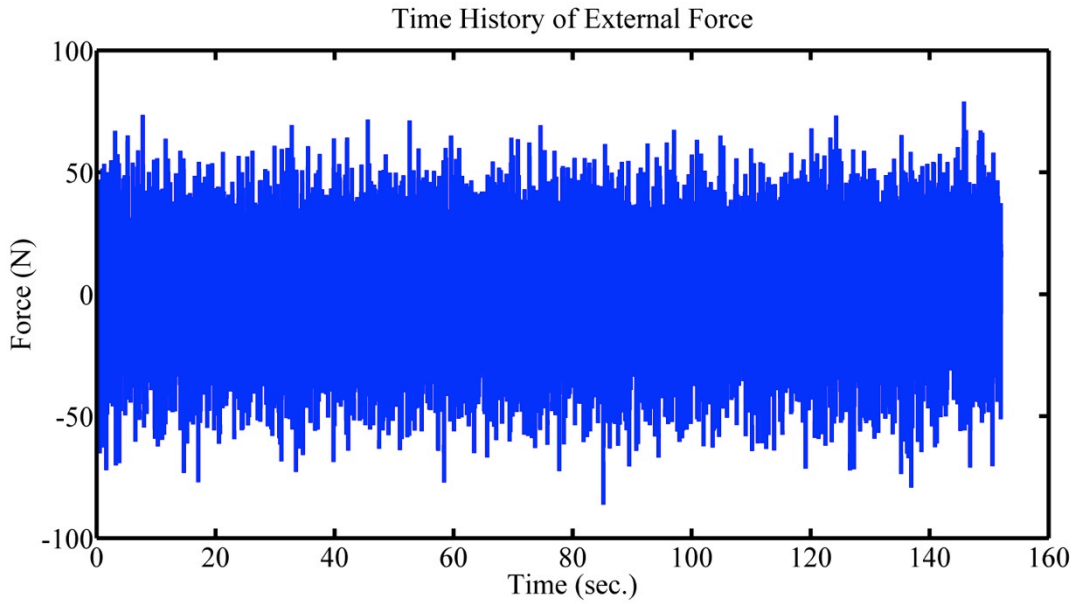

Figure 4-5- Random signal; frequency span of 0-50 Hz

Jumping Excitation

To produce the simulated jumping force, a recommendation in [24] is employed to use a generated load factor (GLF) instead of dynamic load factor (DLF). Accordingly, the crowd jumping force is generated as

$$F_{jump} = mg + \rho_{jump} mg \sum_{i=1}^{i=3} G_{GLF,i} \cos(2\pi i f_{beat} t + \theta_i) \quad \textbf{(4.7)}$$

where

$$mg = g \sum_{i=1}^{N_r} m_{ep} * \phi_r \quad \textbf{(4.8)}$$

ρ_{jump} is the crowd effectiveness factor, m is the mass of the crowd, g is acceleration due to gravity, $G_{GLF,i}$ is the GLF, f_{beat} is the frequency of the crowd activity, t is time and θ_i is the phase difference of the harmonics. Also, m_{ep} is the mass of each

person (assumed to be 80 kg), ϕ_r is the amplitude of the mode shape at the location of the individual jumpers and N_r is the number of people. Because the modelled structure is a SDOF system, the amplitude of the mode shape was set as $\phi_r = 1$. It was also assumed that the number of jumping people on the slab is four each with weight 80kg. The activity frequency was set as the half of the frequency of the structure (i.e. $f_{beat} = 4.46/2$). This leads to the second harmonic of the jumping activity to be tuned to resonance.

Based on [24], scenario 4 is selected where "The whole crowd active". Since the RMS acceleration is used for performance assessment, the phase angles are unimportant and hence $\theta_i = 0$ is chosen. The crowd effectiveness factor (ρ_{jump}) for scenario 4 can be calculated as:

$$\rho_{jump}(f_{beat}) = \text{sech}\,(f_{beat} - 2) \quad \textbf{(4.9)}$$

GLFs for scenario 4 are applied as $G_{GLF,1} = 0.375$, $G_{GLF,2} = 0.095$ and $G_{GLF,3} = 0.026$. The generated force as the result of this approach is shown in Figure 4-6.

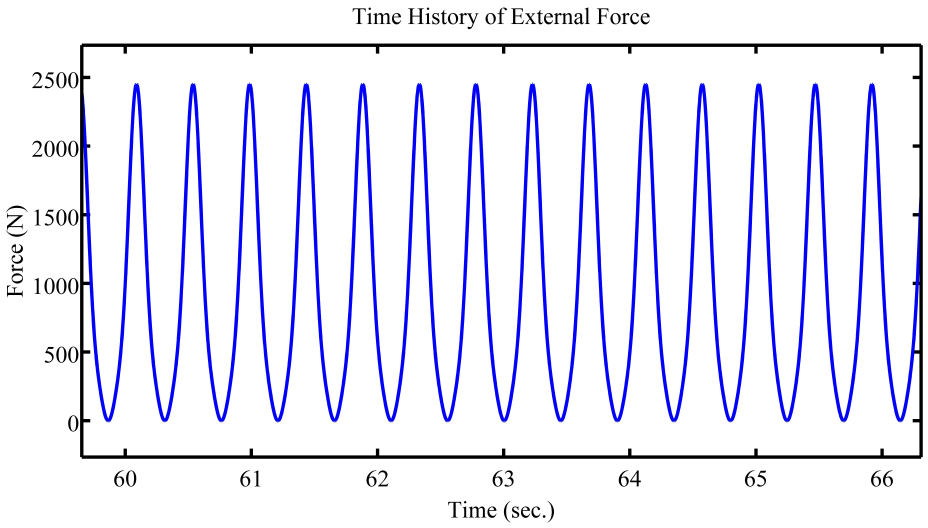

Figure 4-6- Simulated jumping force of four people

4.2.2. Analysis of structural response

As mentioned previously, the performance assessment of the various structural and control configurations was carried out in the frequency and time domains.

4.2.2.1. Comparison of frequency response functions

To generate FRFs from the numerical simulations using random excitation, the acceleration response and force input to the structure were used. The $H_T(f)$ approach was used [168] to properly take account of the effect of the noise on both input and output signals. According to this, $H_T(f)$ can be calculated as:

$$H_T(f) = \frac{G_{yy} - G_{xx} + \sqrt{(G_{xx} - G_{yy})^2 + 4|G_{xy}|^2}}{2G_{yx}} \quad \textbf{(4.10)}$$

where G_{xx} and G_{yy} are the auto spectral density (ASD) functions of the input and output signals respectively. Also G_{xy} and G_{yx} are the cross spectral density (CSD) functions between the input and output. Also, a Hanning window with 50% overlap was applied to the data when calculating the ASD and CSD functions. The magnitude and phase of the calculated FRF functions are shown in Figure 4-7 and Figure 4-8.

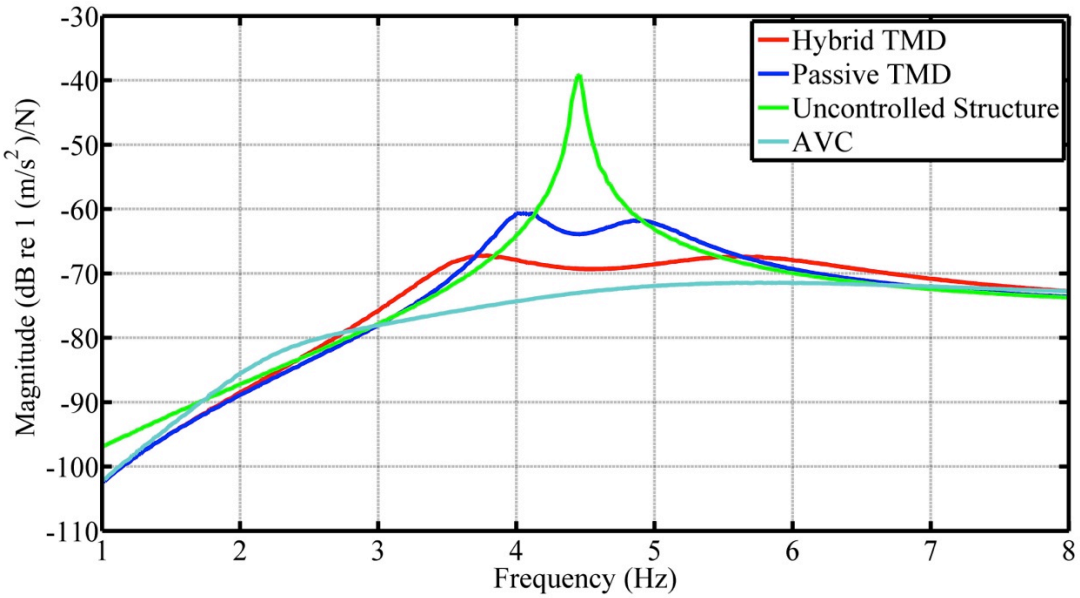

Figure 4-7-- FRF (magnitude) of the uncontrolled structure (green) in comparison with structure with TMD (blue), AMD (cyan) and HTMD (red)

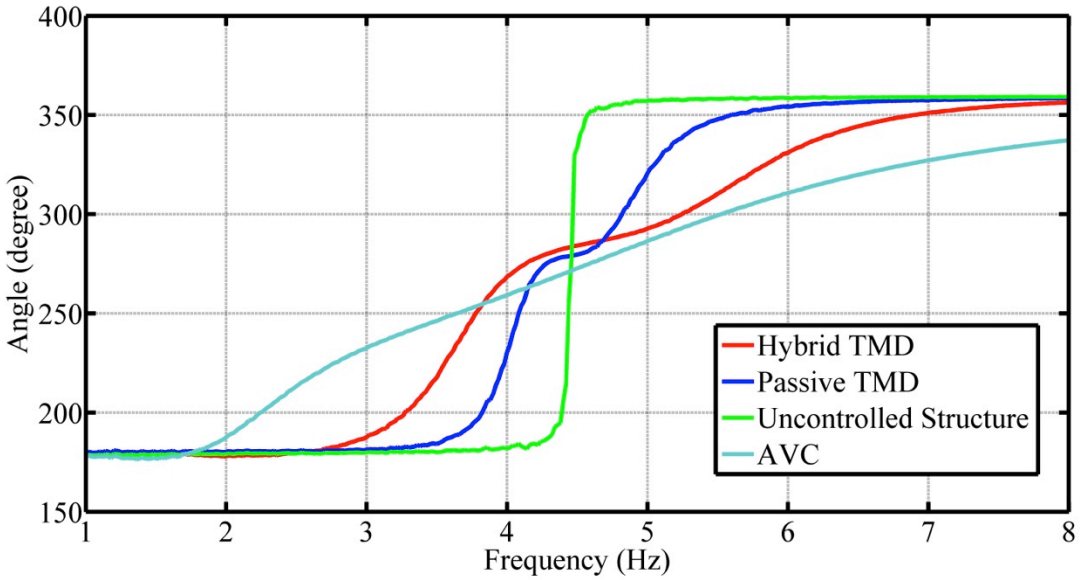

Figure 4-8- FRF (phase) of the uncontrolled structure (green) in comparison with structure with TMD (blue), AMD (cyan) and HTMD (red)

The numerical results of each technique are discussed earlier (in Chapter 3). However, it should be noted that the model used in chapter 3 was Transfer Function method. Herein this chapter, State Space approach and numerical analysis are employed. Same as TF method, HTMD using Genetic Algorithm, HTMD using conventional LQR, HTMD using modified LQR and AMD using Direct Velocity Feedback have 54%, 8%, 27% and 72% reduction respectively in the peak of FRF in comparison with passive TMD. Also, they have 45%, 29%, 35% and 65% reduction respectively in the FRF magnitude at the frequency of the resonant in comparison with passive TMD. It shows that in case of response reduction, AMD has greater reduction in comparison with HTMD. Also, using Genetic Algorithm gains in HTMD has more redution in contrast with conventional and modified LQR.

4.2.2.2.Analysis of jumping excitation

The structural acceleration responses due to the previously described simulated jumping force was calculated then frequency weighted according to [169]. W_k was chosen as the frequency weighting curve in which z-axis of the person is exposed to the vibration.

After weighting the acceleration signal, a number of different assessment criteria were calculated, which were peak acceleration, RMS, running 1 s RMS and maximum transient vibration value (MTVV) of the acceleration response.

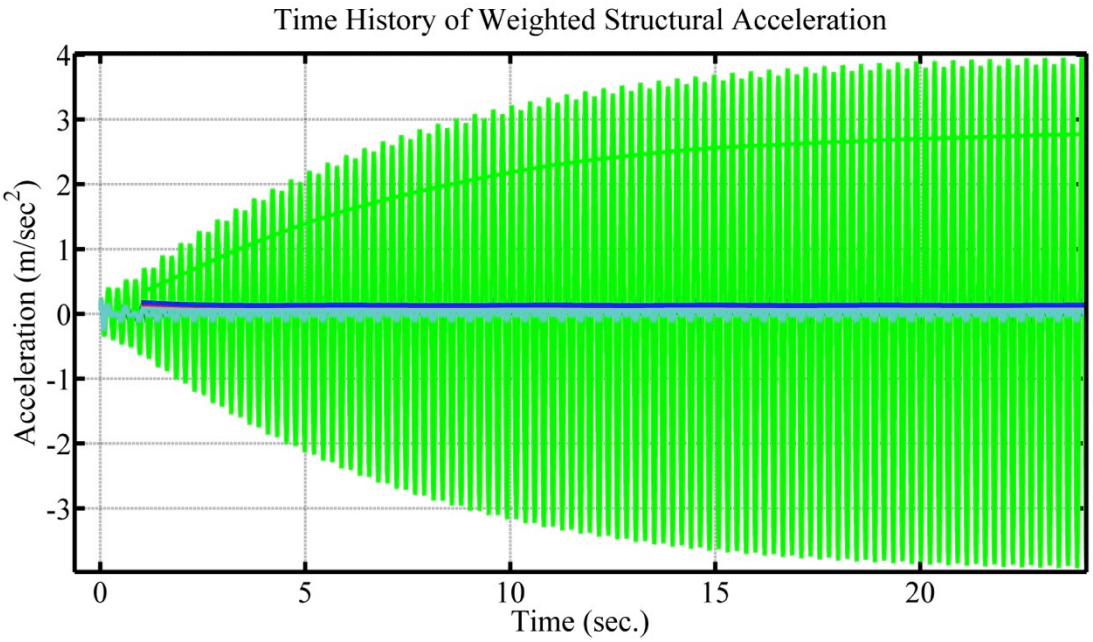

Figure 4-9- Structural weighted acceleration and corresponding running RMS (1 sec.) response from simulated jumping force (4 people); TMD (blue), AMD (cyan), HTMD (red), uncontrolled structure (green)

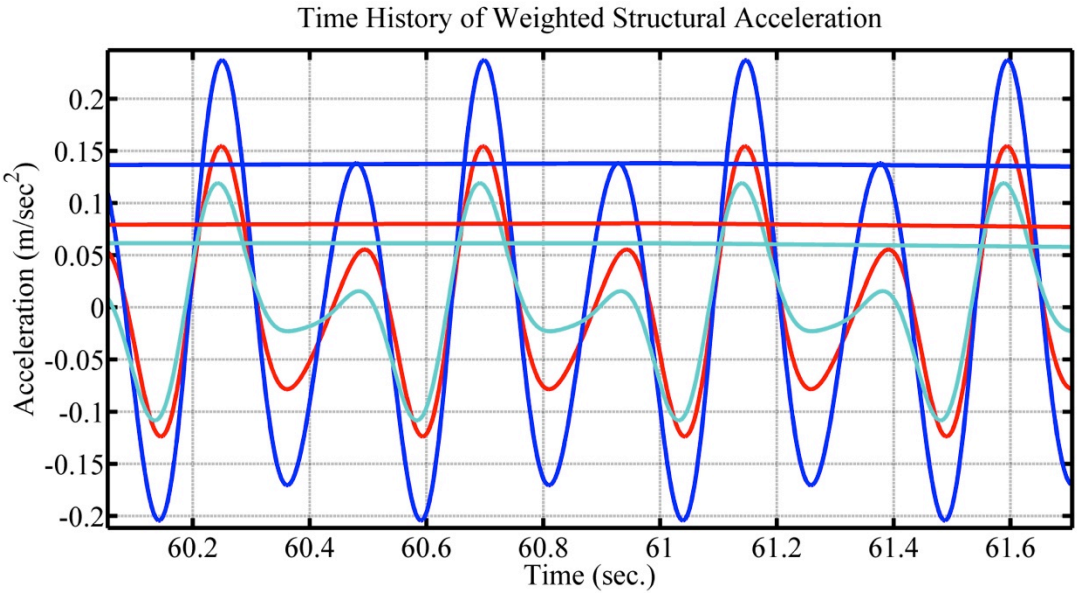

Figure 4-10- Structural weighted acceleration and corresponding running RMS (1 sec.) response from simulated jumping force (4 people); TMD (blue), AMD (cyan), HTMD (red) (zoomed version of Figure 4-9)

As Figure 4-10 and Table 4-3 show, AMD has the highest reduction in peak, and MTVV of structural acceleration in comparison to both uncontrolled structure and structure with passive TMD.

Table 4-3- Simulation results comparison of Time Domain analysis, weighted acceleration of the primary structure

	Uncontrolled Structure	Structure with TMD	Structure with AMD	Structure with HTMD
Peak acceleration (m/s^2)	3.9841	0.2373	0.1192	0.1546
Reduction from uncontrolled structure	-	94%	97%	96%
Reduction from passive TMD	-	-	50%	35%
Weighted MTVV (m/s^2)	2.796	0.1398	0.0633	0.082
Reduction from uncontrolled structure	-	95%	98%	97%
Reduction from passive TMD	-	-	55%	41%

Also, considering on RMS of the acceleration, both AMD and HTMD have large reductions in structural response in comparison with passive TMD. However, comparing AMD and HTMD, there is not a big difference in RMS of the structural acceleration (around 23% reduction).

4.2.2.3.Actuator effort under human jumping excitation

The actuator effort can be checked by considering both input electrical voltage to the amplifier and the force generated by the actuator. It should be noted that the maximum capacity of the actuator in voltage mode is 450 N.

Herein, the voltage command signal to the amplifier and the corresponding generated control force of the actuator are compared with each other for the various control schemes. Similar to the response evaluation, peak, MTVV of the voltage and force are calculated.

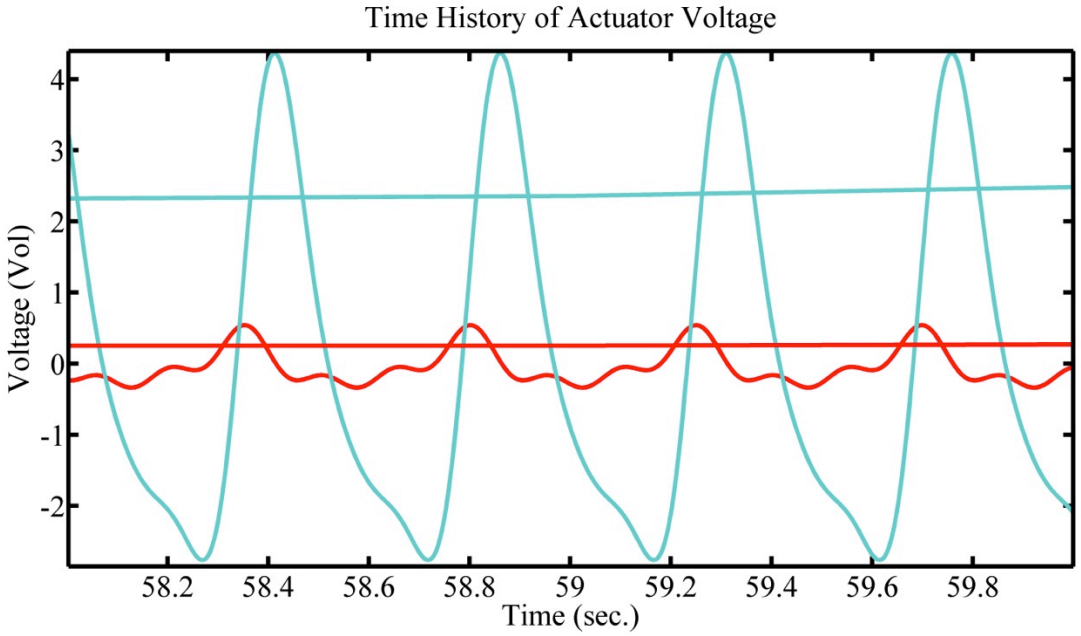

Figure 4-11- Actuator input voltage and corresponding running RMS (1 sec.); response from simulated jumping force (4 people); AMD (cyan), HTMD (red)

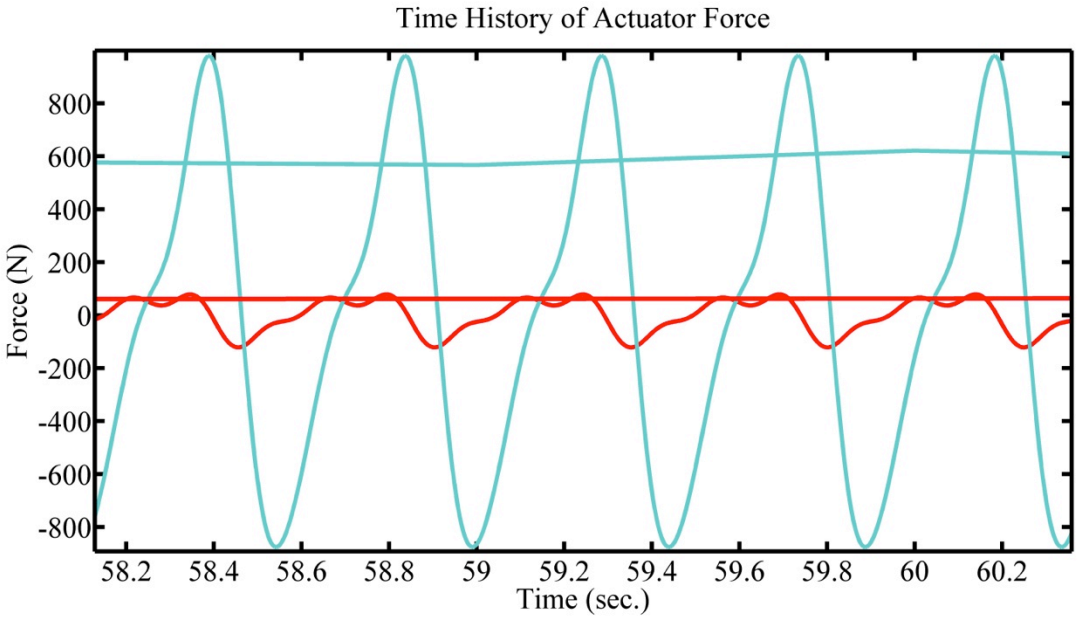

Figure 4-12- Actuator force and corresponding running RMS (1 sec.); response from simulated jumping force (4 people); AMD (cyan), HTMD (red)

As shown in Figure 4-11 and Figure 4-12, the AMD needs a much higher control force in comparison with the HTMD. This force and voltage is higher than the capacity of the actuator and hence cannot be achieved in reality. However, the HTMD has lower demand for actuator force and hence in this case its capacity is not exceeded.

Table 4-4- Actuator force demand from jumping excitation simulations

	AMD	HTMD with GA gains	HTMD with conventional LQR gains	HTMD with modified LQR gains
Peak force (N)	979	78	29	22
Reduction from AMD	-	92%	97%	98%
MTVV (N)	620	66	28	16
Reduction from AMD	-	89%	95%	97%

As can be seen from Table 4-4, when the jumping force has the harmonic component at the structure's frequency (resonant scenario), AMD requires actuator capability around 10 time greater than HTMD. Also HTMD with the gains optimised by modified LQR requires the minimum control effort and input voltage.

4.3. Discussion of simulation results

In this chapter, an optimisation approach using GA was introduced. The goal of this method is to optimise the feedback control gains such that minimum structural response is achieved whilst being in the boundary of the uncontrolled structure's FRF.

It is shown that unlike the other optimisation methods such as conventional and modified LQR techniques, it is possible to combine different states (i.e. displacement, velocity and acceleration of both primary structure and TMD) of the system as feedback signal during the process of optimisation. Also, when compared to the manual optimisation method, the time and cost of calculation is very low and using GA makes it possible to have a smaller frequency increment step. This leads to achieving global optima rather than local ones. Consequently, employing the GA approach leads to the most appropriate gains and hence it was found that these gains gave the best reduction in structural response when using HTMD in comparison with the other optimisation methods utilised.

It is shown that only structure with AMD and HTMD have lower RMS of structural acceleration when the amount of vibration force is high. However, AMD required more power which is out of the practical capability of actuator whereas HTMD can achieve the reduction within the boundary of practical capacity of actuator.

Also it is shown that using HTMD with a different optimisation method (i.e. conventional and modified LQR and GA needs much less power and actuator inertia force in comparison with AMD method. This happens especially when the harmonics of the people's jumping placed at the frequency of the structure (i.e. resonant scenario) and the amount of force is high.

As another comparison, the performance of HTMD is compared with AMD based on both performance (reduction in structural response) and actuator effort. It was shown that the reduction in structural response using AMD is higher than the similar case using HTMD. However, for the particular loading scenario considered the control force demand was very high for the AMD in comparison with the HTMD. This shows that the larger actuator (AMD) is needed where the magnitude of the external excitation force is high.

In conclusion, considering on both structural response and cost, the HTMD has more appropriate performance when simultaneously considering all factors including the structural response reductions in the presence of larger force and also when considering the amount of required power source and actuator inertia force.

As it was noted before, off-tuning is a potential problem in structures such as stadia which could be due to human-structure interaction. Author will introduce new control algorithms to be employed in HTMD in order to deal with this problem. This is considered in the next chapter.

5. HTMD as a solution to off-tuning problems with TMDs

A shorter version of this chapter was presented and published in [162].

5.1. Introduction

A passive tuned mass damper (TMD) is a conventional and generally well accepted method to deal with vibration problems in structures. However, the off-tuning problem is a substantial drawback of this technique, whereby changes in structural natural frequencies may detune the TMDs.

Changes of structural natural frequencies is one of the possible effects of the human-structure interaction phenomenon. It was mentioned earlier that in a structure such as a stadium, the frequency of the structure could change depending on the proportion of active and passive spectators, even if the number of spectators remains the same [38], [39]. Since a TMD is optimally tuned to work in a specific frequency band, changes in the structure or TMD parameters may lead to a deterioration in performance.

In this chapter, the use of an HTMD is proposed for a structure subjected to dynamic excitation and in which off-tuning occurs due to a change in structural dynamic properties. Following a simulation of off-tuning in the structure showing a lack of performance from a detuned passive TMD, two different control schemes are introduced and applied in HTMD to overcome this issue. The performance of such an HTMD system is evaluated by comparing both simulated FRFs and responses due to simulated human excitation.

5.2. Implementation of off-tuning in the structural model

As mentioned before, there are several factors that can cause off-tuning of passive TMDs. These include changes dynamic properties of both the primary structure and the TMD [9], [20].

Herein, to simulate the off-tuning problem, the mass of the primary structure is changed, resulting in a change in natural frequency of the primary structure. It should be noted that in the later experimental work, the off-tuning will be achieved by changing the TMD mass rather than the mass of the primary structure since it is impossible to change the structural mass significantly.

Table 5-1 shows the variation in the mass of the primary structure and the corresponding natural frequencies. As can be seen, there is a change of -41% and +18% in the structural natural frequency when the mass of the structure is scaled by 0.5 and 1.5 respectively. The change in natural frequency causes the passive TMD to be out of tune (off-tuning), hence the TMD is essentially no longer effective.

Table 5-1- Frequency of the structure corresponding to different masses

Structural mass (m_s) kg	Structural frequency (f_s) Hz	Change in frequency
0.5* 7150	6.29	-41%
1.0* 7150	4.46	0%
1.5* 7150	3.63	18%

It should be noted that the natural frequency of the structure can be changed (off-tuning) by changing the stiffness of the instead of mass. However, in this study only changing in the mass is considered.

5.3. Control algorithm

To deal with the off-tuning problem, two control algorithms are proposed. Firstly, direct response feedback with robust gains designed using a GA, in which just one set of gains is calculated and applied to the system for the situation where the frequency of the structure may change in the range 3.63 Hz to 6.29 Hz. This means that the HTMD can perform as an effective vibration mitigation device where the frequency of the structure changes significantly by using just one set of gains.

For the second method, at each frequency (4.45 Hz as the initial tuning frequency and 3.63 Hz and 6.29 Hz as modified frequencies) the system has a set of gains and the appropriate set of gain is chosen depending on the current frequency of the structure. This is an adaptive control method using the GA. The advantages and disadvantages of each method are investigated through simulation.

It should be noted that in both methods, the control signal of the HTMD actuator should be as proposed in Equation (4.1) to ensure good vibration mitigation performance and to provide a solution for off-tuning.

5.3.1. Direct response feedback with robust gains using GA

A similar approach to the one shown in Section 4.1.1 is applied by employing a GA to optimise the feedback gains. However, in this case, instead of having a single m_s, the optimisation problem is specified three mass values (i.e. m_s, $0.5m_s$ and $1.5m_s$) simultaneously.

As shown in Figure 5-1, the objective of the HTMD design is to minimise the response of the structure over a specified band of frequencies (ω_i) for three different frequencies of the primary structure by using appropriate control gains. Hence, the critical values of the GA are the gains of the feedback system, which should be optimized in such a way that reduces the FRF of the structure ($H_{HTMD}(\omega_i)$) as the objective function in three different scenarios simultaneously. Also, similar to the earlier discussion, the FRF of the controlled structure should be inside the boundary of the FRF of the uncontrolled structure ($H_{unc}(\omega_i)$) in all three scenarios. This means that for each ω_i, the response of the controlled structure due to the external force ($H_{HTMD}(\omega_i)$) should be as low as possible. Also for each ω_i of individual m_s, the response of the controlled structure due to the external force ($H_{HTMD}(\omega_i)$) should be less than the response of the uncontrolled structure ($H_{unc}(\omega_i)$) at the same frequency (ω_i). Hence, it is possible to define the problem in optimisation standard language, as discussed earlier.

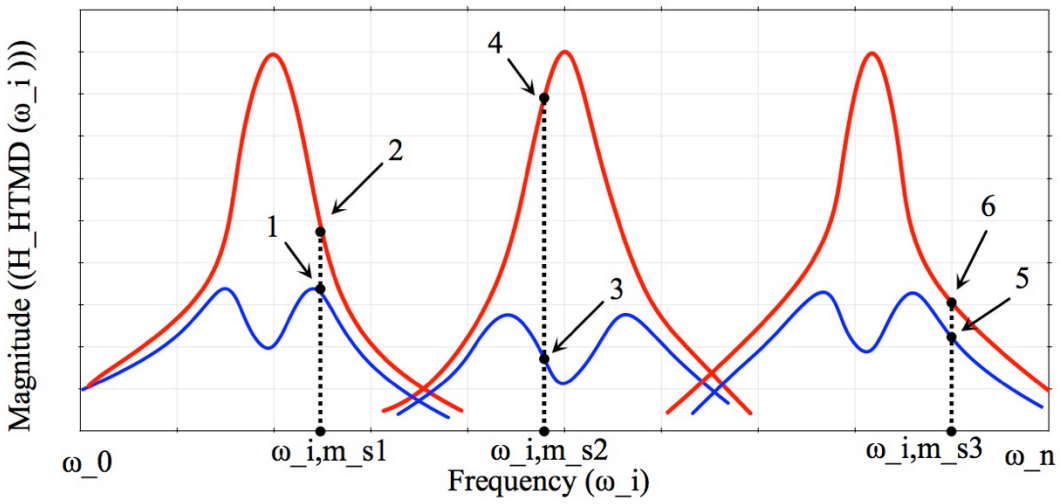

Figure 5-1- FRF magnitude plot of an uncontrolled structure (red) and controlled with HTMD (blue) for three different frequencies of the structure simultaneously

Definition of the optimisation problem

Based on equation (4.3), it is possible again to derive $H_{HTMD}(\omega_i)$, except this time with three different values of m_s instead of one fixed value. Hence, the optimisation problem is to achieve the appropriate gain values of K_1 to K_5 as critical values with following criteria:

$$\text{OF}: \min\left(H_{HTMD}(\omega_i)\right), \quad \omega_0 < \omega_i < \omega_n$$

$$m_{s,i} = \begin{cases} 0.5\text{m}_\text{s} \\ \text{m}_\text{s} \\ 1.5\text{m}_\text{s} \end{cases} \qquad \textbf{(5.1)}$$

and

$$\text{CF}: H_{HTMD}(\omega_i) < H_{unc}(\omega_i) \therefore H_{HTMD}(\omega_i) - H_{unc}(\omega_i) < 0$$

$$\omega_0 < \omega_i < \omega_n \text{ and } m_{s,i} = \begin{cases} 0.5\text{m}_\text{s} \\ \text{m}_\text{s} \\ 1.5\text{m}_\text{s} \end{cases} \qquad \textbf{(5.2)}$$

A similar fitness function as was given in Equation (4.6) can be generated using Equations (5.1) and (5.2). Figure 5-2 shows the plot of the fitness function

employed in the GA. As it illustrates, ω_i is chosen from 0 Hz to 10 Hz with three different structural frequencies simultaneously.

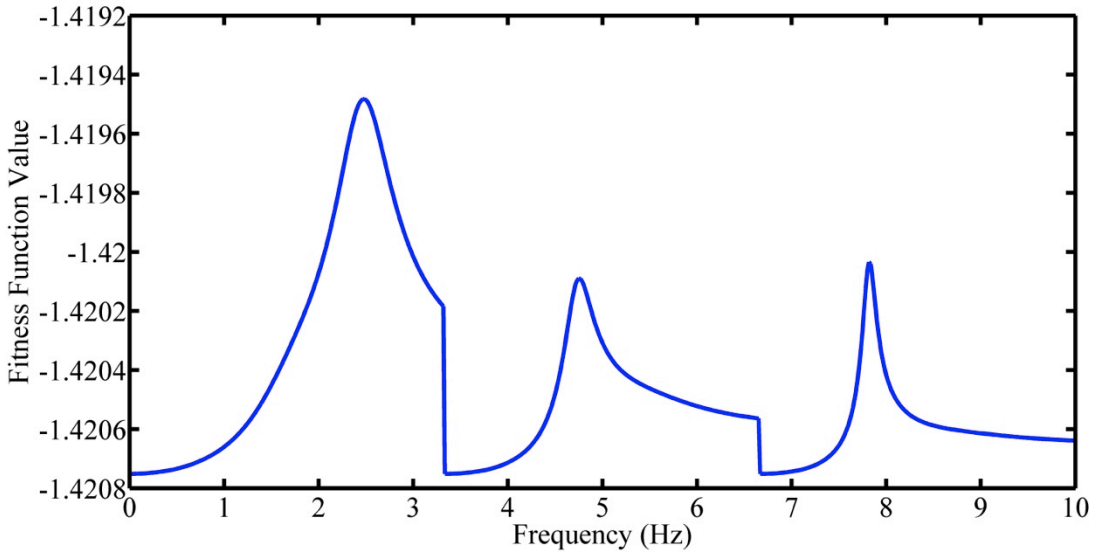

Figure 5-2- Fitness function for robust gain using GA

Using a GA with the properties of Table 3-3 leads to the optimised gains in Table 5-2 after 135 iterations.

Table 5-2- HTMD feedback gains for off-tuning using GA

K_3 (Vol.sec/m)	K_2 (Vol.sec^2/m)	K_1 (Vol /m)	K_4 (Vol.sec/m)	K_5 (Vol.sec^2/m)
0	-6.23	-362.11	-34.47	-0.0149

Applying these gains should lead to a HTMD which can perform at three different frequencies of 4.45 Hz, 3.63 Hz and 6.29 Hz to reduce the structural response in the presence of external excitation force.

Closed loop stability of the control system

As previously noted, the Pole-Zero map and Nyquist plot are both employed to check the stability of the closed loop system. These checks were performed with three different frequencies and gains in Table 5-2

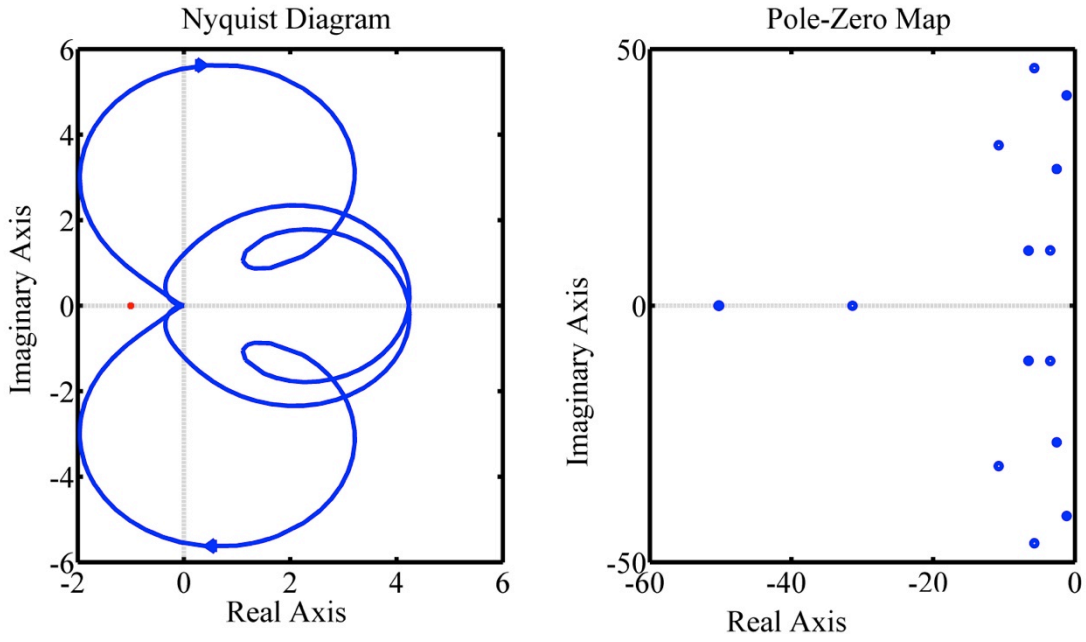

Figure 5-3- Nyquist plot (left) and Pole-Zero map (right) of the closed loop HTMD system using robust gains; f_s=6.29 Hz

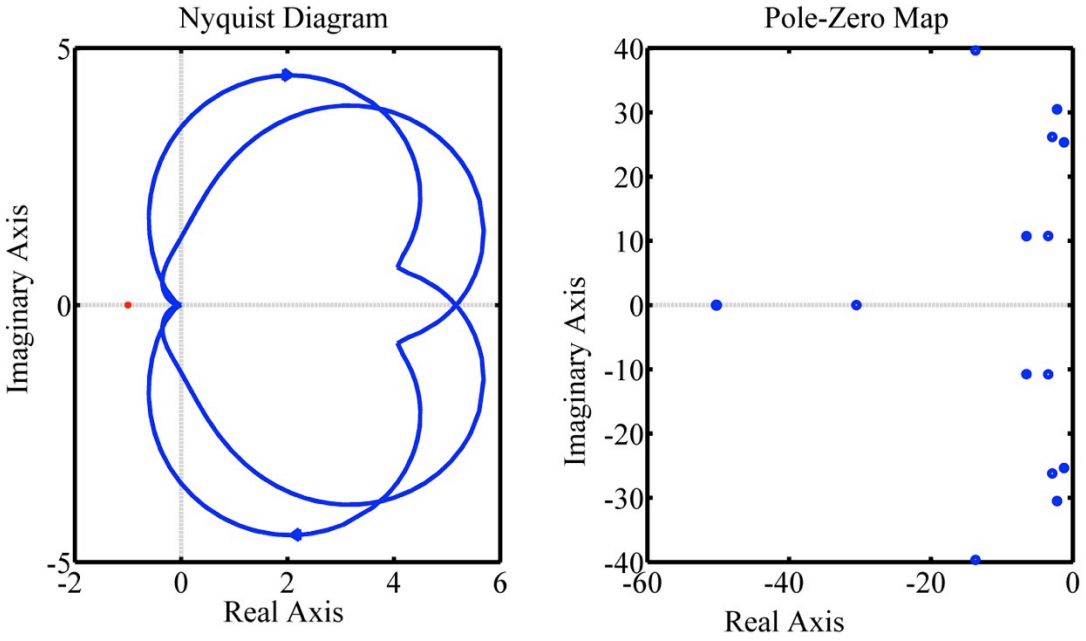

Figure 5-4- Nyquist plot (left) and Pole-Zero map (right) of the closed loop HTMD system using robust gains; f_s=4.46 Hz

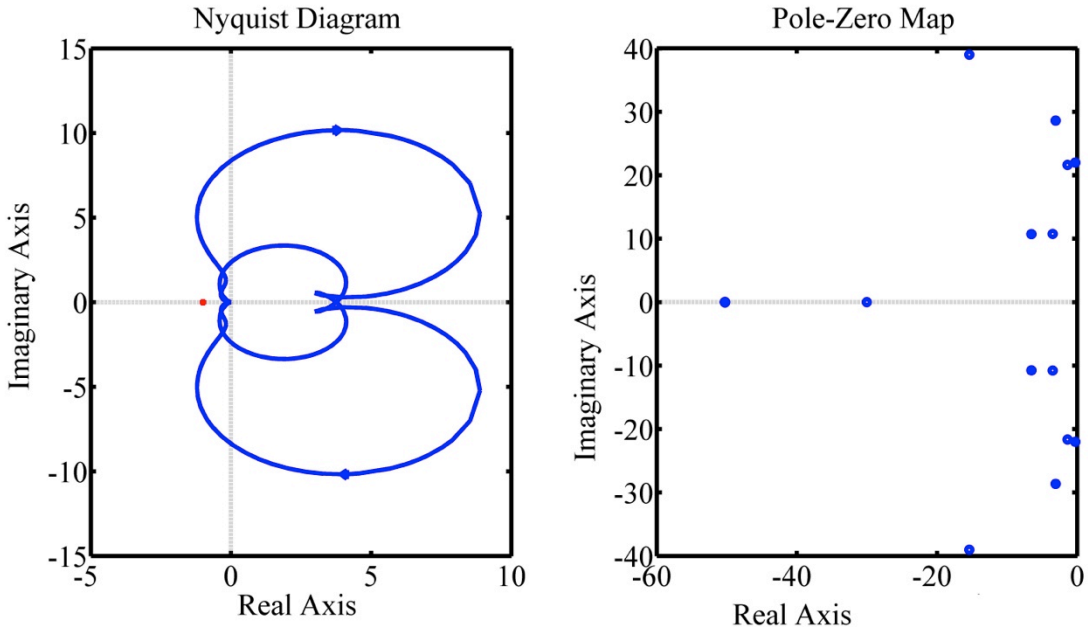

Figure 5-5- Nyquist plot (left) and Pole-Zero map (right) of the closed loop HTMD system using robust gains; f_s=3.63 Hz

As Figure 5-3, Figure 5-4 and Figure 5-5 illustrate, the closed loop system is stable using the proposed gains in the structure with three different frequencies.

5.3.2. Adaptive control method using GA

The adaptive control method using Genetic Algorithm is an approach where the system is solved for different scenarios offline. Then, a database for these situations is generated. For instance there are three different frequencies of the structure due to changing in the primary structural mass. Therefore, there are three individual optimisation problems corresponding to three different structural frequencies.

The solution of these optimisation problems are three sets of gains corresponding to the three different scenarios. These gains form the database of the adaptive control method. Now, the challenge is to determine the frequency of the structure real time and choose the appropriate set of gains from the database while the system is online and the structure is under occupation. To do this, a power spectral density (PSD) approach is proposed to determine the frequency of the primary structure online.

Hence, this method introduces an adaptive HTMD in which the system gains change whilst the structure is under occupation to take account of changes in structural

frequencies caused by human-structure interaction. This is an enhancement of the previous control approach, in which there was only one constant set of gains.

5.3.2.1.Constructing the database for the control system

To generate the database of the control scheme, it is possible to simply employ the same approach as in Section 4.1.1 for three different scenarios separately. This means that the fitness function given in Equation (4.6) is employed three times with individual m_s, $1.5m_s$ and $0.5m_s$ corresponding to structural frequencies of 4.45 Hz, 3.63 Hz and 6.29 Hz respectively. Herein, there are fitness function plots with one peak each in contrast with Figure 5-2 which has one fitness function with three peaks.

Table 5-3 shows the database of the adaptive control scheme, which is the solution of three optimisation problems by employing GA. As can be seen, there are three sets of gains for three different frequencies.

Table 5-3- Database for adaptive control method

Index	m_s (kg)	f_s (Hz)	Off-tuning %	K_3	K_2	K_1	K_4	K_5
1	0.5*7150	6.29	-41%	0	-6.22	-1118.1	-37.1	-0.0004
2	1.0*7150	4.46	0%	0	-5.95	-191.17	-15.28	-0.151
3	1.5*7150	3.63	18%	0	-6.2	-80.4	-22.2	-0.65

It should be noted that the stability of the closed loop system has been checked using a similar approach as before (i.e. by employing pole-zero map and Nyquist plot methods).

5.3.2.2.System identification using PSD of the response

Here the author here expands on the idea of [47] in which the PSD of the response is employed to determine the frequency of the primary structure. In this work, the PSD of the output sensor signal corresponding to the structural acceleration is used for the system identification.

In principle, there should be the frequency components in the output signal corresponding both with the input signal (i.e. excitation force) and structural vibration modes.

Based on the assumption of using a simple SDOF model of the structure and also using the simulated jumping force as in Equation (4.7) where three harmonics of the jumping force are considered, there should be four peaks in the PSD of the system output in an ideal situation. However, it should be noted that the structure here has a HTMD attached. Therefore, there are more frequency components in the output PSD. Also, depending on the frequency of the jumping, the number of the peaks can reduce when the jumping frequency or one of its harmonics coincides with the structure frequencies.

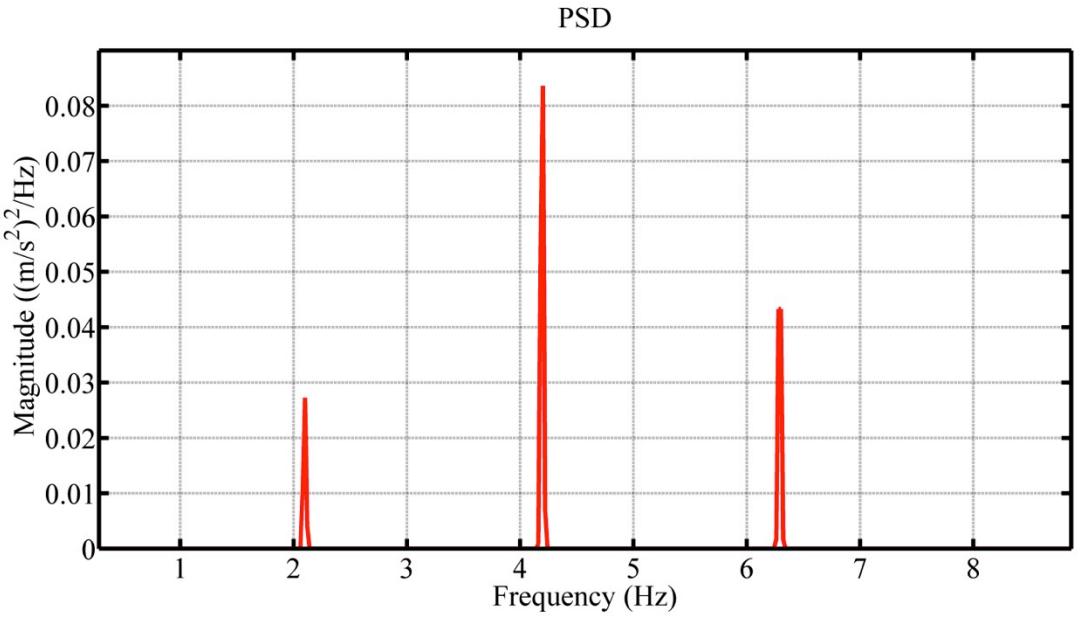

Figure 5-6- PSD of the structural acceleration; f_s = 6.29 Hz with jumping force of 6.29/3 Hz.

To analyse the PSD of the output, nine different scenarios have been considered. These are the combination of three structural frequencies (i.e. 3.36, 4.45 and 6.29 Hz) with three different jumping forces frequencies (i.e. 3.36/2, 4.45/2 and 6.29/3 Hz). Figure 5-6 shows the PSD of the structural response when the frequency of jumping is 6.29/3 Hz and the structural frequency is 6.29 Hz.

There are four peaks in the PSD plot (one is very small) which corresponding to 2.1, 4.2, 6.3 and 8.04 Hz. These are the three harmonics of the jumping force at 6.29/3 Hz in addition to the structural natural frequency in the presence of the HTMD.

Table 5-4 shows the frequency and magnitude of the PSD peaks for nine different scenarios. As is demonstrated, for each set of structural frequency and jumping frequency, the frequency components of the force and structure are generated from PSD. The structural FRF peaks can be seen further in Section (5.4.2.1).

Table 5-4- PSD analysis of the structural acceleration output

f_s (Hz)	External force frequency (Hz)	f_{peak-1} (Hz) & PSD Mag.	f_{peak-2} (Hz) & PSD Mag.	f_{peak-3} (Hz) & PSD Mag.	f_{peak-4} (Hz) & PSD Mag.	f_{peak-5} (Hz) & PSD Mag.
3.63	3.63/2	1.82	2.86	3.64	5.44	-
		0.0225	0.0000	0.0967	0.0030	-
	4.46/2	2.22	2.86	4.46	6.68	-
		0.0777	0.0000	0.1095	0.0016	-
	6.29/3	2.10	2.84	4.2	6.3	-
		0.0641	0.0000	0.1181	0.0022	-
4.46	3.63/2	1.82	3.64	5.44	-	-
		0.0179	0.2118	0.0144	-	-
	4.46/2	2.22	3.66	4.46	6.68	-
		0.0425	0.0000	0.1659	0.0076	-
	6.29/3	2.10	4.20	6.30	-	-
		0.0415	0.1823	0.0121	-	-
6.29	3.63/2	1.82	3.64	5.44	8.02	-
		0.0139	0.0282	0.0469	0.0000	-
	4.46/2	2.22	4.46	5.48	6.68	8.10
		0.0260	0.1556	0.0000	0.0407	0.0000
	6.29/3	2.1	4.2	6.3	8.04	-
		0.0277	0.0891	0.0497	0.0000	-

To employ the result of the PSD method in an online situation where the structure is occupied and the frequency of the structure is altering in real time (e.g. in a live concert event when the number of active people changes together with their jumping frequency) the following method is recommended. In this technique, 8 second blocks of the acceleration time histories of the structure are discretized with a sampling frequency of 512 Hz and the PSD calculated. The peaks of the PSD and their corresponding frequencies are determined and the magnitudes of the PSD peaks are multiplied by their corresponding frequencies.

Solving this method offline for different scenarios (three structural frequencies with three jumping frequencies and four different sets of gains including robust gain from last technique in addition to three sets gains calculated in this method) generates Table 5-5. This table is the index table of the database.

Table 5-5- Index table for adaptive control database

f_{beat}	f_s = 6.29Hz			f_s = 3.63Hz			f_s = 4.46Hz		
	Index	Gain Type	PSD*Freq.	Index	Gain Type	PSD*Freq.	Index	Gain Type	PSD*Freq.
4.46/2	1	Robust	223	13	Robust	56	25	Robust	664
	2	1.0ms	319	14	1.0ms	57	26	1.0ms	204
	3	1.5ms	754	15	1.5ms	70	27	1.5ms	332
	4	0.5ms	191	16	0.5ms	92	28	0.5ms	1513
3.63/2	5	Robust	41	17	Robust	577	29	Robust	184
	6	1.0ms	58	18	1.0ms	200	30	1.0ms	290
	7	1.5ms	31	19	1.5ms	133	31	1.5ms	82
	8	0.5ms	106	20	0.5ms	2008	32	0.5ms	183
6.29/3	9	Robust	116	21	Robust	150	33	Robust	845
	10	1.0ms	112	22	1.0ms	87	34	1.0ms	267
	11	1.5ms	215	23	1.5ms	173	35	1.5ms	227
	12	0.5ms	131	24	0.5ms	169	36	0.5ms	3116

The indices in Table 5-5 are employed to select the appropriate sets of gain in Table 5-3. Consequently, indices 1 to 12 correspond with set 1 of the gain in Table 5-3, indices 13 to 24 are linked to set 3 and 25 to 36 are associated with set 2 of the gains.

Consequently, it is possible to calculate the structural frequency every 8 seconds using the above approach and by applying the appropriate set of gains by linking the measured structural frequency to the control database for every specific segment of time. This operation is performed in pseudo-real time.

5.4. Analytical Study and Simulation

In this section, the proposed control scheme is investigated by performing a numerical simulation using the MATLAB Simulink package [165]. Similar to the last chapter, the proposed state space model that was generated in Chapter 3 is employed and the model of uncontrolled structure, structure with attached TMD and structure with attached HTMD (including both control algorithms to solve off-tuning issue) is used.

To investigate both performance of the system in the case of structural response reduction and also to check the actuator effort and capability, both time and frequency domain responses are investigated.

In addition, two different sets of simulations are executed in the time domain. In the first set, the simulations were implemented separately for individual structural frequencies to achieve the results for each frequency independently. In fact, a simulation was carried out for each structural and input force frequency and the final results were compiled from these simulations.

In the second set of time domain analyses, a new model was created in which the frequency of the structure and input force was altered in real-time. This was done to investigate the response and effect of HTMD due to a system with changing dynamic properties representing changing states of human occupation.

5.4.1. Excitation forces

To perform the three types of simulations (i.e. frequency domain approach and two time domain approaches), three different input forces were applied.

First, similar to Section 4.2.1, random noise with frequency span of 0-50 Hz and magnitude of 2.0V as the input voltage to the amplifier was employed. The results of simulations using this input force are the sets of FRFs between the input force and structural acceleration. These show the performance of controller and reduction in the structural response in different situations.

For the second set of simulations, the same jumping force as was used in Section 4.2.1 was applied. As before, it was assumed that the number of jumping people on the slab was four, each with weight 80 kg. Also as for the SDOF structure, the amplitude of the mode shape is set as $\phi_r = 1$. However, as was mentioned earlier, there are three sets of simulations each with one frequency of the structure and corresponding frequency of jumping. Therefore, three individual jumping forces are produced including jumping with $f_{beat} = 4.46/2$ Hz, $f_{beat} = 3.63/2$ Hz and $f_{beat} = 6.29/3$ Hz which correspond to the structural frequency of $f_s = 4.46$ Hz, $f_s = 3.63$ Hz and $f_s = 6.29$ Hz, respectively. This leads to the second or third harmonic of the jumping activity to coincide with the frequency of the structure. The results of these simulations using this set of input forces are performance comparisons (peak accelerations and MTVV of acceleration) in addition to the actuator inertia force and input voltage. The running time for each of the input forces is set to 120 seconds.

It should be noted that for the jumping frequencies of 3.63 and 4.45 Hz, the second harmonic has been chosen since it is possible to jump at 3.36/2 and 4.45/2 Hz. However, for structural frequency of 6.29 Hz, the third harmonic of 6.29/3 was chosen since it is not possible to jump at 6.29/2 Hz.

For the final input force signal, a combination of the three jumping frequencies mentioned above is employed (Figure 5-7). This excitation time history contains 540 seconds jumping force from four people. It includes up to the third harmonic of jumping. The frequency of the jumping changes every 60 seconds. Also, it will be noted later that at every 180 seconds of the simulation, the frequency of the structure changes. This generates a situation where the structure in three different frequencies experiences three different jumping forces with three different frequencies.

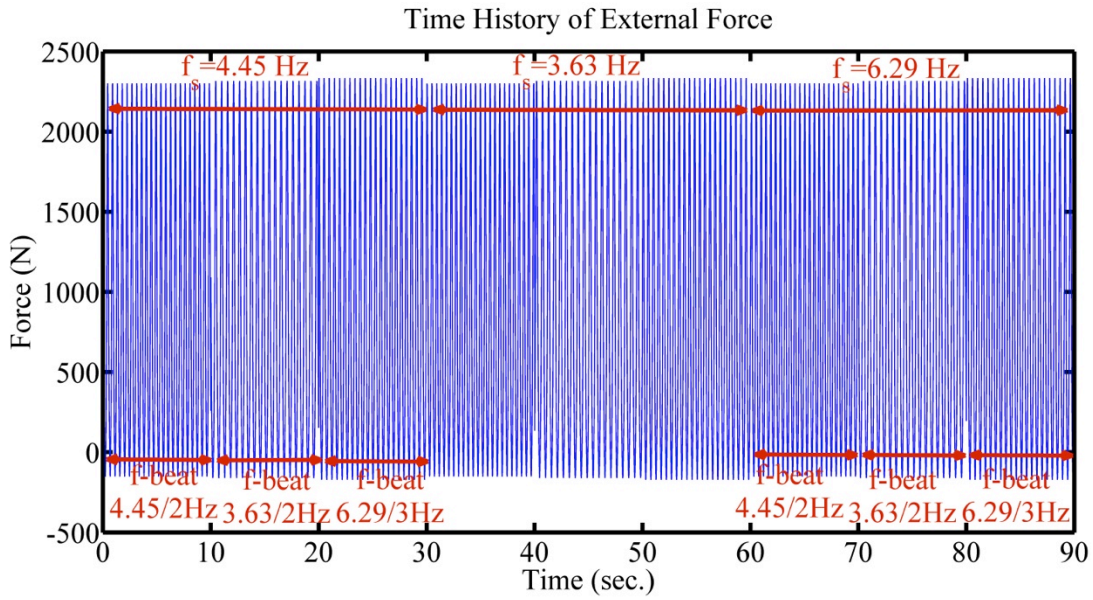

Figure 5-7- Simulated jumping force of 4 people (scaled version on time axis)

Figure 5-8 illustrates the PSD of the generated jumping force. As can be seen, it has all components of three different frequencies including their second and third harmonics at 1.82, 2.1, 2.22, 3.64, 4.2, 4.46, 5.44, 6.3 and 6.7 Hz.

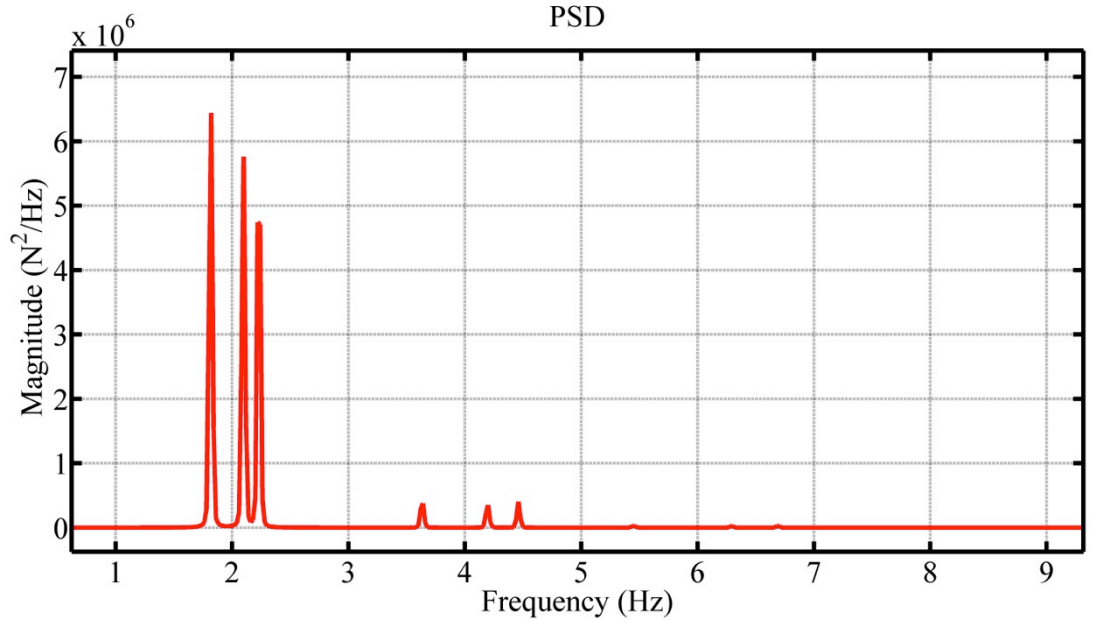

Figure 5-8- PSD of the input force

The result of the third type of simulation using the latest type of jumping force is a set of structural acceleration RMS comparisons for both TMD and HTMD performances and also operation result of the HTMD when the frequency of the

structure and force changes. Also, the RMS of the actuator inertia force is compared in both HTMD control algorithms.

5.4.2. Structural response

The FRFs and responses of the structure are compared for different scenarios. In addition to these, the inertia force and voltage of the actuator are also examined here.

5.4.2.1. Frequency domain response to random excitation

Using the aforementioned random signal in a similar way as in Section 4.2.2.1, the FRFs between external excitation force and structural acceleration were generated for various scenarios. A Hanning window with 50% overlap was applied to the data when calculating FRFs.

The comparison is made between the uncontrolled structure, structure with attached TMD tuned to a frequency of 4.45 Hz and structure with attached HTMD using the two aforementioned control algorithms. The frequency of the structure is altered as noted before to three different frequencies. Also, it should be noted that for the first type of HTMD control algorithm, just one set of gains is used for three different frequencies of the structure. However, on the second type of control algorithm, three different sets of gains are employed each linked to a specific structural frequency.

Direct response feedback with robust gains for individual frequencies

Figure 5-9 shows the magnitude of the FRF of the structure between input force and external excitation. As can be seen, when the frequency of the TMD is tuned to 4.45 Hz (left figure), both TMD and HTMD have similar structural acceleration response at the uncontrolled resonant frequency. However, the HTMD has greater reduction at other frequencies even when the TMD is properly tuned.

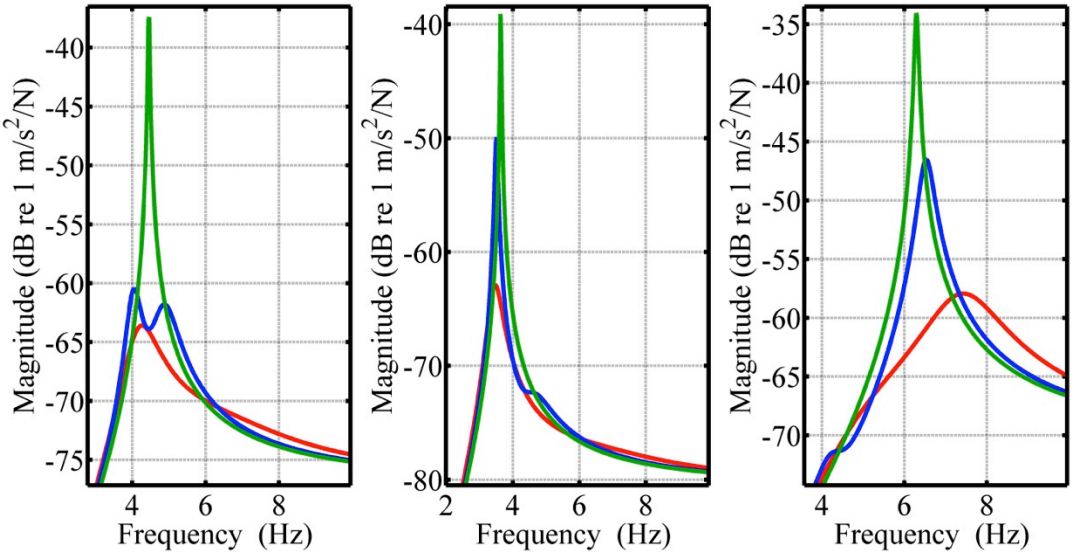

Figure 5-9- FRF of the uncontrolled structure (green) in comparison with structure with TMD (blue) and HTMD (red); off-tuning using robust gains with f_s=4.46 Hz (left), f_s=3.63 Hz (middle) and f_s=6.29 Hz (right),

When the structural natural frequency changes to 3.63 and 6.29 Hz (middle and right figures), the TMD becomes detuned and its performance is reduced. However, the HTMD still shows relatively good performance even when the structural frequency changes.

Table 5-6 compares the results of the simulation for different scenarios for both FRF response at the resonant frequency and also peak of the FRF magnitudes.

Table 5-6- Frequency domain simulation result comparison for different structural frequencies using direct response with robust gain

f_s (Hz)	Type	Maximum response		Response on resonance	
		FRF magnitude ($m/s^2/N$)	Reduction	FRF magnitude ($m/s^2/N$)	Reduction
3.63	Uncontrolled	0.0111	-	0.0111	-
	TMD	0.00319	71%	0.00109	90%
	HTMD	0.000717	94%	0.000594	95%
4.46	Uncontrolled	0.0135	-	0.0135	-
	TMD	0.000949	93%	0.000639	95%
	HTMD	0.000661	95%	0.000622	95%

6.29	Uncontrolled	0.0198	-	0.0198	-
	TMD	0.00472	76%	0.00275	86%
	HTMD	0.00127	94%	0.00079	96%

As the numbers show, the HTMD displays relatively good performance when the TMD becomes detuned. There are the reductions of 78%, 30% and 73% in the FRF maximum response with HTMD compared with passive TMD for the structural frequencies of 3.63 Hz, 4.46 Hz and 6.29 Hz respectively. Also, reductions of 46%, 3% and 71% are achieved based on the response of the FRF at the uncontrolled resonant frequency between HTMD and passive TMD for the structural frequencies of 3.63 Hz, 4.46 Hz and 6.29 Hz respectively.

Adaptive control method using GA for individual frequencies

Figure 5-10 shows the magnitude of the FRF of the structure between input force and external excitation. As noted before, three sets of gain factors are applied for these three scenarios. As the figure illustrates, even when the TMD is tuned (left figure), the HTMD has much larger reduction in the structural acceleration response.

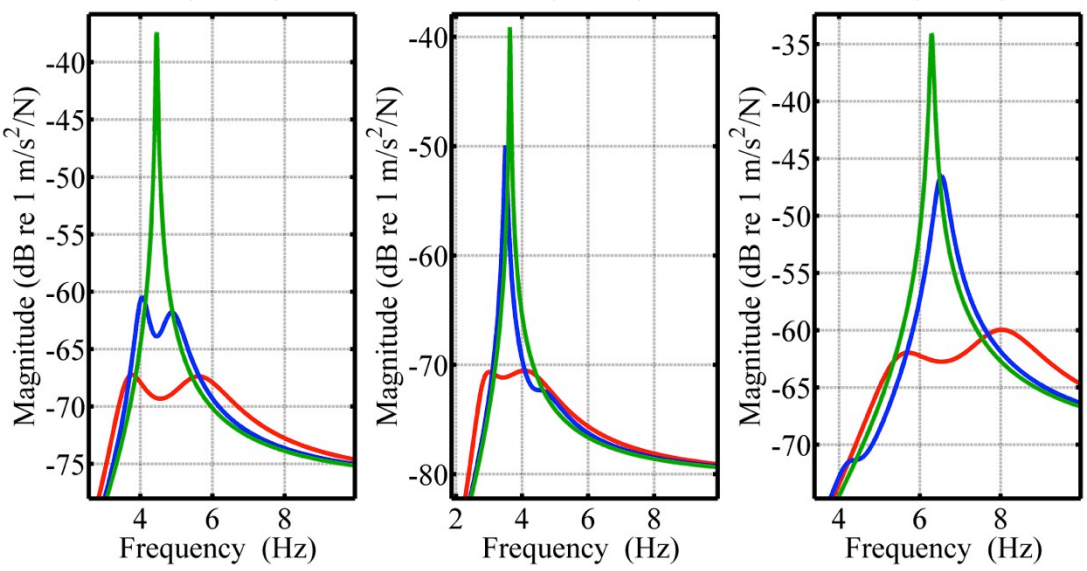

Figure 5-10- FRF of the uncontrolled structure (green) in comparison with structure with TMD (blue) and HTMD (red); off-tuning using adaptive control method with f_s=4.46 Hz (left), f_s=3.63 Hz (middle) and f_s=6.29 Hz (right),

As the frequency of the structure changes (middle and right figure), the performance of the TMD deteriorates. Meanwhile, the HTMD still achieves a large reduction of structural response. Table 5-7 expresses the numerical result of simulation. It can be seen that the HTMD has greater reduction in structural response both at the resonance frequency and peak FRF magnitudes.

Table 5-7- Frequency domain simulation results comparison for different structural frequency using adaptive control method

f_s (Hz)	Type	Maximum response		Response on resonance	
		FRF magnitude ($m/s^2/N$)	Reduction	FRF magnitude ($m/s^2/N$)	Reduction
3.63	Uncontrolled	0.0111	-	0.0111	-
	TMD	0.00319	71%	0.00109	90%
	HTMD	0.000291	97%	0.00028	97%
4.46	Uncontrolled	0.0135	-	0.0135	-
	TMD	0.000949	93%	0.00064	95%
	HTMD	0.000434	97%	0.00034	97%
6.29	Uncontrolled	0.0198	-	0.0198	-
	TMD	0.00472	76%	0.00275	86%
	HTMD	0.001	95%	0.00074	96%

Also, there are the reductions of 91%, 54% and 79% in HTMD FRF maximum response in comparison with passive TMD for the structural frequencies of 3.63, 4.46 and 6.29 Hz, respectively. Also the reduction of 74%, 46% and 73% is achieved based on the response of the FRF at resonance between HTMD and passive TMD for the structural frequencies of 3.63, 4.46 and 6.29 Hz, respectively.

To conclude, based on the FRFs of both proposed control algorithms, the adaptive control method has greater reduction in structural response in comparison with the robust control gains method when the frequency of the structure alters. However, since the performance of the adaptive control method depends on system identification of the structural frequency at time of operation, the third set

simulations will be executed to check the ability of the controller to adapt to changes in the frequencies of the force and structure.

5.4.2.2. Time domain response

Two sets of simulations are performed here. Similar to the frequency domain analysis, the first time domain approach simulates the system at different structural frequencies with their corresponding excitation force individually using the two proposed control algorithms separately. The purpose of this particular simulation is to check the actuator effort.

The second time domain approach is performed to check the performance of the system in a more realistic situation when the frequency of the structure and force may change during operation. In addition, the performance of the proposed system identification method will also be investigated.

The weighted acceleration of the structure according to [169] was used. W_k is chosen as the frequency weighting curve in which z-axis of the person is exposed to the vibration.

Direct response feedback with robust gains for individual frequencies

Here, the performance of the proposed control algorithm using the robust gain control method is investigated. As Table 5-8 and Table 5-9 display, the response of the structure at different structural frequencies with their corresponding external jumping force is investigated. The results are in terms of peak, RMS and MTVV of the weighted acceleration.

As can be seen, in general there is greater reduction in response when the HTMD is employed in comparison with the passive TMD when the frequency of the structure changes. This can be seen in all scenarios when excitation force components coincide with the structural frequency.

Table 5-8- Time domain simulation result comparison for different structural frequency using robust control gains method; comparison of the peak of the structural weighted acceleration (m/s^2)

f_s (Hz)	Type	Peak weighted acceleration(m/s^2)	Reduction from	Reduction from

			uncontrolled structure	structure with TMD
3.63	Uncontrolled	3.1940	-	-
	TMD	0.3020	91%	-
	HTMD	0.1829	94%	39%
4.46	Uncontrolled	3.9841	-	-
	TMD	0.2373	94%	-
	HTMD	0.2287	94%	4%
6.29	Uncontrolled	1.8636	-	-
	TMD	0.3176	83%	-
	HTMD	0.1500	92%	53%

Table 5-9- Time domain simulation result comparison for different structural frequency using robust control gains method; comparison of MTVV of the structural weighted acceleration (m/sec^2)

f_s (Hz)	Type	MTVV(m/sec^2)	Reduction from uncontrolled structure	Reduction from structure with TMD
3.63	Uncontrolled	2.2711	-	-
	TMD	0.2083	91%	-
	HTMD	0.1159	95%	44%
4.46	Uncontrolled	2.7960	-	-
	TMD	0.1398	95%	-
	HTMD	0.1363	95%	3%
6.29	Uncontrolled	1.2751	-	-
	TMD	0.1825	86%	-
	HTMD	0.0754	94%	59%

As was shown in the FRF analysis, using HTMD with robust gain does not have greater reduction in structural response in comparison with passive TMD when the frequency of the excitation force is at resonance and the TMD is tuned. However, when the frequency of the structure changes, the TMD becomes detuned and yet the HTMD performs relatively more consistently.

Adaptive control method using GA for individual frequencies

The performance of the adaptive control method is investigated here. Table 5-10 and Table 5-11 show the time domain analysis results due to different structure frequencies. As these tables reveal, the HTMD performs well in the presence of the off-tuning problem. Also, as noted before, this performance is better in comparison with the HTMD using the robust gain method. The exception to this case is when the frequency of the structure increases in which the reductions are similar between both methods.

Table 5-10- Time domain simulation result comparison for different structural frequency using adaptive control method; comparison of the peak of the structural weighted acceleration

f_s (Hz)	Type	Peak weighted acceleration (m/sec^2)	Reduction from uncontrolled structure	Reduction from structure with TMD
3.63	Uncontrolled	3.1940	-	-
	TMD	0.3020	91%	-
	HTMD	0.1074	97%	64%
4.46	Uncontrolled	3.9841	-	-
	TMD	0.2373	94%	-
	HTMD	0.1546	96%	35%
6.29	Uncontrolled	1.8662	-	-
	TMD	0.3192	83%	-
	HTMD	0.1505	92%	53%

Table 5-11- Time domain simulation result comparison for different structural frequency using adaptive control method; comparison of MTVV of the structural weighted acceleration

f_s (Hz)	Type	MTVV(m/sec^2)	Reduction from uncontrolled structure	Reduction from structure with TMD
3.63	Uncontrolled	2.2711	-	-
	TMD	0.2083	91%	-
	HTMD	0.0582	97%	72%
4.46	Uncontrolled	2.796	-	-
	TMD	0.1398	95%	-
	HTMD	0.082	97%	41%
6.29	Uncontrolled	1.2785	-	-
	TMD	0.1835	86%	-
	HTMD	0.0756	94%	59%

Multi-frequency variable structure model

As is shown in Figure 5-11 and Figure 5-12, when the jumping excitation acts on a structure with altered frequency, the performance of HTMD is generally better than the TMD. This applies for the HTMD with both control methods. However, when the structural frequency is nominal, the HTMD with robust gain has quite a similar performance as the TMD. However, the HTMD with adaptive control has much more reduction even when the frequency of the structure doesn't change in comparison with TMD.

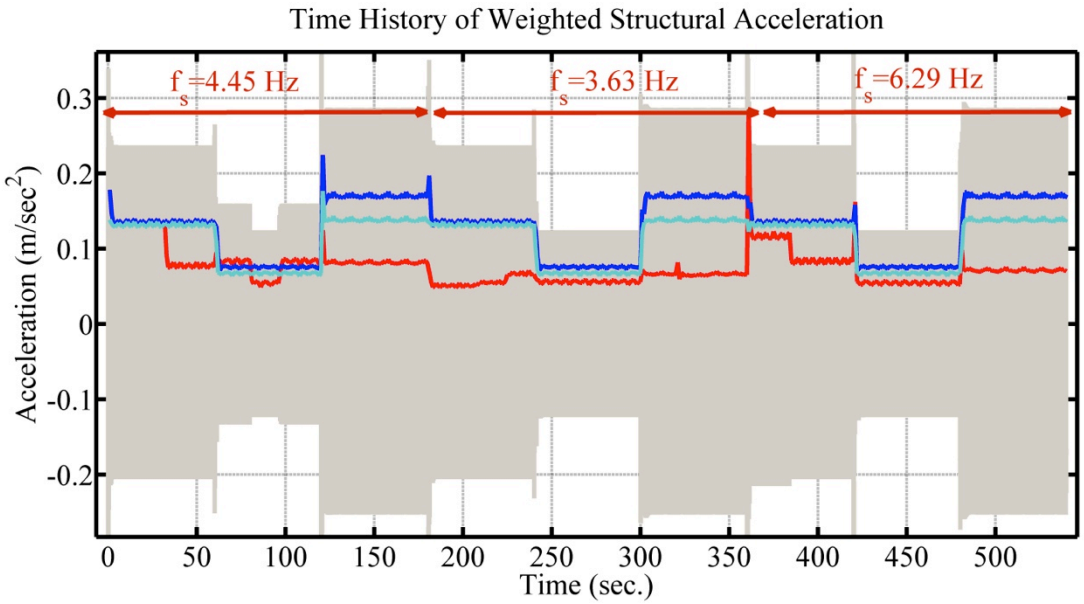

Figure 5-11- Structural weighted acceleration and corresponding running RMS (1 sec.) response from simulated jumping force (4 people); TMD (blue), HTMD with robust gain (cyan), HTMD with adaptive control (red)

Also, based on the figures, at the moment of the changing of the structural frequency, there might be a large peak in response using HTMD with adaptive gain. This looks to happen when two structural frequencies are placed in the same time segment of the PSD, which then has two structural frequencies instead of one.

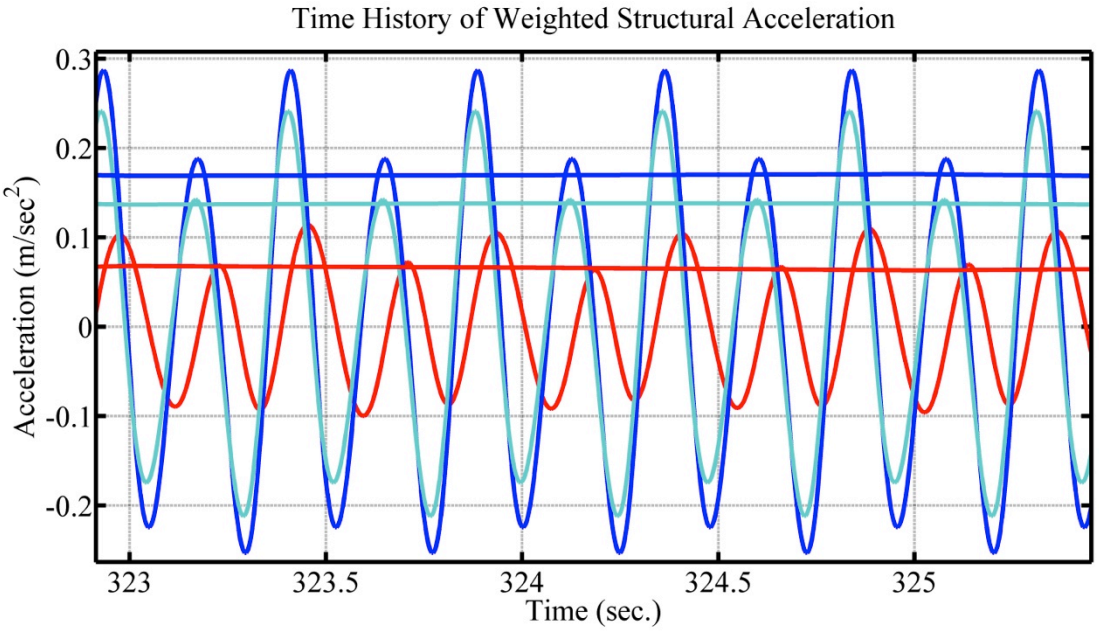

Figure 5-12- Structural weighted acceleration and corresponding running RMS (1 sec.) response from simulated jumping force (4 people); TMD (blue), HTMD

with robust gain (cyan), HTMD with adaptive control (red) (zoomed version of Figure 5-11)

However, it should be considered that when the frequency of the structure doesn't change, if the force frequency has a component except resonant frequency, then HTMD with robust gain causes more reduction in structural response in comparison with passive TMD.

5.4.2.3.Actuator capability and effort

Based on Table 5-12 and Table 5-13, it can be concluded that the amount of inertia force of the actuator depends on the frequency of the structure. When the TMD is tuned, the HTMD maximum required inertia force is higher when robust gain is employed in comparison with adaptive control method.

When the frequency of the structure increases, less force is required in HTMD with adaptive control in comparison with robust gain. However, when the frequency of the structure decreases, it is adaptive control which needs more inertia force for actuator.

Table 5-12- Time domain simulation result comparison for different structural frequency using robust control gains method; comparison of actuator effort

f_s (Hz)	Type	Magnitude
3.63	Peak of inertia force (N)	85
	MTVV of inertia force (N)	60
4.46	Peak of inertia force (N)	96
	MTVV of inertia force (N)	54
6.29	Peak of inertia force (N)	116
	MTVV of inertia force (N)	61

Generally, in all cases, the maximum demanded actuator force is around a quarter of the maximum capacity of the actuator. This shows that a smaller and lower cost actuator would satisfy the requirements of the HTMD for these scenarios.

Table 5-13- Time domain simulation result comparison for different structural frequency using adaptive control method; comparison of actuator's effort

f_s (Hz)	Type	Magnitude
3.63	Peak of inertia force (N)	160
	MTVV of inertia force (N)	86
4.46	Peak of inertia force (N)	78
	MTVV of inertia force (N)	66
6.29	Peak of inertia force (N)	98
	MTVV of inertia force (N)	55

Figure 5-13 displays the time history of the actuator inertia force and its corresponding 1 second running RMS when the multi-frequency simulation is performed. It shows that generally the HTMD with robust control requires less control force compared with adaptive control. Also, when the structure or force frequencies changes, there are quite sudden changes in the control force envelope in adaptive control. However, robust gain shows more fixed pattern in comparison to the adaptive method.

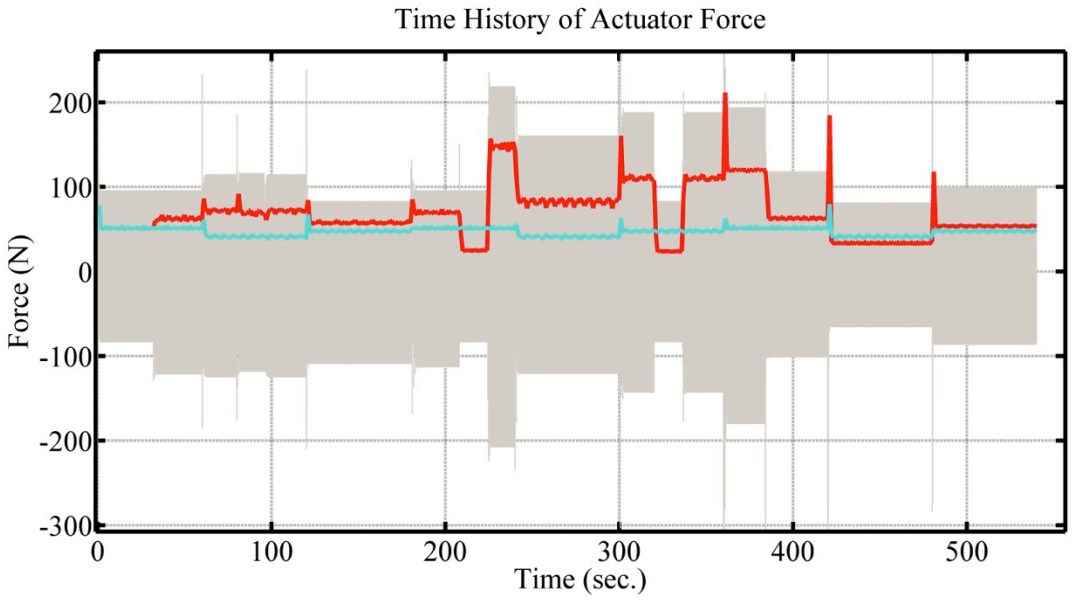

Figure 5-13- Actuator inertia force and corresponding running RMS (1 sec.); response from simulated jumping force (4 people) for 3 frequencies; HTMD with robust gain (cyan), HTMD with adaptive control (red)

Table 5-14- Time domain simulation result comparison for multi-frequency variable structure model; comparison of actuator effort

Type	RMS of actuator inertia force (N)
HTMD with robust gain	47
HTMD with adaptive control	76

Also, as Table 5-14 reveals, HTMD with robust gain method needs almost around 38% less inertia force of actuator in comparison with adaptive method when the frequencies of both the structure and force alter in real time.

5.5. Conclusion and result discussion

In this chapter, two different approaches were introduced to improve the performance of an HTMD in the presence of the off-tuning problem. The goal of these methods was to achieve minimum structural response in the situation in which the structural mass and/or frequency alters.

The gains from each control method were generated and optimised using a GA approach. In the first method, one set of gains was applied to the system to perform over a range of structural frequencies, whereas in the second method, individual sets of gains corresponding with each structural frequency were employed.

It was shown that when the frequency of the structure changes from 4.45 Hz to either 3.63 Hz or 6.29 Hz, the performance of the HTMD deteriorates. This is both in situations where the excitation force (e.g. jumping force) has a component at resonance and when it doesn't.

It is demonstrated that HTMD with adaptive control has greater reduction in structural response in comparison with HTMD with robust gain method when the frequency of the structure does not change or decrease. However, when the frequency of the structure increases, both adaptive and robust control have similar performance and both show greater reduction in comparison with a similarly sized passive TMD.

Also, it is illustrated that the actuator effort is less when using robust gain control method for the cases which the frequency of the structure reduces. However, as the

frequency of the structure increases, the adaptive control requires less power to perform.

It can be argued that based on both response reduction and actuator effort, adaptive control has the best overall performance.

Also, a multi-frequency simulation was performed in which both the frequencies of the structure and force were altered throughout the simulation. It was shown that the adaptive control performed better in comparison with the robust gain approach. This was due to the similar performance of TMD and HTMD with robust gain when the TMD was tuned, whereas the HTMD with adaptive gain had better response reduction in this scenario.

As an important point, although the adaptive control approach in general was more suitable control method in comparison with robust gain method, its performance highly depends on the size of the data base and also the accuracy of the system identification algorithms. With increased size database, the adaptive control approach would be expective to achieve even better performance.

On next chapter author will investigate and verify the proposed HTMD and its control algorithm by building and testing a prototype HTMD in a laboratory structure.

6. Experimental investigation of dynamic performance of a HTMD

A shorter version of this chapter was presented and published in the [170].

6.1. Introduction

The HTMD used in this research work comprised of a TMD with an active inertial actuator attached to the passive mass. This HTMD was designed and built by the author with appropriate technical support. Tests were conducted on the HTMD both while it was on solid ground (stiff laboratory floor) and when it was located on the experimental laboratory structure (post-tensioned slab strip).

The main goal of experiments on the stiff floor was to determine the dynamic properties and performance of the HTMD as a SDOF system, prior to installation on the primary structure. After this, the HTMD was placed on the laboratory slab strip for the main experiments. In general, the following aims were investigated:

- Investigation of the performance of the HTMD and TMD on the slab
- Verify all proposed control algorithms and compare the experimental results with analytical models and simulations
- Investigate the performance of HTMD and TMD in the presence of off-tuning

To achieve these aims, several tests were performed including FRF measurements, time domain measurements using sinusoidal input force, human jumping force at different frequencies and heel-drop tests. Also the force of the active element of HTMD was recorded in all tests.

6.2. Mechanical design and construction of HTMD

TMD parameters

The parameters of the proposed TMD (i.e. mass, stiffness and damping) were summarised in Table 3-4. These parameters were calculated according to the available model of the primary structure (i.e. the laboratory slab).

TMD components

TMD components consist of springs, damper and masses. In this research job, 4 compression springs with the stiffness coefficient of 63.47N/mm are employed. Also, an air damper with viscos behaviour is purchased. However, due to the practical

limitation of the damper, it was decided to remove it and use the active part to produce damping force in the HTMD.

However, it should be noted that the absence of damper does not imply zero damping since there is inherent friction which produces damping inside the system. This is investigated in further parts of this chapter.

As noted before, the HTMD consists of a passive TMD in addition to an active mass damper. Hence, the first step was to design the mechanics of the TMD.

A TMD comprises of three major elements; mass, spring and damper, which determine the performance of TMD. However, from a practical point of view there are other factors which require consideration. These factors include the geometry of the TMD, the physical stability of the TMD, the capacity of the material (i.e. plates of the TMD body), total weight of the TMD, maximum displacement of the TMD mass and friction in its bearings.

Weight of the TMD and handling

It is very important to calculate the precise weight of the TMD. This is necessary both for the dynamic properties of the TMD and also its handling to place it on the target structure

Figure 6-1- placing the TMD on the slab

After construction of the TMD, the weight of the basket without any masses was measured as 110 kg. Also, the weight of the base plate with the four cylinders was 100 kg.

As the total weight is around 220 kg (without additional masses placed in the basket), it is possible to move and lift the TMD using a portable crane. Figure 6-1 shows the lifting and placing operation of the TMD on the laboratory slab strip using a portable crane with a capacity of 400 kg.

TMD geometry design

Figure 6-2 shows rendered images of the TMD. As can be seen, it consists of a base plate which is placed onto the primary structure and hence is the interface between the TMD and the primary structure. On top of this plate, there are four cylinders which have springs inside. Using these cylinders causes the system to have a support reaction force above the centre of gravity of the moving mass, which leads to a more physical stable system. It is possible to use different stiffness springs according to the application at hand.

The springs support the basket which has the masses inside. It is possible to vary the TMD mass by changing the number of mass blocks placed inside this basket.

As shown in the figure, the actuator (active DOF) is placed on the top of the TMD passive mass. Using this arrangement has the advantage of allowing the use of different sized actuators.

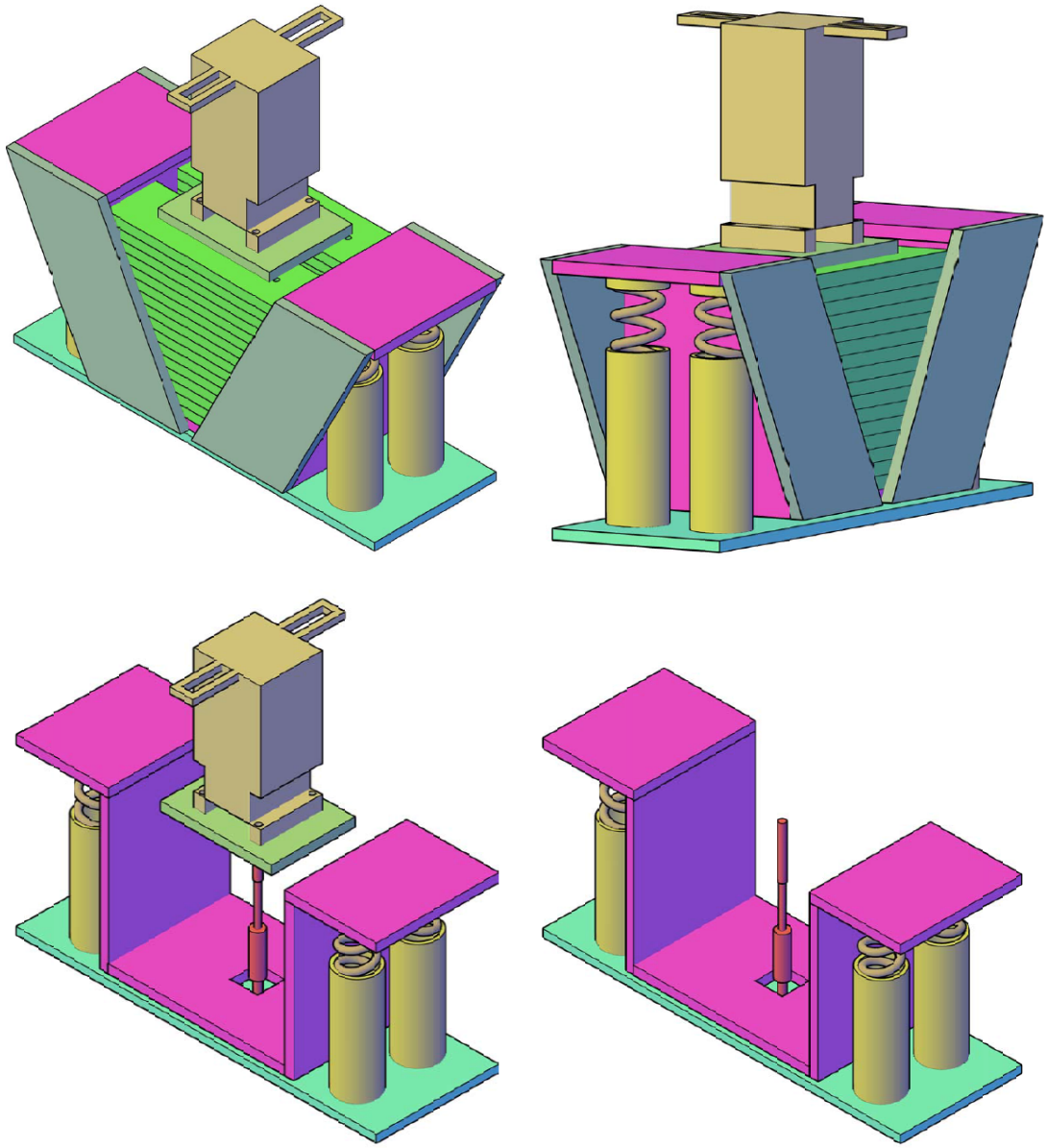

Figure 6-2-Schematic design of HTMD

The base plate of the TMD has size of 130 x 40 cm and the height of the TMD is 58 cm.

Displacement of TMD mass

Maximum displacement of the TMD passive mass is an important factor since it gives the maximum required space below the basket and hence the required height of the cylinders.

To do that, an initial and brief Matlab Simulink simulation was performed with the input force of $10 * 1000\sin(4.5 * 2\pi)$ to just determine the maximum possible displacement of the TMD/HTMD's basket.

This simulation shows that the maximum displacement on TMD's mass is around 80 mm.

6.3. Experimental evaluation of TMD performance

The purpose of this test was to verify the dynamic performance of the constructed TMD/HTMD. Whilst it was located on stiff ground, the shaker on top of the TMD provided an input force and accelerometers on the TMD were used to measure its acceleration response.

Two sets of tests were performed; measurement of frequency response functions and free decay measurements.

Instruments

Figure 6-3- Shaker (left) and amplifier (right)

Figure 6-4- Spectrum analyser (left) and signal conditioner (right)

Endevco 7754A-1000 accelerometers were used to measure the acceleration of the TMD passive mass. These accelerometers were connected to a 16 channel signal conditioner. Also, APS Electrodynamics shakers 400-HF is employed as the actuator. The shaker's driving force is supplied by an Amplifier. Finally, DP730 Data Physics 32-channel spectrum analyser performs the data acquisition and lively FRF measurements.

It should be noted that the dynamic properties of the sensors is neglected for the frequency range of interest since system can be assumed as linear and not dependent on frequency in this range.

6.3.1. Experimental Results

In this experiment, eight 25 kg additional masses were placed on the TMD (in addition to the weight of the basket). However in the set of experiments where the TMD/HTMD was placed on the slab, only six 25 kg masses were used. Also as noted, the damper was removed from the system.

Two accelerometers were used to measure the acceleration response of the TMD; one at the top of the basket and one at the bottom. An additional accelerometer was mounted on the active inertial mass to measure the input force from the active DOF.

FRF test

A random signal with frequency band 0-100 Hz was used as the input force. As can be seen from Figure 6-5, both top and bottom sensors show a very clear modes at 4.37 Hz. Additional modes can be observed at 22.19 and 38.44 Hz, with the latter having greater response at the top of the TMD.

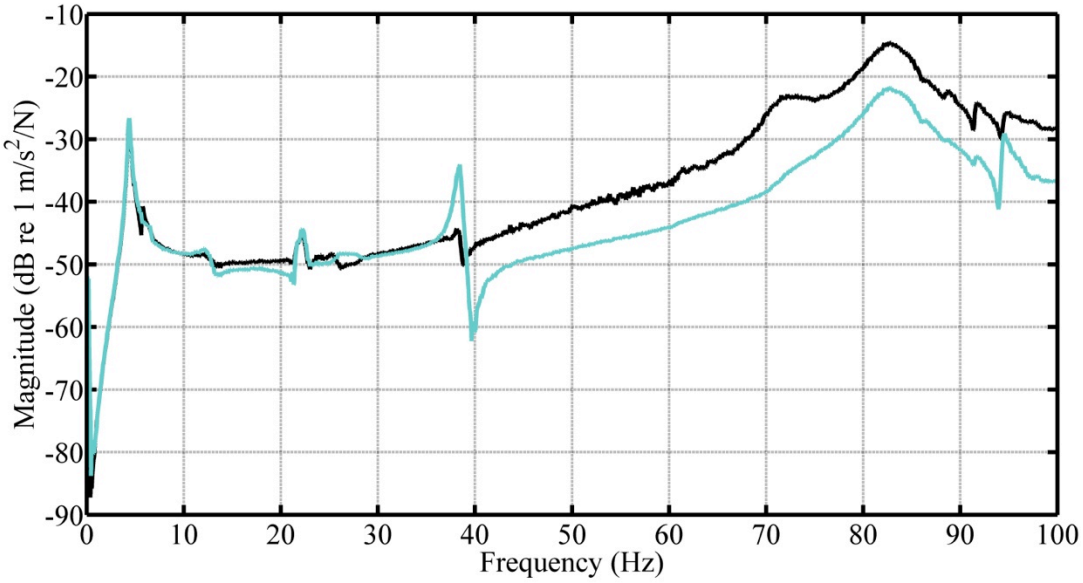

Figure 6-5- FRF magnitude of the TMD placed on the stiff ground; sensor on top of TMD (cyan), sensor at the bottom of the TMD (black)

Free decay test

Two sets of free decay tests were performed to investigate the damping and decay characteristics of the TMD. In the first test, a burst random signal is employed and the shaker is set to off (zero force) after a segment of time. This leads to free-decay response of the TMD. However, the magnitude of the force is restricted since the actuator has a maximum of 450 N inertia force. The second set of tests was carried out using hand-excitation instead of a shaker to produce free-decay response with higher magnitude.

The results of these tests were analysed using a MATLAB-based analysis application called Modal [171]. The damping ratio of the TMD was estimated as 2.8% and 0.41% for the burst signal input and manual excitation respectively. Also, the respective frequencies were estimated as 4.05 Hz and 4.06 Hz.

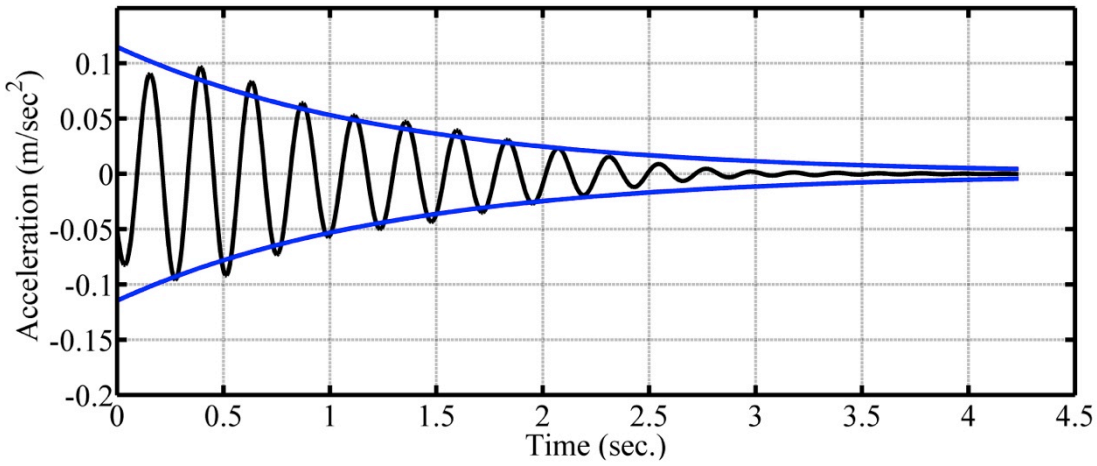

Figure 6-6- Damping estimation of the free-decay response using burst random force from shaker

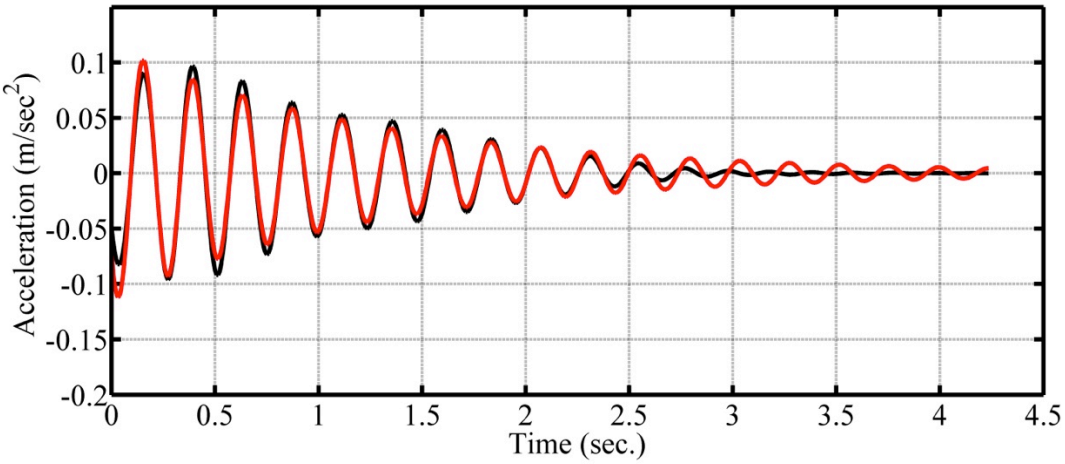

Figure 6-7- Curve fitting of the free-decay response using burst random force from shaker

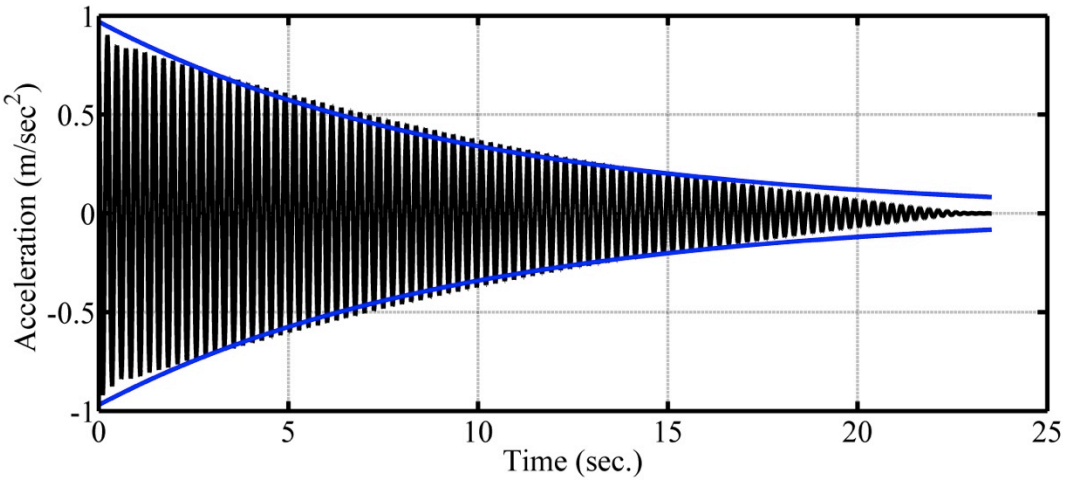

Figure 6-8- damping estimation of the free-decay response using hand excitation

As Figure 6-9 and Figure 6-10 reveal, when the magnitude of the force is low, the amplitude dependency plots show a linear behaviour of frictional damping. This result is similar for higher magnitude of force (hand-excitation) except with less damping result. This confirms the non-linear behaviour of the system's damping.

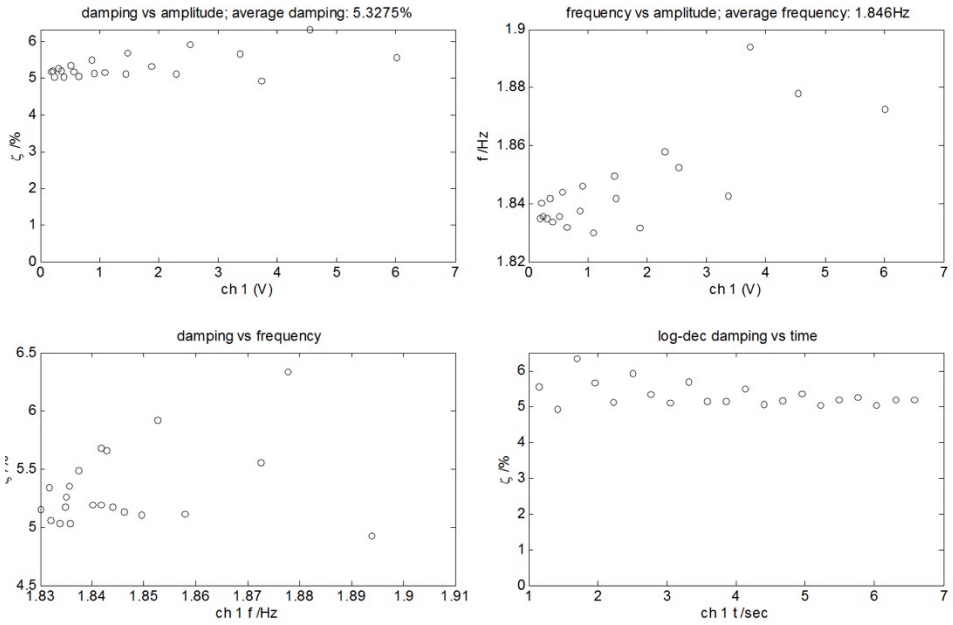

Figure 6-9- Amplitude dependency test on free decay response using burst signal excitation

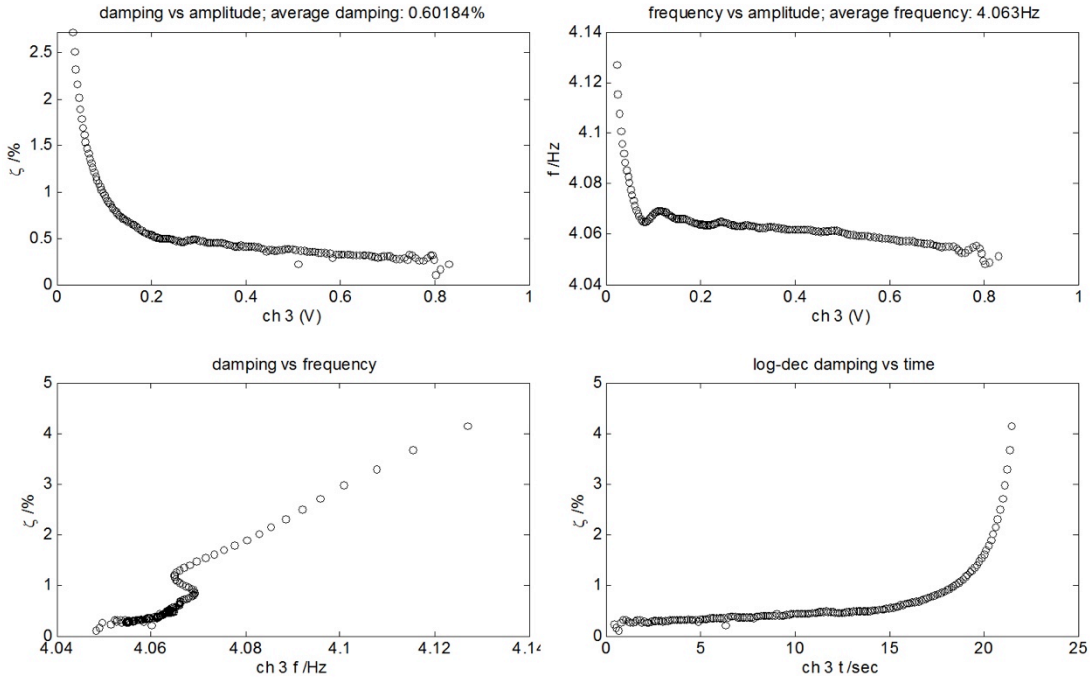

Figure 6-10 Amplitude dependency test on free decay response using hand excitation

6.4. Preparing active damping force on passive TMD

As noted, there was no physical damping element attached to the TMD and the only available damping force was primarily friction in the bearings. To obtain a constant damping force regardless of friction, it is proposed to use the active element of the HTMD to produce a damping force even when it is considered as a passive TMD. This results in a TMD with an active (simulated viscous) damping force. As noted earlier, to produce the active damping force of both TMD and HTMD, the velocity of the TMD passive mass should be used as the feedback signal. In addition, the displacement and acceleration of the TMD were also employed for tuning purposes. However, the gains and corresponding control forces were very low and considered negligible.

6.4.1. Parameters optimisation

Herein, the author used a similar GA approach as described previously to optimise the proposed gains to achieve a damping force which leads to a TMD with a similar performance as the desired passive TMD.

However, the difference is the constraint function which is the FRF magnitude of the structure with attached desired passive TMD. This means the optimisation problem is

changed to a new one in which the feedback gains are optimised subject to the constraint of the FRF of the passive TMD.

Also, the minimisation problem is converted to a maximisation to achieve as close as possible the FRF of the desired passive TMD. Table 6-1 illustrates the optimised gains using this method.

Table 6-1- Optimised gains for HTMD acting as a TMD

K_3 (Vs/m)	K_2 (V.s^2/m)	K_1 (V/m)	K_4 (Vs/m)	K_5 (V.s^2/m)
0.000	0.000	-3.094	-1.816	-0.111

6.4.2. Analytical and experimental verification

The performance of the proposed TMD with active damping force was investigated both analytically and experimentally against the performance of the desired TMD with pure viscous damping.

Figure 6-11 displays the structural FRF magnitude with a TMD attached. As it shows, both practical (blue line) and analytical simulation (red line) TMDs using proposed feedback gains are acting the same as the required and desired passive TMD (green line) mentioned and designed before.

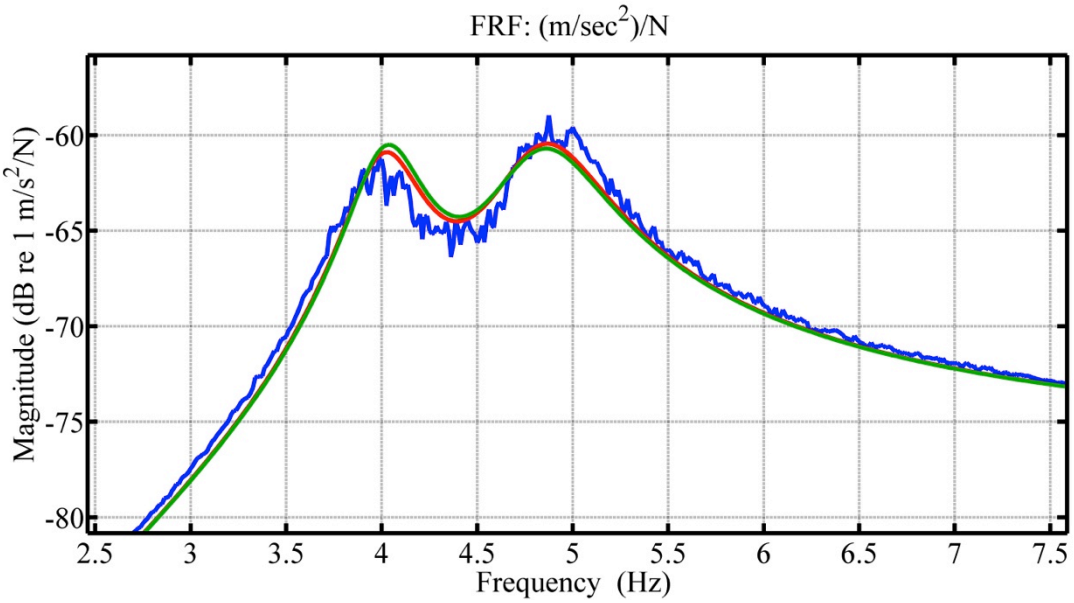

Figure 6-11- FRF of the desired analytical TMD (green), practical TMD with active damping force (blue) and analytical model of TMD with active damping force (red)

6.5. Application of HTMD to laboratory structure

Two main sets of tests were executed. Firstly, the performance of HTMD was compared against that of the passive TMD. This comparison was carried out both in the frequency domain (using FRFs) and in the time domain using a range of input forces. For comparative purposes, the performance of the HTMD was also compared against an active control scheme.

Secondly, the performance of the HTMD was compared against passive TMD in the presence of off-tuning, both in the frequency and time domains.

Figure 6-12- Laboratory slab strip; empty (left) and attached with HTMD (right)

Instruments and test grids

In addition to the same instrumentation described in Section 6.3, a dSPACE control unit was employed to implement the feedback control schemes on the structure.

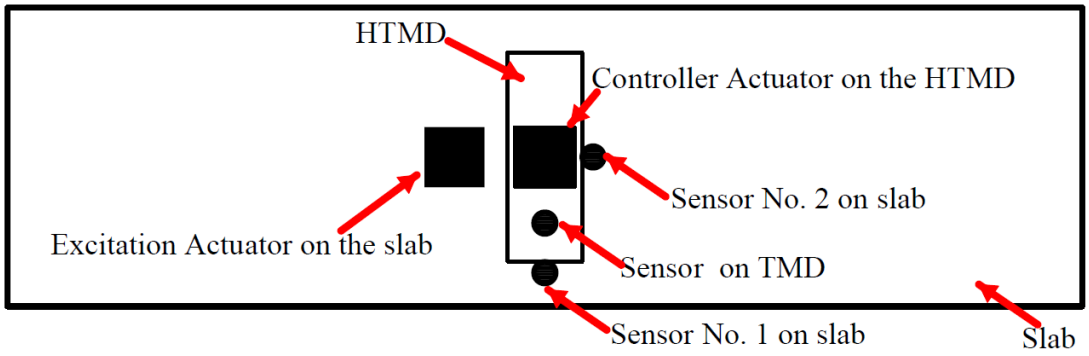

Figure 6-13- arrangement of the equipment on the laboratory slab (sensors are accelerometers)

As shown in Figure 6-13, in addition to the actuator on the HTMD (active part), a similar actuator is located on the slab, next to the HTMD, to apply external force to the primary structure. Five accelerometers were employed; one on the TMD passive mass to measure the response of the TMD, two on the structure (one below and one next to the HTMD) to measure the response of the structure and one on each of the actuators to measure the corresponding inertia forces.

The locations of the accelerometers on the structure were chosen to be at the nodal point of the target mode. Also, a low pass filter was applied to avoid measurement noise due to dynamics of the accelerometers [7], [46], [150].

As shown in Figure 6-15, the control cabinet including the shaker amplifier, signal conditioner, spectrum analyser and dSPACE control unit was placed next to the slab.

Figure 6-14- HTMD and instrumentation arrangements on the laboratory structure (back and front view)

Figure 6-15- HTMD and controller cabinet arrangements on the laboratory structure

For measurements where it was necessary to measure the response of the uncontrolled structure, the TMD/HTMD basket was locked as shown in Figure 6-16. This was to minimise the requirement to mount and dismount the TMD/HTMD on the slab, which was a difficult and time-consuming operation. This was done by placing wooden chocks below the TMD basket. However, it should be noted that the weight of the TMD/HTMD then had to be considered as an additional passive mass attached to the primary structure which was included in the analytical models.

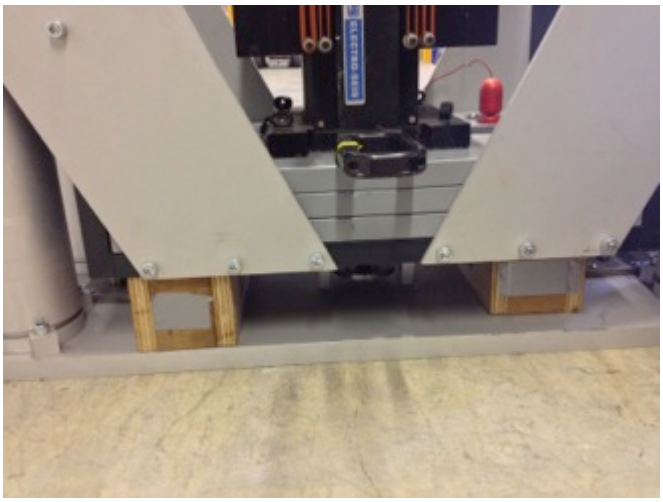

Figure 6-16- locked TMD on the structure for measurements on the uncontrolled structure

Filter Design

In order to remove the DC offset and low frequency noise of the signal and also remove the higher frequency part of the signal, a band pass filter is required. The high pass part of the filter was intended to remove the DC-offset of the sensors and low frequency noises using high-pass filter. In addition to this, since the performance of the system is important for the frequency below 50Hz and the first vibration mode is targeted to be controlled, a low pass filter is applied to avoid the high frequencies component of the response.

This band-pass filter is placed before each integrator block in the controller block diagram (Figure 6-19). Also, the lower and higher bands of the frequencies are set to 0.7 Hz and 50 Hz respectively. The proposed band-pass filter is a second order Butterworth filter. This type of filter is characterized by a magnitude response that is maximally flat in the pass band [165].

The Transfer Function of the filter is generated using MATLAB [165] as follow:

$$G_{filter} = \frac{9.595 * 10^4 s^2}{s^4 + 438.1 s^3 + 9.872 * 10^4 s^2 + 6.053 * 10^5 s + 1.909 * 10^6} \quad \textbf{(6.1)}$$

Figure 6-17 shows the Bode plot of the proposed filter.

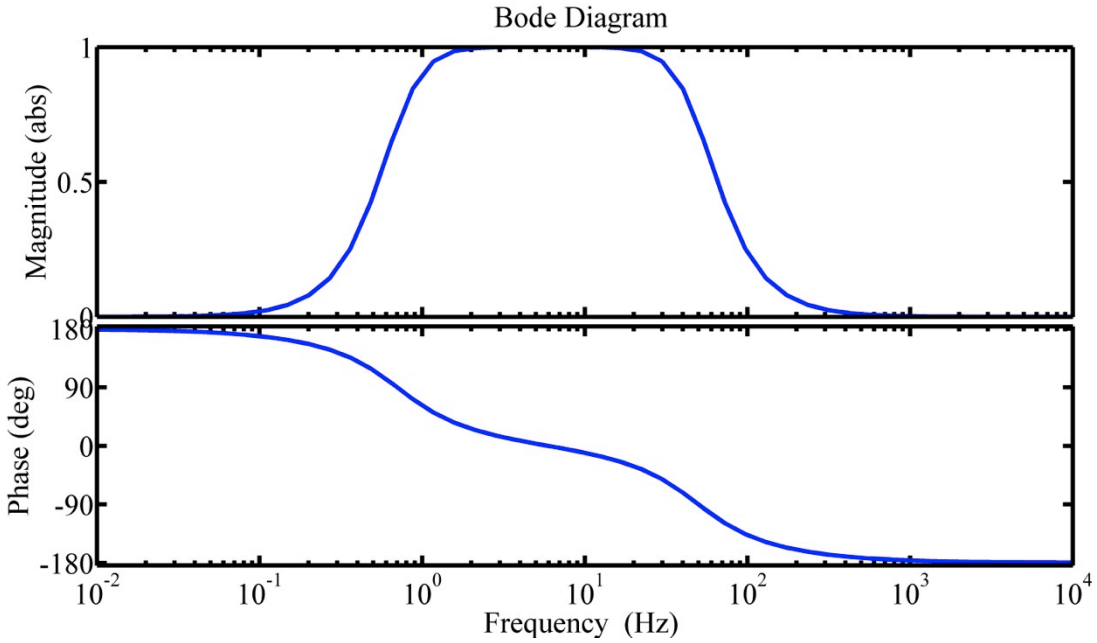

Figure 6-17- Bode plot of the band-pass filter

Controller Unit

As noted before, a dSPACE control unit was employed in this research to implement the designed control algorithms. This was a dSPACE model ACE1103 consisting of a DS1103 PowerPC GX/1 GHz controller board and CLP1103 LED panel (Figure 6-18).

Figure 6-18- dSPACE control unit

The proposed control algorithm (Figure 6-19) was uploaded to the dSPACE unit. As is shown, two measured signals are used for control. The first is the acceleration of TMD and the second is the acceleration of the main structure (sensor No. 1 in Figure

6-13). As is shown in Figure 6-19, integrator blocks are used to obtain velocity and displacement of each signal. These are multiplied by the control gains and summed to generate the control signal, which is fed back to the shaker amplifier.

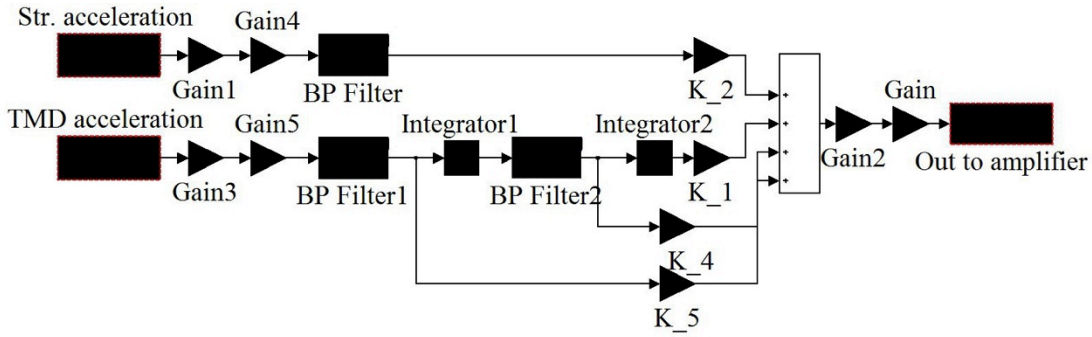

Figure 6-19- MATLAB Simulink model uploaded to dSPACE control unit

6.5.1. Analytical model verification

The proposed analytical model of HTMD was verified by performing a FRF test on the structure when the HTMD was in operation. It should be noted that to have more accurate feedback gains, a new model was generated including the designed band-pass filter.

Table 6-2- Optimised gains for laboratory HTMD

K_3 (Vs/m)	K_2 (Vs^2/m)	K_1 (V/m)	K_4 (Vs/m)	K_5 (Vs^2/m)
0.000	-6.156	-277.332	-22.695	-0.052

Table 6-2 shows the result of the optimisation of the revised structural/TMD properties using the previously described GA approach. Setting these gains in the dSPACE controller unit and performing a FRF test with the frequency span of 10Hz resulted in Figure 6-20. As can be seen, the experimental results correlate well with the analytical model of the structure/HTMD system. The presence of noice can be seen below the frequency of 1Hz. This is the accelerometer dynamics.

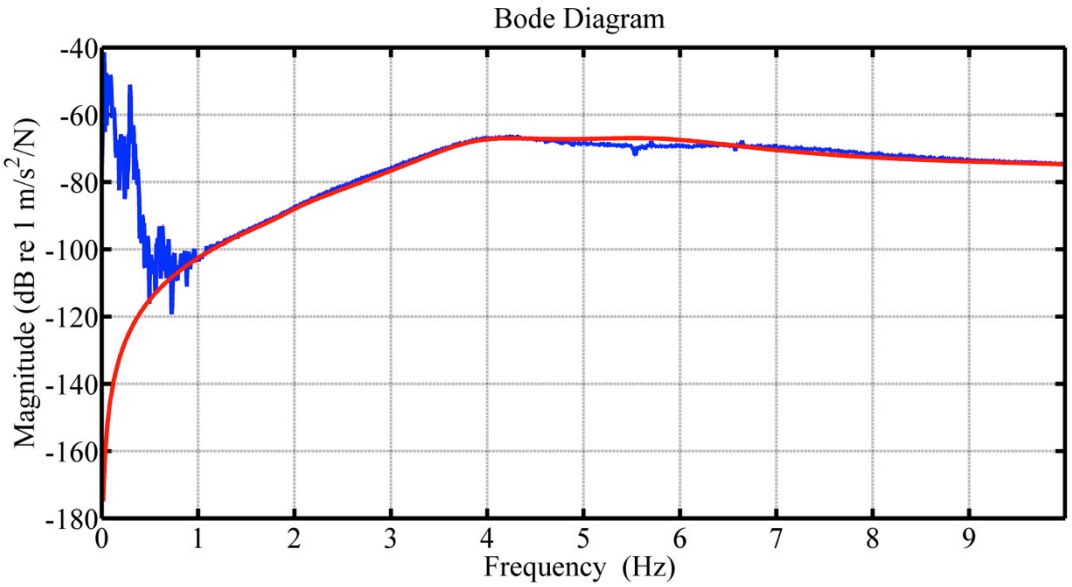

Figure 6-20- comparison of the FRF of analytical model of HTMD (red) with experimental HTMD (blue)

6.5.2. FRF measurements

For the FRF measurements, band-limited random noise signals was employed with frequency bands of:

- 0-10 Hz to see in detail the effect of the HTMD/TMD on the target control mode, and
- 0-100 Hz to check the effect of TMD/HTMD on higher modes.

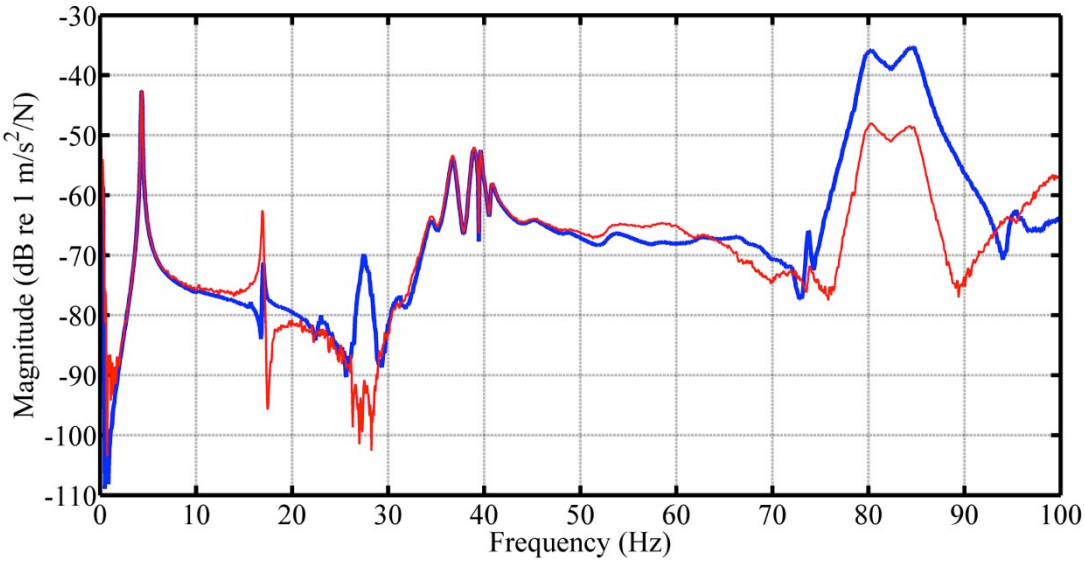

Figure 6-21- FRFs of the uncontrolled structure with responses at accelerometer No 1 (blue) and 2 (red) and excitation at shaker location

Figure 6-21 shows the FRF of the uncontrolled structure from both sensor No 1 and No 2. As can be seen, there is a torsional mode at 27 Hz (sensor No. 1 bottom of TMD) and bending mode at 17 Hz (sensor No. 2 next to TMD).

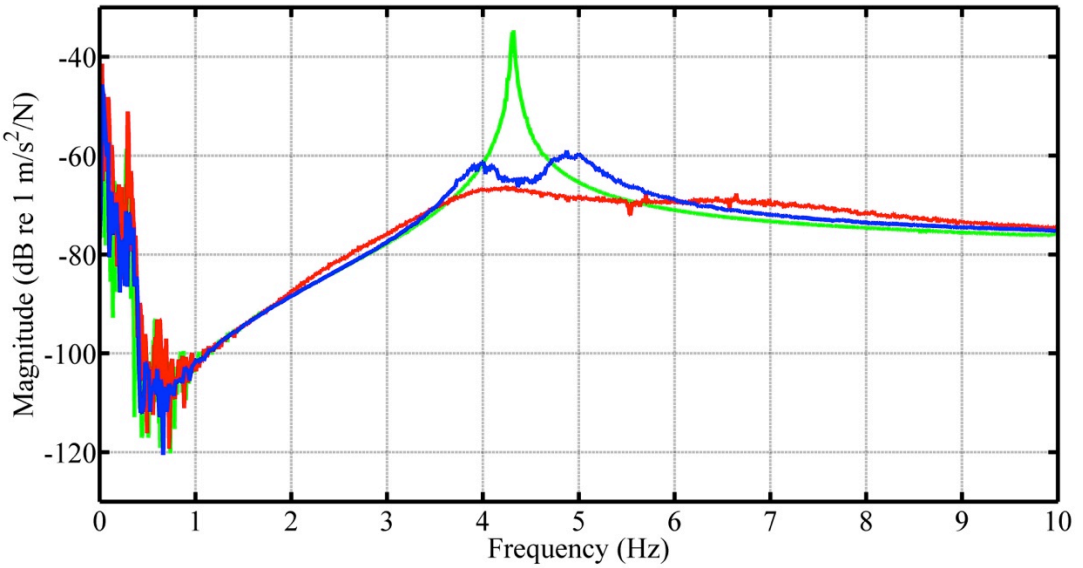

Figure 6-22- Experimental FRF magnitude comparison of the uncontrolled structure (green), structure with TMD (blue) and structure with HTMD (red); frequency span of 10 Hz

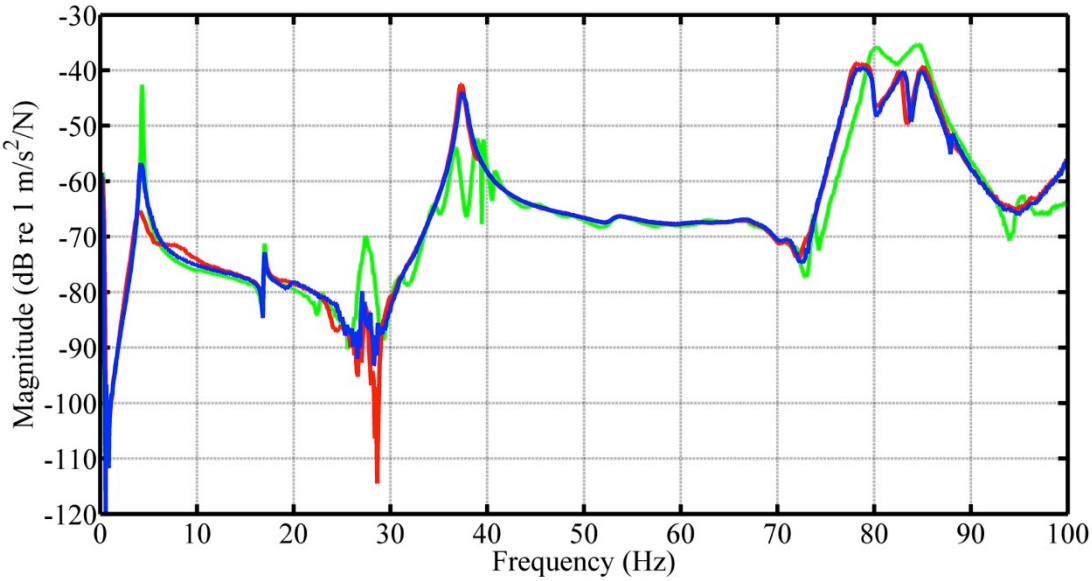

Figure 6-23- Experimental FRF magnitude comparison of the uncontrolled structure (green), structure with TMD (blue) and structure with HTMD (red); frequency span of 100 Hz

As can be seen in Figure 6-22, both the TMD and HTMD achieve a significant reduction in structural acceleration response. Also, it can be seen that the HTMD has higher reduction than the TMD and the response of the structure with HTMD is almost completely inside the boundary of the response of the uncontrolled structure.

In addition, as Figure 6-23 illustrates, there is no significant reduction in response of using HTMD/TMD on higher modes. However, at around 38Hz, there is a response amplification using TMD/HTMD which is the local mode of the TMD, as shown before. The local mode herein means that this is an existing mode in the TMD.

Table 6-3- Experimental result comparison of different control methods

	Uncontrolled Structure	Structure with TMD	Structure with HTMD
Max. response magnitude ($m/s^2/N$)	0.01853	0.00112	0.00049
Reduction of the max. response	-	94%	97%
Response magnitude at resonance frequency of uncontrolled structure ($m/s^2/N$)	0.01853	0.00056	0.00047
Reduction of response at resonance frequency of uncontrolled structure	-	97%	97%

Table 6-3 compares the experimental results of the structural acceleration FRF. It shows 56% and 16% reduction in maximum response and resonant response of structure with HTMD in comparison with structure with TMD.

6.5.3. Measurement of responses to controlled excitations

For the comparison of responses in the time domain, three sets of experiments were performed including using sinusoidal input force (from shaker to check the performance at resonance), jumping force (from a human participant) and a heel-drop test (to check the response on impulse input and have a rough FRF).

Sinusoidal input force

Two sinusoidal input forces were applied to the structure using excitation actuator, their frequencies being those of the frequency of the uncontrolled structure resonance and the frequency of the largest peak of the FRF with passive TMD applied. The magnitude of the force in both scenarios was set to the maximum capability of the actuator (i.e. 2 V).

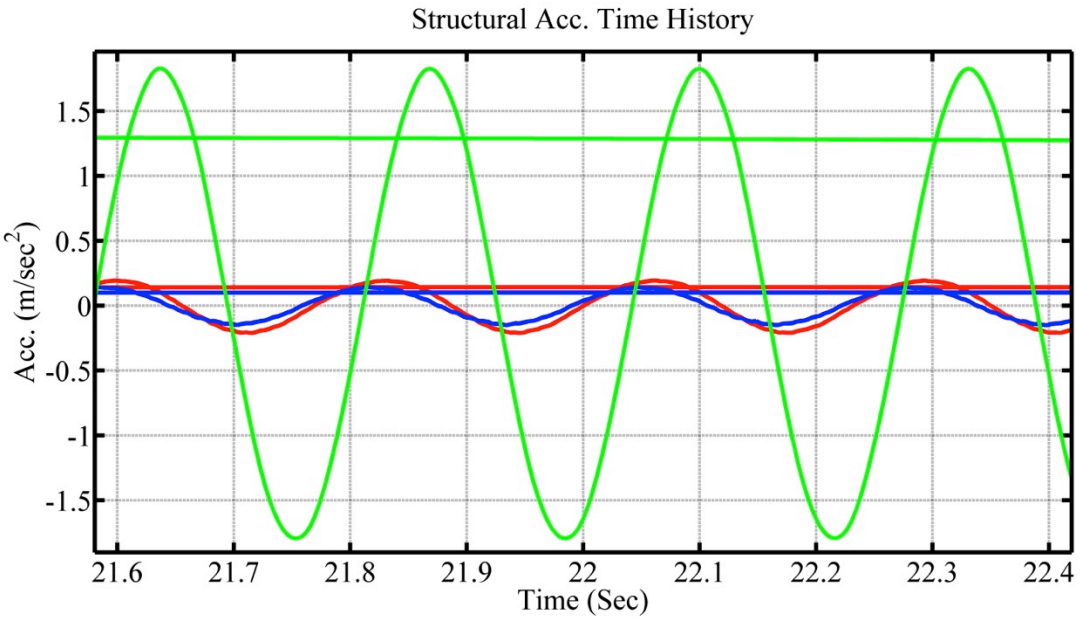

Figure 6-24- Experimental time history of structural acceleration response and corresponding 1 second running RMS of the uncontrolled structure (green), structure with TMD (blue) and structure with HTMD (red); sinusoidal input force with frequency of 4.35Hz

Based on the previous FRF comparison, both TMD and HTMD have similar performance for response reduction at the resonant frequency of the uncontrolled structure. This is verified from the sinusoidal time domain response at this frequency, as shown in Figure 6-24.

However, at the frequency of the maximum FRF peak of the structure/TMD system (i.e. 4.88 Hz), the HTMD showed a large reduction in structural response in comparison with the passive TMD. This is verified in Figure 6-25. Table 6-4 compares the result of time domain using these two sinusoidal inputs. As is shown, at the sinusoidal input with frequency 4.88 Hz, the HTMD gives 79% and 80% reduction in peak acceleration and MTVV of the acceleration respectively in comparison with the passive TMD.

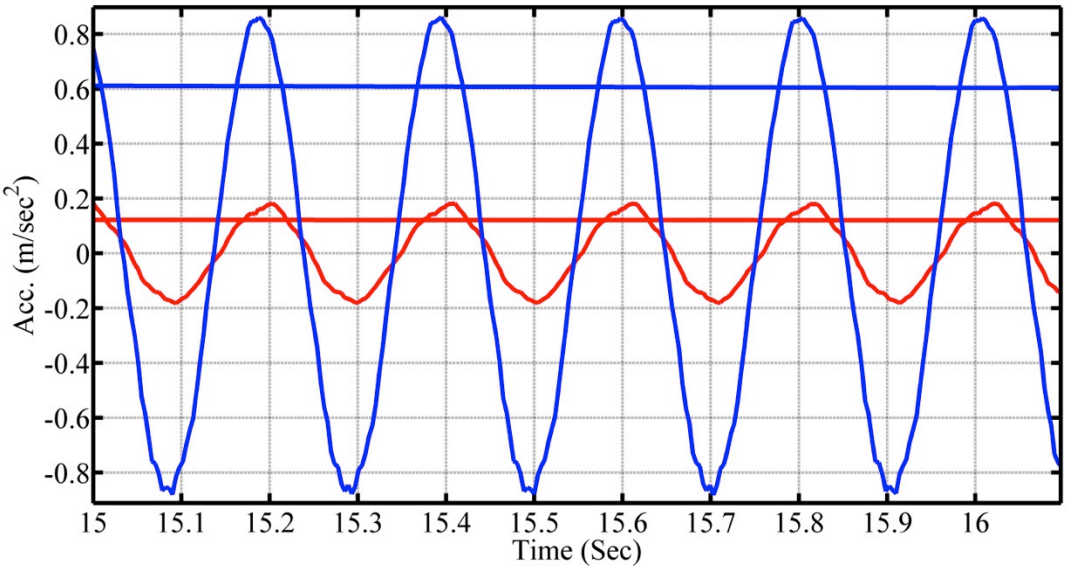

Figure 6-25- Experimental time history of structural acceleration response and corresponding 1 second running RMS of the structure with TMD (blue) and structure with HTMD (red); sinusoidal input force with frequency of 4.88Hz

Table 6-4- Experimental time domain result comparison of different control methods; sinusoidal input force on the structure

	Peak Acc. (m/s^2)			MTVV of Acc. (m/s^2)		
	Unc.	TMD	HTMD	Unc.	TMD	HTMD
Sinusoidal @4.35 Hz	1.839	0.144	0.1928	1.306	0.09956	0.1394
Reduction	-	92%	90%	-	92%	89%
Sinusoidal @4.88 Hz	-	0.8599	0.1816	-	0.6118	0.1211
Reduction	-	-	-	-	-	-

Jumping force

Similar to the sinusoidal input force, two jumping frequencies were applied to the structure. In this test, a human participant jumped on the structure with a frequency such that the second harmonic coincided with the natural frequency of the uncontrolled structure and also at the peak of the FRF with passive TMD, i.e. 2.16 Hz (i.e. 4.32/2 Hz) and 2.44 Hz (4.88/2 Hz) respectively.

With second harmonic of jumping tuned to the structural natural frequency, both TMD and HTMD have similar amount of structural response reduction, as is shown in Figure 6-26. However, at the FRF peak frequency (i.e. second harmonic of 2.44 Hz), the HTMD has much greater reduction in structural response (Figure 6-27). These observations support the results from the FRF measurements. A comparison of the jumping test results is shown in Table 6-5.

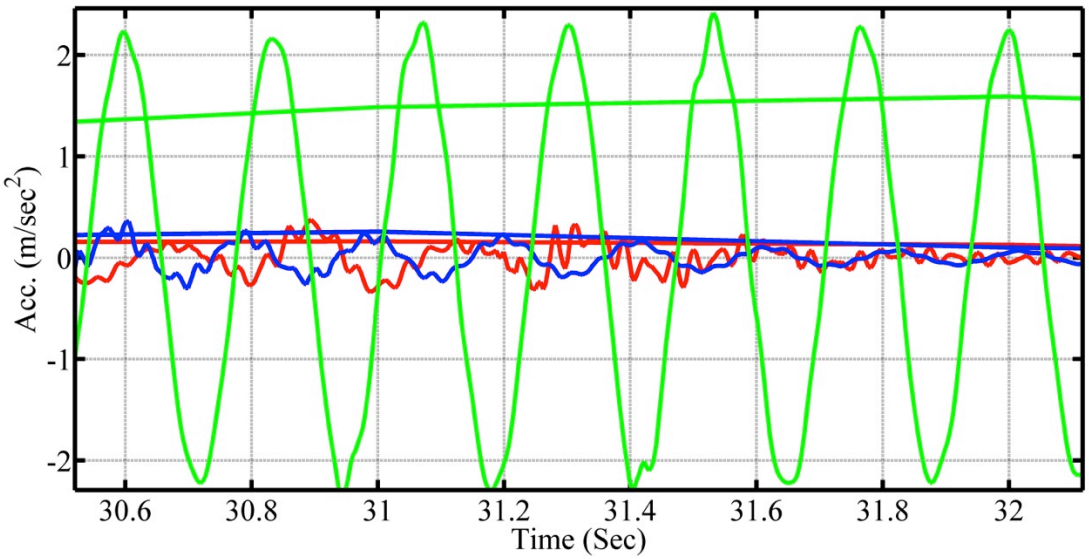

Figure 6-26- Experimental time history of structural acceleration response and corresponding 1 second running RMS of the uncontrolled structure (green), structure with TMD (blue) and structure with HTMD (red); jumping input force with frequency of 2.16 Hz

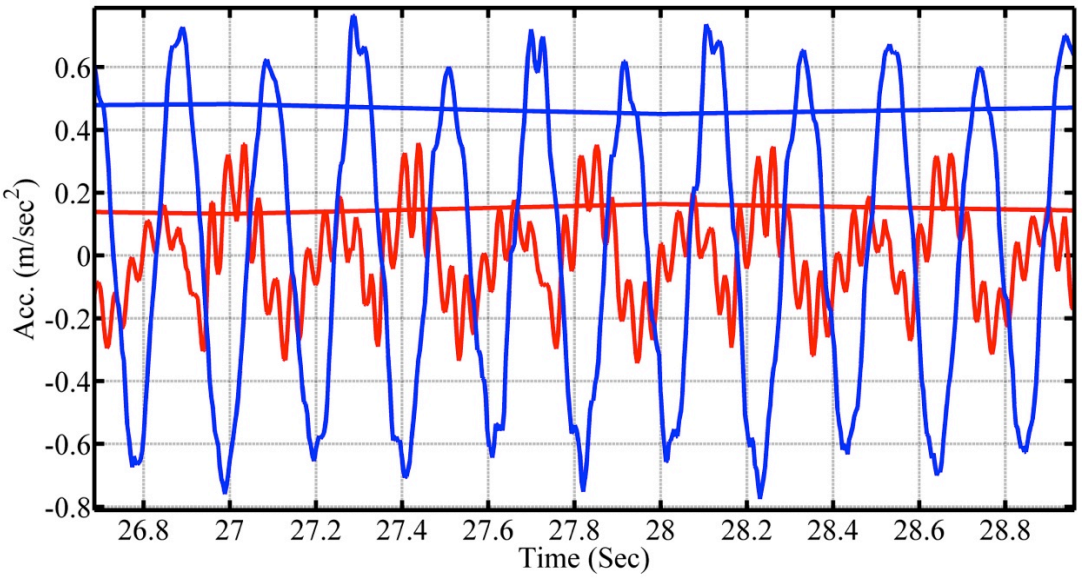

Figure 6-27 Experimental time history of structural acceleration response and corresponding 1 second running RMS of the structure with TMD (blue) and structure with HTMD (red); jumping input force with frequency of 2.44 Hz

Table 6-5- Experimental time domain result comparison of different control methods; jumping on the structure

	Peak Acc. (m/s^2)			MTVV of Acc. (m/s^2)		
	Unc.	TMD	HTMD	Unc.	TMD	HTMD
Jumping @2.16 Hz	2.37	0.3577	0.3762	1.59	0.1178	0.1327
Reduction	-	85%	84%	-	93%	92%
Jumping @2.44 Hz	-	0.7643	0.3542	-	0.4824	0.1325
Reduction	-	-	-	-	-	-

According to this table, at the jumping frequency of 2.16 Hz, HTMD has 54% and 73% reduction in peak acceleration and MTVV of the acceleration respectively in comparison with TMD.

Heel Drop

To investigate the free vibration decay of the structural response for different configurations, the heel-drop test was implemented on the structure. In these tests, the time for the response to reduce to 1% of its peak was examined for the uncontrolled structure, the structure with TMD and the structure with HTMD attached (Figure 6-28, Figure 6-29 and Figure 6-30).

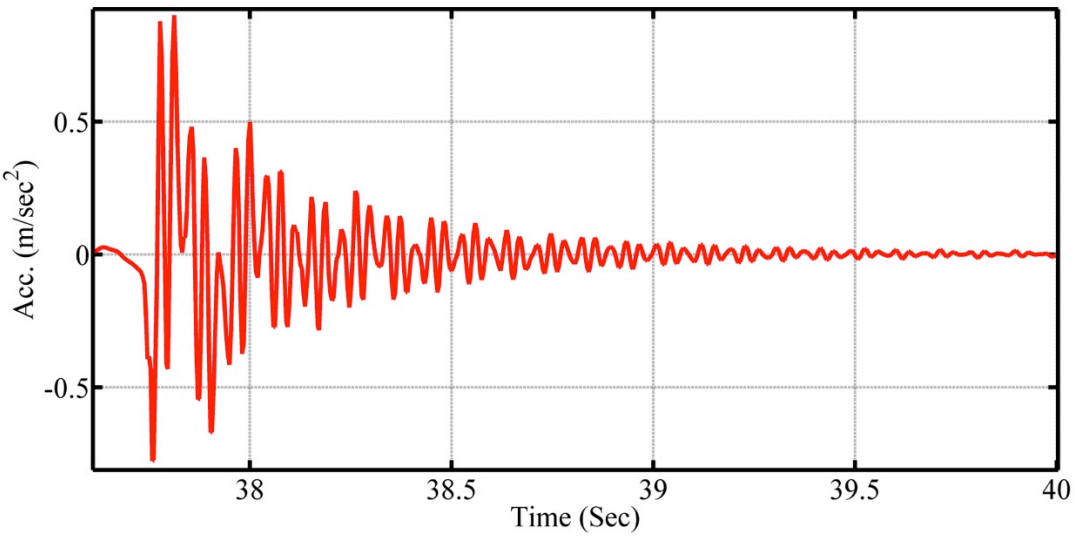

Figure 6-28- Experimental time history of structural acceleration response to heel-drop test on the structure with HTMD

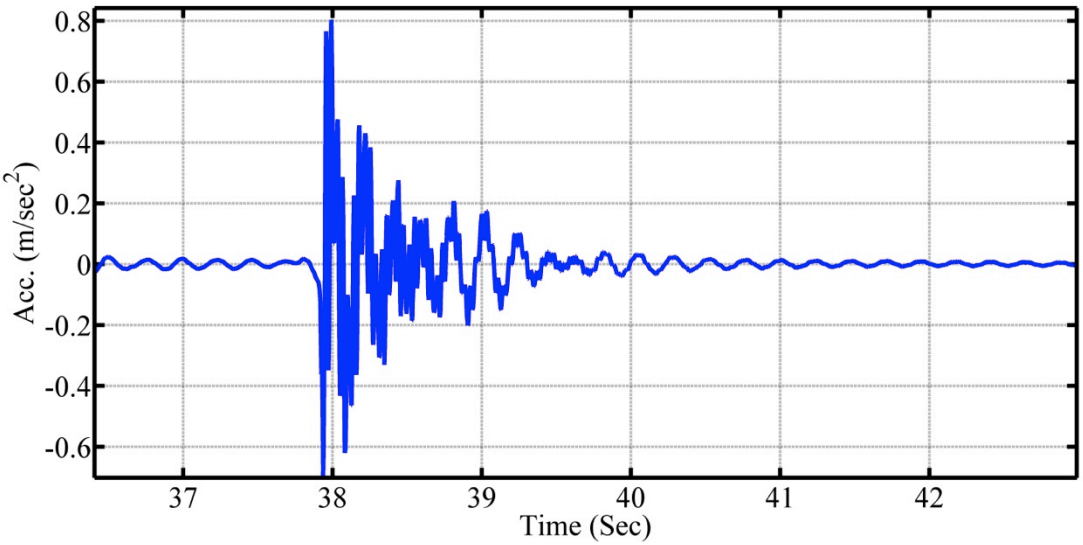

Figure 6-29- Experimental time history of structural acceleration response to heel-drop test on the structure with TMD

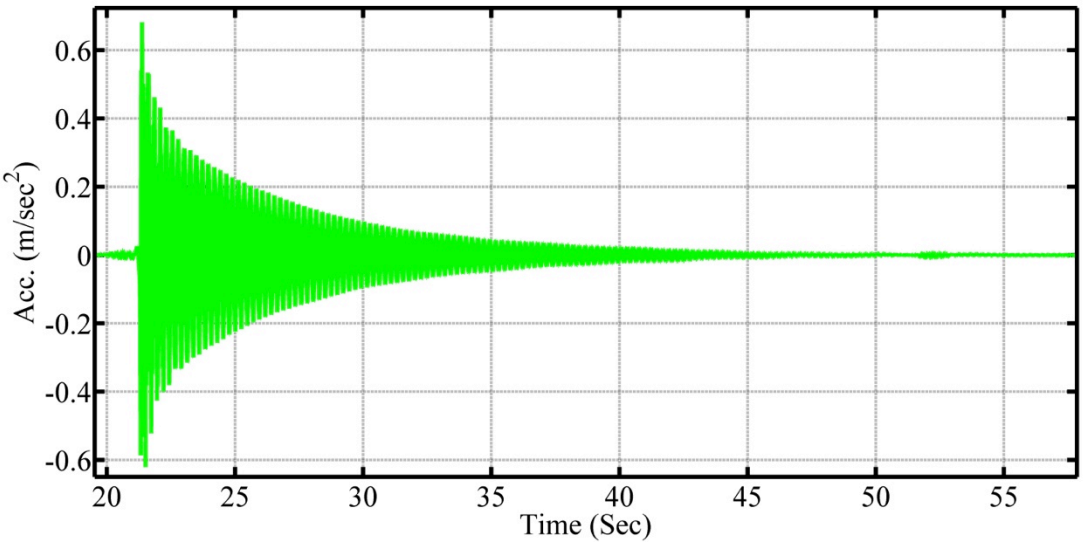

Figure 6-30- Experimental time history of structural acceleration response to heel-drop test on the uncontrolled structure

Table 6-6- Decay time to achieve 1% of the peak response

	Uncontrolled Structure	Structure with TMD	Structure with HTMD
Decay Time (s)	26.1	3.5	2.5
Comparison	-	87%	90%

Table 6-6 compares the result in these three scenarios. According to this, the HTMD has faster decay time compared with the passive TMD.

6.5.4. Experimental determination of actuator effort

To investigate the required control force, the control force was recorded in all of the above scenarios. As can be seen in Figure 6-31 to Figure 6-35, in all cases the required control force from the actuator was less than its capacity. The maximum actuator forces were 60, 91, 318 and 378 N for sinusoidal input with 4.35 Hz and 4.88 Hz and jumping forces at 2.16 Hz and 2.44 Hz, respectively. The MTVV of actuator force for jumping at 2.16 Hz and 2.44 Hz are 122 N and 139 N respectively.

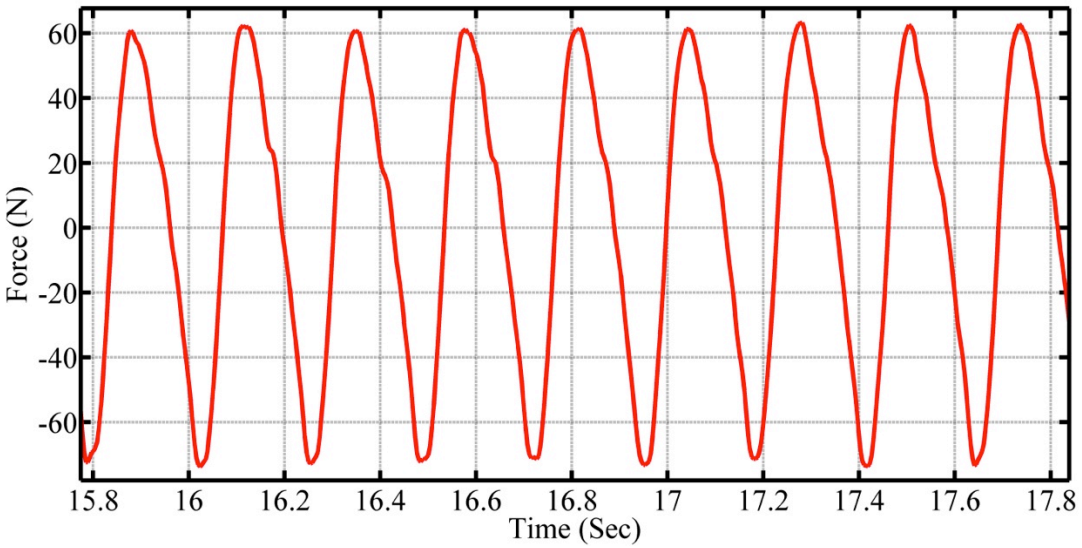

Figure 6-31- Experimental actuator control force of HTMD with harmonic input force with frequency of 4.35Hz

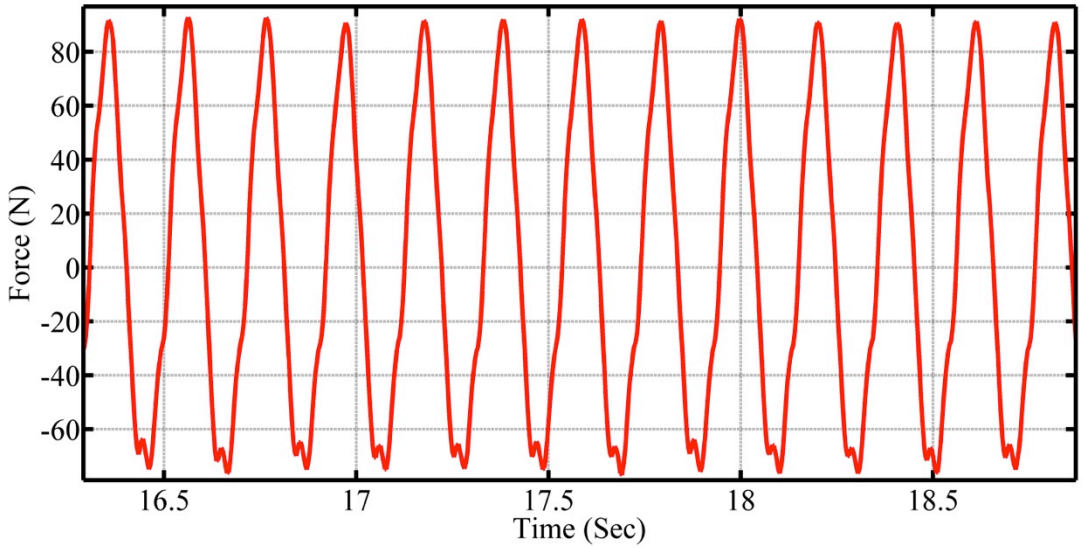

Figure 6-32- Experimental actuator control force of HTMD with harmonic input force with frequency of 4.88Hz

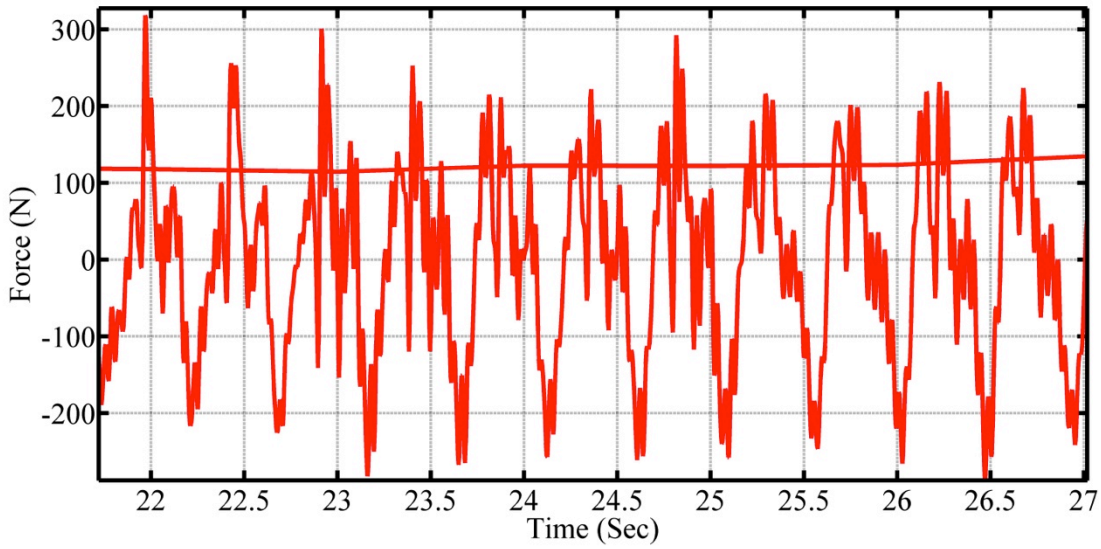

Figure 6-33- Experimental actuator control force and corresponding 1 second running RMS of HTMD with jumping input force with frequency of 2.16 Hz

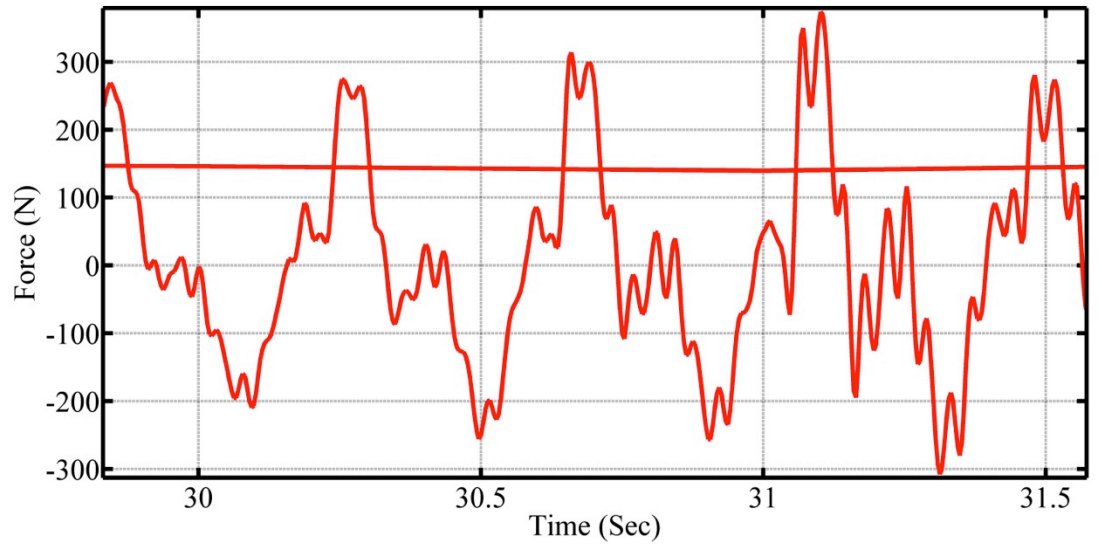

Figure 6-34- Experimental actuator control force and corresponding 1 second running RMS of HTMD with jumping input force with frequency of 2.44 Hz

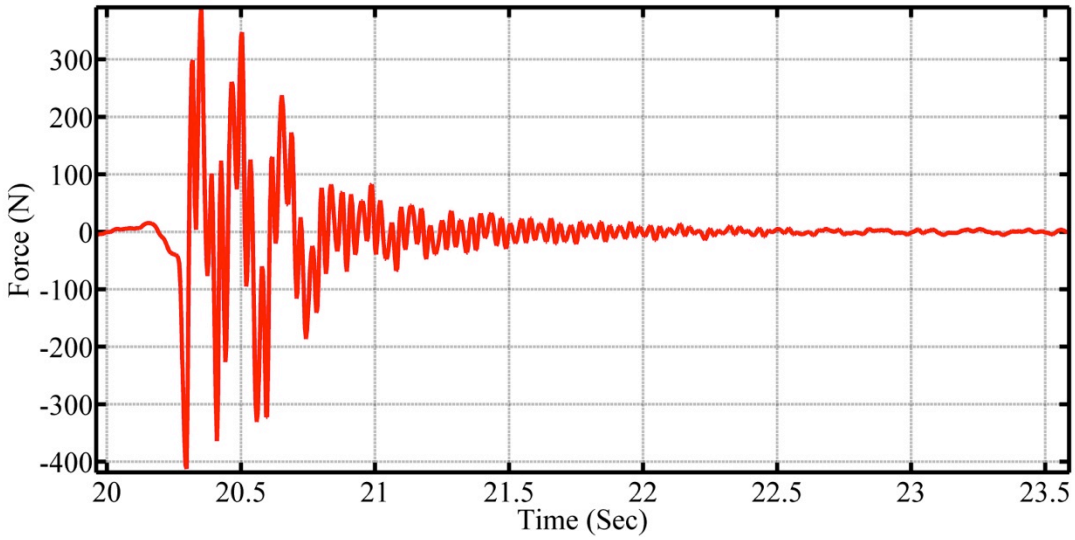

Figure 6-35- Experimental actuator control force of HTMD for heel-drop test

6.5.5. HTMD vs AMD

In another set of measurements, the performance of the HTMD was compared against the AMD (active control method) using the direct velocity feedback scheme. Table 6-7 shows the employed gains in both HTMD and AMD. It should be noted that in this test, the band-pass filter with frequency range 0.7 to 100 Hz was employed. Hence, new gains were obtained from the optimisation problem. The performance was investigated in both the frequency domain (i.e. through FRF measurements) and time domain using human participants jumping .

Table 6-7- Optimised gains for laboratory HTMD and AMD

Device	K_3 (Vs/m)	K_2 (Vs^2/m)	K_1 (V/m)	K_4 (Vs/m)	K_5 (Vs^2/m)
HTMD	0.000	-5.926	-438.024	-25.864	-0.215
AMD	-300.000	0.000	0.000	0.000	0.000

FRF measurements

A random noise signal with frequency band of 0 to 100 Hz as input force was employed to investigate the frequency response of the structure in different scenarios. As can be seen in Figure 6-36, both HTMD and AMD have very positive effects on response reduction of the structure in comparison with the uncontrolled

structure. It can also be seen that the AMD has greater decrease in structural response in comparison with the HTMD.

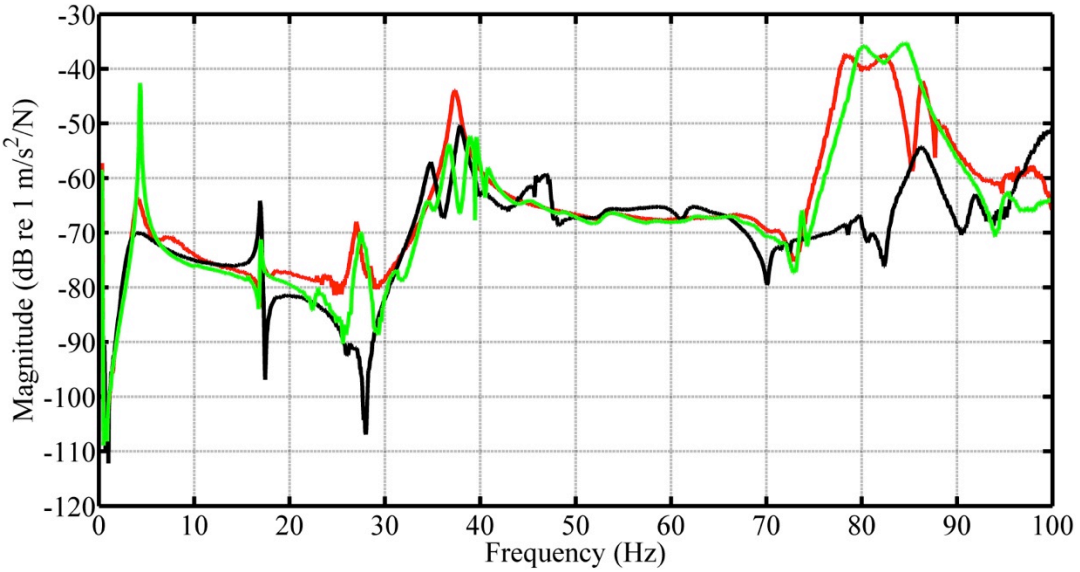

Figure 6-36- Experimental FRF magnitude comparison of the uncontrolled structure (green), structure with AMD (black) and structure with HTMD (red); frequency span of 100 Hz

As noted previously, at a frequency of 38 Hz, there is an amplification in response when the HTMD is used since this is a local mode of the HTMD device which exist in the HTMD. Figure 6-37 shows a zoomed FRF plot around the first two vibration modes of the slab, where it can be seen that although AMD has more reduction in response in comparison with HTMD, it has a negative effect (increase in structural response) on second mode of the structure (around 17 Hz). However, the HTMD does not have a significant effect on other modes, including the second mode of vibration.

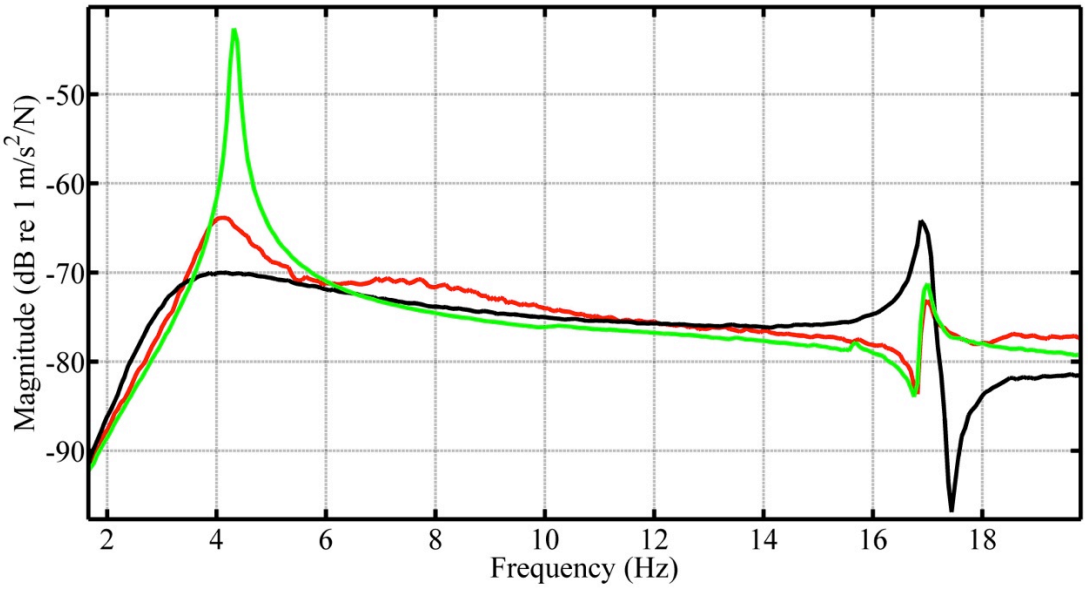

Figure 6-37- Experimental FRF magnitude comparison of the uncontrolled structure (green), structure with AMD (black) and structure with HTMD (red); (zoomed of Figure 6-36)

Table 6-8- Experimental FRF numerical comparison of different control methods

	Uncontrolled Structure	Structure with AMD	Structure with HTMD
Max. FRF magnitude ($m/s^2/N$)	0.00742	0.00031	0.00064
Reduction of the FRF peak	-	96%	91%
FRF magnitude at uncontrolled resonance ($m/s^2/N$)	0.00742	0.00031	0.00058
Reduction of FRF magnitude at uncontrolled resonance	-	96%	92%

Table 6-8 compares the magnitudes of the FRFs due to the various control scenarios. As can be seen, AMD and HMTD have greater response reduction for the first mode of vibration in comparison with TMD. Also there is 52% and 47% in maximum

response and at the uncontrolled resonant frequency for the AMD in comparison with the HTMD.

Experimental time domain response

For the time domain measurements, a single human participant carried out a bouncing excitation at a frequency of 2.25 Hz. As both Figure 6-38 and Table 6-9 show, the performance of the HTMD and AMD are similar, which was also demonstrated by the FRF plot in Figure 6-37.

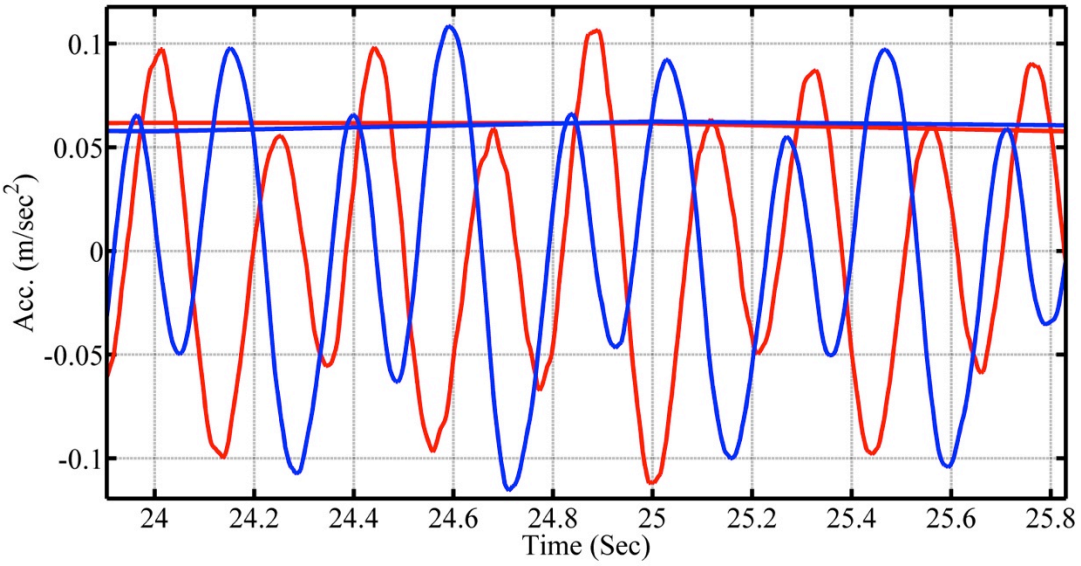

Figure 6-38- Experimental time history of structural acceleration response and corresponding 1 second running RMS of the structure with AMD (blue) and structure with HTMD (red); bouncing at 2.25 Hz

Table 6-9- Summary of experimental time domain results of HTMD and AMD control methods; bouncing on the structure

	Peak Acc. (m/s^2)		MTVV of Acc. (m/s^2)	
	AMD	HTMD	AMD	HTMD
Bouncing @2.25 Hz	0.1082	0.1067	0.05777	0.06185
Reduction	-	1%	-	7%

Experimental actuator effort control

In the above measurements, the actuator control forces were monitored. Figure 6-39 compares the actuator forces between the AMD and HTMD for the random noise signal with the frequency band of 0-100 Hz. It shows a higher force demand for the AMD in comparison with the HTMD.

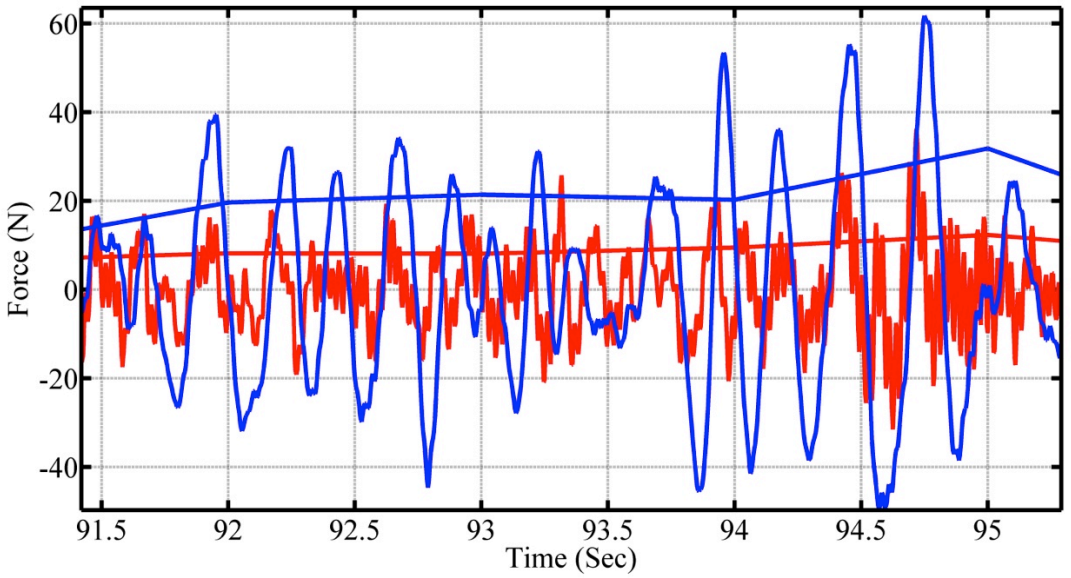

Figure 6-39- Experimental actuator control force and corresponding 1 second running RMS of HTMD (red) and AMD (blue) with input force of random noise of 0-100 Hz

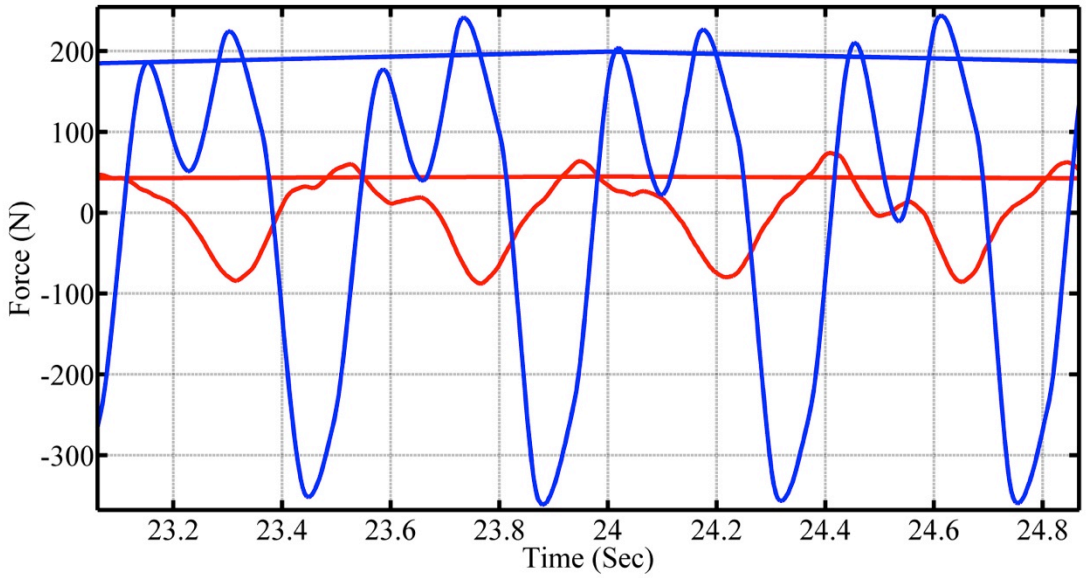

Figure 6-40- Experimental actuator control force and corresponding 1 second running RMS of HTMD (red) and AMD (blue) with bouncing at 2.25 Hz

Figure 6-40 compares the actuator forces between AMD and HTMD due to excitation from the human bouncing force. Similar to the random force, it reveals much higher actuator effort in AMD in comparison with HTMD.

Table 6-10- Experimental actuator control force of HTMD and AMD control methods

	Peak Force (N)		MTVV of Force (N)	
	AMD	HTMD	AMD	HTMD
Random force	82	36	33	13
Reduction	-	56%	-	61%
Bouncing @2.25 Hz	240	60	199	45
Reduction	-	75%	-	77%

Table 6-10 compares the results from both types of input. It shows that the HTMD requires less than half of the actuator capacity in comparison with AMD. This is even less when the excitation force has a component at the structural resonant frequency.

6.6. Investigating the performance of HTMD for off-tuning

As discussed before, passive TMDs can become out of tune in some structures when the structural natural frequency changes, for example in a stadium due to human-structure interaction. In this section, the effect of off-tuning on the performance of the passive TMD and HTMD in the same scenarios are investigated experimentally.

6.6.1. Implementation of off-tuning in the structural model

Since there was practical restriction for implementing off-tuning on the primary structure (laboratory slab), the dynamic properties of the TMD were changed by adding or removing inertial mass. This led to changes in the mass and frequency of the TMD and generated off-tuning situations in the structure/TMD system (Figure 6-41). The TMD mass was changed from 340 kg (tuned scenario) to 250, 500 and 700 kg. It should be noted that there are other ways to change the laboratory structure's properties which will be explained in last chapter.

Similar to previously, FRF and time domain response measurements were carried out and the actuator force was monitored.

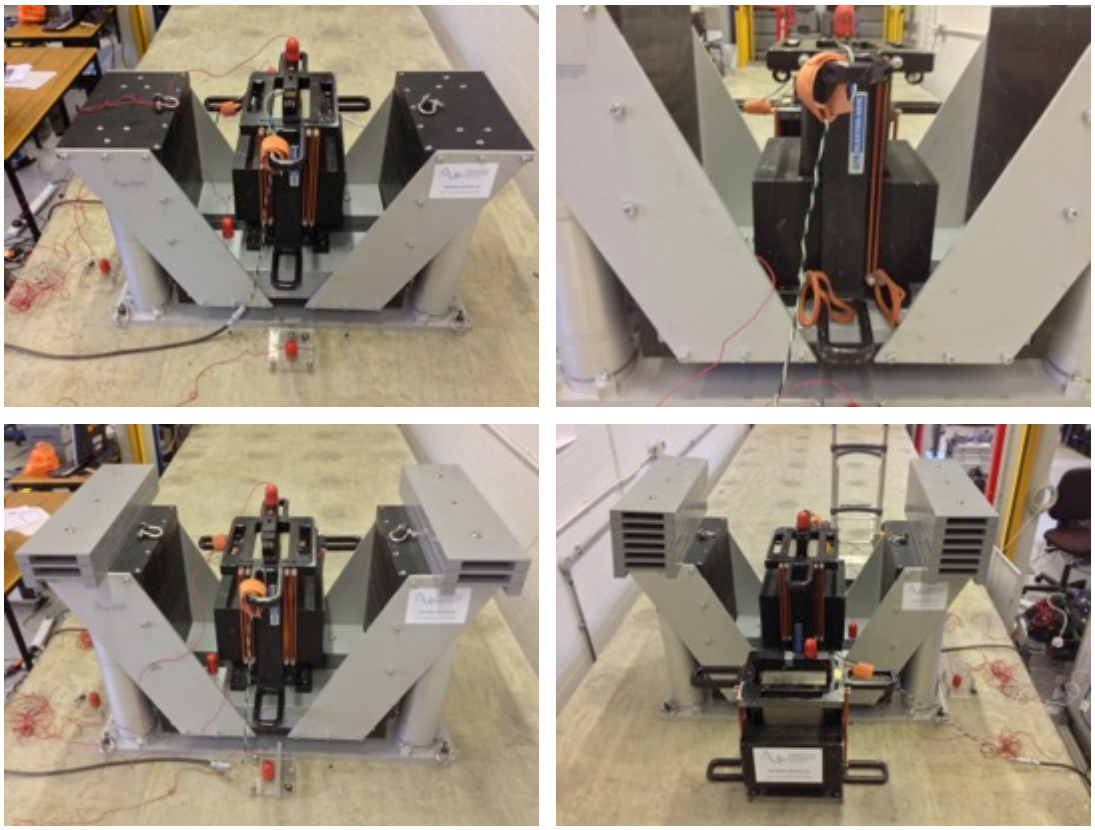

Figure 6-41-practical implementation of off-tuning to the TMD/HTMD; m_p=340 kg (top-left), m_p=250 kg masses (top right), m_p=500 kg masses (bottom left), m_p=700 kg masses (bottom right)

6.6.2. Control algorithm and gain optimisation

Similar control algorithm (robust control method) and gain optimisation introduced in the simulations in Chapter 5 were applied here. The only difference was the presence of the band-pass filter required for the measurements. Table 6-11 shows the feedback gains result from the GA. These gains were applied using the dSPACE control unit for all off-tuning scenarios.

Table 6-11- Optimised gains for robust control method of laboratory HTMD (off-tuning gains)

K_3 (Vs/m)	K_2 (Vs^2/m)	K_1 (V/m)	K_4 (Vs/m)	K_5 (Vs^2/m)
0.000	-6.252	-396.835	-30.743	-0.089

6.6.3. FRF measurements

Two different random noise inputs with frequency band of 0-10 Hz and 0-100 Hz were applied to the structure for the different scenarios.

Figure 6-42, Figure 6-43 and Figure 6-44 show the FRF magnitude of the structural acceleration response in different scenarios. As these show, the performance of the passive TMD deteriorates when the off-tuning is applied to the system.

Also, as these figures show, the HTMD FRF is almost completely inside the boundary of uncontrolled structure at all frequencies. Also, based on Figure 6-45, Figure 6-46 and Figure 6-47 except at the frequency of 38 Hz (i.e. the local mode of the TMD), there is little effect on higher modes from both TMD and HTMD.

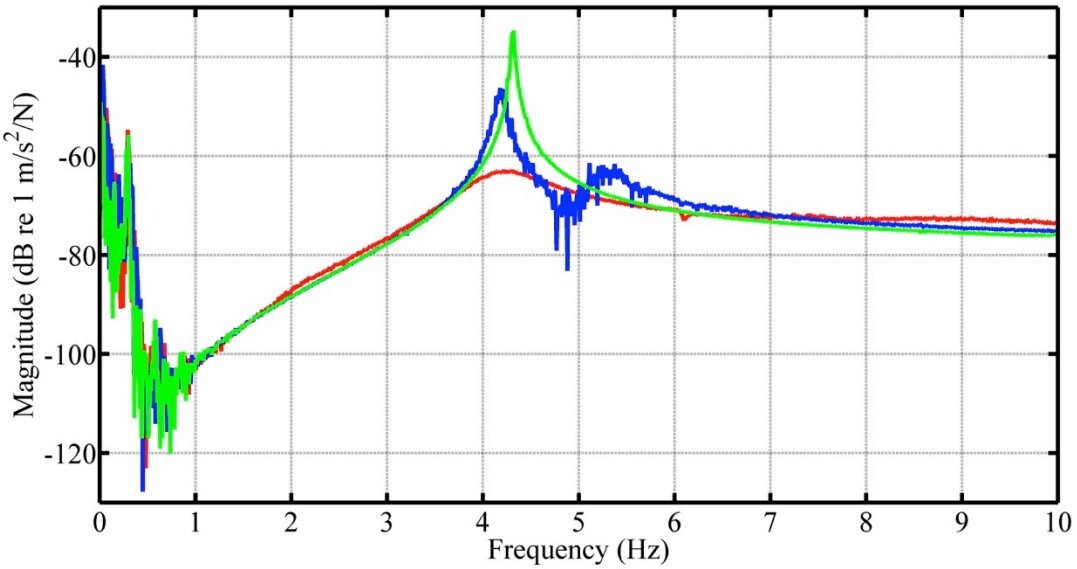

Figure 6-42- FRF comparison of structure with m_p=250 kg; uncontrolled structure (green), structure with TMD (blue), structure with HTMD (red); frequency span of 10 Hz

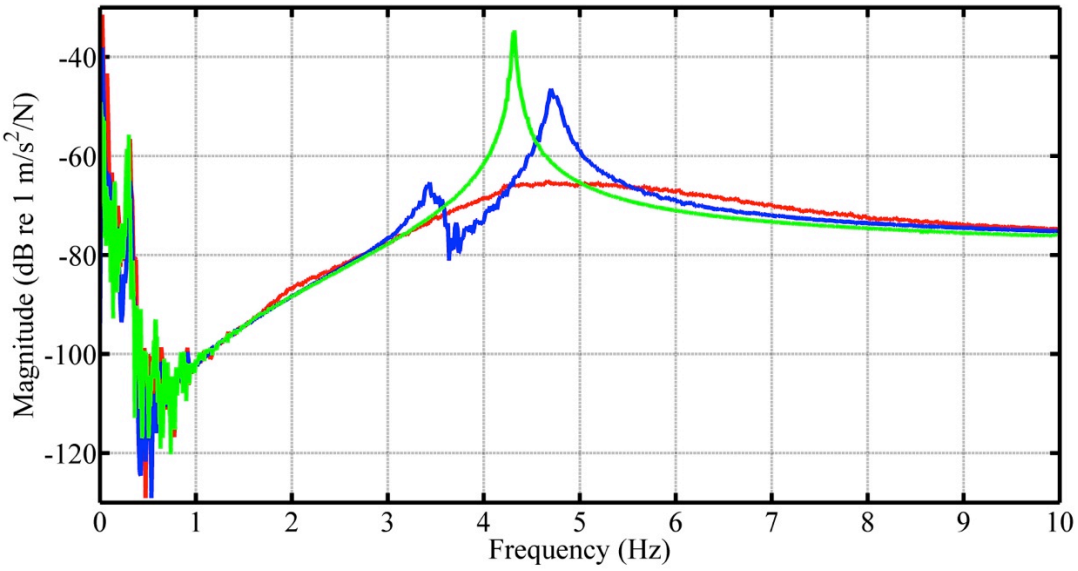

Figure 6-43- FRF comparison of structure with m_p=500 kg; uncontrolled structure (green), structure with TMD (blue), structure with HTMD (red)); frequency span of 10 Hz

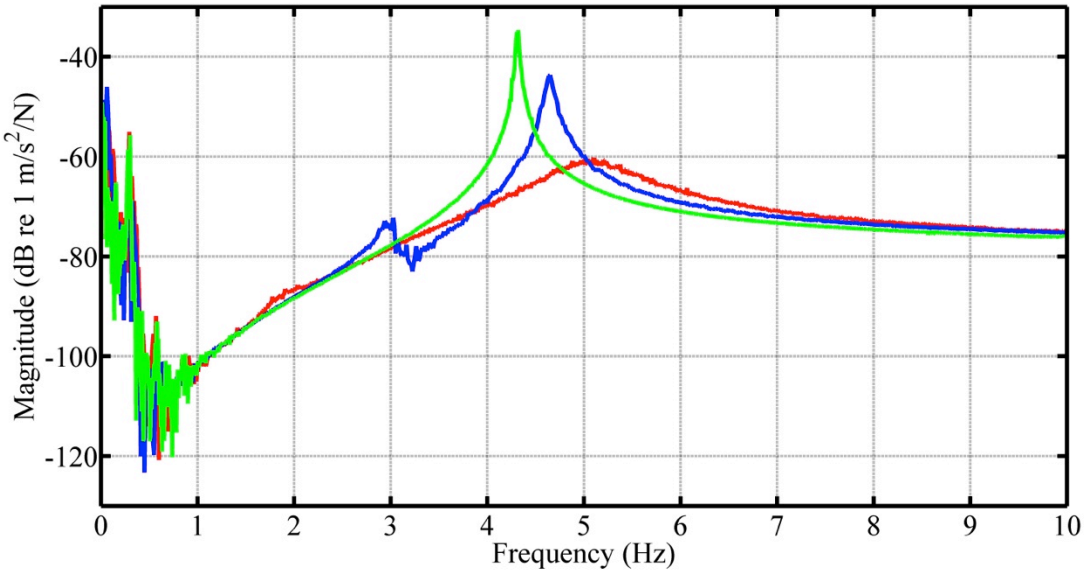

Figure 6-44- FRF comparison of structure with m_p=700 kg; uncontrolled structure (green), structure with TMD (blue), structure with HTMD (red)); frequency span of 10 Hz

Table 6-12 compares the FRF magnitude in different scenarios between TMD and HTMD. As can be seen, the performance of the HTMD has at least 85% greater reduction in comparison with passive TMD for these off-tuning scenarios.

Table 6-12- Comparison of the FRF magnitude with different frequencies of the TMD and HTMD

	TMD mass	Max. FRF magnitude ($(m/s^2)/N$)	Reduction of max. FRF magnitude
TMD	500	0.004772	-
HTMD		0.0005455	89%
TMD	700	0.006545	-
HTMD		0.0009721	85%
TMD	250	0.004857	-
HTMD		0.00070771	85%

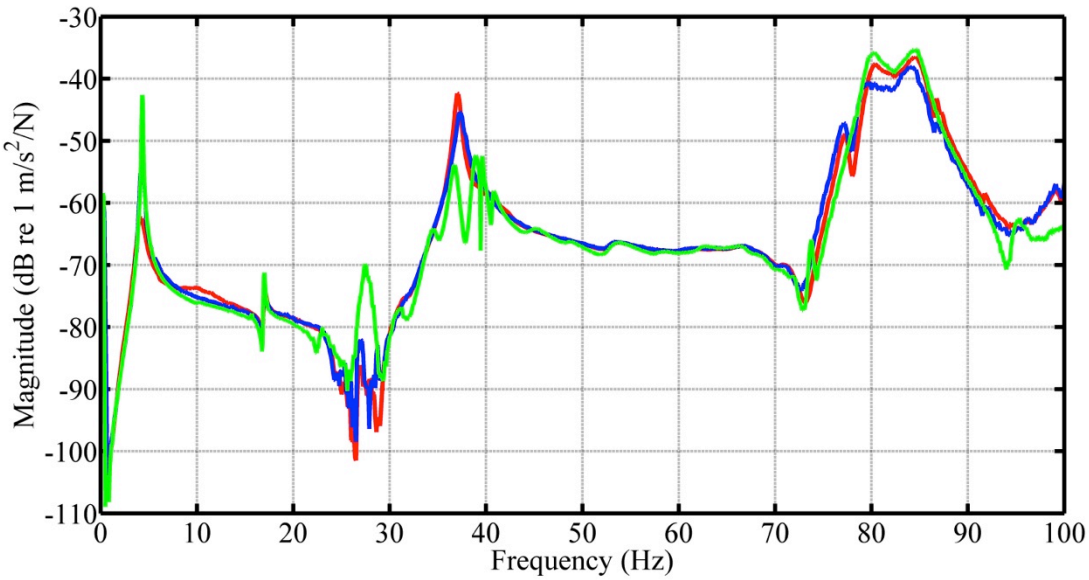

Figure 6-45- FRF comparison of structure with m_p=250 kg; uncontrolled structure (green), structure with TMD (blue), structure with HTMD (red); frequency span of 100 Hz

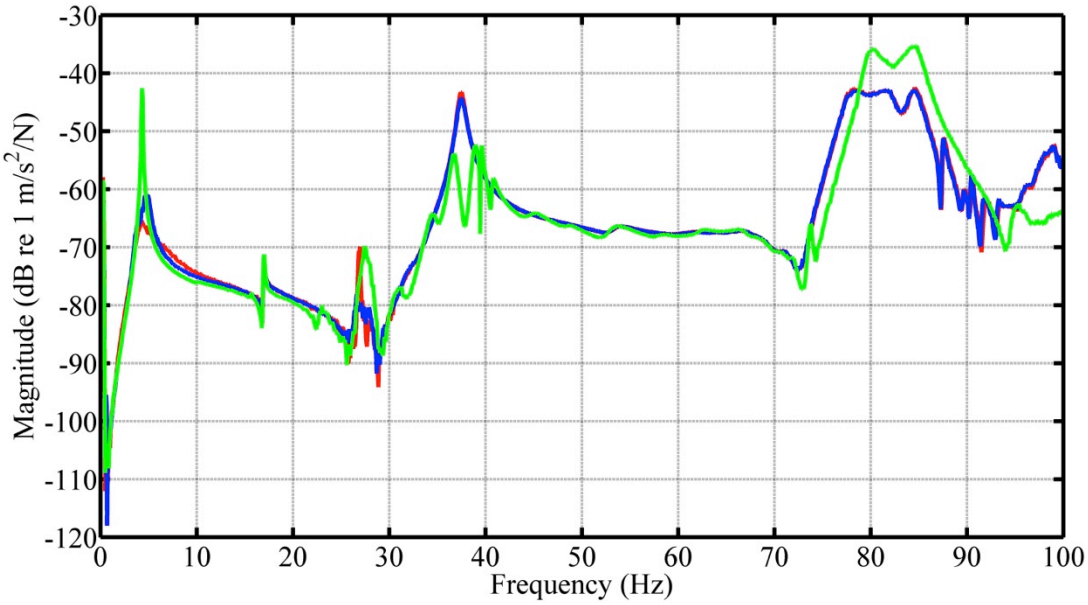

Figure 6-46- FRF comparison of structure with m_p=500 kg; uncontrolled structure (green), structure with TMD (blue), structure with HTMD (red); frequency span of 100 Hz

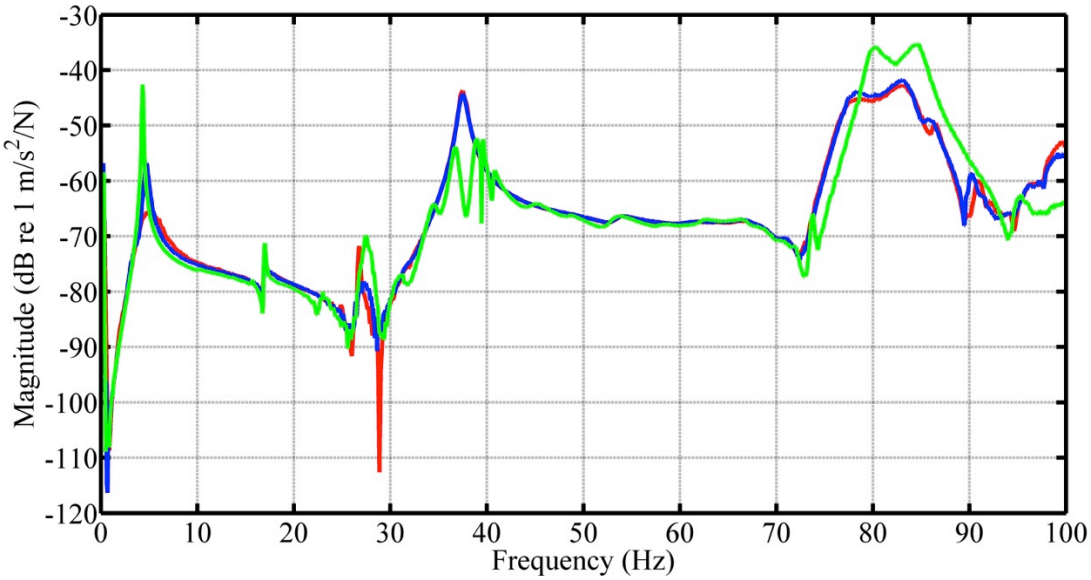

Figure 6-47- FRF comparison of structure with m_p=700 kg; uncontrolled structure (green), structure with TMD (blue), structure with HTMD (red); frequency span of 100 Hz

6.6.4. Measurement of responses to controlled excitations

Similar to earlier experiments, both sinusoidal and jumping tests were performed on the structure for different off-tuning scenarios. The responses of the structure were compared between TMD and HTMD.

Sinusoidal input force

The sinusoidal input force applied to the structure in various scenarios had a frequency corresponding with the uncontrolled structural natural frequency. As shown in Figure 6-49 and Figure 6-50, the HTMD is more effective than the passive TMD in the presence of off-tuning.

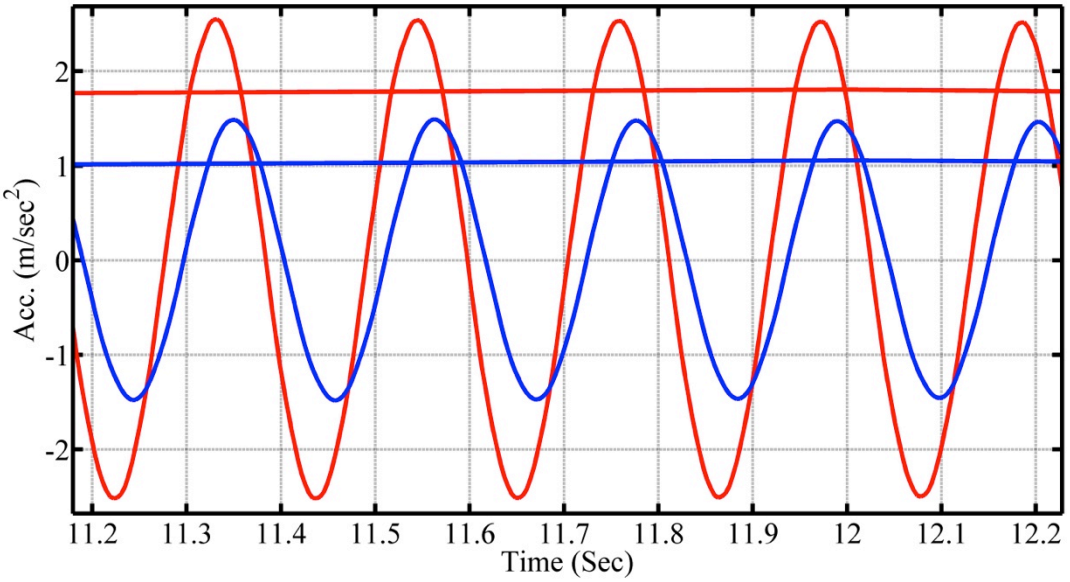

Figure 6-48- Experimental time history of structural acceleration response and corresponding 1 second running RMS of the structure with TMD (blue) and structure with HTMD (red); sinusoidal input force with frequency of 4.70 Hz; m_p=700 kg

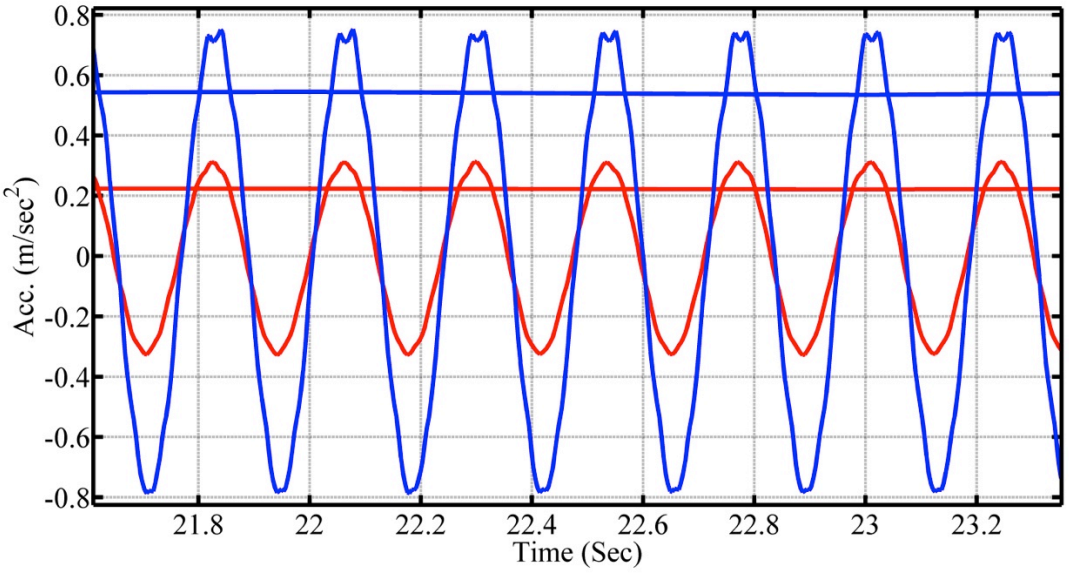

Figure 6-49- Experimental time history of structural acceleration response and corresponding 1 second running RMS of the structure with TMD (blue) and

structure with HTMD (red); sinusoidal input force with frequency of 4.22 Hz; m_p=250 kg

However according to the Figure 6-48, the performance of the HTMD deteriorates for the scenario of m_p=700, which is due to actuator saturation.

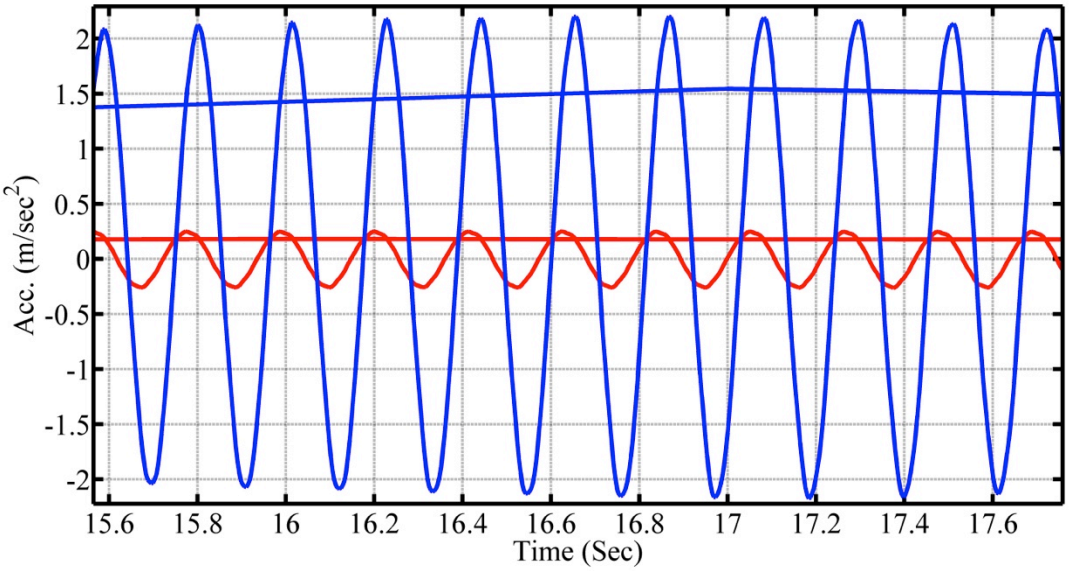

Figure 6-50- Experimental time history of structural acceleration response and corresponding 1 second running RMS of the structure with TMD (blue) and structure with HTMD (red); sinusoidal input force with frequency of 4.70Hz; m_p=500 kg

Also, as Table 6-13 shows, except for the case m_p=700, the HTMD is much more effective in reducing structural response than the passive TMD.

Table 6-13- Experimental time domain result comparison between TMD and HTMD in off-tuning situation; sinusoidal input force on the structure

Scenario	Peak Acc. (m/s^2)		MTVV of Acc. (m/s^2)	
	TMD	HTMD	TMD	HTMD
Sinusoidal @ 4.70Hz, m_p=700 kg	1.492	2.534	1.056	1.806
Reduction	-	-70%	-	-71%
Sinusoidal @ 4.22Hz, m_p=250 kg	0.7471	0.3098	0.545	0.2234
Reduction	-	59%	-	59%
Sinusoidal @ 4.70Hz, m_p=500 kg	2.182	0.2504	1.545	0.1775
Reduction	-	89%	-	89%

Jumping force

The human jumping force was applied to the structure with frequency component of the resonant (peak of the FRFs) for individual scenarios. As can be seen from Figure 6-51 and Figure 6-52, the HTMD is more effective in the presence of the off-tuning than the passive TMD.

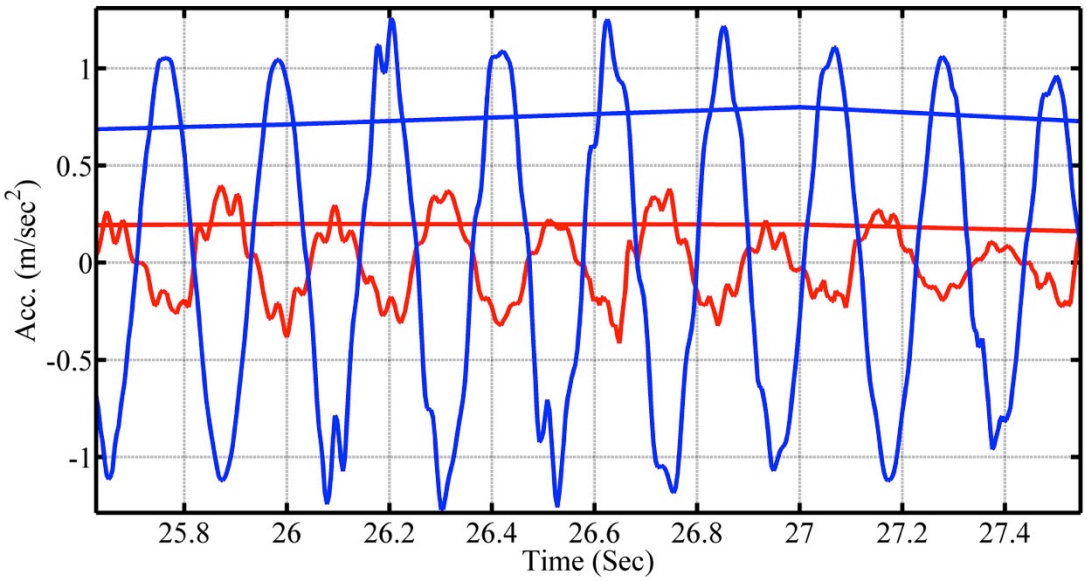

Figure 6-51- Experimental time history of structural acceleration response and corresponding 1 second running RMS of the structure with TMD (blue) and structure with HTMD (red); jumping input force with frequency of 2.30Hz; m_p=700 kg

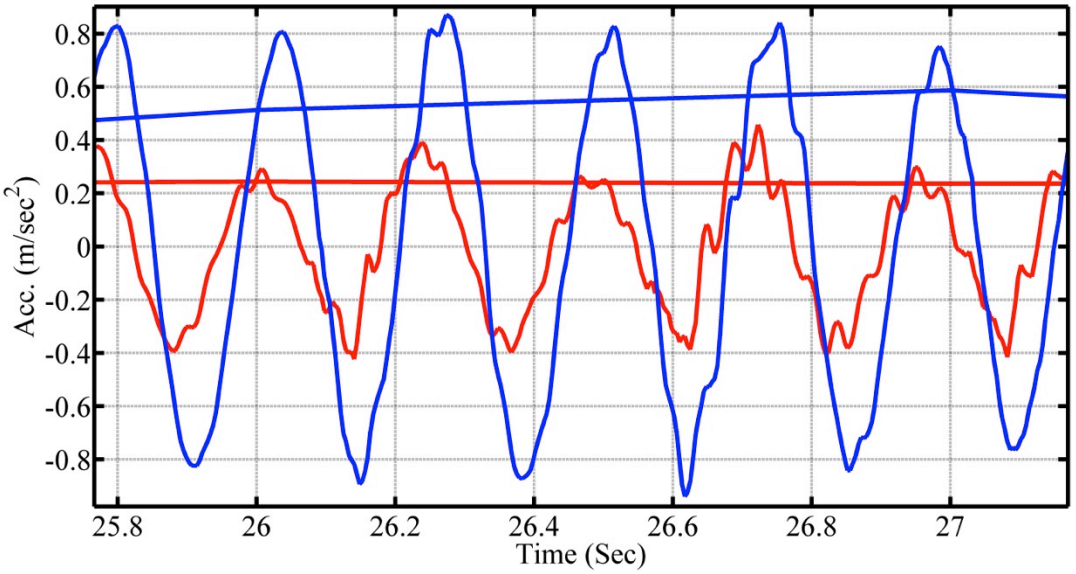

Figure 6-52 Experimental time history of structural acceleration response and corresponding 1 second running RMS of the structure with TMD (blue) and structure with HTMD (red); jumping input force with frequency of 2.12Hz; m_p=250 kg

The numerical results from these measurements are compared in Table 6-14. The HTMD has at least 50% more reduction for cases when off-tuning is present in comparison with the passive TMD in the presence of human jumping force.

Table 6-14- Experimental time domain result comparison between TMD and HTMD in off-tuning situation; jumping input force on the structure

Scenario	Peak Acc. (m/s^2)		MTVV of Acc. (m/s^2)	
	TMD	HTMD	TMD	HTMD
Jumping @2.30 Hz, m_p=700 kg	1.256	0.3695	0.8	0.1964
Reduction	-	71%	-	75%
Jumping @2.12 Hz, m_p=250 kg	0.8702	0.4572	0.5865	0.2363
Reduction	-	47%	-	60%

6.6.5. Experimental determination of actuator effort

The actuator control force was recorded and plotted for the different excitation and off-tuning scenarios. In all cases except the previously mentioned scenario (i.e. jumping force at 4.70 Hz with TMD of m_p=700 kg), the actuator was operating within its capacity.

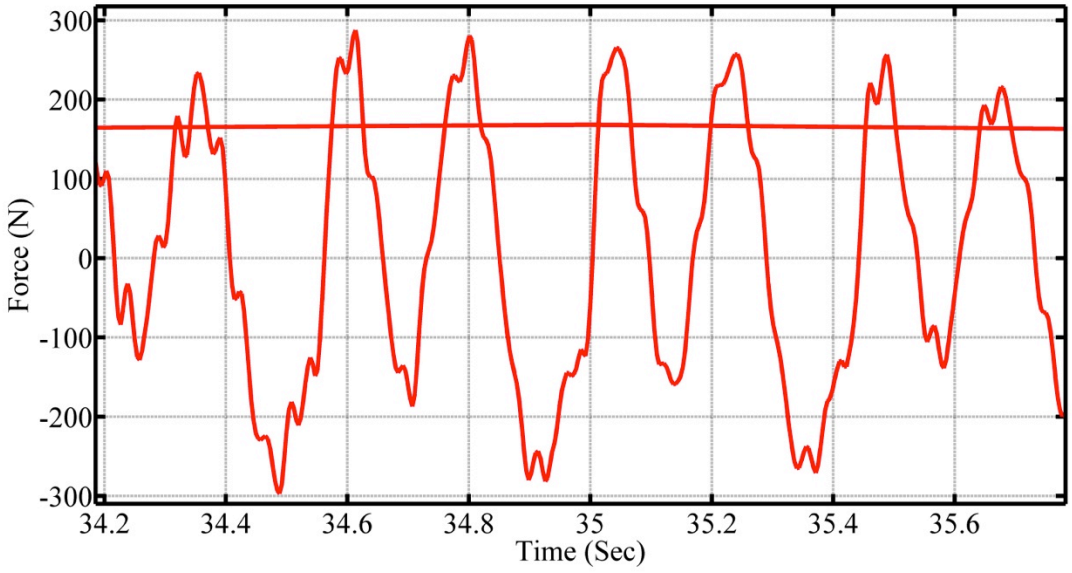

Figure 6-53- Experimental actuator control force of HTMD with jumping input force with frequency of 2.30 Hz, m_p =700 kg

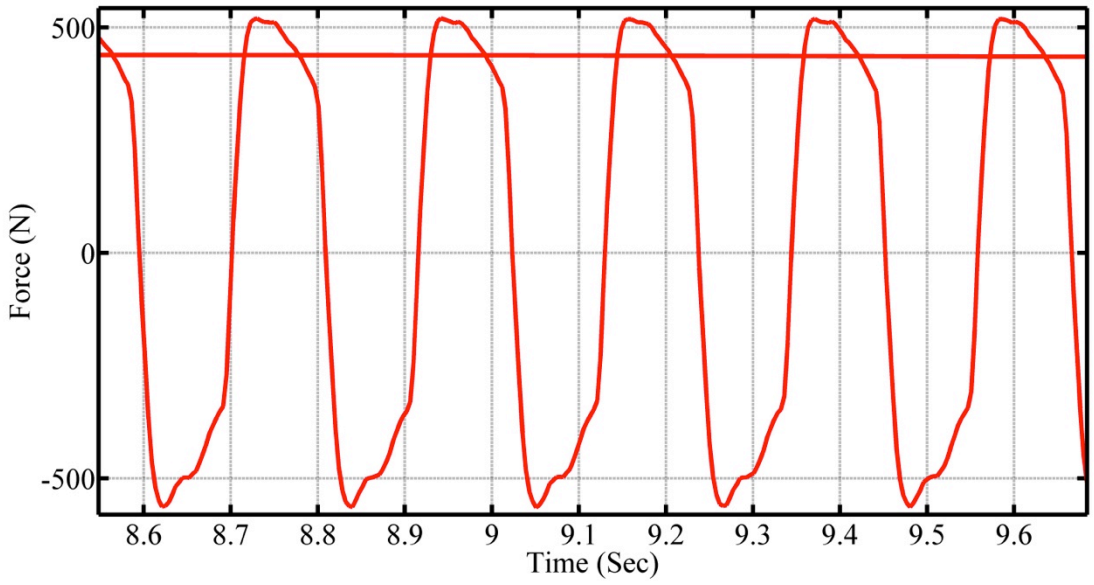

Figure 6-54- Experimental actuator control force of HTMD with sinusoidal input force with frequency of 4.70 Hz, m_p =700 kg

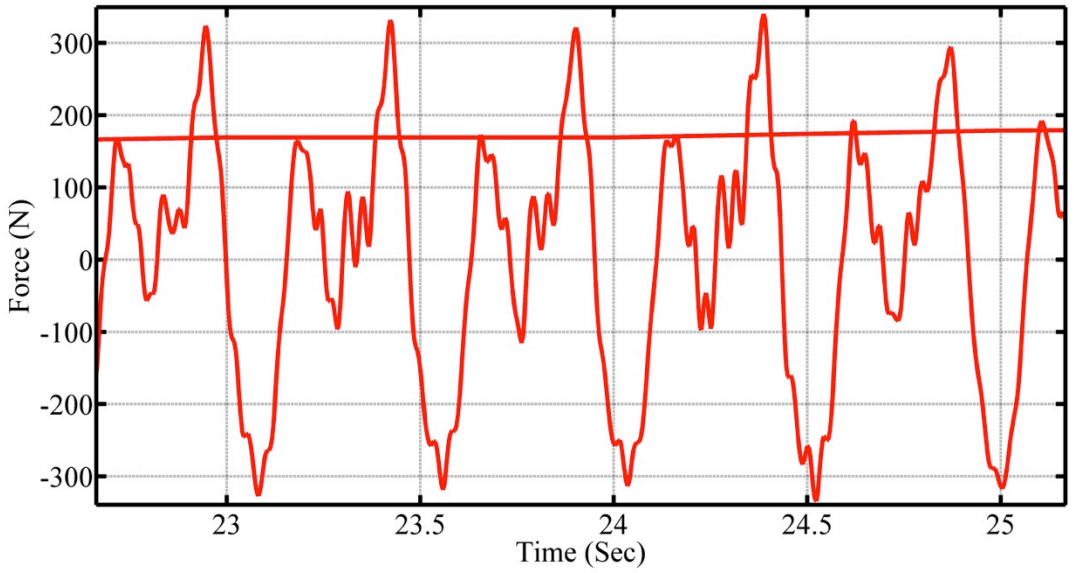

Figure 6-55- Experimental actuator control force of HTMD with jumping input force with frequency of 2.12 Hz, m_p =250 kg

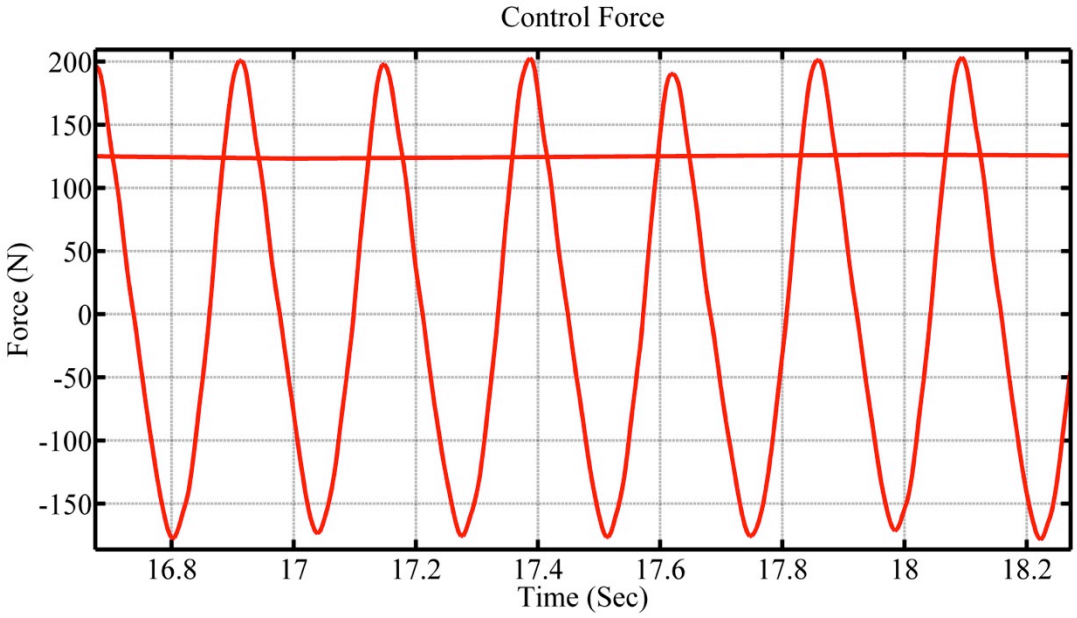

Figure 6-56- Experimental actuator control force of HTMD with sinusoidal input force with frequency of 4.22 Hz, m_p =250 kg

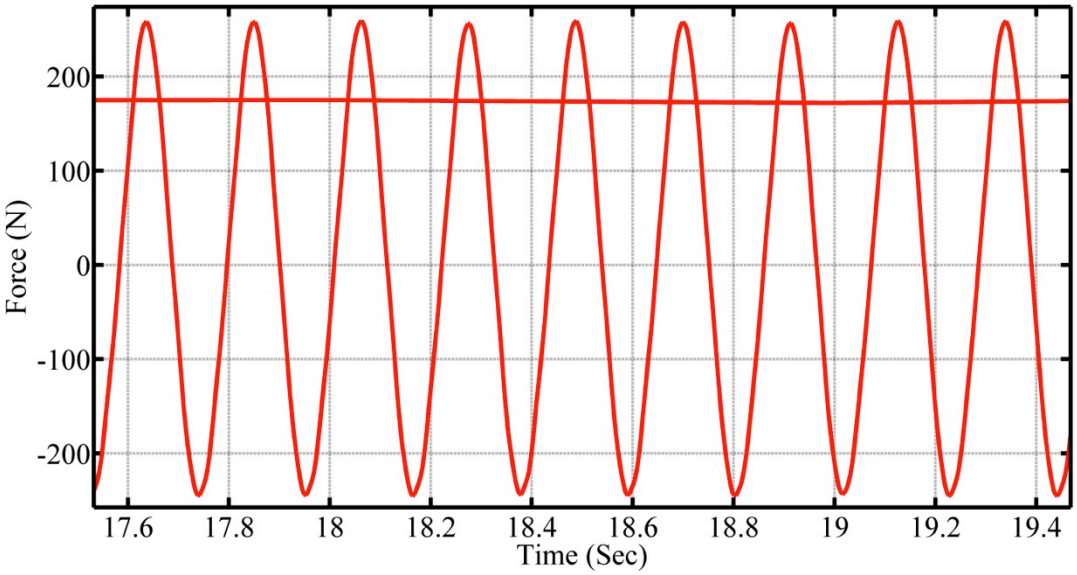

Figure 6-57- Experimental actuator control force of HTMD with sinusoidal input force with frequency of 4.70 Hz, m_p =500 kg

Table 6-15- Experimental actuator control force of HTMD in off-tuning scenarios

Scenario	Peak Force (N)	MTVV of Force (N)
Jumping @ 2.30 Hz, m_p=700 kg	280	168
Sinusoidal @ 4.70 Hz, m_p=700 kg	518	438
Jumping @ 2.12 Hz, m_p=250 kg	321	169
Sinusoidal @ 4.22 Hz, m_p=250 kg	198	123
Sinusoidal @ 4.70 Hz, m_p=500 kg	257	175

Table 6-15 illustrates the maximum actuator force for the above experiments. It should be noted that the maximum capacity of the actuator is around 450 N.

6.7. Conclusion and result discussion

In this chapter, the design and construction of a laboratory HTMD was presented, which was then used for a range of experiments. The aim of this chapter was to verify the analytical models proposed previously and to experimentally investigate the performance of the HTMD on the laboratory structure.

After explaining the design restriction and procedure, different tests were executed to approach the dynamic properties and behaviour of the HTMD/TMD. It was decided to remove the physical damper from TMD/HTMD since it did not work as expected. Instead, the damping force of the HTMD/TMD was designed to be generated by the actuator as an active damping force. The performance of this TMD with active damping force was compared with desired TMD with physical damper and it was demonstrated that the proposed TMD had the characeteristics of the desired TMD.

The measurements on the laboratory structure demonstrated in general that the the HTMD was more effective for response reduction than the passive TMD. Also from time domain tests it was demonstrated that for different types of input force, HTMD can have more reduction with available capacity of the actuator.

After implementing a number of off-tuning scenarios on the TMD/HTMD, it was demonstrated that although the TMD performance deteriorates when out of tune, the

HTMD continues to be effective and is still effective in reducing the structural response.

Finally, the performance of HTMD was compared against that of the AMD. It was demonstrated that although AMD had more reduction in the structural response in the targeted mode, it had a negative effect on the second mode of vibration. Meanwhile, the HTMD reduces the response of the structure only in the targeted mode without having a negative effect on the second mode of vibration. Also, it was shown that the AMD required higher control force from the actuator in comparison with the HTMD. This shows that in the presence of a high level of vibration magnitude, HTMD is potentially more efficient in comparison with the AMD.

After proposing HTMD and relevant control algorithm in earlier chapters and then practically test and verify these, author uses the proposed HTMD is a simulation model of a real stadium occupied by spectators. This will be the topic of next chapter.

7. Simulation of HTMD implementation on a stadium structure

A shorter version of this chapter was presented and published in [149] and [162].

7.1. Introduction

Off-tuning is one of the key disadvantages of passive TMDs, which are accepted as appropriate and established vibration control devices. In stadium structures, this issue may be the result of crowd-structure interaction which can lead to changes in structural natural frequencies. Because a TMD is designed to work at a particular frequency, this variation in the dynamics of the primary structure causes the TMD to become detuned and hence less efficient.

In this chapter the data presented in [38], [39] have been used to create a model of a stadium structure. Both transfer function and state space models are employed. These two models are used both in gain optimisation and analytical studies, respectively.

Next, similar approaches as were presented in Sections 3.3.3 are used to design a TMD and HTMD and carry out simulations of the modelled structure. Similar investigations as were described previously for the laboratory structure are performed for the stadium structure by examining both frequency and time domain responses. Both structural acceleration response and the actuator effort are compared between the uncontrolled structure and the structure with TMD and HTMD.

Finally, the proportion of active people in the stadium is changed to simulate changes in structural dynamic properties and to and induce an off-tuning situation. The ability of the two proposed control algorithms to deal with off-tuning are determined and compared against the passive TMD.

7.2. Grandstand model

The structure for this research work is a stand in a football stadium in the United Kingdom (Figure 7-1) [39]. There is a short segment of upper tier seating in one of the corners of the stadium that is of particular interest. The length of this part is 18.9 m and it has a cantilever length of about 7 m. Previous in-service vibration monitoring results carried out whilst the stadium was used for a concert event show that this area is quite lively [39].

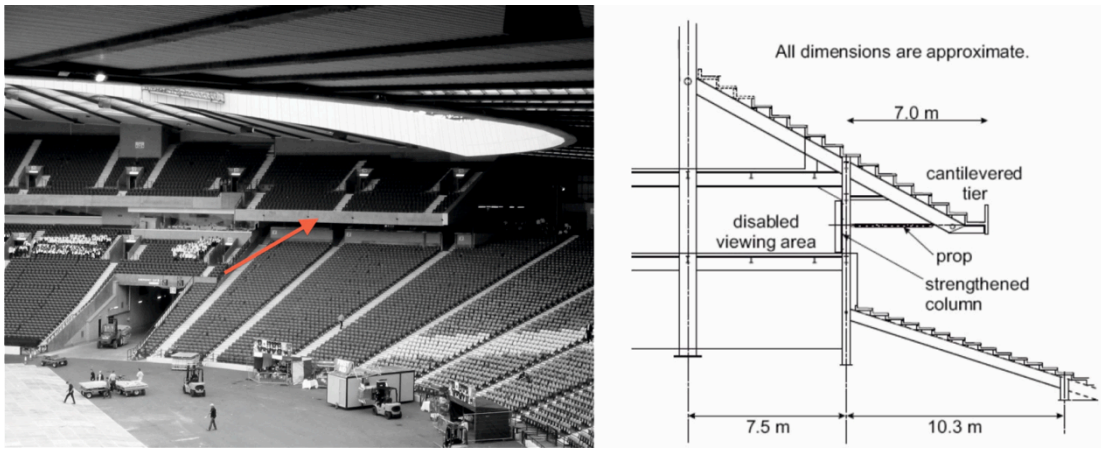

Figure 7-1- View of the modelled seating deck (left) and cross section of the tier (right) [39]

Through both ambient vibration test [39] and updating of the finite element (FE) model of the empty structure [172], the modal properties of the structure were determined. The first local vertical mode appears at approximately 4.34 Hz. From both the auto-spectral density of the acceleration response of the structure and also from appropriate modelling of the stadium in the presence of both active and passive spectators structure considering human-structure interaction [172], the frequency reduced from 4.34 to 3.20 Hz, which coincided with the second harmonic of the musical beat the one song which produced maximum response, which had a beat frequency of 1.6 Hz.

Table 7-1- Dynamic properties of the stadium

Structure	Frequency (Hz)	Damping Ratio (%)	Modal Mass (kg)	Modal Damping (Ns/m)	Modal Stiffness (N/m)
Empty	4.34	3.70	82,811	167,105	61,578,233
Full	3.20	11.00	108,019	567,396	61,578,233

The proposed structural model is a 3 degree of freedom (3DOF) idealisation encompassing the empty structure and the active and passive spectators (Figure 7-2). The subscripts *s*, *p*, *a*, *as* and *ps* stand for structure, passive part of TMD/HTMD, actuator, active spectator and passive spectator, respectively.

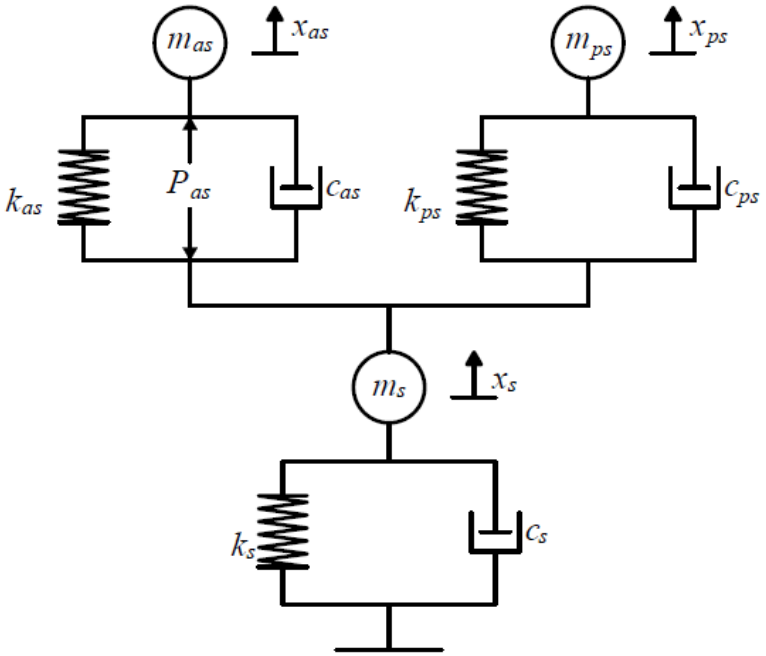

Figure 7-2- 3DOF model of the stadium cantilever with active and passive spectators

Based on Figure 7-2, the set of equations of motion of the system is given by:

$$
\begin{aligned}
&\text{a)}\quad m_s\ddot{x}_s(t) + \left(c_s + c_{as} + c_{ps}\right)\dot{x}_s(t) - c_{as}\dot{x}_{as}(t) - c_{ps}\dot{x}_{ps}(t) + \\
&\qquad \left(k_s + k_{as} + k_{ps}\right)x_s(t) - k_{as}x_{as}(t) - k_{ps}x_{ps}(t) = P_{as}(t) \\
&\text{b)}\quad m_{as}\ddot{x}_{as}(t) - c_{as}\dot{x}_s(t) + c_{as}\dot{x}_{as}(t) - k_{as}x_s(t) + k_{as}x_{as}(t) = -P_{as}(t) \\
&\text{c)}\quad m_{ps}\ddot{x}_{ps}(t) - c_{ps}\dot{x}_s(t) + c_{ps}\dot{x}_{ps}(t) - k_{as}x_s(t) + k_{as}x_{ps}(t) = 0
\end{aligned}
\qquad \textbf{(7.1)}
$$

m_{as} and m_{ps} are the mass of active and passive spectators. Also, P_{as} is the motion induced force produced within the active body unit.

Table 7-2 shows the recommended frequencies and damping ratios of the active and passive spectators according to [24]. In the first instance, the passive TMD is used based on a design assumption of active/passive spectator ratio of 40%:60%.

Table 7-2- Dynamic properties of the passive and active spectators

Crowd	Population	Frequency (Hz)	Damping Ratio (%)
Active	40%	2.3	25
Passive	60%	5	40

Table 7-3 shows the frequency of the first vertical mode of the structure when the ratio of active/passive spectators changes. As can be seen, the frequency of the structure varies from 2.71 to 4.17 Hz when the percentage of active people changes from 1% to 80% respectively. This is a -30% to 15% change in frequency in comparison with 3.20 Hz as the initial design frequency of the TMD.

Table 7-3- Variation of spectator active/passive ratio and corresponding frequencies of the first vertical mode

Scenario	Active people (%)	Mass of Active people m_{as} (kg)	Mass of Passive people m_{ps} (kg)	Frequency of the first vertical mode structure (Hz)	Changing of the frequency of the main structure (%)
1	1%	970	96005	2.71	15%
2	5%	4849	92126	2.74	14%
3	10%	9698	87278	2.79	13%
4	20%	19395	77580	2.9	9%
5	30%	29093	67883	3.02	6%
6	40%	38790	58185	3.2	0%
7	60%	58185	38790	3.57	-12%
8	80%	77580	19395	4.17	-30%

7.2.1. Transfer function model of the structure

To generate a transfer function model of the uncontrolled structure, equation (7.1) is converted from time domain to Laplace domain:

a) $$m_s s^2 X_s(s) + \left(c_s + c_{as} + c_{ps}\right) s X_s(s) - c_{as} s X_{as}(s) - c_{ps} s X_{ps}(s) + \quad \textbf{(7.2)}$$

$$\left(k_s + k_{as} + k_{ps}\right)X_s(s) - k_{as}X_{as}(s) - k_{ps}X_{ps}(s) = P_{as}(s)$$

b) $m_{as}s^2X_{as}(s) - c_{as}sX_s(s) + c_{as}sX_{as}(s) - k_{as}X_s(s) + k_{as}X_{as}(s) = -P_{as}(s)$

c) $m_{ps}s^2X_{ps}(s) - c_{ps}sX_s(s) + c_{ps}sX_{ps}(s) - k_{as}X_s(s) + k_{as}X_{ps}(s) = 0$

Rearranging (7.2) in terms of $X_s(s)$, $X_p(s)$, $X_{as}(s)$, $X_{ps}(s)$ and $P_{as}(s)$ leads to:

a) $\left[m_ss^2X_s(s) + \left(c_s + c_{as} + c_{ps}\right)s + \left(k_s + k_{as} + k_{ps}\right)\right]X_s(s) - [\,c_{as}s + k_{as}]\,X_{as}(s) - \left[\,c_{ps}s + k_{ps}\right]X_{ps}(s) = P_{as}(s)$

b) $[m_{as}s^2 + c_{as}s + k_{as}]X_{as}(s) - [c_{as}s + k_{as}]X_s(s) = -P_{as}(s)$

c) $\left[m_{ps}s^2 + c_{ps}s + k_{ps}\right]X_{as}(s) - [c_{ps}s + k_{ps}]X_s(s) = 0$ **(7.3)**

Defining $G_{s,1,TMD,S}$, $G_{s,2,TMD,S}$, $G_{s,3,TMD,S}$, $G_{s,4,TMD,S}$, $G_{p,1,S}$, $G_{as,1,S}$, $G_{as,2,S}$ and $G_{ps,1,S}$ by considering the acceleration as the output of each block (i.e. by multiplying s^2 term) as follows:

$$G_{s,1,unc,S} = \frac{X_s(s)s^2}{P_{as}(s)} = \frac{s^2}{m_ss^2 + \left(c_s + c_{as} + c_{ps}\right)s + \left(k_s + k_{as} + k_{ps}\right)} \quad \textbf{(7.4)}$$

$$G_{s,2,unc,S} = \frac{X_s(s)s^2}{X_{as}(s)s^2} = \frac{[\,c_{as}s + k_{as}]}{m_ss^2 + \left(c_s + c_{as} + c_{ps}\right)s + \left(k_s + k_{as} + k_{ps}\right)} \quad \textbf{(7.5)}$$

$$G_{s,3,unc,S} = \frac{X_s(s)s^2}{X_{ps}(s)s^2} = \frac{\left[\,c_{ps}s + k_{ps}\right]}{m_ss^2 + \left(c_s + c_{as} + c_{ps}\right)s + \left(k_s + k_{as} + k_{ps}\right)} \quad \textbf{(7.6)}$$

$$G_{as,1,S} = \frac{X_{as}(s)s^2}{X_s(s)s^2} = \frac{[c_{as}s + k_{as}]}{[m_{as}s^2 + c_{as}s + k_{as}]} \quad \textbf{(7.7)}$$

$$G_{as,2,S} = \frac{X_{as}(s)s^2}{P_{as}(s)} = \frac{-s^2}{[m_{as}s^2 + c_{as}s + k_{as}]} \quad \textbf{(7.8)}$$

$$G_{ps,1,S} = \frac{X_{ps}(s)s^2}{X_s(s)s^2} = \frac{\left[c_{ps}s + k_{ps}\right]}{\left[m_{ps}s^2 + c_{ps}s + k_{ps}\right]} \quad \textbf{(7.9)}$$

Substituting equations (7.4) to (7.9) into equation (7.3) and rearranging leads to:

$$\begin{aligned} &a)\ \ddot{x}_s = P_{as}G_{s,1,unc,S} + \ddot{x}_{as}G_{s,2,unc,S} + \ddot{x}_{ps}G_{s,3,unc,S} \\ &b)\ \ddot{x}_{as} = P_{as}G_{as,2,S} + \ddot{x}_sG_{as,1,S} \\ &c)\ \ddot{x}_{ps} = \ddot{x}_sG_{ps,1,S} \end{aligned} \quad \textbf{(7.10)}$$

Rearranging equations (7.10) in terms of $\ddot{x}_s$ and P_{as} results in:

$$\ddot{x}_s = P_{as}\mathrm{G_{s,1,unc,S}} + (P_{as}\mathrm{G_{as,2,S}} + \ddot{x}_s\mathrm{G_{as,1,S}})\mathrm{G_{s,2,unc,S}} + (\ddot{x}_s\mathrm{G_{ps,1,S}})\mathrm{G_{s,3,unc,S}} \quad \textbf{(7.11)}$$

Rearranging equation (7.11) generates the transfer function of the uncontrolled structure between the force from human occupants P_{as} and the acceleration of the primary structure $\ddot{x}_s$.

$$H_{unc,S} = \frac{\ddot{x}_s}{P_{as}} = -(G_{s,1,unc,S} + G_{as,2,S} * G_{s,2,unc,S})/(G_{as,1,S} * G_{s,2,unc,S} + G_{ps,1,S} * G_{s,3,unc,S} - 1) \quad \textbf{(7.12)}$$

The transfer function in equation (7.12) is depicted in Figure 7-3.

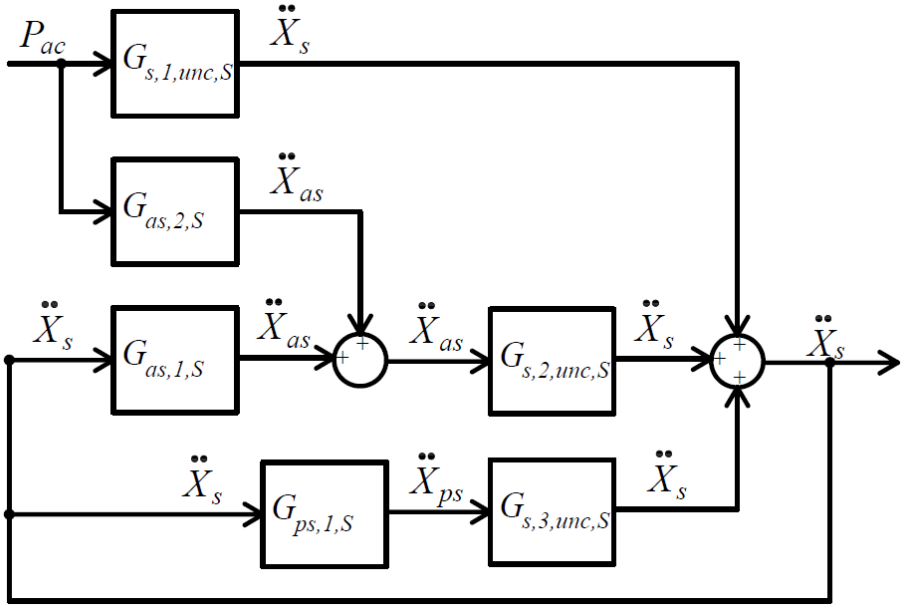

Figure 7-3- Block diagram arrangement of the uncontrolled stadium as a 3DOF system

7.2.2. State space model of the structure

Based on equation (7.1), the states of uncontrolled structure are introduced as

$$\begin{Bmatrix} X_{1,unc,S} = x_s \\ X_{2,unc,S} = \dot{x}_s \\ X_{3,unc,S} = x_{as} \\ X_{4,unc,S} = \dot{x}_{as} \\ X_{5,unc,S} = x_{ps} \\ X_{6,unc,S} = \dot{x}_{ps} \end{Bmatrix} \quad \textbf{(7.13)}$$

Hence, the SS representation of the system in the form of $\dot{X}_{unc,S} = A_{unc,S}X_{unc,S} + B_{unc,S}U_{unc,S}$ is developed as

$$\begin{Bmatrix} \dot{X}_{1,unc,S} \\ \dot{X}_{2,unc,S} \\ \dot{X}_{3,unc,S} \\ \dot{X}_{4,unc,S} \\ \dot{X}_{5,unc,S} \\ \dot{X}_{6,unc,S} \end{Bmatrix} = \begin{bmatrix} 0 & 1 & 0 & \cdots \\ -\frac{(k_s + k_{as} + k_{ps})}{m_s} & -\frac{(c_s + c_{as} + c_{ps})}{m_s} & \frac{k_{as}}{m_s} & \cdots \\ 0 & 0 & 0 & \cdots \\ \frac{k_{as}}{m_{as}} & \frac{c_{as}}{m_{as}} & -\frac{k_{as}}{m_{as}} & \cdots \\ 0 & 0 & 0 & \cdots \\ \frac{k_{ps}}{m_{ps}} & \frac{c_{ps}}{m_{ps}} & 0 & \cdots \end{bmatrix} \quad \textbf{(7.14)}$$

$$\begin{matrix} \cdots & 0 & 0 & 0 \\ \cdots & \frac{c_{as}}{m_s} & \frac{k_{ps}}{m_s} & \frac{c_{ps}}{m_s} \\ \cdots & 1 & 0 & 0 \\ \cdots & -\frac{c_{as}}{m_{as}} & 0 & 0 \\ \cdots & 0 & 0 & 1 \\ \cdots & 0 & -\frac{k_{ps}}{m_{ps}} & -\frac{c_{ps}}{m_{ps}} \end{matrix} \begin{Bmatrix} X_{1,unc,S} \\ X_{2,unc,S} \\ X_{3,unc,S} \\ X_{4,unc,S} \\ X_{5,unc,S} \\ X_{6,unc,S} \end{Bmatrix} + \begin{bmatrix} 0 \\ \frac{1}{m_s} \\ 0 \\ \frac{-1}{m_{as}} \\ 0 \\ 0 \end{bmatrix} \{P_{as}\}$$

To obtain displacement, velocity and acceleration of the system as outputs in the form of $Y_{unc,S} = C_{unc,S}X_{unc,S} + D_{unc,S}U_{unc,S}$, the output matrix is established as

$$\begin{Bmatrix} Y_{1,unc,S} \\ Y_{1,unc,S} \\ Y_{1,unc,S} \end{Bmatrix} = \begin{bmatrix} 1 & 0 & 0 & \cdots \\ 0 & 1 & 0 & \cdots \\ -\frac{(k_s + k_{as} + k_{ps})}{m_s} & -\frac{(c_s + c_{as} + c_{ps})}{m_s} & \frac{k_{as}}{m_s} & \cdots \end{bmatrix}$$

$$\begin{matrix} \cdots & 0 & 0 & 0 \\ \cdots & 0 & 0 & 0 \\ \cdots & \frac{c_{as}}{m_s} & \frac{k_{ps}}{m_s} & \frac{c_{ps}}{m_s} \end{matrix} \begin{Bmatrix} X_{1,unc,S} \\ X_{2,unc,S} \\ X_{3,unc,S} \\ X_{4,unc,S} \\ X_{5,unc,S} \\ X_{6,unc,S} \end{Bmatrix} + \begin{bmatrix} 0 \\ 0 \\ \frac{1}{m_s} \end{bmatrix} \{P_{as}\} \quad \textbf{(7.15)}$$

This proposed state space model was employed in the subsequent analytical simulations.

7.3. Grandstand model with attached TMD

Figure 7-4 shows the model of the grandstand with a TMD attached to it. It is a 4DOF system model including empty structure, active spectators, passive spectators and the TMD.

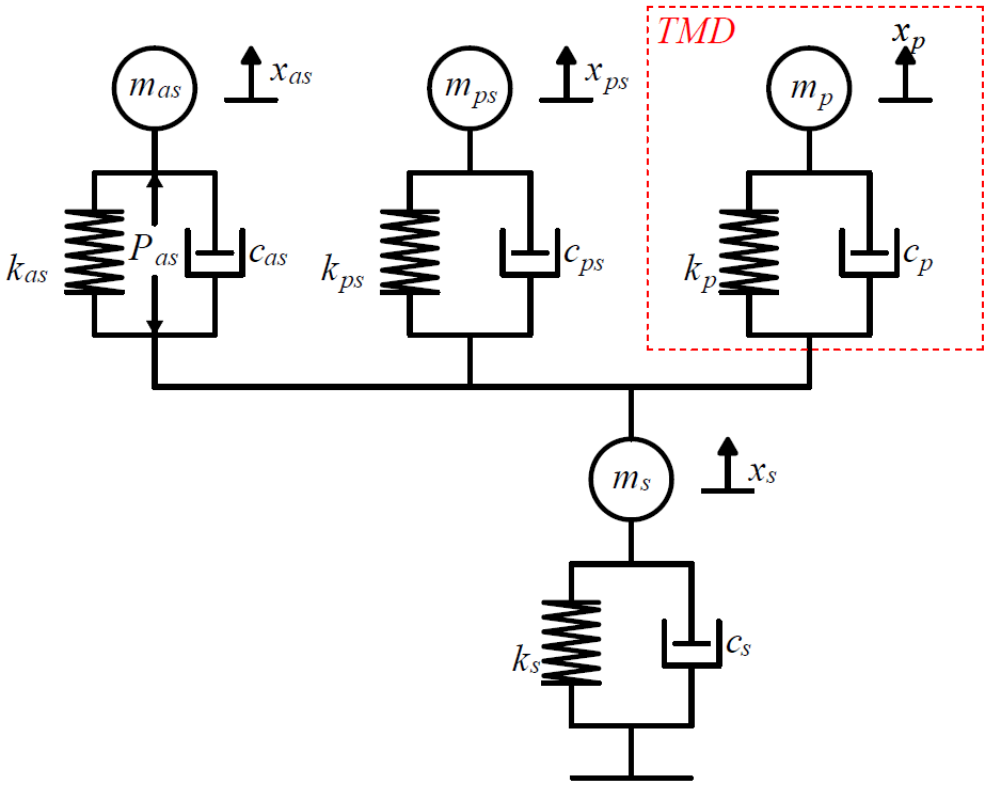

Figure 7-4- 4DOF model of the stadium cantilever with active and passive spectators and mounted TMD

The properties of the designed TMD are summarised in Table 7-4. These properties has been calculated as Section 3.3.3.

Table 7-4-TMD parameters employed in stadium model

$\bar{m}$	$\bar{f}$	f_p (Hz)	ξ_p	m_p (kg)	c_p (Ns/m)	k_p (N/m)
2.6%	0.98	3.15	5.1%	2,174	4,412	850,786

Based on Figure 7-4, the set of equations of motion of the proposed 4DOF system is generated as :

a) $m_s\ddot{x}_s(t) + (c_s + c_p + c_{as} + c_{ps})\dot{x}_s(t) - c_p * \dot{x}_p(t) - c_{as}\dot{x}_{as}(t) - c_{ps}\dot{x}_{ps}(t) + (k_s + k_p + k_{as} + k_{ps})x_s(t) - k_p x_p(t) - k_{as}x_{as}(t) - k_{ps}x_{ps}(t) = P_{as}(t)$

b) $m_p\ddot{x}_p(t) - c_p\dot{x}_s(t) + c_p\dot{x}_p(t) - k_p x_s(t) + k_p x_p(t) = 0$ **(7.16)**

c) $m_{as}\ddot{x}_{as}(t) - c_{as}\dot{x}_s(t) + c_{as}\dot{x}_{as}(t) - k_{as}x_s(t) + k_{as}x_{as}(t) = -P_{as}(t)$

d) $m_{ps}\ddot{x}_{ps}(t) - c_{ps}\dot{x}_s(t) + c_{ps}\dot{x}_{ps}(t) - k_{as}x_s(t) + k_{as}x_{ps}(t) = 0$

7.3.1. Transfer function model of the structure

The transfer function of the 4DOF system was generated by converting the equation (7.16) from time domain to Laplace domain as:

a) $m_s s^2 X_s(s) + (c_s + c_p + c_{as} + c_{ps}) s X_s(s) - c_p s X_p(s) - c_{as} s X_{as}(s) - c_{ps} s X_{ps}(s) + (k_s + k_p + k_{as} + k_{ps}) X_s(s) - k_p X_p(s) - k_{as} X_{as}(s) - k_{ps} X_{ps}(s) = P_{as}(s)$

b) $m_p s^2 X_p(s) - c_p s X_s(s) + c_p X_p(s) - k_p X_s(s) + k_p X_p(s) = 0$ **(7.17)**

c) $m_{as} s^2 X_{as}(s) - c_{as} s X_s(s) + c_{as} s X_{as}(s) - k_{as} X_s(s) + k_{as} X_{as}(s) = -P_{as}(s)$

d) $m_{ps} s^2 X_{ps}(s) - c_{ps} s X_s(s) + c_{ps} s X_{ps}(s) - k_{as} X_s(s) + k_{as} X_{ps}(s) = 0$

Rearranging (7.17) in terms of $X_s(s)$, $X_p(s)$, $X_{as}(s)$, $X_{ps}(s)$ and $P_{as}(s)$ leads to:

a) $[m_s s^2 X_s(s) + (c_s + c_p + c_{as} + c_{ps}) s + (k_s + k_p + k_{as} + k_{ps})] X_s(s) - [c_p s + k_p] X_p(s) - [c_{as} s + k_{as}] X_{as}(s) - [c_{ps} s + k_{ps}] X_{ps}(s) = P_{as}(s)$

b) $[m_p s^2 + c_p s + k_p] X_p(s) - [c_p s + k_p] X_s(s) = 0$ **(7.18)**

c) $[m_{as} s^2 + c_{as} s + k_{as}] X_{as}(s) - [c_{as} s + k_{as}] X_s(s) = -P_{as}(s)$

d) $[m_{ps} s^2 + c_{ps} s + k_{ps}] X_{as}(s) - [c_{ps} s + k_{ps}] X_s(s) = 0$

Defining $G_{s,1,TMD,S}$, $G_{s,2,TMD,S}$, $G_{s,3,TMD,S}$, $G_{s,4,TMD,S}$, $G_{p,1,S}$, $G_{as,1,S}$, $G_{as,2,S}$ and $G_{ps,1,S}$ by considering the acceleration as the output of each block (i.e. by multiplying s^2 term) as follows:

$$G_{s,1,TMD,S} = \frac{X_s(s)s^2}{P_{as}(s)} = \frac{s^2}{m_s s^2 + (c_s + c_p + c_{as} + c_{ps})s + (k_s + k_p + k_{as} + k_{ps})} \quad \textbf{(7.19)}$$

$$G_{s,2,TMD,S} = \frac{X_s(s)s^2}{X_p(s)s^2} = \frac{[\,c_p s + k_p\,]}{m_s s^2 + (c_s + c_p + c_{as} + c_{ps})s + (k_s + k_p + k_{as} + k_{ps})} \quad \textbf{(7.20)}$$

$$G_{s,3,TMD,S} = \frac{X_s(s)s^2}{X_{as}(s)s^2} = \frac{[\,c_{as} s + k_{as}\,]}{m_s s^2 + (c_s + c_p + c_{as} + c_{ps})s + (k_s + k_p + k_{as} + k_{ps})} \quad \textbf{(7.21)}$$

$$G_{s,4,TMD,S} = \frac{X_s(s)s^2}{X_{ps}(s)s^2} = \frac{[\,c_{ps} s + k_{ps}\,]}{m_s s^2 + (c_s + c_p + c_{as} + c_{ps})s + (k_s + k_p + k_{as} + k_{ps})} \quad \textbf{(7.22)}$$

$$G_{p,1,S} = \frac{X_p(s)s^2}{X_s(s)s^2} = \frac{[c_p s + k_p]}{[m_p s^2 + c_p s + k_p]} \quad \textbf{(7.23)}$$

Substituting equations (7.19) to (7.23) into the equation (7.18) results in:

$$\begin{aligned} &a)\ \ddot{x}_s = P_{as} G_{s,1,TMD,S} + \ddot{x}_p G_{s,2,TMD,S} + \ddot{x}_{as} G_{s,3,TMD,S} + \ddot{x}_{ps} G_{s,4,TMD,S} \\ &b)\ \ddot{x}_p = \ddot{x}_s G_{p,1,S} \\ &c)\ \ddot{x}_{as} = P_{as} G_{as,2,S} + \ddot{x}_s G_{as,1,S} \\ &d)\ \ddot{x}_{ps} = \ddot{x}_s G_{ps,1,S} \end{aligned} \quad \textbf{(7.24)}$$

Rearranging equations (7.24) in terms of $\ddot{x}_s$ and P_{as} results in:

$$\ddot{x}_s = P_{as}\mathrm{G_{s,1,unc,S}} + (\ddot{x}_s\mathrm{G_{p,1,S}})\mathrm{G_{s,2,TMD,S}} + (P_{as}\mathrm{G_{as,2,S}} + \ddot{x}_s\mathrm{G_{as,1,S}})\mathrm{G_{s,2,unc,S}} + (\ddot{x}_s\mathrm{G_{ps,1,S}})\mathrm{G_{s,3,unc,S}} \quad (7.25)$$

The transfer function of the system between external force P_{as} and primary structure acceleration $\ddot{x}_s$ is derived as:

$$H_{TMD,S} = \frac{\ddot{x}_s}{P_{as}} = -(G_{s,1,TMD,S} + G_{as,2,S} * G_{s,3,TMD,S})/(G_{as,1,S} * G_{s,3,TMD,S} + G_{p,1,S} * G_{s,2,TMD,S} + G_{ps,1,S} * G_{s,4,TMD,S} - 1) \quad (7.26)$$

The transfer function block diagram of this system is depicted in Figure 7-5.

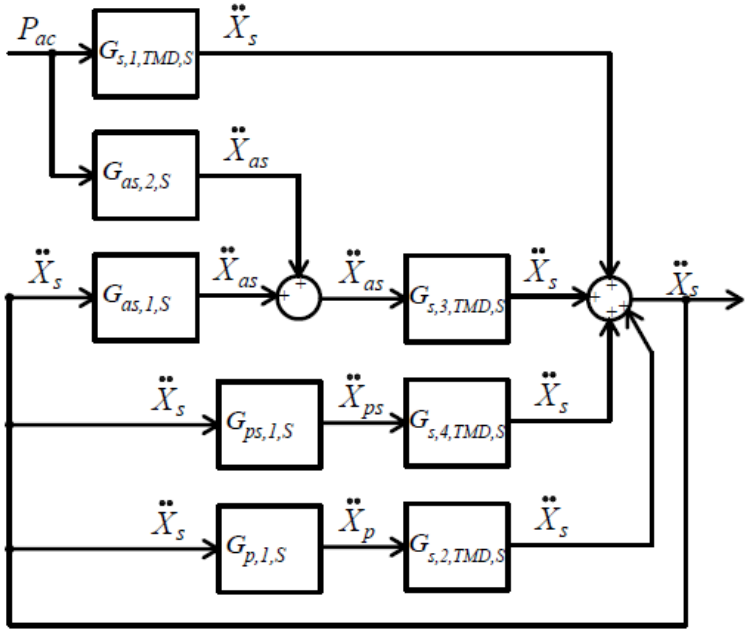

Figure 7-5- Block diagram arrangement of the stadium with TMD as a 4DOF system

7.3.2. State space model of the system

Based on equation (7.16), the states of the system are introduced as:

$$\begin{Bmatrix} X_{1,TMD,S} = x_s \\ X_{2,TMD,S} = \dot{x}_s \\ X_{3,TMD,S} = x_p \\ X_{4,TMD,S} = \dot{x}_p \\ X_{5,TMD,S} = x_{as} \\ X_{6,TMD,S} = \dot{x}_{as} \\ X_{7,TMD,S} = x_{ps} \\ X_{8,TMD,S} = \dot{x}_{ps} \end{Bmatrix} \quad \textbf{(7.27)}$$

Hence, the SS representation of the model in the form of $\dot{X}_{TMD,S} = A_{TMD,S}X_{TMD,S} + B_{TMD,S}U_{TMD,S}$ becomes

$$\begin{Bmatrix} \dot{X}_{1,TMD,S} \\ \dot{X}_{2,TMD,S} \\ \dot{X}_{3,TMD,S} \\ \dot{X}_{4,TMD,S} \\ \dot{X}_{5,TMD,S} \\ \dot{X}_{6,TMD,S} \\ \dot{X}_{7,TMD,S} \\ \dot{X}_{8,TMD,S} \end{Bmatrix} = \begin{bmatrix} 0 & 1 & 0 & 0 & \cdots \\ -\frac{(k_s + k_p + k_{as} + k_{ps})}{m_s} & -\frac{(c_s + c_p + c_{as} + c_{ps})}{m_s} & \frac{k_p}{m_s} & \frac{c_p}{m_s} & \cdots \\ 0 & 0 & 0 & 1 & \cdots \\ \frac{k_p}{m_p} & \frac{c_p}{m_p} & -\frac{k_p}{m_p} & -\frac{c_p}{m_p} & \cdots \\ 0 & 0 & 0 & 0 & \cdots \\ \frac{k_{as}}{m_{as}} & \frac{c_{as}}{m_{as}} & 0 & 0 & \cdots \\ 0 & 0 & 0 & 0 & \cdots \\ \frac{k_{ps}}{m_{ps}} & \frac{c_{ps}}{m_{ps}} & 0 & 0 & \cdots \end{bmatrix} \quad \textbf{(7.28)}$$

$$\begin{bmatrix} \cdots & 0 & 0 & 0 & 0 \\ \cdots & \frac{k_{as}}{m_s} & \frac{c_{as}}{m_s} & \frac{k_{ps}}{m_s} & \frac{c_{ps}}{m_s} \\ \cdots & 0 & 0 & 0 & 0 \\ \cdots & 0 & 0 & 0 & 0 \\ \cdots & 0 & 1 & 0 & 0 \\ \cdots & -\frac{k_{as}}{m_{as}} & -\frac{c_{as}}{m_{as}} & 0 & 0 \\ \cdots & 0 & 0 & 0 & 1 \\ \cdots & 0 & 0 & -\frac{k_{ps}}{m_{ps}} & -\frac{c_{ps}}{m_{ps}} \end{bmatrix} \begin{Bmatrix} X_{1,TMD,S} \\ X_{2,TMD,S} \\ X_{3,TMD,S} \\ X_{4,TMD,S} \\ X_{5,TMD,S} \\ X_{6,TMD,S} \\ X_{7,TMD,S} \\ X_{8,TMD,S} \end{Bmatrix} + \begin{bmatrix} 0 \\ \frac{1}{m_s} \\ 0 \\ 0 \\ 0 \\ -\frac{1}{m_{as}} \\ 0 \\ 0 \end{bmatrix} \{P_{as}\}$$

To obtain displacement, velocity and acceleration of the structure and TMD as outputs in the form of $Y_{TMD,S} = C_{TMD,S}X_{TMD,S} + D_{TMD,S}U_{TMD,S}$, the output matrix is introduced as

$$\begin{Bmatrix} Y_{1,TMD,S} \\ Y_{2,TMD,S} \\ Y_{3,TMD,S} \\ Y_{4,TMD,S} \\ Y_{5,TMD,S} \\ Y_{6,TMD,S} \end{Bmatrix} =$$

$$= \begin{bmatrix} 1 & 0 & 0 & 0 & \cdots \\ 0 & 1 & 0 & 0 & \cdots \\ -\frac{(k_s + k_p + k_{as} + k_{ps})}{m_s} & -\frac{(c_s + c_p + c_{as} + c_{ps})}{m_s} & \frac{k_p}{m_s} & \frac{c_p}{m_s} & \cdots \\ 0 & 0 & 1 & 0 & \cdots \\ 0 & 0 & 0 & 1 & \cdots \\ \frac{k_p}{m_p} & \frac{c_p}{m_p} & -\frac{k_p}{m_p} & -\frac{c_p}{m_p} & \cdots \end{bmatrix} \quad \textbf{(7.29)}$$

$$\begin{bmatrix} \cdots & 0 & 0 & 0 & 0 \\ \cdots & 0 & 0 & 0 & 0 \\ \cdots & \frac{k_{as}}{m_s} & \frac{c_{as}}{m_s} & \frac{k_{ps}}{m_s} & \frac{c_{ps}}{m_s} \\ \cdots & 0 & 0 & 0 & 0 \\ \cdots & 0 & 0 & 0 & 0 \\ \cdots & 0 & 0 & 0 & 0 \end{bmatrix} \begin{Bmatrix} X_{1,TMD,S} \\ X_{2,TMD,S} \\ X_{3,TMD,S} \\ X_{4,TMD,S} \\ X_{5,TMD,S} \\ X_{6,TMD,S} \\ X_{7,TMD,S} \\ X_{8,TMD,S} \end{Bmatrix} + \begin{bmatrix} 0 \\ 0 \\ \frac{1}{m_s} \\ 0 \\ 0 \\ 0 \end{bmatrix} \{P_{as}\}$$

7.4. Grandstand model with attached HTMD

As noted earlier, the HTMD consists of a passive TMD in addition to an inertial actuator. Figure 7-6 illustrates the 5DOF model including the empty structure, active spectators, passive spectators, passive TMD and actuator.

The actuator used in this chapter is similar to those employed in earlier chapters for the laboratory simulations and testing. However, since the scale of the force and vibration is much larger, it is assumed that the capacity of the actuator is higher than 450 N by removing the saturation block in the simulations.

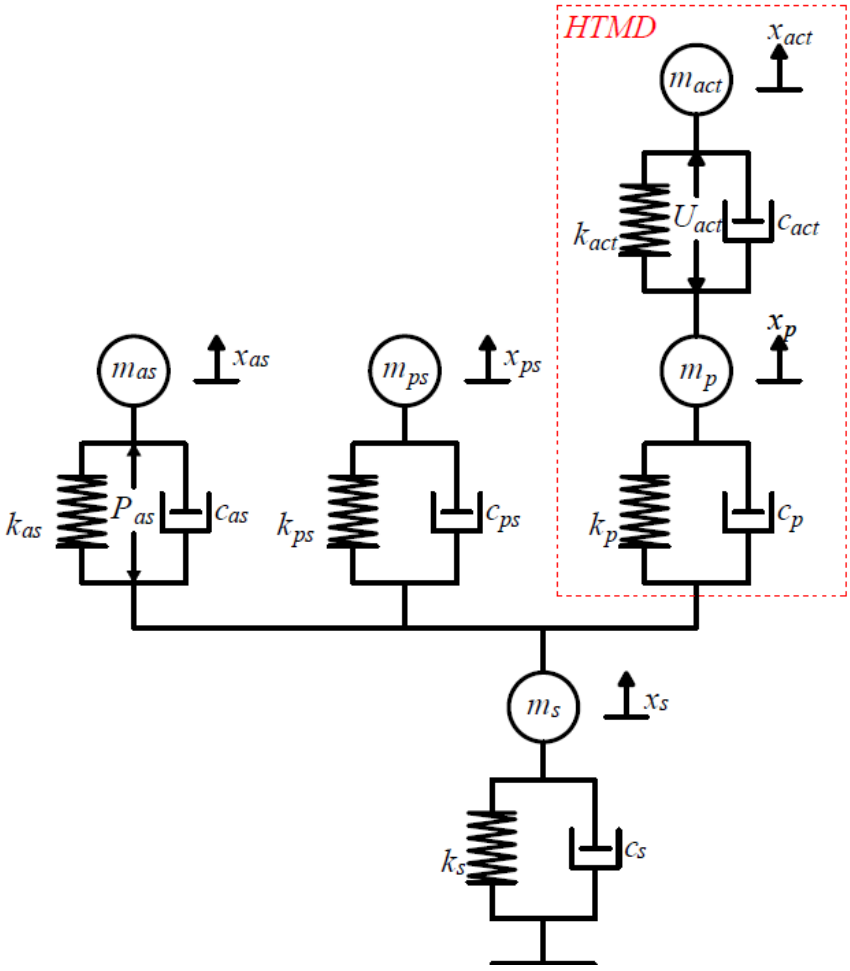

Figure 7-6- 5DOF model of the stadium cantilever with active and passive spectators and mounted HTMD

Based on Figure 7-6, the set of equations of motion of the proposed 5DOF system is generated as:

a) $m_s\ddot{x}_s(t) + (c_s + c_p + c_{as} + c_{ps})\dot{x}_s(t) - c_p\dot{x}_p(t) - c_{as}\dot{x}_{as}(t) - c_{ps} *$ **(7.30)**

$\dot{x}_{ps}(t) + (k_s + k_p + k_{as} + k_{ps})x_s(t) - k_p x_p(t) - k_{as}x_{as}(t) - k_{ps}x_{ps}(t) = P_{as}(t)$

b) $m_p\ddot{x}_p(t) - c_p\dot{x}_s(t) + c_p\dot{x}_p(t) - k_p x_s(t) + k_p x_p(t) = F_{I,act}(t)$

c) $m_{as}\ddot{x}_{as}(t) - c_{as}\dot{x}_s(t) + c_{as}\dot{x}_{as}(t) - k_{as}x_s(t) + k_{as}x_{as}(t) = -P_{as}(t)$

d) $m_{ps}\ddot{x}_{ps}(t) - c_{ps}\dot{x}_s(t) + c_{ps}\dot{x}_{ps}(t) - k_{as}x_s(t) + k_{as}x_{ps}(t) = 0$

e) $m_{act}\ddot{x}_{act}(t) + (m_{act}\varepsilon_{act} + c_{act})\ddot{x}_{act}(t) + (c_{act}\varepsilon_{act} + k_{act})\dot{x}_a(t) + (k_a\varepsilon_{act})x_{act}(t) = v_{act}m_{act}V_{in,act}(t)$

Also, as was derived in earlier chapters, the actuator degree of freedom is replaced by its inertia force (i.e. $F_{I,act}$) acting on the TMD mass.

7.4.1. Transfer function model of the structure

The transfer function of the 5DOF system is generated by converting equation (7.30) from the time domain to the Laplace domain. Defining $G_{p,2,S}$ based on the acceleration as the output of each block (i.e. by multiplying s^2 term) as follows:

$$G_{p,2,S} = \frac{X_p(s)s^2}{F_{I,act}(s)} = \frac{s^2}{m_p s^2 + c_p s + k_p} \quad \textbf{(7.31)}$$

Substituting and rearranging these equations as before leads to :

a) $\ddot{x}_s = P_{ac}G_{s,1,TMD,S} + \ddot{x}_p G_{s,2,TMD,S} + \ddot{x}_{as}G_{s,3,TMD,S} + \ddot{x}_{ps}G_{s,4,TMD,S}$

b) $\ddot{x}_p = \ddot{x}_s G_{p,1,S} + F_{I,act}G_{p,2,S}$

c) $\ddot{x}_{as} = P_{ac}G_{as,2,S} + \ddot{x}_s G_{as,1,S}$ **(7.32)**

d) $\ddot{x}_{ps} = \ddot{x}_s G_{ps,1,S}$

Regenerating equation (7.32) in terms of $\ddot{x}_s$ and P_{as} and also rewriting the equation of motion of the actuator as part a and b of equation (7.33) gives:

a) $\ddot{x}_s = P_{as}G_{s,1,unc,S} + (\ddot{x}_s G_{p,1,S} + F_{I,act}G_{p,2,S})G_{s,2,TMD,S} + (P_{as}G_{as,2,S} + \ddot{x}_s G_{as,1,S})G_{s,2,unc,S} + (\ddot{x}_s G_{ps,1,S})G_{s,3,unc,S}$ **(7.33)**

b) $F_{I,act} = V_{in,act} * G_{act} = (K_3\dot{x}_s + K_2\ddot{x}_s + K_1 x_p + K_4\dot{x}_p + K_5\ddot{x}_p) * G_{act}$

Combining part a and b of equation (7.33) results in:

$$\ddot{x}_s = -(G_{s,1,TMD,S}P_{as} + G_{as,2,S}G_{s,3,TMD,S}P_{as})/(G_{as,1,S}G_{s,3,TMD,S} + G_{p,1,S}G_{s,4,TMD,S} - (G_{s,2,TMD,S}(G_{p,1,S} + G_{act}G_{p,2,S}(K_2 + G_{int}K_3)))/(G_{act}G_{p,2,S}(K_1{G_{int}}^2 + K_4G_{int} + K_5) - 1) - 1) \quad \textbf{(7.34)}$$

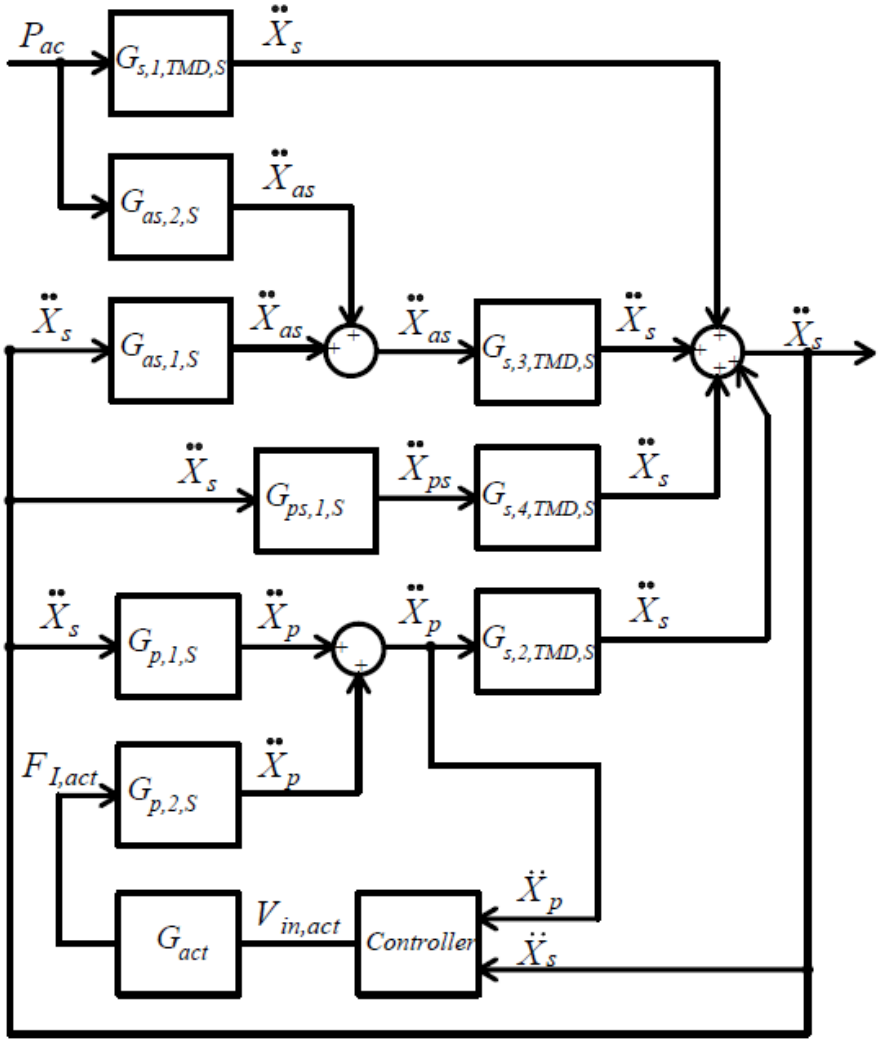

Figure 7-7- Block diagram arrangement of the stadium with HTMD as a 5DOF system

Therefore, the transfer function of the system between the human force P_{as} and acceleration of the primary structure $\ddot{x}_s$ is derived as:

$$H_{HTMD,S} = \frac{\ddot{x}_s}{P_{as}} = -(G_{s,1,TMD,S} + G_{as,2,S}G_{s,3,TMD,S})/(G_{as,1,S}G_{s,3,TMD,S} + G_{ps,1,S}G_{s,4,TMD,S} - (G_{s,2,TMD,S}(G_{p,1,S} + G_{act}G_{p,2,S}(K_2 + G_{int}K_3)))/(G_{act}G_{p,2,S}(K_1{G_{int}}^2 + K_4G_{int} + K_5) - 1) - 1) \quad \textbf{(7.35)}$$

It should be noted that K_1 to K_5 are similar types of feedback gains as defined in Section 3.6.

7.4.2. State space model of the system

Based on equation (7.30), the states of the system are introduced as

$$\begin{Bmatrix} X_{1,HTMD,S} = x_s \\ X_{2,HTMD,S} = \dot{x}_s \\ X_{3,HTMD,S} = x_p \\ X_{4,HTMD,S} = \dot{x}_p \\ X_{5,HTMD,S} = x_{as} \\ X_{6,HTMD,S} = \dot{x}_{as} \\ X_{7,HTMD,S} = x_{ps} \\ X_{8,HTMD,S} = \dot{x}_{ps} \\ X_{9,HTMD,S} = x_{act} \\ X_{10,HTMD,S} = \dot{x}_{act} \\ X_{11,HTMD,S} = \ddot{x}_{act} \end{Bmatrix} \quad \textbf{(7.36)}$$

Hence, the SS representation of the system in the form of $\dot{X}_{\mathrm{H}TMD,S} = A_{\mathrm{H}TMD,S}X_{\mathrm{H}TMD,S} + B_{\mathrm{H}TMD,S}U_{\mathrm{H}TMD,S}$ becomes:

$$
\begin{Bmatrix}
\dot{X}_{1,HTMD,S} \\ \dot{X}_{2,HTMD,S} \\ \dot{X}_{3,HTMD,S} \\ \dot{X}_{4,HTMD,S} \\ \dot{X}_{5,HTMD,S} \\ \dot{X}_{6,HTMD,S} \\ \dot{X}_{7,HTMD,S} \\ \dot{X}_{8,HTMD,S} \\ \dot{X}_{9,HTMD,S} \\ \dot{X}_{10,HTMD,S} \\ \dot{X}_{11,HTMD,S}
\end{Bmatrix} =
\begin{bmatrix}
0 & 1 & \cdots \\
-\frac{(k_s + k_p + k_{as} + k_{ps})}{m_s} & -\frac{(c_s + c_p + c_{as} + c_{ps})}{m_s} & \cdots \\
0 & 0 & \cdots \\
\frac{k_p}{m_p} & \frac{c_p}{m_p} & \cdots \\
0 & 0 & \cdots \\
\frac{k_{as}}{m_{as}} & \frac{c_{as}}{m_{as}} & \cdots \\
0 & 0 & \cdots \\
\frac{k_{ps}}{m_{ps}} & \frac{c_{ps}}{m_{ps}} & \cdots \\
0 & 0 & \cdots \\
0 & 0 & \cdots \\
0 & 0 & \cdots
\end{bmatrix}
$$

$$
\begin{bmatrix}
\cdots & 0 & 0 & 0 & 0 & 0 & 0 & \cdots \\
\cdots & \frac{k_p}{m_s} & \frac{c_p}{m_s} & \frac{k_{as}}{m_s} & \frac{c_{as}}{m_s} & \frac{k_{ps}}{m_s} & \frac{c_{ps}}{m_s} & \cdots \\
\cdots & 0 & 1 & 0 & 0 & 0 & 0 & \cdots \\
\cdots & -\frac{k_p}{m_p} & -\frac{c_p}{m_p} & 0 & 0 & 0 & 0 & \cdots \\
\cdots & 0 & 0 & 0 & 1 & 0 & 0 & \cdots \\
\cdots & 0 & 0 & -\frac{k_{as}}{m_{as}} & -\frac{c_{as}}{m_{as}} & 0 & 0 & \cdots \\
\cdots & 0 & 0 & 0 & 0 & 0 & 1 & \cdots \\
\cdots & 0 & 0 & 0 & 0 & -\frac{k_{ps}}{m_{ps}} & -\frac{c_{ps}}{m_{ps}} & \cdots \\
\cdots & 0 & 0 & 0 & 0 & 0 & 0 & \cdots \\
\cdots & 0 & 0 & 0 & 0 & 0 & 0 & \cdots \\
\cdots & 0 & 0 & 0 & 0 & 0 & 0 & \cdots
\end{bmatrix}
$$

$$
\begin{bmatrix}
\cdots & 0 & 0 & 0 \\
\cdots & 0 & 0 & 0 \\
\cdots & 0 & 0 & 0 \\
\cdots & 0 & 0 & 0 \\
\cdots & 0 & 0 & 0 \\
\cdots & 0 & 0 & 0 \\
\cdots & 0 & 0 & 0 \\
\cdots & 0 & 0 & 0 \\
\cdots & 0 & 1 & 0 \\
\cdots & 0 & 0 & 1 \\
\cdots & -\frac{(k_{act}\varepsilon_{act})}{m_{act}} & -\frac{(c_{act}\varepsilon_{act} + k_{act})}{m_{act}} & -\frac{(m_{act}\varepsilon_{act} + c_{act})}{m_{act}}
\end{bmatrix}
\cdots
$$

(7.37)

$$\cdots \begin{Bmatrix} X_{1,HTMD,S} \\ X_{2,HTMD,S} \\ X_{3,HTMD,S} \\ X_{4,HTMD,S} \\ X_{5,HTMD,S} \\ X_{6,HTMD,S} \\ X_{7,HTMD,S} \\ X_{8,HTMD,S} \\ X_{9,HTMD,S} \\ X_{10,HTMD,S} \\ X_{11,HTMD,S} \end{Bmatrix} + \begin{bmatrix} 0 & 0 & 0 \\ \frac{1}{m_s} & 0 & 0 \\ 0 & 0 & 0 \\ 0 & \frac{1}{m_p} & 0 \\ 0 & 0 & 0 \\ -\frac{1}{m_{as}} & 0 & 0 \\ 0 & 0 & 0 \\ 0 & 0 & 0 \\ 0 & 0 & 0 \\ 0 & 0 & 0 \\ 0 & 0 & v_{act} \end{bmatrix} \begin{Bmatrix} P_{as} \\ F_{I,act} \\ V_{in,act} \end{Bmatrix}$$

It should be noted the TF of the actuator (actuator dynamics) is included in the SS representation. To achieve the output as displacement, velocity and acceleration of the structure and TMD, and also displacement, velocity and inertia force of actuator in the form of $Y_{\mathrm{H}TMD,S} = C_{\mathrm{H}TMD,S} X_{\mathrm{H}TMD,S} + D_{\mathrm{H}TMD,S} U_{\mathrm{H}TMD,S}$, the output matrix is introduced as:

$$\begin{Bmatrix} Y_{1,HTMD,S} \\ Y_{2,HTMD,S} \\ Y_{3,HTMD,S} \\ Y_{4,HTMD,S} \\ Y_{5,HTMD,S} \\ Y_{6,HTMD,S} \\ Y_{7,HTMD,S} \\ Y_{8,HTMD,S} \\ Y_{9,HTMD,S} \end{Bmatrix} \cdots$$

$$= \begin{bmatrix} 1 & 0 & 0 & 0 & \cdots \\ 0 & 1 & 0 & 0 & \cdots \\ -\frac{(k_s + k_p + k_{as} + k_{ps})}{m_s} & -\frac{(c_s + c_p + c_{as} + c_{ps})}{m_s} & \frac{k_p}{m_s} & \frac{c_p}{m_s} & \cdots \\ 0 & 0 & 1 & 0 & \cdots \\ 0 & 0 & 0 & 1 & \cdots \\ \frac{k_p}{m_p} & \frac{c_p}{m_p} & -\frac{k_p}{m_p} & -\frac{c_p}{m_p} & \cdots \\ 0 & 0 & 0 & 0 & \cdots \\ 0 & 0 & 0 & 0 & \cdots \\ 0 & 0 & 0 & 0 & \cdots \end{bmatrix} \quad \textbf{(7.38)}$$

$$\cdots \begin{bmatrix} \cdots & \frac{k_{as}}{m_s} & \frac{c_{ps}}{m_s} & \frac{k_{as}}{m_s} & \frac{c_{ps}}{m_s} & 0 & 0 & 0 \\ \cdots & 0 & 0 & 0 & 0 & 0 & 0 & 0 \\ \cdots & 0 & 0 & 0 & 0 & 0 & 0 & 0 \\ \cdots & 0 & 0 & 0 & 0 & 0 & 0 & 0 \\ \cdots & 0 & 0 & 0 & 0 & 0 & 0 & 0 \\ \cdots & 0 & 0 & 0 & 0 & 0 & 0 & 0 \\ \cdots & 0 & 0 & 0 & 0 & 1 & 0 & 0 \\ \cdots & 0 & 0 & 0 & 0 & 0 & 1 & 0 \\ \cdots & 0 & 0 & 0 & 0 & 0 & 0 & m_{act} \end{bmatrix} \begin{Bmatrix} X_{1,HTMD,S} \\ X_{2,HTMD,S} \\ X_{3,HTMD,S} \\ X_{4,HTMD,S} \\ X_{5,HTMD,S} \\ X_{6,HTMD,S} \\ X_{7,HTMD,S} \\ X_{8,HTMD,S} \\ X_{9,HTMD,S} \\ X_{10,HTMD,S} \\ X_{11,HTMD,S} \end{Bmatrix} \cdots$$

$$\cdots + \begin{bmatrix} 0 & 0 & 0 \\ 0 & 0 & 0 \\ \frac{1}{m_s} & 0 & 0 \\ 0 & 0 & 0 \\ 0 & 0 & 0 \\ 0 & \frac{1}{m_p} & 0 \\ 0 & 0 & 0 \\ 0 & 0 & 0 \\ 0 & 0 & 0 \end{bmatrix} * \begin{Bmatrix} P_{as} \\ F_{I,act} \\ V_{in,act} \end{Bmatrix}$$

7.5. HTMD control algorithm

To optimise the feedback gains, a similar approach as depicted in an earlier chapter (Section 4.1.1) was employed by using a GA. To set the upper and lower band of the gains, the root locus method was applied. Table 7-5 summarises the ranges of these gains based on the stability of the closed-loop system.

Table 7-5- Stability range of the gains

Type of response feedback	Gain Range
K_3, Velocity of the main structure, $X_{Resp} = \dot{x}_s$	[-4040,0]
K_2, Acceleration of the main structure, $X_{Resp} = \ddot{x}_s$	[-207,0]
K_1, Displacement of the TMD, $X_{Resp} = x_p$	[-5670,0]
K_4, Velocity of the TMD, $X_{Resp} = \dot{x}_p$	[-261,0]
K_5, Acceleration of the TMD, $X_{Resp} = \ddot{x}_p$	[-22,0]

Employing the transfer functions derived earlier (eq. 7.35), the optimised feedback gains for the scenario when the ratio of active/passive spectators is 40:60 were calculated. The result of the optimisation is shown in Table 7-6.

Table 7-6- Optimised performance gains for stadium model with HTMD

K_3 (Vs/m)	K_2 (Vs^2/m)	K_1 (V/m)	K_4 (Vs/m)	K_5 (Vs^2/m)
0.000	-40	-4125	-60	-11

A similar approach as was used in Section 5.3 to determine the appropriate gains for off-tuning scenarios. Both approaches were used for the off-tuning design; robust gain and adaptive control.

By applying the derived transfer functions of the system and using the GA method, the gains for both control methods were generated. These are shown in Table 7-7 and Table 7-8.

Table 7-7- Optimised adaptive control gains for stadium model with HTMD

Scenario	Active people (%)	K_3	K_2	K_1	K_4	K_5
1	1%	0	0	-44.16	-2	0
2	5%	0	0	-41.4	-1.8	0
3	10%	0	0	-35.88	-1.7	0
4	20%	0	0	-27.6	-1.2	0
5	30%	0	0	-16.56	-0.7	0
6	40%	-40	-4125	-60.72	-11	-40
7	60%	-40	-1375	-22.08	-1.6	-40
8	80%	-10	-4400	-8.28	-2.2	-10

As noted before, when using the robust control approach just one set of gains was used to deal with the off-tuning in different scenarios. Conversely, for the adaptive control approach, different sets of gains were used for the various proportions of active occupants.

Table 7-8- Optimised robust control gains for stadium model with HTMD

K_3 (Vs/m)	K_2 (Vs^2/m)	K_1 (V/m)	K_4 (Vs/m)	K_5 (Vs^2/m)
0.000	-50	-475	-99	-0.6739

7.6. Analytical simulation

The generated state space models were used to simulate the modelled structure in different scenarios. These included the uncontrolled structure, structure with attached TMD and finally structure with attached HTMD.

Similar to previous simulations, both FRFs and time domain responses were investigated. In addition to the structural response comparison, the actuator effort and required control force was also explored.

7.6.1. Excitation forces

Similar to the earlier chapter (section 4.2.1), two types of forces were used. For FRF simulations a random noise signal with frequency span of 0-50 Hz and magnitude of 2.0 V as the input voltage to the actuator amplifier. This was applied directly to the structure DOF.

To simulate the input force for the time domain response analyses, the recommendation of [24] was applied. This is similar to the force that was used in the earlier chapter. In this case the motion induced force is produced as a force couple applied to both the body unit and the structure (i.e. P_{as}). Accordingly, this can be generated as:

$$P_{as} = \rho_{jump} mg \sum_{i=1}^{i=3} G_{GLF,i} \cos\left(2\pi i f_{beat} t + \theta_i\right) \quad \textbf{(7.39)}$$

where

$$mg = g \sum_{i=1}^{N_r} m_{ep} \phi_r \quad \textbf{(7.40)}$$

and ρ_{jump} is the crowd effectiveness factor, m is the mass of the crowd, g is the gravity acceleration, $G_{GLF,i}$ is a generated load factor (GLF) for harmonic i, f_{beat} is

the frequency of the crowd activity (music beat in this model), t is time and θ_i is the phase difference for harmonic i. Also m_{ep} is the mass of each person (i.e. 80 kg), ϕ_r is the amplitude of the mode shape at the location of each individual and N_r is the number of people.

For this particular structure, there were seven rows in the grandstand each with 45 people. Hence, each row's people weights should be multiplied to its corresponding mode shape amplitude (with the maximum of $\phi_r = 1$ at the tip of cantilever).

The beat frequency was set as the half of the frequency of the structure for each scenario. This meant that, depending on the ratio of active/passive spectators, the frequency of the human activity is assumed to vary as well. This led to the second harmonic of the jumping activity always to be applied at the structural resonant frequency for each scenario.

Based on [24], the scenario 4 condition is selected where "The whole crowd active". Since the RMS of the acceleration is used, $\theta_i = 0$ is chosen (due to summing the responses using SRSS method). The crowd effectiveness factor (ρ_{jump}) for scenario 4 can be calculated as:

$$\rho_{jump}(f_{beat}) = \text{sech}\,(f_{beat} - 2) \quad \textbf{(7.41)}$$

The GLFs for scenario 4 were applied as $G_{GLF,1} = 0.375$, $G_{GLF,2} = 0.095$ and $G_{GLF,3} = 0.026$. The generated modal force as the result of this approach is shown in Figure 7-8.

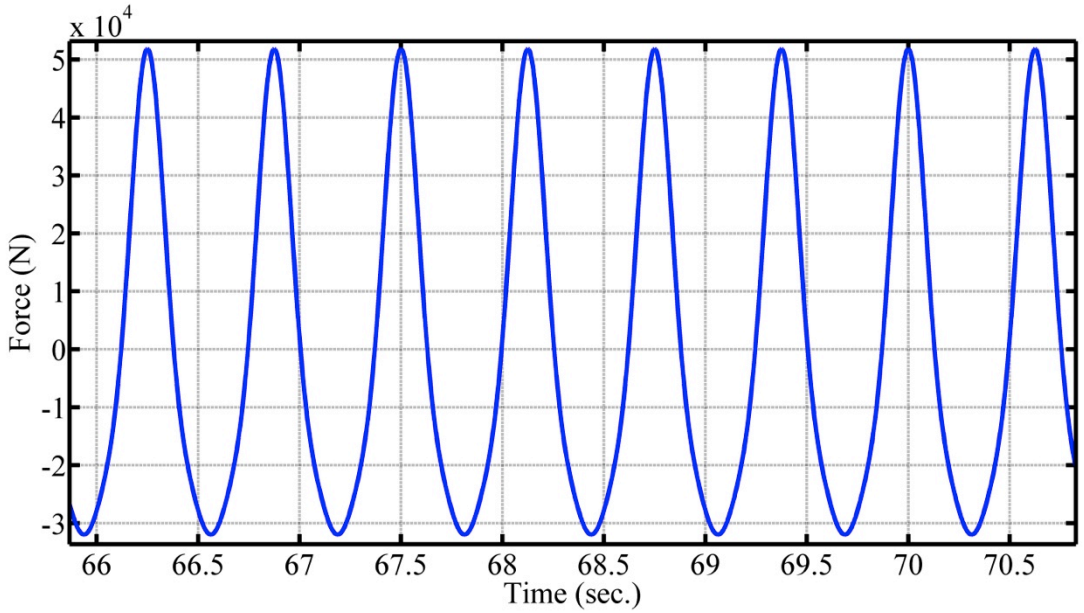

Figure 7-8- Extract from the modal force time history from an active spectator

7.6.2. Results from simulations

Results are given here for both the FRF simulations and the time domain responses due to human excitation.

It should be noted that each part of the analysis contains three parts. Firstly, the proposed feedback gains for the 40:60 scenario in which the performance of HTMD is compared against the tuned TMD.

Secondly, the performance of HTMD in the off-tuning scenario using the robust gain method is investigated by changing the frequency of the human/structure system by varying the ratio of active/passive people.

Finally, the performance of the HTMD is compared against the passive TMD with the same off-tuning scenarios using adaptive control gains.

7.6.2.1. FRF simulations

The results of simulations using band-limited random input force are the sets of FRFs between the excitation and resulting structural acceleration. It should be noted the crowd's DOF is included in the simulation. These show the performance of controller for different control scenarios. A Hanning window with 50% overlap was applied to the data when calculating FRFs.

Structural response reduction using HTMD

Figure 7-9 shows the FRFs between the structural acceleration response and input force applied to the structure DOF for the scenario where the TMD is tuned to the structure (40:60 ratio of active/passive people). As can be seen, both the passive TMD and HTMD reduce the structural response compared with the uncontrolled structure. However, the performance of the HTMD is better in comparison with passive TMD.

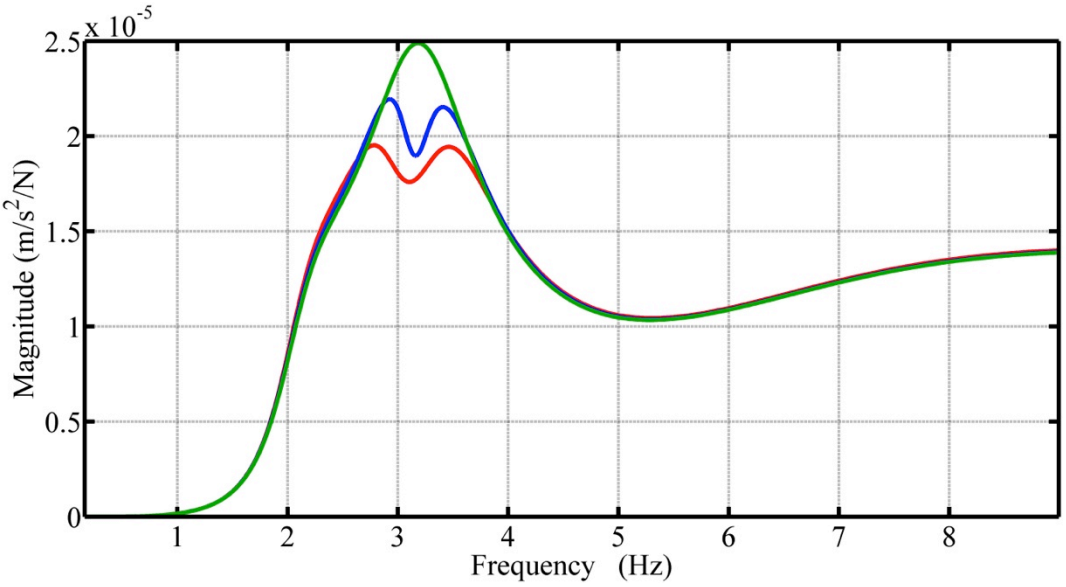

Figure 7-9- FRF magnitude comparison of the stadium model; uncontrolled structure (green), structure with TMD (blue) and HTMD (green)

Table 7-9 shows the key numerical results corresponding with the FRF plots. Although the TMD is well tuned, the FRF including HTMD still has around 11% greater reduction in comparison with the passive TMD.

Table 7-9- FRF reduction comparison of the stadium model

Type	FRF magnitude at highest peak $(m/s^2)/N$			FRF magnitude at uncontrolled resonant frequency $(m/s^2)/N$		
	Unc.	TMD	HTMD	Unc.	TMD	HTMD
Magnitude	2.49E-05	2.19E-05	1.95E-05	2.49E-05	1.90E-05	1.78E-05
Reduction from unc.	-	12%	22%	-	24%	29%

Reduction from TMD	-	-	11%	-	-	6%

Off-tuning scenario using robust gain approach

The active/passive crowd ratio was varied as described previously, resulting in a range of dominant frequencies of the human/structure system in the range of 2.71 to 4.17 Hz. The single set of robust gains were used for all of these configurations.

Figure 7-10 to Figure 7-17 show the FRFs of the uncontrolled structure, structure with TMD and HTMD. In scenario 6 (i.e. f_s=3.20Hz with active/passive ratio of 40:60), the passive TMD is tuned. As can be seen from Figure 7-15 shows, when the robust gain method is employed for the tuned scenario, the maximum response of the structure with HTMD is mainly within the boundary of the TMD response.

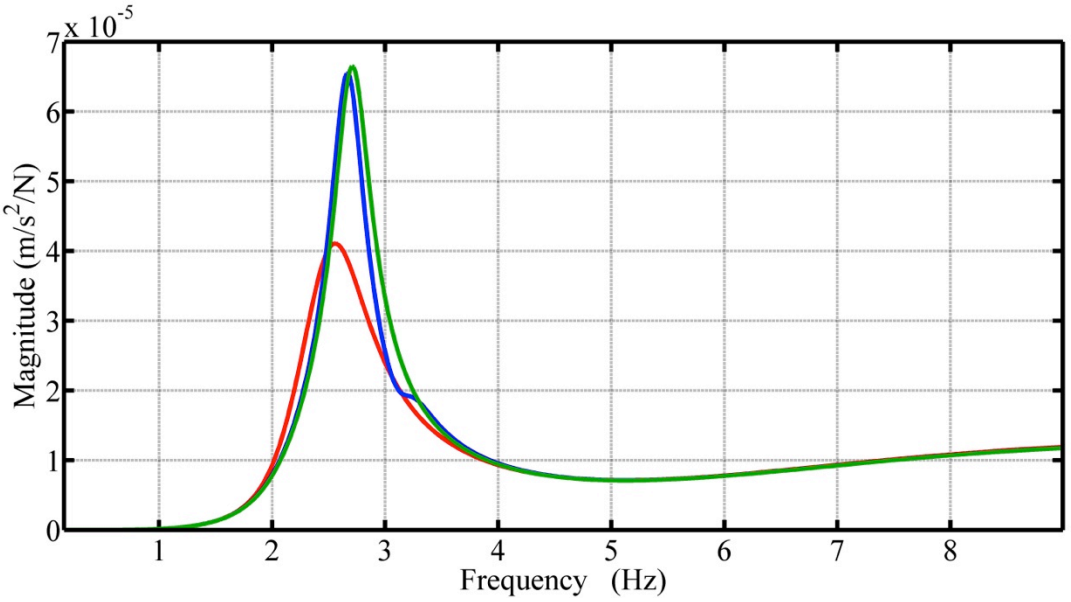

Figure 7-10- FRF magnitude comparison of the structural acceleration of the stadium model in the presence of off-tuning using Robust Gains method; scenario 1(1:99); uncontrolled structure (green), structure with TMD (blue) and HTMD (green)

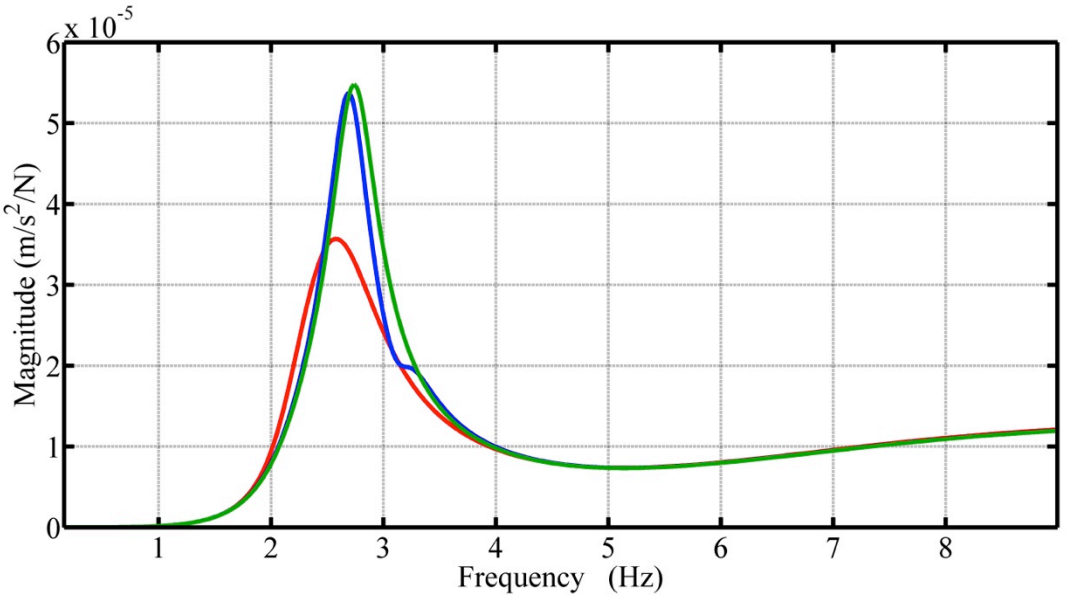

Figure 7-11- FRF magnitude comparison of the structural acceleration of the stadium model in the presence of off-tuning using Robust Gains method; scenario 2 (5:95); uncontrolled structure (green), structure with TMD (blue) and HTMD (green)

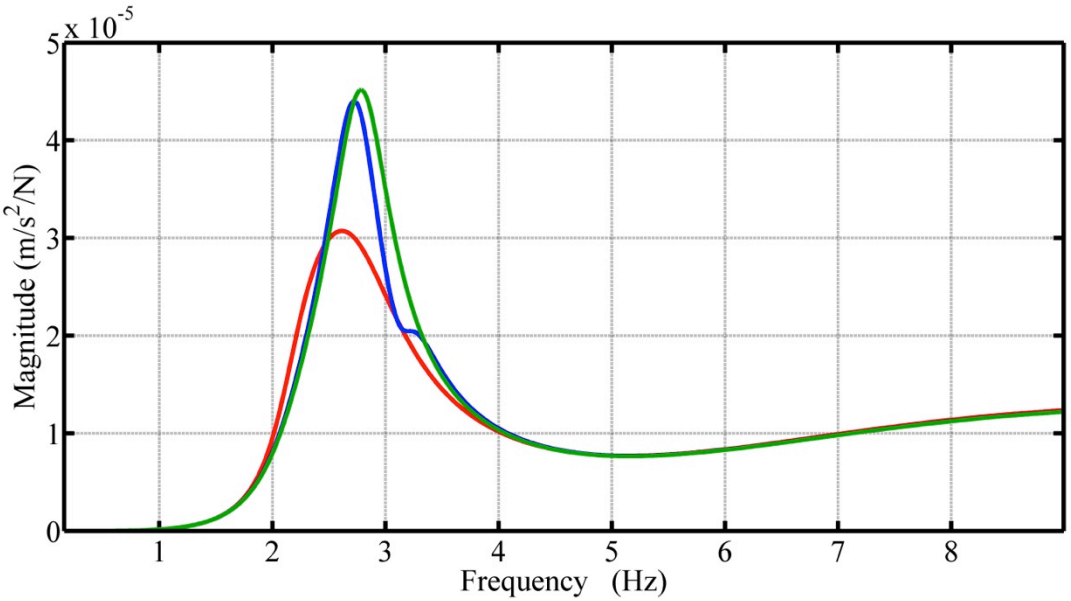

Figure 7-12- FRF magnitude comparison of the structural acceleration of the stadium model in the presence of off-tuning using Robust Gains method; scenario 3 (10:90); uncontrolled structure (green), structure with TMD (blue) and HTMD (green)

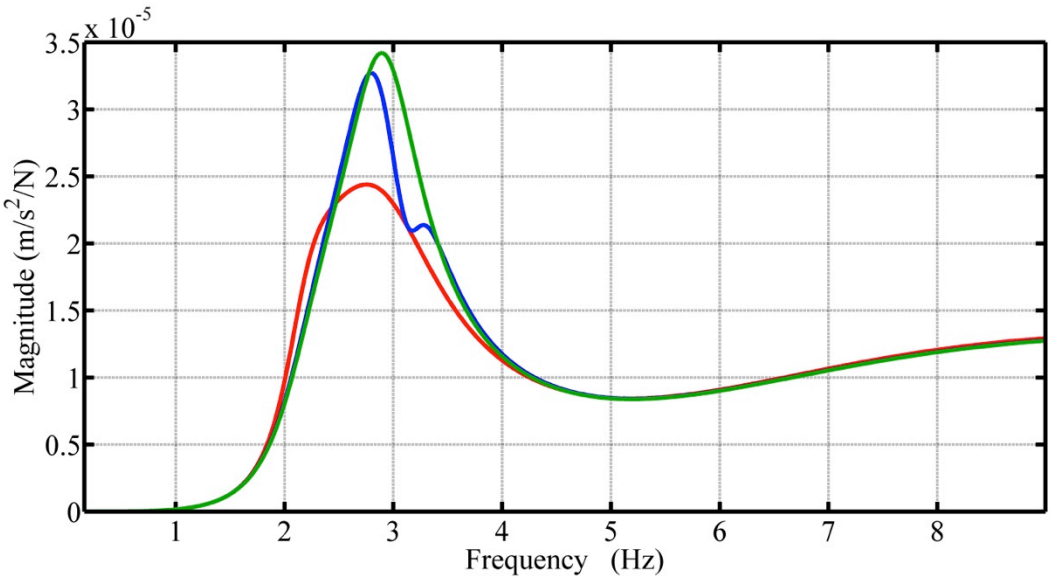

Figure 7-13- FRF magnitude comparison of the structural acceleration of the stadium model in the presence of off-tuning using Robust Gains method; scenario 4 (20:80); uncontrolled structure (green), structure with TMD (blue) and HTMD (green)

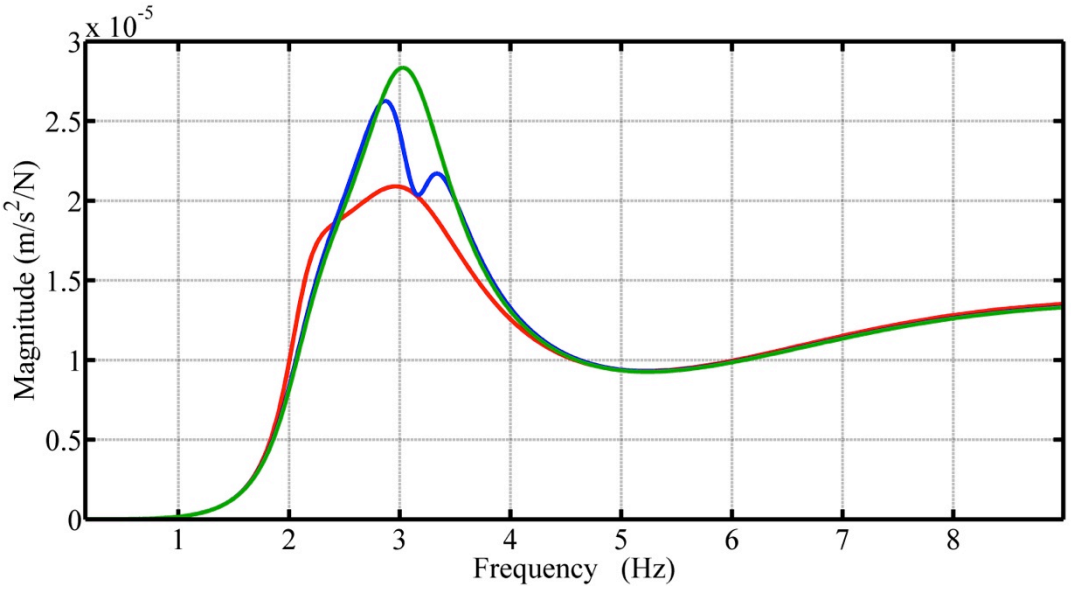

Figure 7-14- FRF magnitude comparison of the structural acceleration of the stadium model in the presence of off-tuning using Robust Gains method; scenario 5 (30:70); uncontrolled structure (green), structure with TMD (blue) and HTMD (green)

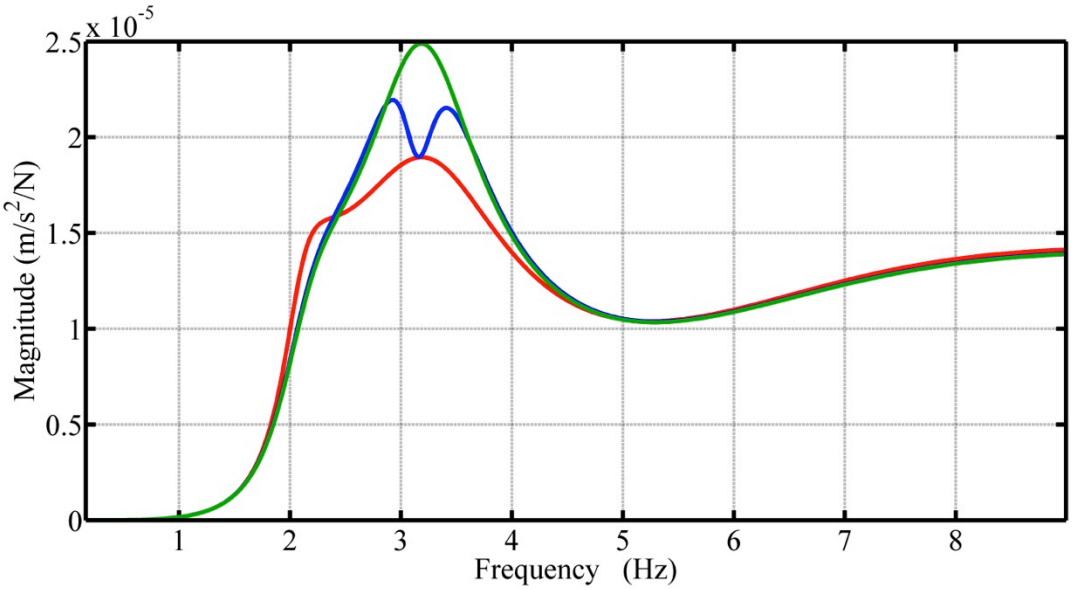

Figure 7-15- FRF magnitude comparison of the structural acceleration of the stadium model in the presence of off-tuning using Robust Gains method; scenario 6 (40:60); uncontrolled structure (green), structure with TMD (blue) and HTMD (green)

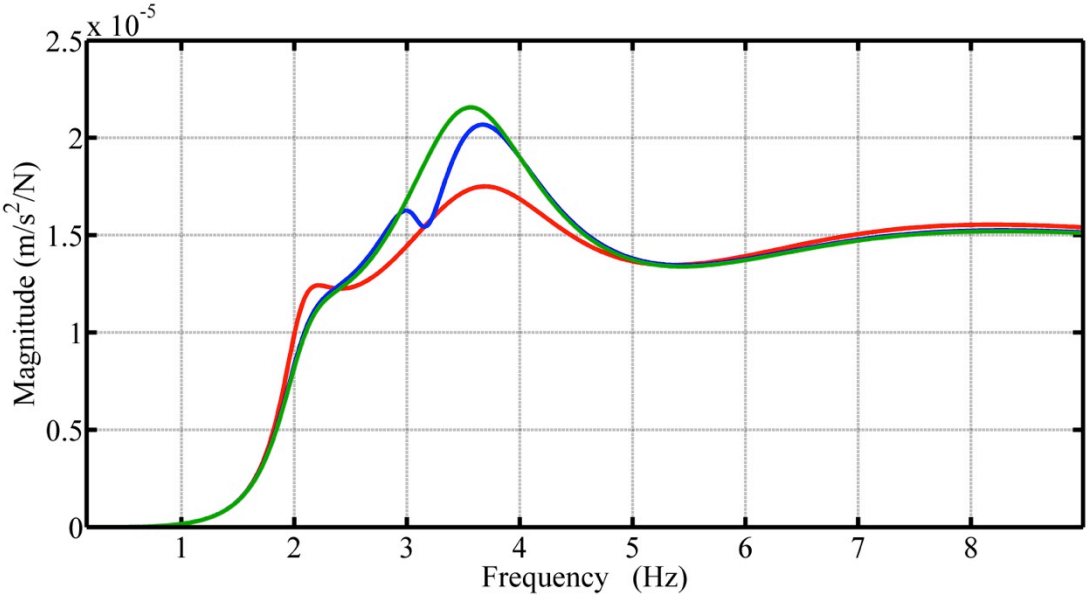

Figure 7-16- FRF magnitude comparison of the structural acceleration of the stadium model in the presence of off-tuning using Robust Gains method; scenario 7 (60:40); uncontrolled structure (green), structure with TMD (blue) and HTMD (green)

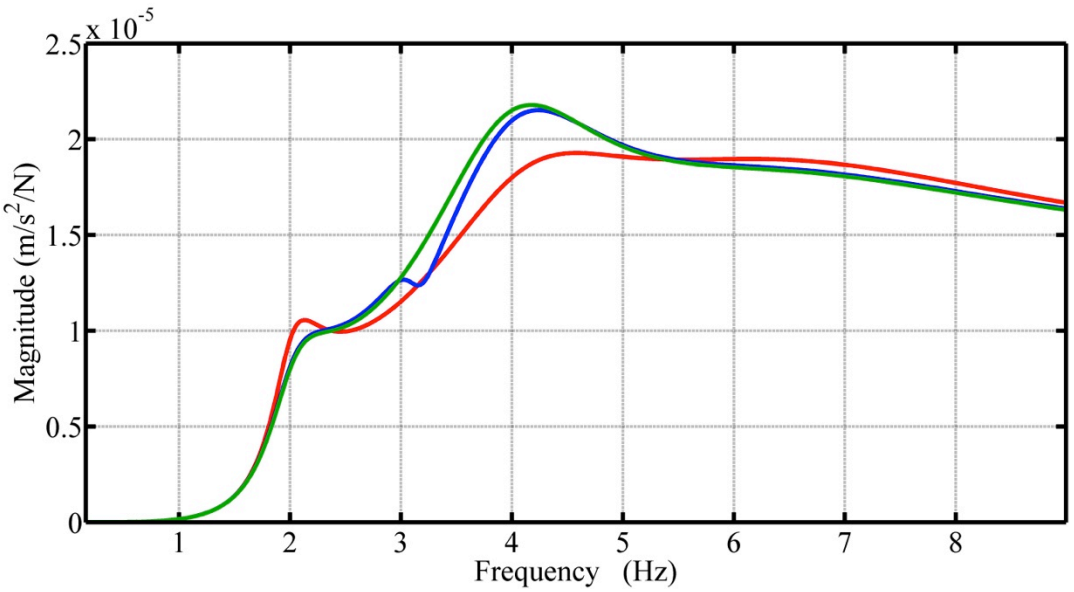

Figure 7-17- FRF magnitude comparison of the structural acceleration of the stadium model in the presence of off-tuning using Robust Gains method; scenario 8 (80:20); uncontrolled structure (green), structure with TMD (blue) and HTMD (green)

As Figure 7-10 to Figure 7-17 show, when the frequency of the structure changes from 3.20 Hz due to the varying crowd configurations, the TMD becomes detuned and hence its performance is reduced. However, the HTMD is capable of compensating for this lack of tuning and hence shows relatively good performance for all crowd configurations.

Table 7-10- FRF reduction comparison of the stadium model in the presence of off-tuning using Robust Gain control method

Scenario	Type	FRF magnitude at highest peak (m/s^2)/N			FRF magnitude at uncontrolled resonant frequency (m/s^2)/N		
		Unc.	TMD	HTMD	Unc.	TMD	HTMD
1	Magnitude	6.65E-05	6.55E-05	4.11E-05	6.65E-05	6.34E-05	3.70E-05
	Red. Unc.	-	2%	38%	-	5%	44%
	Red. TMD	-	-	37%	-	-	42%
2	Magnitude	5.48E-05	5.37E-05	3.56E-05	5.48E-05	5.21E-05	3.30E-05
	Red. Unc.	-	2%	35%	-	5%	40%
	Red. TMD	-	-	34%	-	-	37%
3	Magnitude	4.52E-05	4.40E-05	3.07E-05	4.52E-05	4.25E-05	2.91E-05
	Red. Unc.	-	3%	32%	-	6%	36%
	Red. TMD	-	-	30%	-	-	32%
4	Magnitude	3.42E-05	3.27E-05	2.44E-05	3.42E-05	3.10E-05	2.39E-05
	Red. Unc.	-	4%	29%	-	9%	30%
	Red. TMD	-	-	25%	-	-	23%
5	Magnitude	2.83E-05	2.63E-05	2.09E-05	2.83E-05	2.35E-05	2.08E-05
	Red. Unc.	-	7%	26%	-	17%	27%
	Red. TMD	-	-	21%	-	-	11%
6	Magnitude	2.49E-05	2.19E-05	1.90E-05	2.49E-05	1.90E-05	1.90E-05
	Red. Unc.	-	12%	24%	-	24%	24%
	Red. TMD	-	-	13%	-	-	0%
7	Magnitude	2.16E-05	2.07E-05	1.75E-05	2.16E-05	2.05E-05	1.74E-05
	Red. Unc.	-	4%	19%	-	5%	19%
	Red. TMD	-	-	15%	-	-	15%
8	Magnitude	2.18E-05	2.15E-05	1.92E-05	2.18E-05	2.15E-05	1.87E-05
	Red. Unc.	-	1%	12%	-	1%	14%
	Red. TMD	-	-	11%	-	-	13%

As can be seen from Table 7-10, when the dominant frequency of the human/structure system is much lower than the tuning frequency (Scenario 1), the HTMD has 42% further reduction in the structural response in comparison with passive TMD.

Meanwhile when the frequency of the human/structure system increases, although the reduction in structural response with HTMD is less in comparison with the scenario of the structure with lower frequencies than the tuning frequency. Nevertheless, there is still almost 13% reduction in comparison with passive TMD.

Also as the figures show, the FRF of the structure with HTMD is almost inside the boundary of the uncontrolled structure and structure with TMD and this avoids amplification in response for non-resonant frequencies.

Off-tuning scenario using adaptive control approach

Herein, a different control approach as section 5.3.2 is employed on the similar off-tuning scenarios. However, in the current method for individual structural frequencies, a specified set of gains is employed.

Figure 7-18 to Figure 7-25 demonstrate the FRF of the structure in different scenarios. As can be seen, the HTMD can reduce the response over a range of scenarios with different dominant frequencies of the human/structure system compared with the passive TMD.

In addition, the FRFs of the structure with HTMD are almost completely inside the boundary of the FRFs of the uncontrolled structure and structure with passive TMD. This avoids the amplification of the response at non-resonant frequencies.

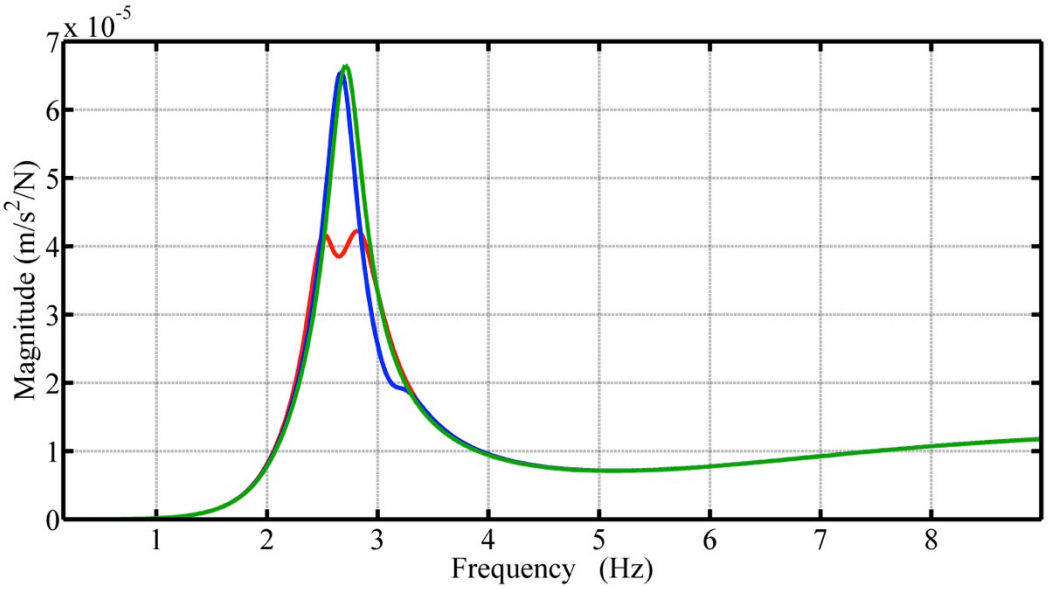

Figure 7-18- FRF magnitude comparison of the structural acceleration of the stadium model in the presence of off-tuning using Adaptive Control method; scenario 1 (1:99); uncontrolled structure (green), structure with TMD (blue) and HTMD (green)

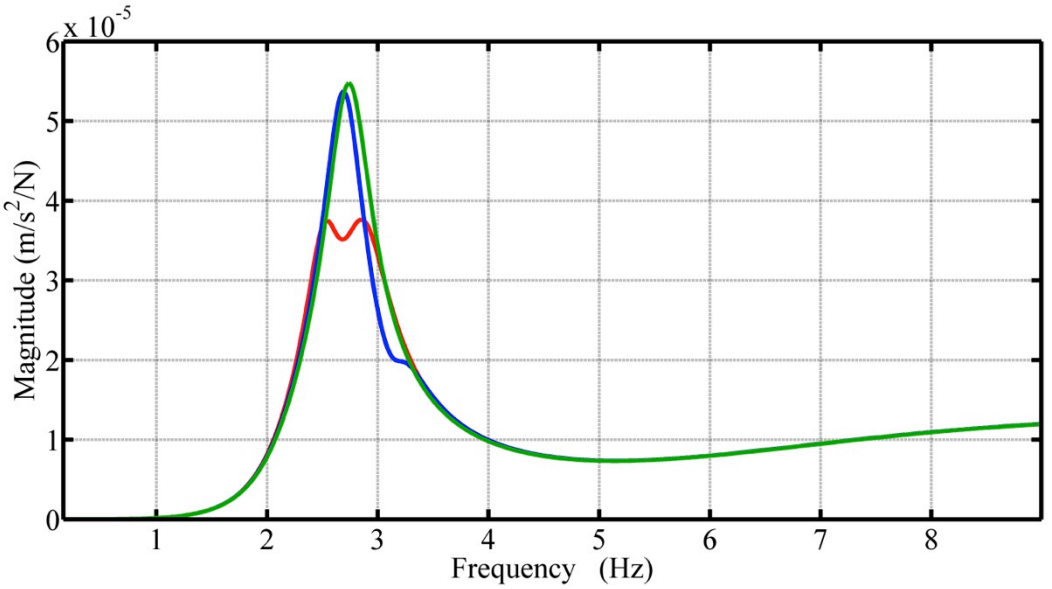

Figure 7-19- FRF magnitude comparison of the structural acceleration of the stadium model in the presence of off-tuning using Adaptive Control method; scenario 2 (5:95); uncontrolled structure (green), structure with TMD (blue) and HTMD (green)

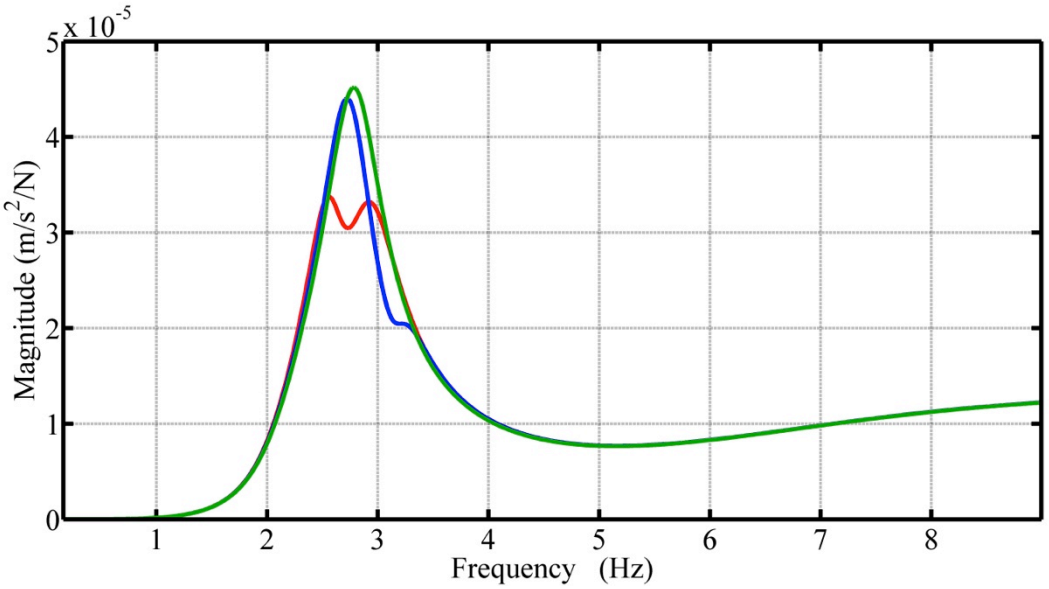

Figure 7-20- FRF magnitude comparison of the structural acceleration of the stadium model in the presence of off-tuning using Adaptive Control method; scenario 3 (10:90); uncontrolled structure (green), structure with TMD (blue) and HTMD (green)

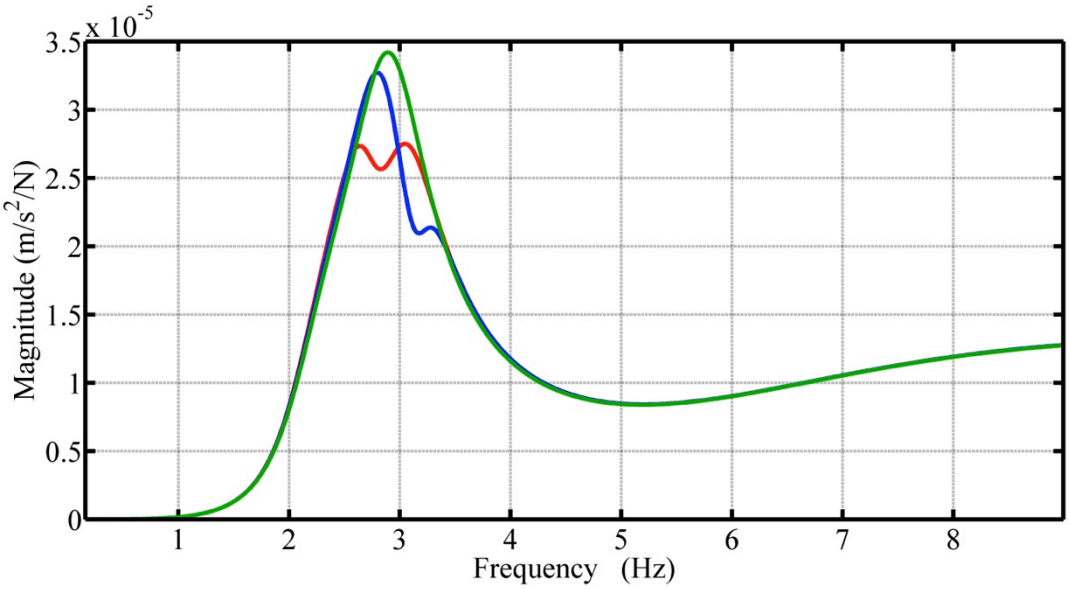

Figure 7-21- FRF magnitude comparison of the structural acceleration of the stadium model in the presence of off-tuning using Adaptive Control method; scenario 4(20:80); uncontrolled structure (green), structure with TMD (blue) and HTMD (green)

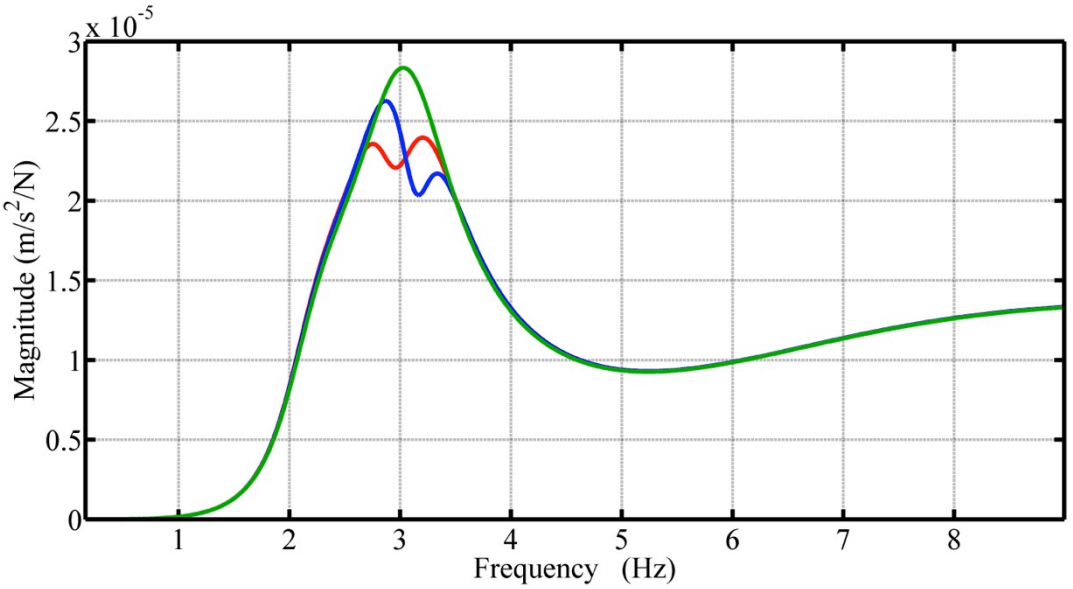

Figure 7-22- FRF magnitude comparison of the structural acceleration of the stadium model in the presence of off-tuning using Adaptive Control method; scenario 5(30:70); uncontrolled structure (green), structure with TMD (blue) and HTMD (green)

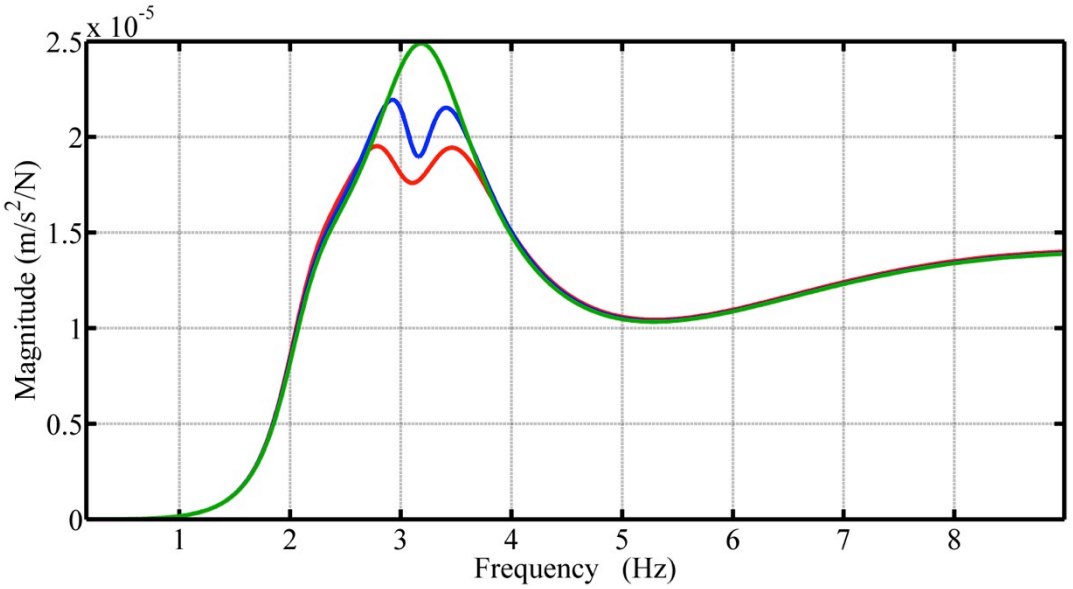

Figure 7-23- FRF magnitude comparison of the structural acceleration of the stadium model in the presence of off-tuning using Adaptive Control method; scenario 6 (40:60); uncontrolled structure (green), structure with TMD (blue) and HTMD (green)

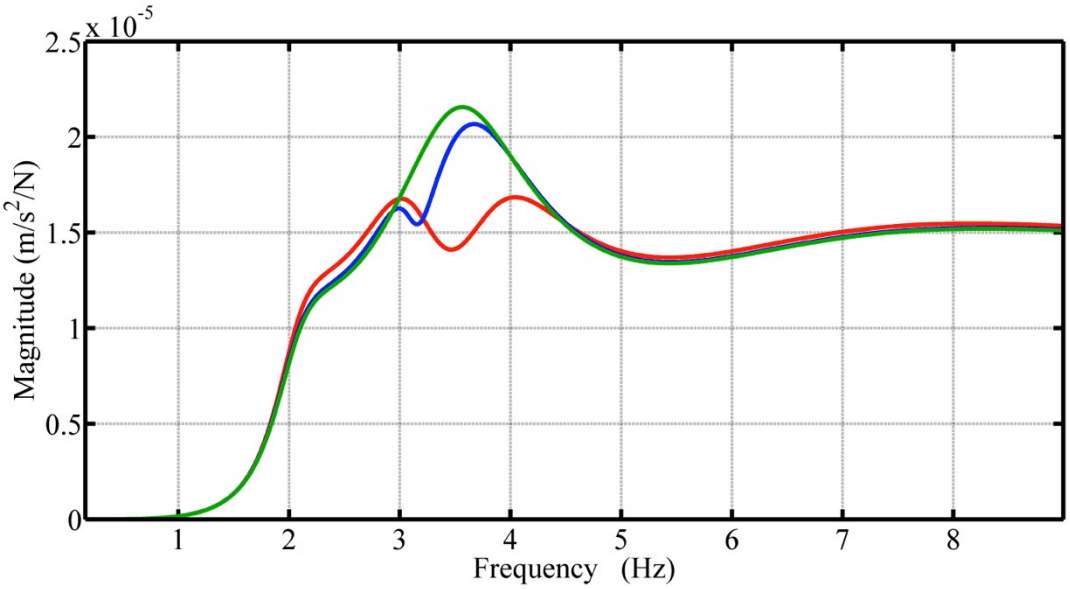

Figure 7-24- FRF magnitude comparison of the structural acceleration of the stadium model in the presence of off-tuning using Adaptive Control method; scenario 7 (60:40); uncontrolled structure (green), structure with TMD (blue) and HTMD (green)

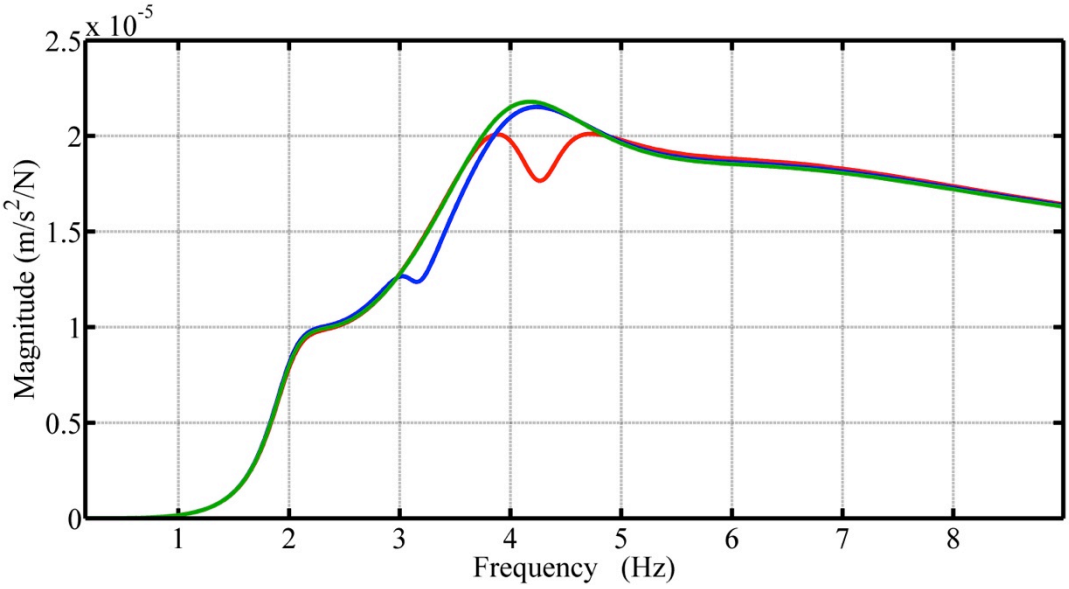

Figure 7-25- FRF magnitude comparison of the structural acceleration of the stadium model in the presence of off-tuning using Adaptive Control method; scenario 8 (80:20); uncontrolled structure (green), structure with TMD (blue) and HTMD (green)

Figure 7-23 shows the FRFs of the structure for the well-tuned TMD scenario. In this case the adaptive control approach gives similar gains as for the robust control

approach and hence the HTMD again has around 11% more reduction in comparison with the passive TMD.

Table 7-11 shows the numerical results from the FRF analysis for the adaptive control approach. As can be seen, when the frequency of the human/structure system reduces, the HTMD has better performance compared with when the frequency of the human-structure system increases. This is a similar conclusion to the robust gains method.

Table 7-11 also shows that when the dominant frequency of the human/structure system increases (higher number of active people), the adaptive control method causes more reduction initially in comparison with robust gain approach. However, when number of active spectators increases (i.e. higher structural frequencies), both adaptive control and robust gain have similar performance of response reduction.

Table 7-11- FRF reduction comparison of the stadium model in the presence of off-tuning using adaptive control gains

Scenario	Type	FRF magnitude at highest peak (m/s^2)/N			FRF magnitude at uncontrolled resonant frequency (m/s^2)/N		
		Unc.	TMD	HTMD	Unc.	TMD	HTMD
1	Magnitude	6.65E-05	6.55E-05	4.23E-05	6.65E-05	6.34E-05	3.95E-05
	Red. Unc.	-	2%	36%	-	5%	41%
	Red. TMD	-	-	35%	-	-	38%
2	Magnitude	5.48E-05	5.37E-05	3.75E-05	5.48E-05	5.21E-05	3.58E-05
	Red. Unc.	-	2%	32%	-	5%	35%
	Red. TMD	-	-	30%	-	-	31%
3	Magnitude	4.52E-05	4.40E-05	3.38E-05	4.52E-05	4.25E-05	3.11E-05
	Red. Unc.	-	3%	25%	-	6%	31%
	Red. TMD	-	-	23%	-	-	27%
4	Magnitude	3.42E-05	3.27E-05	2.73E-05	3.42E-05	3.10E-05	2.61E-05
	Red. Unc.	-	4%	20%	-	9%	24%
	Red. TMD	-	-	17%	-	-	16%
5	Magnitude	2.83E-05	2.63E-05	2.36E-05	2.83E-05	2.35E-05	2.24E-05
	Red. Unc.	-	7%	17%	-	17%	21%
	Red. TMD	-	-	10%	-	-	5%
6	Magnitude	2.49E-05	2.19E-05	1.95E-05	2.49E-05	1.90E-05	1.78E-05
	Red. Unc.	-	12%	22%	-	24%	29%
	Red. TMD	-	-	11%	-	-	6%
7	Magnitude	2.16E-05	2.07E-05	1.68E-05	2.16E-05	2.05E-05	1.44E-05
	Red. Unc.	-	4%	22%	-	5%	33%
	Red. TMD	-	-	19%	-	-	30%
8	Magnitude	2.18E-05	2.15E-05	2.01E-05	2.18E-05	2.15E-05	1.82E-05
	Red. Unc.	-	1%	8%	-	1%	17%
	Red. TMD	-	-	7%	-	-	15%

7.6.2.2. Time domain response to simulated human loading

The response of the structure is compared here for the various scenarios in terms of peak, 1 second running RMS and MTVV of weighted acceleration. The weighted acceleration of the structure according to [169] was used. W_k was chosen as the frequency weighting curve in which z-axis of the person is exposed to the vibration.

Structural response reduction using HTMD

Table 7-12 shows the acceleration response of the structure due to the occupied structure with 45*7 people. This is for the scenario when 60% of the people are jumping with the frequency of the half of the dominant frequency of the human/structure system.

Table 7-12- Time domain result comparison of the stadium model

Type	Comparison	Unc.	TMD	HTMD
Peak (m/s^2)	Magnitude	0.243	0.189	0.180
	Red. Unc.	-	22%	26%
	Red. TMD	-	-	5%
RMS (m/s^2)	Magnitude	0.149	0.113	0.107
	Red. Unc.	-	24%	29%
	Red. TMD	-	-	6%
MTVV (m/s^2)	Magnitude	0.156	0.119	0.113
	Red. Unc.	-	24%	28%
	Red. TMD	-	-	5%

In this scenario, as the TMD is tuned, both HTMD and TMD exhibit good performance in terms of reduction of structural response. However, the HTMD still has slightly better performance, as was observed in the FRF analysis.

Off-tuning scenarios using robust gains approach

Figure 7-26 shows a portion of the time history of structural acceleration from scenario 1, which has lower dominant frequency of the combined human/structure system than the original TMD tuning frequency. As can be seen, the structure with

HTMD has lower amplitude acceleration response in comparison to the structure with only a passive TMD.

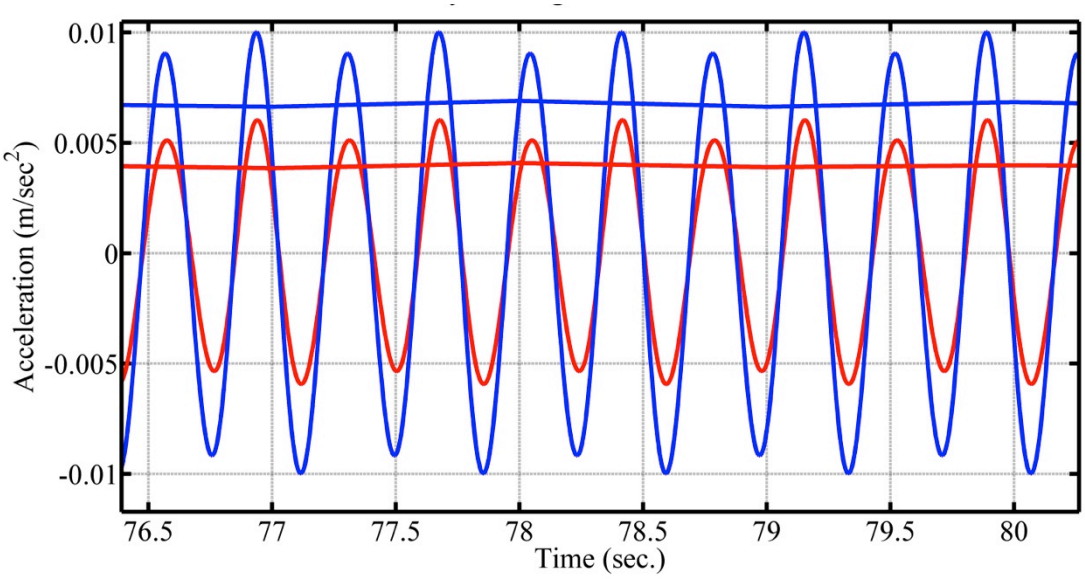

Figure 7-26- Comparison of the structural acceleration and the corresponding 1 second running RMS in Scenario 1 (1:99) using Robust Gains method; TMD (blue) and HTMD (red)

Also, Table 7-13 and Table 7-14 summarise the numerical results from the time domain simulations of response to crowd excitation. These are the peak, and MTVV of the weighted acceleration of the uncontrolled structure, structure with TMD and HTMD.

These confirm the results from the FRF analysis, that there is a reduction in performance from the TMD when the human/structure dominant frequency changes yet the performance of the HTMD remains relatively good.

Table 7-13- Comparison of time domain response of the stadium model in the presence of off-tuning using robust gains method; peak acceleration of the structure

Scenario	Type	Peak of weighted acceleration (m/s^2)		
		Unc.	TMD	HTMD
1	Magnitude	0.011	0.010	0.006
	Red. Unc.	-	10%	46%
	Red. TMD	-	-	40%
2	Magnitude	0.047	0.043	0.028
	Red. Unc.	-	10%	41%
	Red. TMD	-	-	35%
3	Magnitude	0.081	0.073	0.051
	Red. Unc.	-	11%	37%
	Red. TMD	-	-	30%
4	Magnitude	0.135	0.117	0.092
	Red. Unc.	-	14%	31%
	Red. TMD	-	-	21%
5	Magnitude	0.184	0.149	0.133
	Red. Unc.	-	19%	28%
	Red. TMD	-	-	10%
6	Magnitude	0.243	0.189	0.185
	Red. Unc.	-	22%	24%
	Red. TMD	-	-	2%
7	Magnitude	0.421	0.395	0.356
	Red. Unc.	-	6%	15%
	Red. TMD	-	-	10%
8	Magnitude	0.931	0.910	0.938
	Red. Unc.	-	2%	-1%
	Red. TMD	-	-	-3%

Table 7-14- Time Domain result comparison of the stadium model in the presence of off-tuning using robust gains method; MTVV of the acceleration of the structure

Scenario	Type	MTVV of weighted acceleration (m/s^2)		
		Unc.	TMD	HTMD
1	Magnitude	0.008	0.007	0.004
	Red. Unc.	-	9%	46%
	Red. TMD	-	-	41%
2	Magnitude	0.033	0.030	0.019
	Red. Unc.	-	9%	41%
	Red. TMD	-	-	36%
3	Magnitude	0.056	0.050	0.035
	Red. Unc.	-	10%	37%
	Red. TMD	-	-	31%
4	Magnitude	0.090	0.079	0.062
	Red. Unc.	-	13%	31%
	Red. TMD	-	-	22%
5	Magnitude	0.119	0.099	0.087
	Red. Unc.	-	17%	27%
	Red. TMD	-	-	12%
6	Magnitude	0.156	0.119	0.118
	Red. Unc.	-	24%	24%
	Red. TMD	-	-	1%
7	Magnitude	0.252	0.234	0.210
	Red. Unc.	-	7%	17%
	Red. TMD	-	-	10%
8	Magnitude	0.481	0.465	0.470
	Red. Unc.	-	3%	2%
	Red. TMD	-	-	-1%

Off-tuning scenarios using adaptive control approach

Figure 7-27 shows a portion of the time history of structural acceleration from scenario 1, which has lower dominant frequency of the combined human/structure system than the original TMD tuning frequency. As can be seen, the structure with HTMD using the adaptive control approach has lower amplitude acceleration response in comparison to the structure with only a passive TMD.

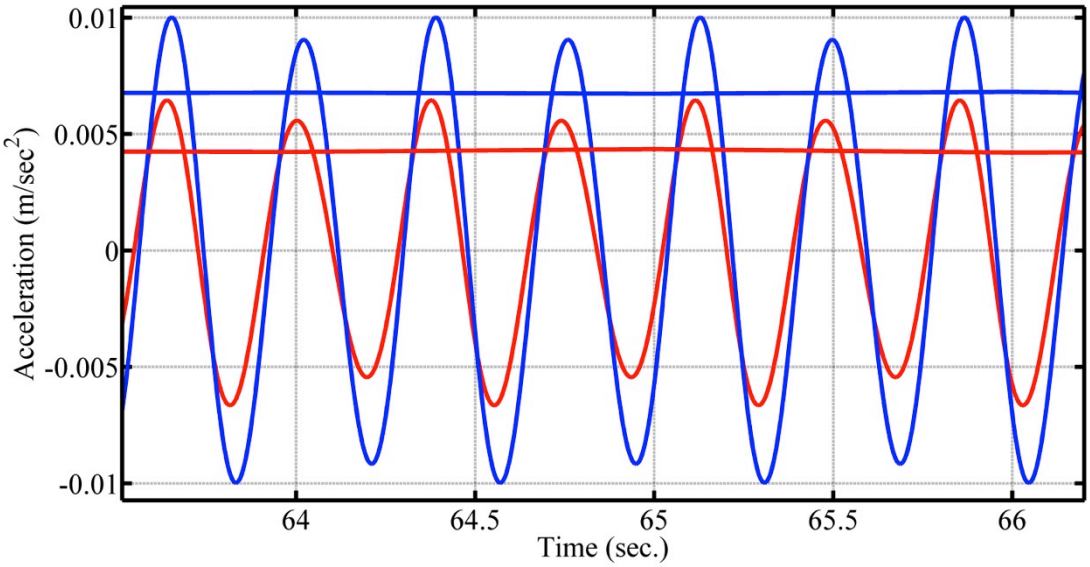

Figure 7-27- Comparison of the structural acceleration and the corresponding 1 second running RMS in Scenario 1 using Adaptive Control method; TMD (blue) and HTMD (red)

Table 7-15 and Table 7-16 summarise the numerical results of the time domain response analyses. These show a similar conclusion as the FRF analysis.

Table 7-15- Time Domain result comparison of the stadium model in the presence of off-tuning using Adaptive Control method; peak acceleration of the structure

Scenario	Type	Peak of weighted acceleration (m/s^2)		
		Unc.	TMD	HTMD
1	Magnitude	0.011	0.010	0.007
	Red. Unc.	-	10%	40%
	Red. TMD	-	-	34%
2	Magnitude	0.047	0.043	0.031
	Red. Unc.	-	10%	35%
	Red. TMD	-	-	27%
3	Magnitude	0.081	0.073	0.056
	Red. Unc.	-	11%	31%
	Red. TMD	-	-	23%
4	Magnitude	0.135	0.117	0.103
	Red. Unc.	-	14%	23%
	Red. TMD	-	-	11%
5	Magnitude	0.184	0.149	0.145
	Red. Unc.	-	19%	21%
	Red. TMD	-	-	2%
6	Magnitude	0.243	0.189	0.180
	Red. Unc.	-	22%	26%
	Red. TMD	-	-	5%
7	Magnitude	0.421	0.395	0.310
	Red. Unc.	-	6%	26%
	Red. TMD	-	-	22%
8	Magnitude	0.931	0.910	0.822
	Red. Unc.	-	2%	12%
	Red. TMD	-	-	10%

Table 7-16- Time Domain result comparison of the stadium model in the presence of off-tuning using Adaptive Control method; MTVV of the acceleration of the structure

Scenario	Type	MTVV of weighted acceleration (m/s^2)		
		Unc.	TMD	HTMD
1	Magnitude	0.008	0.007	0.005
	Red. Unc.	-	9%	42%
	Red. TMD	-	-	36%
2	Magnitude	0.033	0.030	0.021
	Red. Unc.	-	9%	36%
	Red. TMD	-	-	30%
3	Magnitude	0.056	0.050	0.038
	Red. Unc.	-	10%	32%
	Red. TMD	-	-	25%
4	Magnitude	0.090	0.079	0.068
	Red. Unc.	-	13%	25%
	Red. TMD	-	-	14%
5	Magnitude	0.119	0.099	0.093
	Red. Unc.	-	17%	22%
	Red. TMD	-	-	6%
6	Magnitude	0.156	0.119	0.113
	Red. Unc.	-	24%	28%
	Red. TMD	-	-	5%
7	Magnitude	0.252	0.234	0.182
	Red. Unc.	-	7%	28%
	Red. TMD	-	-	22%
8	Magnitude	0.481	0.465	0.425
	Red. Unc.	-	3%	12%
	Red. TMD	-	-	9%

7.6.2.3.Actuator effort

The actuator effort can be examined based on the inertia force through the actuator predicted by the time domain simulations. It should be noted that the restriction of the maximum capacity of the actuator (i.e. 450 N) was removed due to the larger scale of the simulation and the assumption that larger actuators would be designed for such a purpose.

Figure 7-28 shows the time history of the actuator effort for Scenario 6, when the TMD is well-tuned.

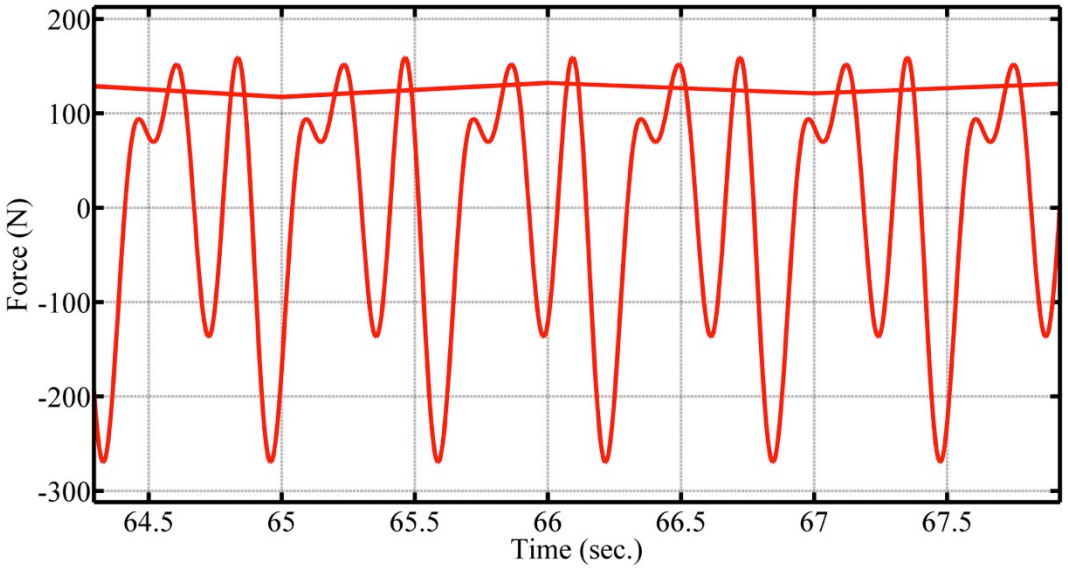

Figure 7-28- Time history of the actuator force in HTMD and the corresponding 1 second running RMS

Also, Table 7-17 shows the numerical result of the actuator force in the same scenario. As can be seen, although the scale of the excitation force is very high and 60% of people jumping at the most onerous frequency, still the amount of the required active force is low and is less than the maximum capacity of the available actuator.

Table 7-17- HTMD actuator force in stadium model

Peak force (N)	RMS of the force (N)	MTVV of the force (N)
159	127	134

Off-tuning scenarios using robust gains approach

Figure 7-29 illustrates the time history of the actuator force for one of the off-tuning scenarios when robust gains method was employed for the HTMD.

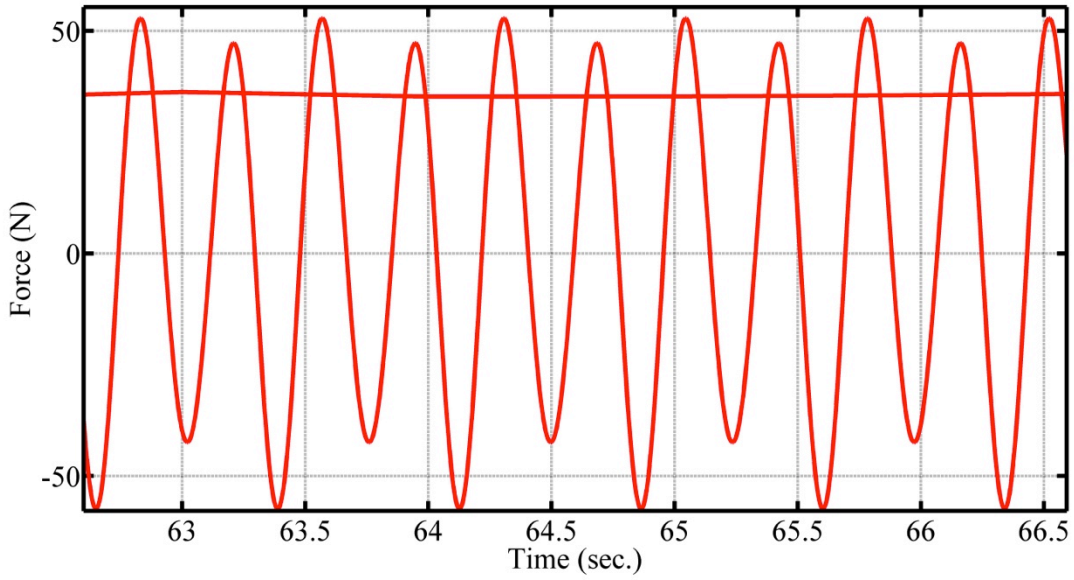

Figure 7-29- Time history of the actuator force in HTMD and the corresponding 1 second running RMS in Scenario 1 using Robust Gains method

Table 7-18- HTMD actuator force in stadium model in the presence of off-tuning using Robust Gains

Scenario	Peak force (N)	RMS of the force (N)	MTVV of the force (N)
1	53	36	38
2	222	148	158
3	349	230	250
4	425	286	322
5	372	331	370
6	1127	607	645
7	5196	2827	2962
8	13365	10969	11348

Also, Table 7-18 shows the numerical results of the actuator force for the full range of different scenarios. As can be seen, except the last two scenarios (when 80% of people are active and jumping on resonant frequency), the required actuator force within the capacity of the available laboratory actuator.

Off-tuning scenarios using the adaptive control approach

Figure 7-30 shows the actuator effort for off-tuning Scenario 1 when the adaptive control approach was implemented for the HTMD.

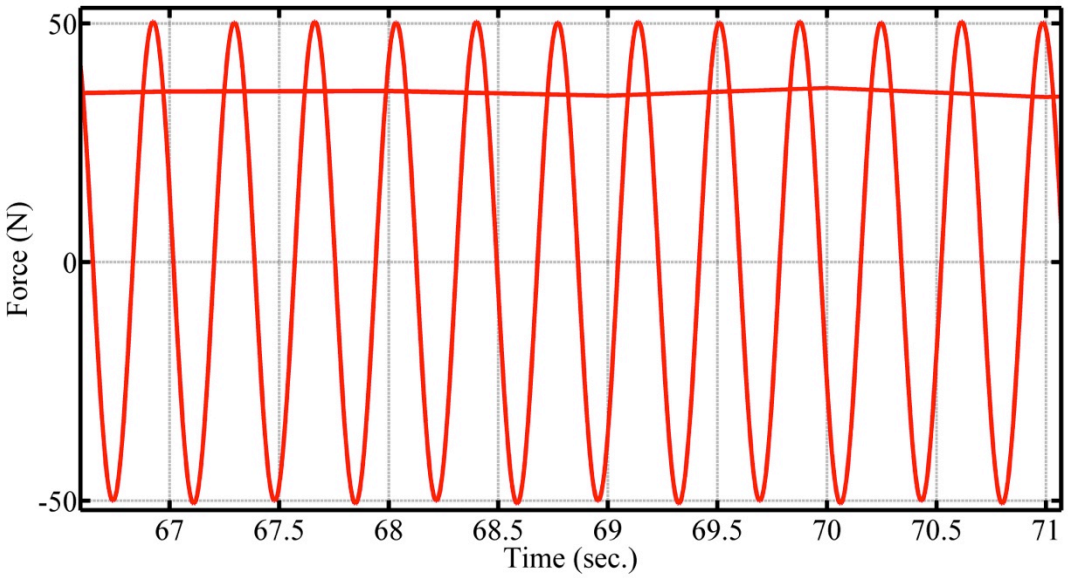

Figure 7-30- Time history of the actuator force in HTMD and the corresponding 1 second running RMS in Scenario 1 using Adaptive Control method

Also, Table 7-19 shows the numerical results of the required actuator control force for the full range of scenarios. Also, it illustrates that the amount of required force in higher frequencies is less in comparison with HTMD with robust gain method.

Table 7-19- HTMD actuator force in stadium model in the presence of off-tuning using Adaptive Control

Scenario	Peak force (N)	RMS of the force (N)	MTVV of the force (N)
1	50	36	37
2	203	143	148
3	331	234	241

4	391	276	281
5	326	230	232
6	159	127	134
7	3687	1764	1866
8	4845	3121	3255

7.7. Conclusion and result discussion

In this chapter a model of a real stadium cantilever was used with the size of 7*45 people as the primary structure. This was a 3DOF system including empty structure, active and passive spectators. Similar control algorithms and gain optimisation methods as introduced before were applied to this structure. This was for both response reductions in tuned and out-of-tune scenarios with respect to the passive TMD component.

It was shown that when the percentage of the active spectators changes in the structure, the frequency of the structure varies as well. This means that the employed TMD becomes relatively out-of-tune and hence relatively less effective. Meanwhile, the HTMD with both of the proposed control techniques could still reduce the structural response, even in the presence of off-tuning.

It was shown that the HTMD performance was relatively better when the frequency of the structure reduced from tuning frequency in comparison with increase in the structural frequency. Also, the required actuator effort was less when using adaptive control in comparison with robust gains.

To conclude, it is recommended to design the HTMD for the worst scenario (more active people) as the tuning frequency since the performance of HTMD is much better when the frequency of the structure reduces.

8. Conclusions and recommendations for further work

Chapters 3 to 7 of this thesis have presented detailed conclusions from the analytical and experimental studies. Here, a summary of the key conclusions is given and recommendations are made for avenues of further research that may be explored.

8.1. Conclusions

A generic model of a SDOF representation of an uncontrolled structure, structure controlled with passive TMD, AMD and HTMD in both state space and transfer function formulations was developed.

It was concluded that it is not suitable to use conventional gain optimisation methods such as conventional or modified LQR in HTMD since it is a 3DOF system and these methods are restricted to fewer gain combinations or may result in local minimums instead of global ones. Hence, a genetic algorithm (GA) approach was introduced as a comprehensive search method. A new method was introduced to convert the problem of choice of HTMD gains to standard optimisation problem language and then utilising GA to solve this optimisation problem.

It was found that employing GA is an appropriate optimisation method to determine suitable sets of gains for implementation in a HTMD. The resulting HTMD demonstrated improved (reduced) structural response in contrast with the same HTMD with gains optimised using other methods (manual, conventional LQR and modified LQR).

Also, it was concluded that structural acceleration plus the velocity of the TMD mass are two appropriate sets of feedback parameters which have the most effect on the HTMD performance for both reducing the response of the primary structure and also tuning the HTMD (e.g. actively control the HTMD damping). Two methods were also introduced and employed to check the stability of the closed loop system.

Following choice of appropriate feedback control gains, the operation of HTMD was compared with the uncontrolled structure and the structure controlled with TMD and AMD. It was concluded that the HTMD provides higher reduction in structural response at resonance in contrast with TMD. Also, compared against AMD, it was found that the HTMD requires less power (actuator effort) to reduce the structural

response for the same scenario when DVF (Direct Velocity Feedback) control method is employed in AMD.

The performance of a TMD and HTMD in the presence of off-tuning (i.e. when the frequency of the structure changes) was also investigated. Two control algorithms were introduced to deal with this based on GA optimisation. The performance of both control techniques was compared and the benefits and disadvantages of each were studied. It was concluded that in addition to the two proposed gains, feedback of the acceleration and displacement of the TMD mass provide two new gains for re-tuning and modifying the HTMD frequency. The results show that when off-tuning occurs in the structure, the passive TMD does not operate efficiently. However, the HTMD can still effectively reduce the structural response by its properties in real time.

The two proposed control algorithms were also compared together and it was concluded that one method has more structural response reduction, whereas the other one needs less actuator effort (power) to reduce the structural response.

The design and construction of a prototype HTMD was presented. The built HTMD had the same properties as the one used in the analytical studies (simulations). The aim was to verify the developed analytical models and to experimentally investigate the performance of the HTMD on the laboratory structure. In addition, the suggested control algorithms were verified using these laboratory experiments.

Similar to the analytical simulation, it was demonstrated that the HTMD reduces the response of the structure in comparison with the passive TMD. Also, it was shown that the HTMD required less power in comparison with the AMD. The stability of the closed loop system was investigated and it was concluded that the proposed methods can be utilised to check and ensure the stability of the HTDM.

As to the other part of the experimental investigation, the performance of the HTMD in off-tuning was investigated experimentally and it was concluded that the HTMD can still reduce the structural response when the frequency of the primary structure changes. It was also concluded that although the AMD can decrease the structural response in off-tuning, HTMD requires less actuator effort.

Finally, the performance of HTMD was investigated using a simulation model of an actual stadium, which had both active and passive spectators. Both state-space and transfer function models of this structure were developed as uncontrolled, controlled with TMD and controlled with HTMD.

It was demonstrated that when the structural frequency changes (due to the variation in the ratio of active and passive spectators), the HTMD had better performance in structural response reduction in comparison with passive TMD. This was achieved with the proposed HTMD and actuator and hence it was concluded that the HTMD has potential application in real stadium. This is especially so for the scenarios when the spectator activity (such as jumping) has a harmonic close a structural frequency (resonance scenario).

To summarise, considering both structural response and cost of the actuator, the hybrid tuned mass damper (HTMD) is an appropriate and effective device to reduce structural vibration due to human activities in stadiums, which can adapt to off-tuning caused by variation in the crowd configuration during real events.

8.2. Recommendations for further work

As was shown previously, the performance of HTMD in off-tuning using an adaptive control method depends on the size of the database and the on-line system identification. Further work is required to develop a larger database for the adaptive control approach to deal with the off-tuning problem. The proposed database should consider all possible frequencies with fewer increments. A larger database would probably result in improved structural response reduction and lower actuator cost. Also, further work is required to develop and improved on-line system identification method on which the adaptive gains are selected.

Also, it would be beneficial to investigate the performance of the HTMD in a real stadium cantilever structure with both actuator excitation and also in the presence of a crowd. In this thesis, the proposed control algorithms were implemented in a laboratory structure. However, the performance of the HTMD in a real stadium (the last chapter of this study) should also be tested and verified experimentally. This opens more challenges including finding the appropriate HTMD location, restriction

and protection of the HTMD in a real concert or sport event, health and safety issues, mobility of the HTMD to the site, etc.

It would be beneficial to investigate the performance of employing multi-HMTD (several HTMDs) in larger structures and to develop the appropriate control algorithms for both structural response reduction and also dealing with off-tuning as a potential problem in grandstands.

Power-cut is one of the possible problems could happen in the operation time of HTMD. Since power cut causes the actuator to be out of work and hence, an extra degree of freedom system on top of TMD without no tuning, it could even increase the vibration of the structure. Hence, author recommends of using/manufacturing an actuator with a locking/ emergency mechanism which stop/lock the mass of the actuator in the event of power cut. This can be extend to design a control algorithm to also stop/lock the actuator when the system becomes unstable or even un-expected structural response is monitored.

As it was noted earlier, in order to investigate off-tuning effect in the experimental studies, the properties of the TMD/HTMD changed instead of the primary structure. However, it is recommended for future experimental studies that the dynamic properties of the primary slab is changed by using actuator beneath the slab or employing human participant and changing their numbers.

Finally, it would be valuable to design an appropriate actuator specifically for the HTMD, considering the appropriate damping and frequency of the actuator itself, the frequency range of the operation and optimised power consumption.

9. References

[1] M. Kasperski and H. J. Niemann, “Man induced vibrations of a stand structure,” *Proc., EURODYN*, pp. 977–983, 1993.

[2] C. M. Wang, N. Yan, and T. Balendra, “Control on Dynamic Structural Response Using Active-Passive Composite-Tuned Mass Dampers,” *J. Vib. Control*, vol. 5, no. 3, pp. 475–489, May 1999.

[3] K. R. Crescent, N. Yang, C. M. Wang, T. Balendra, and N. Yan, “Composite mass dampers for vibration control of wind-excited towers,” *J. Sound Vib.*, vol. 213, no. 2, pp. 301–316, Jun. 1998.

[4] C. Seiler, O. Fischer, P. Huber, and B. B. Ag, “Semi-active MR dampers in TMD ’ s for vibration control of footbridges , Part 2 : Numerical analysis and practical realisation,” in *Proceedings of the International Conference on the Design and Dynamic Behaviour of Footbridges*, 2002, pp. 20–22.

[5] I. M. Díaz and P. Reynolds, “On-off nonlinear active control of floor vibrations,” *Mech. Syst. Signal Process.*, vol. 24, no. 6, pp. 1711–1726, Aug. 2010.

[6] I. Diaz, D. Nyawako, and P. Reynolds, “On-off nonlinear velocity feedback control for cancelling floor vibrations,” in *Proceedings of the 4th European Conference on Structural Control*, 2008, pp. 175–82.

[7] I. M. Díaz and P. Reynolds, “Acceleration feedback control of human-induced floor vibrations,” *Eng. Struct.*, vol. 32, no. 1, pp. 163–173, Jan. 2010.

[8] C. a. A. Ã. Jones, P. Reynolds, and a. Pavic, “Vibration serviceability of stadia structures subjected to dynamic crowd loads: A literature review,” *J. Sound Vib.*, vol. 330, no. 8, pp. 1531–1566, Apr. 2011.

[9] M. Setareh, “Floor vibration control using semi-active tuned mass dampers,” *Can. J. Civ. Eng.*, vol. 29, no. 1, pp. 76–84, Feb. 2002.

[10] A. Bahar, F. Pozo, L. Acho, J. Rodellar, and A. Barbat, “Parameter identification of large-scale magnetorheological dampers in a benchmark building,” *Comput. Struct.*, vol. 88, no. 3–4, pp. 198–206, 2010.

[11] G. W. Housner, L. A. Bergman, T. K. Caughey, A. G. Chassiakos, R. O. Claus, S. F. Masri, R. E. Skelton, T. T. Soong, B. F. Spencer, and J. T. P. Yao, “Structural Control: Past, Present, and Future,” *J. Eng. Mech.*, vol. 123, no. 9, pp. 897–971, 1997.

[12] Y. Nakamura, K. Tanaka, M. Nakayama, and T. Fujita, “Hybrid mass dampers using two types of electric servomotors: AC servomotors and linear-induction

servomotors," *Earthq. Eng. Struct. Dyn.*, vol. 30, no. 11, pp. 1719–1743, Nov. 2001.

[13] A. Occhiuzzi, M. Spizzuoco, and G. Serino, "Semi-active MR dampers in TMD ' s for vibration control of footbridges , Part 1 : Numerical modelling and control algorithm," in *Footbridge 2002$\$ Proceedings of the International Conference on the Design and Dynamic Behaviour of Footbridges*, 2002, pp. 1–10.

[14] Y. Arfiadi, M. N. S. Hadi, Y. Ar, and M. N. S. H. R, "Passive and active control of three-dimensional buildings," *Earthq. Eng. Struct. Dyn.*, vol. 29, no. 3, pp. 377–396, Mar. 2000.

[15] K. Shiba, S. Mase, Y. Yabe, and K. Tamura, "Active/passive vibration control systems for tall buildings," *Smart Mater. Struct.*, vol. 7, no. 5, pp. 588–598, Oct. 1998.

[16] K. Seto, "Control of vibration in civil structures," *Proc. Inst. Mech. Eng. Part I J. Syst. Control Eng.*, vol. 218, no. 7, pp. 515–529, 2004.

[17] D. S. Nyawako and P. Reynolds, "Technologies for mitigation of human-induced vibrations in civil engineering structures," *Shock Vib. Dig.*, vol. 39, no. 6, pp. 465–493, Nov. 2007.

[18] T. Soong and J. B. F. Spencer, "Supplemental energy dissipation: state-of-the-art and state-of-the-practice," *Eng. Struct.*, vol. 24, no. 3, pp. 243–259, Mar. 2002.

[19] L. M. Jansen and S. J. Dyke, "Semiactive Control Strategies for MR Dampers: Comparative Study," *J. Eng. Mech.*, vol. 126, no. 8, p. 795, 2000.

[20] M. Setareh, "Application of semi-active tuned mass dampers to base-excited systems," *Earthq. Eng. Struct. Dyn.*, vol. 30, no. 3, pp. 449–462, 2001.

[21] A. Ahlawat and A. Ramaswamy, "Multi-objective optimal design of FLC driven hybrid mass damper for seismically excited structures," *Earthq. Eng. ...*, vol. 1479, no. June 2001, pp. 1459–1479, 2002.

[22] L. Hong-nan, H.-N. Li, and Z. G. Chiang, "Intelligent Algorithm Based Semi-Active Control for MR Damper for Structures ,*," *Processing*, vol. 3 , pp. 2428–2432, 2004.

[23] B. R. B. Ellis, T. Ji, and J. D. J. Littler, "The response of grandstands to dynamic crowd loads," *Proc. ICE - Struct. Build.*, vol. 140, no. 4, pp. 355–365, Jan. 2000.

[24] Institution of Structural Engineers, IStructE, and I. of S. Engineers, *Dynamic Performance Requirements for Permanent Grandstands Subject to Crowd Action: Recommendations for Management, Design and Assessment*, vol.

SD/03/26, no. November. London: The Institution of Structural Engineers, The Department for Communities and Local Government, The Department for Culture Media and Sport, 2008, pp. 1–22.

[25] J. G. Parkhouse and D. J. Ewins, "Crowd-induced rhythmic loading," *Struct. Build.*, vol. 159, no. SB5, pp. 247–259, 2006.

[26] B. R. E. Dsc, J. D. Littler, and B. R. Ellis, "Response of cantilever grandstands to crowd loads. Part 2: load estimation," *Proc. ICE - Struct. Build.*, vol. 157, no. 5, pp. 297–307, Jan. 2004.

[27] A. Caprioli, P. Reynolds, M. Vanali, and E. Zappa, "Comparison of the effects of a moving crowd on different grandstands during similar events," in *IMAC XXIV*, 2006, pp. 1–9.

[28] B. R. Ellis, T. Ji, and J. D. Littler, "The response of grandstands to dynamic loads induced by crowds," vol. ; Sydney, p. -, 1994.

[29] B. R. Ellis, T. Ji, and J. D. Littler, "Crowd actions and grandstands," vol. 71; Birmingham, pp. 277–282.

[30] J. D. Littler, "The dynamic response of a three tier cantilever grandstand." Balkema, Rotterdam, pp. 623–628, 1999.

[31] D. Nyawako and P. Reynolds, "Active control of human induced floor vibrations," in *Proc. 26th Int. Modal Analysis Conf.(Orlando, FL)*, 2008.

[32] A. Ebrahimpour and R. L. Sack, "A review of vibration serviceability criteria for floor structures," *Comput. Struct.*, vol. 83, no. 28–30, pp. 2488–2494, Nov. 2005.

[33] J. Sim, M. S. Williams, and a. Blakeborough, "Statistical analysis of structural vibrations due to crowd jumping loads," *Proc. ICE - Struct. Build.*, vol. 161, no. 2, pp. 65–75, Jan. 2008.

[34] J. Sim, M. Williams, and a. Blakeborough, "Modelling effects of passive crowds on grandstand vibration," *Struct. Build.*, vol. 159, no. SB5, pp. 261–272, Jan. 2006.

[35] Z. Ibrahim, "The Effects of Crowds on Dynamic Characteristics of Stadia Structures," University of Sheffield, Department of Civil and Structural Engineering, 2006.

[36] B. Ellis, T. Ji, and C. Eng, "Human–structure interaction in vertical vibrations," *Proc. Instn Civ. Engrs Structs Bldgs*, vol. 122, pp. 1–9, 1997.

[37] A. Blakeborough and M. S. Williams, "Human Structure Interaction in Cantilever Grandstands," *Struct. Dyn. Oxford Univ.*, 2007.

[38] A. Pavic and P. Reynolds, “Experimental verification of novel 3DOF model for grandstand crowd- structure dynamic interaction,” *26th Int. Modal Anal. …*, vol. 6399, 2008.

[39] P. Reynolds and A. Pavic, “The dynamic performance of sports stadia under crowd dynamic loading at concert events,” *Sixth Eur. Conf. Dyn. EURODYN*, pp. 473–479, 2005.

[40] P. Reynolds and A. Pavic, “Vibration performance of a large cantilever grandstand during an international football match,” *ASCE J. Perform. Constr. Facil.*, vol. 20, no. 3, pp. 202–212, 2006.

[41] R. Mitchell, Y. Kim, T. El-Korchi, and Y.-J. Cha, “Wavelet-neuro-fuzzy control of hybrid building-active tuned mass damper system under seismic excitations,” *J. Vib. Control*, Jul. 2012.

[42] T. T. Soong and G. F. Dargush, *Passive Energy Dissipation Systems in Structural Engineering*. New York,: Wiley, 1997.

[43] M. C. Constantinou, T. T. Soong, and G. F. Dargush, “Passive energy dissipation systems for structural design and retrofit,” *Passiv. Energy Dissipation Syst. Struct. Des. Retrofit*, p. -–, 1998.

[44] R. D. Hanson and T. T. Soong, “Seismic design with supplemental energy dissipation devices,” *EERI Monogr. No. 8*, 2001.

[45] M. Sakamoto and T. Kobori, “Research, development and practical applications on structural response control of buildings,” *Smart Mater. Struct.*, vol. 4, no. 1A, pp. A58–A74, Mar. 1995.

[46] F. Weber, G. Feltrin, and O. Huth, “Guidelines for structural control,” *Struct. Eng. Res. Lab.*, no. March, 2006.

[47] G. Aguirre, M. Gorostiaga, T. Porchez, and J. Muñoa, “Self-tuning semi-active tuned-mass damper for machine tool chatter suppression,” in *ISMA2012-USD2012*, 2012, pp. 109–124.

[48] N. D. Sims, “Vibration absorbers for chatter suppression: A new analytical tuning methodology,” *J. Sound Vib.*, vol. 301, no. 3–5, pp. 592–607, Apr. 2007.

[49] H. R. R. Ji, Y. J. J. Moon, C. H. H. Kim, and I. W. W. Lee, “Structural vibration control using semiactive tuned mass damper,” in *Proceedings of the 18th KKCNN symposium on civil engineering-KAIST6*, 2005, vol. 30, no. 3, pp. 449–462.

[50] R. COLLINS, B. Basu, and B. BRODERICK, “Control strategy using bang–bang and minimax principle for FRF with ATMDs,” *Eng. Struct.*, vol. 28, no. 3, pp. 349–356, Feb. 2006.

[51] I. Nishimura, T. Yamada, M. Sakamoto, and T. Kobori, “Control performance of active-passive composite tuned mass damper,” *Smart Mater. Struct.*, vol. 7, no. 5, pp. 637–653, Oct. 1998.

[52] I. Nishimura, T. Kobori, and M. Sakamoto, “Active passive composite tuned mass damper,” *Proc. Semin. Seism. Isol.*, pp. 737–748, 1993.

[53] A. Bozer and G. Altay, “Hybrid tracking controller with attached tuned mass damper,” *Struct. Control Heal. Monit.*, p. n/a–n/a, Sep. 2011.

[54] J. Connor, *Introduction to structural motion control*, Massachuse. Massachusetts Institute of Technology,: Prentice Hall, 2002.

[55] C. Li, “Multiple active – passive tuned mass dampers for structures under the ground acceleration,” *Earthq. Eng. & Struct. Dyn.*, vol. 964, no. August 2002, pp. 949–964, 2003.

[56] Y. L. Cheung, W. O. Wong, and L. Cheng, “Optimization of a hybrid vibration absorber for vibration control of structures under random force excitation,” *J. Sound Vib.*, vol. 332, no. 3, pp. 494–509, Feb. 2013.

[57] J.-S. Bae, J.-H. Hwang, J.-H. Roh, J.-H. Kim, M.-S. Yi, and J. H. Lim, “Vibration suppression of a cantilever beam using magnetically tuned-mass-damper,” *J. Sound Vib.*, vol. 331, no. 26, pp. 5669–5684, Dec. 2012.

[58] J. Suhardjo, B. F. Spencer, and A. Kareem, “Active control of wind excited buildings: A frequency domain based design approach,” *J. Wind Eng. Ind. Aerodyn.*, vol. 43, no. 1–3, pp. 1985–1996, Jan. 1992.

[59] J. Suhardjo, J. Spencer, and M. K. Sain, “Feedback-feedforward control of structures under seismic excitation,” *Struct. Saf.*, vol. 8, no. 1–4, pp. 69–89, 1990.

[60] T. T. Soong, *Active Structural Control: Theory and Practice*. Essex, England, 1990.

[61] G. W. Housner, T. T. Soong, and S. F. Masri, “Second generation of active structural control in civil engineering,” in *Proceedings of the First World Conference on Structural Control*, 1994, pp. 3–18.

[62] S. J. Dyke, B. F. S. Jr., P. Quast, and M. K. Sain, “Role of control-structure interaction in protective system design,” *J. Eng. Mech.*, vol. 121, no. 1, pp. 322–338, 1995.

[63] T. Kobori, “Future direction on research and development of seismic-response-controlled structure,” in *Proc. 1st World Conf. on Struct. Control*, 1994, pp. 19–31.

[64] P. B. SHING, M. E. Dixon, N. KERMICHE, R. Su, and D. M. FRANGOPOL, "CONTROL OF BUILDING VIBRATIONS WITH ACTIVE/PASSIVE DEVICES," *Earthq. Eng. Struct. Dyn.*, vol. 25, no. 10, pp. 1019–1039, Oct. 1996.

[65] F. Y. Cheng and H. Jiang, "Hybrid Control of Seismic Structures with Optimal Placement of Control Devices," *J. Aerosp. Eng.*, vol. 11, no. 2, p. 52, 1998.

[66] F. E. Udwadia, S. Tabaie, and F. E. Udwadia., "PULSE CONTROL OF SINGLE-DEGREE-OF-FREEDOM SYSTEM," *ASCE J Eng Mech Div*, vol. 107, no. 6, pp. 997–1009, 1981.

[67] R. A. Lund, *Active damping of large structures in winds*. New York: North Holland, 1980.

[68] L. Li, G. Song, and J. Ou, "Hybrid active mass damper (AMD) vibration suppression of nonlinear high-rise structure using fuzzy logic control algorithm under earthquake excitations," *Struct. Control Heal. Monit.*, vol. 18, no. 6, pp. 698–709, Oct. 2011.

[69] K. Yang, L. Cui, and H. Huang, "A robust control method of a hybrid vibration absorber for vibration suppression in a wide frequency band considering large structural parameter variations," *Proc. Inst. Mech. Eng. Part I J. Syst. Control Eng.*, vol. 227, no. 3, pp. 308–319, Mar. 2013.

[70] J. Morison and D. Karnopp, "COMPARISON OF OPTIMIZED ACTIVE AND PASSIVE VIBRATION ABSORBERS.," in *14th Annu. Joint Automatic Control Conf*, 1973, pp. 932–938.

[71] S. Chatterjee, "Optimal active absorber with internal state feedback for controlling resonant and transient vibration," *J. Sound Vib.*, vol. 329, no. 26, pp. 5397–5414, Dec. 2010.

[72] D. C. Batterbee and N. D. Sims, "Hardware-in-the-loop simulation of magnetorheological dampers for vehicle suspension systems," *Proc. Inst. Mech. Eng. Part I J. Syst. Control Eng.*, vol. 221, no. 2, pp. 265–278, Jan. 2007.

[73] T. Kobori, M. Takahashi, T. Nasu, N. Niwa, and K. Ogasawara, "Seismic response controlled structure with active variable stiffness system," *Earthq. Eng. Struct. Dyn.*, vol. 22, no. 11, pp. 925–941, 1993.

[74] S. Kamagata and T. Kobori, "Autonomous adaptive control of active variable stiffness systems for seismic ground motion," in *Proc. 1 World Conf. on Struct. Control*, 1994, pp. 33–42.

[75] R. L. Sack and W. Patten, "Semiactive hydraulic structural control," in *Proc. Int. Workshop on Struct. Control*, 1994, pp. 417–431.

[76] A. Dominguez, R. Sedaghati, and I. Stiharu, “Modeling and application of MR dampers in semi-adaptive structures,” *Comput. Struct.*, vol. 86, no. 3–5, pp. 407–415, 2008.

[77] F. Pozo, L. Acho, A. RodrÃguez, and G. Pujol, “Nonlinear modeling of hysteretic systems with double hysteretic loops using position and acceleration information,” *Nonlinear Dyn.*, vol. 57, no. 1–2, pp. 1–12, 2009.

[78] F. Ikhouane and J. Rodellar, *Identification and Control Using the Bouc-Wen Model*. John Wiley and Sons , 2007, p. -–.

[79] L. Hong-Nan and C. Zhi-Guo, “Intelligent algorithm based semi-active control for MR damper for structures,” in *Fifth World Congress on Intelligent Control and Automation (IEEE Cat. No.04EX788)*, 2001, vol. 3, no. 6, pp. 2428–2432.

[80] D. C. Batterbee, N. D. Sims, and A. Plummer, “Hardware-in-the-loop-simulation of a vibration isolator incorporating magnetorheological fluid damping,” *2nd ECCOMAS Themat. Conf. Smart Struct. Mater. Lisbon, Port.*, 2005.

[81] L. R. Miller, “An approach to semi-active control of multi-degree-of-freedom systems,” *An Approach to Semi-active Control Multi-degree-of-freedom Syst.*, p. -–, 1988.

[82] B. Spencer Jr, M. K. K. Sain, and B. F. Spencer, “Controlling buildings: a new frontier in feedback,” *Control Syst. Mag. IEEE*, vol. 17, no. 6, pp. 19–35, 1997.

[83] J. D. Carlson, “The promise of controllable fluids,” *Proc. Actuator*, vol. 94, pp. 266–270, 1994.

[84] J. D. Carlson and K. D. Weiss, “A growing attraction to magnetic fluids,” *Mach. Des.*, no. 15, pp. 61–64, 1994.

[85] J. D. Carlson, D. M. Catanzarite, and K. A. S. Clair, “Commercial magneto-rheological fluid devices,” *Int. J. Mod. Phys. B*, vol. 10, no. 23–24, pp. 2857–2865, 1996.

[86] J. D. Carlson, “Magnetorheological fluids engineering applications today and tomorrow,” in *2nd ECCOMAS Thematic Conference on Smart structures and materials, Lisbon, Portugal, 18-21*, 2005.

[87] F. Gordaninejad, M. Saiidi, B. C. Hansen, E. O. Ericksen, and F.-K. Chang, “Magneto-rheological fluid dampers for control of bridges,” *J. Intell. Mater. Syst. Struct.*, vol. 13, no. 2–3, pp. 167–180, 2002.

[88] H. Search, C. Journals, A. Contact, M. Iopscience, S. Mater, I. P. Address, S. J. Dyke, B. F. Spencer, M. K. Sain, and J. D. Carlson, “Modeling and control

of magnetorheological dampers for seismic response reduction," *Smart Mater. Struct.*, vol. 5, no. 5, pp. 565–575, Oct. 1996.

[89] D. C. Batterbee and N. D. Sims, "Vibration isolation using smart fluid dampers: A benchmarking study," *Smart Struct. Syst.*, vol. 1, no. 3, pp. 235–256, 2005.

[90] S. J. Dyke, B. F. Spencer, M. K. Sain, and J. D. Carlson, "An experimental study of MR dampers for seismic protection," *Smart Mater. Struct.*, vol. 7, no. 5, pp. 693–703, 1998.

[91] S. J. Dyke, J. S. B.F., M. K. Sain, and J. D. Carlson, "Seismic response reduction using magnetorheological dampers," in *Proceedings of the IFAC World Congress*, 1996, pp. 145–150.

[92] B. F. Spencer, J. D. Carlson, M. K. Sain, and G. Yang, "On the current status of magnetorheological dampers: Seismic protection of full-scale structures ," 1997, vol. 1 , pp. 458–462.

[93] B. F. S. Jr., S. J. S. Dyke, M. K. Sain, J. D. Carlson, B. S. Jr, and B. F. Spencer, "Phenomenological Model for Magnetorheological Dampers," *J. Eng. ...*, vol. 123, no. 3, p. 230, 1997.

[94] S. J. Dyke and B. F. Spencer, "Seismic response control using multiple MR dampers," *Proc. 2nd Int. Work. Struct. Control*, pp. 163–173, 1996.

[95] B. F. Spencer, E. A. Johnson, and J. C. Ramallo, "Smart isolation for seismic control ," 1999, pp. 169–174.

[96] G. A. Baker, E. A. Johnson, J. S. B.F., and Y. Fujino, "Modeling and semiactive damping of stay cables ," 1999.

[97] K. Sunakoda, H. Sodeyama, N. Iwata, H. Fujitani, and S. Soda, "Dynamic characteristics of magneto-rheological fluid damper ," 2000.

[98] W. M. Winslow, "Method and Means for Translating Electrical Impulses into Mechanical Force ." US Patent No. 2,417,850., USA, 1947.

[99] J. Rabinow, "The magnetic fluid clutch," *AIEE Trans.*, vol. 67 , pp. 1308–1315, 1948.

[100] "Lord Corporation," *Rheonetic MR fluid*. p. -–, 2001.

[101] K. D. Weiss, J. D. Carlson, and D. A. Nixon, "Viscoelastic properties of magneto- and electro-rheological fluids," *J. Intell. Mater. Syst. Struct.*, vol. 5, no. 6, pp. 772–775, 1994.

[102] J. M. Ginder, L. C. Davis, and L. D. Elie, “Rheology of magnetorheological fluids: Models and measurements,” *Int. J. Mod. Phys. B*, vol. 10, no. 23–24, pp. 3293–3303, 1996.

[103] F. Yi, S. J. Dyke, S. Frech, and J. D. Carlson, “Investigation of magnetorheological dampers for earthquake hazard mitigation,” *Proceeding 2nd World Conf. Struct. Control*, pp. 349–358, 1998.

[104] F. Yi, S. J. Dyke, J. M. Caicedo, and J. D. Carlson, “Seismic response control using smart dampers ,” 1999, vol. 2 , pp. 1022–1026.

[105] S. J. Dyke, F. Yi, and J. D. Carlson, “Application of magnetorheological dampers to seismically excited structures,” *Proc., Int. Modal Anal. Conf.*, p. -– , 1999.

[106] W. M. Winslow, “Induced fibration of suspensions,” *J. Appl. Phys.*, vol. 20, no. 12, pp. 1137–1140, 1949.

[107] T. Pinkaew and Y. Fujino, “Effectiveness of semi-active tuned mass dampers under harmonic excitation,” *Eng. Struct.*, vol. 23, no. 7, pp. 850–856, Jul. 2001.

[108] M. Abe, T. Igusa, and C. Engineering, “SEMI-ACTIVE DYNAMIC VIBRATION ABSORBERS FOR CONTROLLING TRANSIENT RESPONSE,” *J. Sound Vib.*, vol. 198, no. 5, pp. 547–569, Dec. 1996.

[109] J.-H. Koo, M. Ahmadian, M. Setareh, and T. Murray, “In Search of Suitable Control Methods for Semi-Active Tuned Vibration Absorbers,” *J. Vib. Control*, vol. 10, no. 2, pp. 163–174, Feb. 2004.

[110] F. Weber, C. Boston, and G. Feltrin, “Controlled Viscous-Friction Damping of Stay Cables with MR Dampers,” in *4th International Conference on Structural Health Monitoring of Intelligent Infrastructure (SHMII-4)*, 2009, no. July, pp. 2–8.

[111] B. F. Spencer, S. J. Dyke, and H. S. Deoskar, “Benchmark problems in structural control. Part I: Active mass driver system,” 1997, pp. 1265–1269.

[112] A. S. Ahlawat and A. Ramaswamy, “Multiobjective Optimal Fuzzy Logic Controller Driven Active and Hybrid Control Systems for Seismically Excited Nonlinear Buildings,” *J. Eng. Mech.*, vol. 130, no. 4, p. 416, 2004.

[113] I. Nagashima, R. Maseki, Y. Asami, J. Hirai, and H. Abiru, “Performance of hybrid mass damper system applied to a 36-storey high-rise building,” *Earthq. Eng. Struct. Dyn.*, vol. 30, no. 11, pp. 1615–1637, Nov. 2001.

[114] T. Fujinami, Y. Saito, M. Morishita, Y. Koike, and K. Tanida, “A hybrid mass damper system controlled by H control theory for reducing bending–torsion

vibration of an actual building," *Earthq. Eng. Struct. Dyn.*, vol. 30, no. 11, pp. 1639–1653, 2001.

[115] M. Watakabe, M. M. Tohdo, O. Chiba, N. Izumi, H. Ebisawa, T. Fujita, and M. Tohdo, "Response control performance of a hybrid mass damper applied to a tall building," *Earthq. Eng. Struct. Dyn.*, vol. 30, no. 11, pp. 1655–1676, Nov. 2001.

[116] M. Higashino and S. Aizawa, "Application of active mass damper system in actual buildings ," 1993, pp. 194–205.

[117] T. T. Soong, A. M. Reinhorn, S. Aizawa, and M. Higashino, "Recent structural applications of active control technology," *J. Struct. Control*, vol. 1, no. 2, pp. 5–21, 1994.

[118] S. Yamazaki, N. Nagata, and H. Abiru, "Tuned active dampers installed in the Minato Mirai (MM) 21 landmark tower in Yokohama," *J. Wind Eng. Ind. Aerodyn.*, vol. 43, no. 1–3, pp. 1937–1948, Jan. 1992.

[119] T. Fujita, "Application of hybrid mass damper with convertible active and passive modes using hydraulic actuator to high-rise building," in *Proceedings of 1994 American Control Conference - ACC '94*, 1994, vol. 1, no. June, pp. 1067–1072.

[120] T. Yamada, T. Kobori, and I. Nishimura, "Dynamic vibration absorber ." Japan Patent Bureau S63-156171 , 1988.

[121] Y. L. L. Cheung, W. O. O. Wong, and L. Cheng, "Design optimization of a damped hybrid vibration absorber," *J. Sound Vib.*, vol. 331, no. 4, pp. 750–766, Feb. 2012.

[122] J. Yuan, "Hybrid vibration absorption by zero/pole-assignment," *J. Vib. Acoust.*, vol. 122, no. October, pp. 466–469, 2000.

[123] R. Lewandowski and J. Grzymislawska, "Dynamic behaviour of composite mass damper for control of wind-excited vibration," in *AMAS Workshop on Smart Materials and Structures*, 2003, pp. 131–140.

[124] J. D. Marshall and F. A. Charney, "Seismic response of steel frame structures with hybrid passive control systems," *Earthq. Eng. Struct. Dyn.*, p. n/a–n/a, Jul. 2011.

[125] J. J. Kim and H. Amick, "Active vibration control in fabs," *Semicond. Int.*, vol. 20, no. Si 97, pp. 1–6, 1997.

[126] I. Nagashima and Y. Shinozaki, "Variable gain feedback control technique of active mass damper and its application to hybrid structural control," *Earthq. Eng. Struct. Dyn.*, vol. 26, no. 8, pp. 815–838, 1997.

[127] C. Li, "Multiple active-passive tuned mass dampers for structures under the ground acceleration," *Earthq. Eng. Struct. Dyn.*, vol. 32, no. 6, pp. 949–964, May 2003.

[128] I. Nishimura, "Active passive composite tuned mass damper," *Proc. ATC17-1 (San Fr.*, pp. 737–743, 1992.

[129] H.-N. Li, S. Yan, and G. Lin, "State-of-the-art review for intelligent structural control," *Earthq. Eng. Eng. Vib.*, vol. 19, no. 2, pp. 29–36, 1999.

[130] J. Florescu and A. Bu, "State-Space PD Feedback Control," *Int. J. Comput. Information, ...*, pp. 52–56, 2009.

[131] R. L. Sack, C. C. Kuo, H. C. Wu, L. Liu, and W. N. Patten, "Seismic motion control via semiactive hydraulic actuators," *Proc., U.S. 5th Nat. Conf. Earthq. Engrg.*, vol. 2 , pp. 311–320, 1994.

[132] S. J. Dyke, B. F. S. Jr., P. Quast, M. K. Sain, D. C. K. Jr., and T. T. Soong, "Acceleration feedback control of MDOF structures," *J. Eng. Mech.*, vol. 122, no. 9, pp. 907–917, 1996.

[133] S. J. Dyke, B. F. S. Jr., P. Quast, D. C. K. Jr., and M. K. Sain, "Implementation of an active mass driver using acceleration feedback control," *Microcomput. Civ. Eng.*, vol. 11, no. 5, pp. 305–323, 1996.

[134] T. Abdelaziz and M. Valášek, "STATE DERIVATIVE FEEDBACK BY LQR FOR LINEAR TIME-INVARIANT SYSTEMS," *Proc. 16th IFAC World Congr.*, 2005.

[135] T. Abdelaziz and M. Valášek, "Direct algorithm for pole placement by state-derivative feedback for multi-inputlinear systems - nonsingular case," *Kybernetika*, vol. 41, no. 5, 2005.

[136] M. S. Kumar and S. Vijayarangan, "Design of LQR controller for active suspension system," *INDIAN J. ...*, vol. 13, no. June, pp. 173–179, 2006.

[137] P. Lu, S. Chen, and Y. Zheng, "Artificial Intelligence in Civil Engineering," *Math. Probl. Eng.*, vol. 2012, pp. 1–22, 2012.

[138] S. Sivanandam and S. Deepa, *Introduction to Genetic Algorithms*. New York: Springer, 2007.

[139] S. S. Rao, *Engineering Optimization*, Fourth Edi. Hoboken, NJ, USA: John Wiley & Sons, Inc., 2009.

[140] Y. L. Cheung and W. O. Wong, "H∞ and H2 optimizations of a dynamic vibration absorber for suppressing vibrations in plates," *J. Sound Vib.*, vol. 320, no. 1–2, pp. 29–42, Feb. 2009.

[141] Y.-A. He and T. Guo, "Active structural control based on genetic algorithms," *J. Vib. Eng.*, vol. 12 , pp. 182–187, 1999.

[142] H.-N. Li, Z.-G. Chang, and B.-D. Zhao, "Study on optimization of structural vibration control by GA," *Earthq. Eng. Eng. Vib.*, vol. 22, no. 5, pp. 92–96, 2002.

[143] A. S. Ahlawat and A. Ramaswamy, "Multiobjective optimal FLC driven hybrid mass damper system for torsionally coupled, seismically excited structures," *Earthq. Eng. Struct. Dyn.*, vol. 31, no. 12, pp. 2121–2139, Dec. 2002.

[144] D. S. Nyawako and P. Reynolds, "LQR controller for an in-service floor," *Exp. Mech.*, 2010.

[145] D. Nyawako, P. Reynolds, and M. Hudson, "Investigating PID controllers for mitigation of human-induced floor vibrations," in *EURODYN*, 2011.

[146] D. Nyawako and P. Reynolds, "Response-dependent velocity feedback control for mitigation of human-induced floor vibrations," *Smart Mater. Struct.*, vol. 18, no. 7, pp. 1–14, Jul. 2009.

[147] P. Reynolds, I. M. Diaz, and D. S. Nyawako, "Vibration testing and active control of an office floor," in *27th International Modal Analysis Conference (IMAC XXVII), Orlando, Florida, USA*, 2009.

[148] D. S. Nyawako and P. Reynolds, "Active control of human induced floor vibrations." p. -, 2007.

[149] N. Noormohammadi and P. Reynolds, "Control of human induced vibrations in stadia using a hybrid tuned mass damper," in *Noise and Vibration Engineering, ISMA2012*, 2012, pp. 1119–1132.

[150] D. S. Nyawako and P. Reynolds, "LQR controller for an in-service floor," *Dyn. Civ. Struct. Vol. 4*, pp. 227–237, 2011.

[151] P. Reynolds, "The Effects of Raised Access Flooring on the Vibrational Performance of Long-Span Concrete Floors," University of Sheffield, 2000.

[152] J. P. den Hartog, *Mechanical Vibrations*. Mineola, New York: Dover Publications Inc., 1985, p. -436.

[153] H.-C. Tsai and G.-C. Lin, "Optimum tuned-mass dampers for minimizing steady-state response of support-excited and damped systems," *Earthq. Eng. Struct. Dyn.*, vol. 22, no. 11, pp. 957–973, Nov. 1993.

[154] Matlab, *Matlab Optimization Toolbox User's Guide*. 2012.

[155] VES, "Vibration Engineering Section Handbook," 2012. [Online]. Available: https://sites.google.com/a/sheffield.ac.uk/ves-handbook/.

[156] "Instruction manual, Electro-seis, Model 113 Shaker." APS Dynamics, Inc., p. -, 1996.

[157] E. Shahabpoor, P. Reynolds, and D. Nyawako, "A Comparison of Direct Velocity, Direct and Compensated Acceleration Feed-back Control Systems in Mitigation of Low-frequency Floor Vibrations," *Dyn. Civ. Struct. Vol. 4*, pp. 177–187, 2011.

[158] S. Ohrui, T. Kobori, S. Mitsuta, N. Koshika, I. Nishimura, K. Sasaki, A. Kondo, I. Fukushima, and M. Sakamoto, "An Active-Passive Composite Tuned Mass Damper for Vibration Control of A Building," in *Second International Conference on Motion and Vibration Control*, 1994, pp. 569–574.

[159] I. Nishimura, T. Kobori, M. Sakamoto, N. Koshika, K. Sasaki, S. Ohrui, H. Search, C. Journals, A. Contact, M. Iopscience, S. Mater, and I. P. Address, "Active tuned mass damper," *Smart Mater.*, vol. 1, no. 4, pp. 306–311, Dec. 1992.

[160] I. Nishimura, M. Sakamoto, T. Yamada, N. Koshika, and T. Kobori, "Acceleration feedback method applied to active-passive composite tuned mass damper," *J. Struct. Control*, vol. 1, no. 1–2, pp. 103–116, 1994.

[161] I. Fukushima, K. Sasaki, I. Nishimura, N. Koshika, M. Sakamoto, and T. Kobori, "Development and application of active-passive composite tuned mass damper to high-rise building," *Proc. Pacific …*, 1995.

[162] N. Noormohammadi and P. Reynolds, "Employing hybrid tuned mass damper to solve off-tuning problems for controlling human induced vibration in stadia," in *IMAC XXXI*, 2013.

[163] R. C. Dorf and R. H. Bishop, *Modern Control Systems*, 12th ed. New Jersey: Prentice Hall, 2001.

[164] British Standards, "BS6472: 1992, Guide to evaluation of human exposure to vibrations in buildings," *Br. Stand.*, 1992.

[165] Matlab Inc., *Simulink 7 Getting Started Guide*. 2009.

[166] V. Kadirkamanathan, "Lecture Notes, State-Space, Non-Linear and Optimal Control," Department of Automatic Control and Systems, University of Sheffield, 2011.

[167] Data Physics Corporation, "Getting Started with SignalCalc Mobilyzer," 2002.

[168] K. Shin and J. K. Hammond, *Fundamentals of signal processing for sound and vibration engineers*, vol. 10, no. 2. Wiley, 2008.

[169] British Standards, "BS ISO 2631-1:1997," *BSI Stand. Publ.*, 1997.

[170] N. Noormohammadi and P. Reynolds, " Experimental investigation of dynamic performance of a prototype hybrid tuned mass damper under human excitation ," 2013, vol. 8688, p. 86880W–86880W–13.

[171] J. M. W. Brownjohn, *Modal*. Singapore, 2000.

[172] A. Pavic and P. Reynolds, "Experimental verification of novel 3DOF model for grandstand crowd-structure interaction," in *26th International Modal Analysis Conference (IMAC XXVI)*, 2008, p. -.

10.Bibliography

A. Ghaffari, *Control and Dynamic Systems*, 1st ed., K. N. Toosi University of Technolog, Tehran, Iran (1997).

C. Chen, *Linear System Theory and Design*, Third, M. R. Lightner, Ed., OXFORD UNIVERSITY PRESS, New York (1998).

F. Edition and K. Ogata, *Modern Contro Engineering*, 4th ed., in *Control Engineering*, 4th ed., Aeeizb, Tehran (2002).

G. Hart and K. Wong, *Structural Dynamics for structural engineers*, W. Anderson, Ed., John Wiley & Sons, Inc., New York (1999).

J. P. Lynch, "Active structural control research at Kajima Corporation," in *The National Science Foundation's Summer Institute in Japan Program*, Stanford University (1998).

J. Wilkie, M. A. Johnson, and R. Katebi, *Control Engineering: An Introductory Course*, Palgrave (2002).

M. Hatch, *Vibration simulation using MATLAB and ANSYS*, CHAPMAN & HALL/CRC, Boca Raton (2001).

N. D. Lagaros, V. Plevris, C. C. Mitropoulou, L. Johnston, H. A. Probst, J. Gamon, and K. Wolfe, *Design Optimization of Active and Passive Structural Control Systems*, Information Science Reference, Hershey (2012).

N. PERANDIN and O. S. BURSI, "MITIGATION OF CROWD - INDUCED VIBRATION IN A STADIUM STRUCTURE," UNIVERSITÀ DEGLI STUDI DI TRENTO (2005).

P. Venkataraman, *Applied optimization with MATLAB programming*, John Wiley & Sons, New York (2009).

W. Gawronski, *Advanced structural dynamics and active control of structures*, F. F. Ling, Ed., Springer New York (2004).

Y. Kwon and H. Bang, *The finite element method using MATLAB*, CRC Press, Boca Raton (2000).